Program and Abstract Volume

LPI Contribution No. 1843

LUNAR AND PLANETARY INSTITUTE

USRA

Fourth International Planetary Dunes Workshop: Integrating Models, Remote Sensing, and Field Data

May 19–22, 2015 • City, State

INSTITUTIONAL SUPPORT

Universities Space Research Association (USRA)

Lunar and Planetary Institute

CONVENERS

Timothy Titus
U.S. Geological Survey

SCIENCE ORGANIZING COMMITTEE

Timothy Titus
U.S. Geological Survey

Joshua Bandfield
Space Science Institute

Mary Bourke
Trinity College Dublin

Lori Fenton
Carl Sagan Center at the SETI Institute

Rosalyn Hayward
U.S. Geological Survey

Briony Horgan
Purdue University

Jani Radebaugh
Brigham Young University

James Zimbelman
Smithsonian Institute

Lunar and Planetary Institute 3600 Bay Area Boulevard Houston TX 77058-1113

LPI Contribution No. 1843

Compiled in 2015 by

Meeting and Publication Services
Lunar and Planetary Institute
USRA Houston
3600 Bay Area Boulevard, Houston TX 77058-1113

This material is based upon work supported by NASA under Award No. NNX08AC28A. Any opinions, findings, and conclusions or recommendations expressed in this volume are those of the author(s) and do not necessarily reflect the views of the National Aeronautics and Space Administration.

The Lunar and Planetary Institute is operated by the Universities Space Research Association under a cooperative agreement with the Science Mission Directorate of the National Aeronautics and Space Administration.

Abstracts in this volume may be cited as

Author A. B. (2015) Title of abstract. In *Fourth International Planetary Dunes Workshop: Integrating Models, Remote Sensing, and Field Data,* p. XX. LPI Contribution No. 1843, Lunar and Planetary Institute, Houston.

ISSN No. 0161-5297

Preface

This volume contains abstracts that have been accepted for presentation at the Fourth International Planetary Dunes Workshop: Integrating Models, Remote Sensing, and Field Data, May 19–22, 2015, Boise, Idaho.

Administration and publications support for this meeting were provided by the staff of the Meeting and Publication Services Department at the Lunar and Planetary Institute.

Technical Guide to Sessions

Tuesday, May 19, 2015

8:30 a.m.	Lookout Room	Workshop Welcome and Introduction Remarks
8:45 a.m.	Lookout Room	Bedform Morphology
1:00 p.m.	Lookout Room	Wind Regimes and Bedform Response
5:00 p.m.	Lookout Room	Field Trip Update
5:30 p.m.	Lookout Room	Introduce and Advertise Your Poster
6:00 p.m.	Lookout Room	Poster Session

Wednesday, May 20, 2015

7:30 a.m.	Towne Place Suites Parking Lot	Bruneau Dunes Field Trip

Thursday, May 21, 2015

8:30 a.m.	Lookout Room	Dune Migration and Transport
1:00 p.m.	Lookout Room	Sediment Flux and Composition

Friday, May 22, 2015

8:30 a.m.	Lookout Room	Ripples and Lidar
10:15 a.m.	Lookout Room	Workshop Discussion and Wrap-Up
11:45 a.m.	Lookout Room	COSI-Corr Tutorial

Contents

Program

Tuesday, May 19, 2015
WORKSHOP WELCOME AND INTRODUCTION REMARKS
8:30 a.m. Lookout Room

Chairs: **Timothy Titus**
Josh Bandfield

8:30 a.m. Bandfield J *
Welcome Remarks and Logistics

8:35 a.m. Titus T *
Workshop Objectives and Goals

8:40 a.m. Zimbelman J *
Update on the Icarus Special Issue

BEDFORM MORPHOLOGY
8:45 a.m. Lookout Room

Aeolian Bedforms Observed on a Variety of Planetary Surfaces, Including Comets, Venus, Mars and Earth.

Chairs: **Hezi Yizhaq**
Matthew Chojnacki

8:45 a.m. Tirsch D. * Mottola S. Otto K. Kührt E. Jaumann R. Arnold G. Grothues H.-G. Hamm M. Michaelis H. Pelivan I. Proffe G. Scholten F. Schröder S. Bibring J.-P.
Morphology of Aeolian Bedforms on 67P/Churyumov-Gerasimenko **[#8024]**
We describe and anylyze various aeolian bedforms found on the comet 67P/Churyumov-Gerasimenko imaged by ROLIS and OSIRIS data.

9:15 a.m. Kreslavsky M. A. * Bondarenko N. V.
Aeolian Bedforms Associated with Radar-Dark Diffuse Features on Venus **[#8035]**
With few exceptions, asymmetric aeolian bedforms are absent in the central parts of extended crater-related deposits on Venus but are persistent in their peripheral parts. We discuss possible explanations of this phenomenon.

9:45 a.m. Lorenz R. D. *
Heights of Fortuna-Meshknet Dunes (Al-Uzza Undae), Venus, from Magellan Radarclinometry **[#8004]**
I re-examine Magellan images of Al-Uzzae, applying radarclinometric techniques used for Cassini. I find dune heights of ~40m, suggesting the dunes are not 'fully-grown' given their wavelength, perhaps due to limited sand supply.

10:15 a.m. Geissler P. E. * Wilgus J. T.
Antidunes on Mars? **[#8039]**
Transverse aeolian ridges (TARs) may have formed by a process different from either ripples or dunes.

10:45 a.m. Vaz D. A. * Sarmento P. T. K. Fenton L. K. Barata M. T. Michaels T. I.
Object-Based Dune Mapping and Characterization on Mars: Data Comparison and Accuracy Assessment **[#8045]**
We evaluate qualitatively and quantitatively a new methodology that enables the automated mapping and characterization of martian dune fields using CTX image mosaics.

11:15 a.m. Tsoar H. *
The Puzzle of Linear Dunes on Planets **[#8005]**
There are several types of linear dunes in the world's deserts where most of them are found on Mars and Titan. In my lecture I will cover what we do and do not know about these dunes.

11:45 a.m. DISCUSSION

Tuesday, May 19, 2015
WIND REGIMES AND BEDFORM RESPONSE
1:00 p.m. Lookout Room

How Aeolian Features Record and Respond to Wind Regimes, both Measured and Modeled.

Chairs: **Laura Kerber**
William Anderson

1:00 p.m. Narteau C. * Courrech du Pont S. Lü P. Dong Z. Rodriguez S. Fernandez-Cascales L.
Two Independent Dune Growth Mechanism in Laboratory and Landscape-Scale Experiments **[#8043]**
We identify two independent dune growth mechanisms in laboratory and landscape-scale experiments that can together provide less uncertainties on the estimation of the wind regime that have been responsible for the development of bedforms.

1:30 p.m. Lv P. * Narteau C. Dong Z. B.
Raked Linear Dunes as an Example of the Coexistence of two Modes of Crest Orientation **[#8009]**
Here we show that the raked linear dune morphology results from the coexistence of two dune growth mechanisms.

2:00 p.m. Lucas A. Rodriguez S. * Narteau C. Charnay B. Courrech du Pont S. Tokano T. Garcia A. Thiriet M. Hayes A. G. Lorenz R. D. Aharonson O.
Growth Mechanism and Dune Orientation on Titan **[#8011]**
Herein, we present a comprehensive analysis of Titan's dune orientations by coupling a new dune growth mechanism with actual wind fields generated by climate modelling.

2:30 p.m. BREAK

3:00 p.m. Newman C. E. * Richardson M. I. Bridges N. T. Lewis K. W. Gómez-Elvira J. Navarro S. Marín Jiménez M.
Winds and Aeolian Activity in Gale Crater on Mars: Model Results and Comparison with Observations **[#8034]**
We will show comparisons between measured winds in Gale Crater, aeolian features seen by MSL, and predictions from the MarsWRF model. We will also use MarsWRF to predict dune characteristics over the rest of Gale, focusing on active dunes near MSL.

3:30 p.m. Middlebrook W. Ewing R. C. * Ayoub F. Bridges N. T. Smith I. Spiga A.
Boundary Conditions and the Aeolian Sediment State of the Olympia Undae Dune Field, Mars **[#8051]**
We evaluate the boundary conditions in Olympia Undae. We map two and three dimensional dune parameters from two locations proximal and distal to Planum Boreum and constrain sediment fluxes. We compare our results with a mesoscale atmospheric model.

4:00 p.m. Michaels T. I. * Fenton L. K.
A Tale of Two Wind Paradigms: Unraveling a Paradox in Meridiani Planum, Mars **[#8032]**
High-resolution atmospheric modeling is used to make sense of two observed dominant wind paradigms (that each somehow affect only certain aeolian features/areas) in Meridiani Planum.

4:30 p.m. DISCUSSION

Tuesday, May 19, 2015
FIELD TRIP UPDATE
5:00 p.m. Lookout Room

Bruneau Dunes Field Trip Update Including Logistics Arrangements.

Chairs: **James Zimbelman**
Josh Bandfield

5:00 p.m. Zimbelman J. R. *
Field Trip to the Bruneau Dunes and the Snake River Plains Basalts **[#8010]**
The May 20 field trip involves stops to view the Snake River Plain basalts (near Boise) and to hike on the Bruneau Dunes, which are within a state park about 68 miles from Boise.

INTRODUCE AND ADVERTISE YOUR POSTER
5:30 p.m. Lookout Room

A One Minute Opportunity to Introduce Your Poster with one PowerPoint Slide..

Chairs: **Timothy Titus**
Rosalyn Hayward

5:30 p.m. *Poster Introductions*

Tuesday, May 19, 2015
POSTER SESSION
6:00 p.m. Lookout Room

Williams D. A.
Update on NASA's Planetary Aeolian Laboratory **[#8001]**
This presentation will provide the community a status update on the Planetary Aeolian Laboratory and future plans.

Runyon K. D. Lisse C. M. Cheng A. F. Bridges N. T. Lewis K.
Controls on and Implications of Aeolian Geomorphology on Comet 67P **[#8037]**
Simple mathematical modelling and physical arguments suggest putative aeolian geomorphologies on Comet 67P are indeed aeolian and most likely ripples formed from jets and amorphous outgassing.

Neakrase L. D. V.
Terrestrial Analogs for Venusian Dunes: Sub-Aqueous, Seafloor Dune Fields **[#8023]**
Terrestrial seafloor dune fields could serve as a more appropriate analog for venusian dunes due to similarities in the higher-pressure fluid environment in which they form, including remote sensing techniques for discerning dune morphologies.

Lorenz R. D. Fenton L. Lancaster N.
The Tallest Dunes in the Solar System? Dune Heights on Earth, Mars, Titan and Venus **[#8031]**
Whose dunes are tallest? / Many Mars dunes seem stunted / But Russell wins out.

Lorenz R. D. Radebaugh J.
Giant Linear Dunes as the Formation Pathway to Megabarchan Chains: Titan and the Rub 'Al Khali **[#8003]**
We suggest megabarchans cannot grow from barchans. Rather sand accumulates as giant linear dunes in a bidirectional regime which has since become more unidirectional. We see this pattern on Titan and in the field in the .United Arab Emirates.

Bishop B. B. Radebaugh J. R. Christiansen E. H. Lewis R. C.
Geographic Position of Dunes Relative to the Belet Sand Sea Margins and Correlation with Dune Width and Spacing **[#8055]**
Dune width variability in Belet's sand sea decreases with increasing distance to the margin. Distinct groups of width data at 100 km intervals from the sand sea margin showed a decreasing standard deviation with increasing distance from the margin.

Charnay B. Barth E. Rafkin S. Narteau C. Lebonnois S. Rodriguez S. Courrech du Pont S. Lucas A.
Methane Storms as a Driver of Titan's Dune Orientation **[#8046]**
We propose that the eastward propagation of Titan's dune is caused by tropical methane storms producing fast eastward gusts thanks to a coupling with the superrotation.

Radebaugh J. Lorenz R. D. Paillou P. Northrup D.
Morphologies, Morphometries and SAR Brightnesses of Yardangs and Dunes on Earth and Titan **[#8048]**
Yardangs, Earth, Titan / Wind erodes, not deposits / SAR can tell apart.

Northrup D. Radebaugh J. Lorenz R. D. Bishop B. Lewis R. C. Christiansen E. H.
Comparative Analysis of Yardang Morphologies in China **[#8053]**
A study on yardang morphologies in the Dunhuang Yardang field of western China. Yardang length, width, spacing, and sinuosity were measured to better understand yardang morphologies and aid in distinguishing yardangs from dunes on celestial bodies.

Jessar A. D. Zimbelman J. R. Hennig L. A.
TARs on Mars: A Study of the Spatial Variability and Physical Characteristics of Martian Transverse Aeolian Ridges **[#8022]**
We present the results from our analysis of HiRISE images from a 70°E–80°E pole-to-pole swath, in which we examined both the spatial variability and morphology of Martian Transverse Aeolian Ridges. We also propose new image analysis techniques.

Scheidt S. P. Palafox L. F. Hamilton C. W. Zimbelman J. R.
Automated Detection of Transverse Aeolian Ridges on Mars Using Convolutional Neural Networks and a Field-Based Terrestrial Orthoimage Training Set **[#8047]**
This work uses field-based photogrammetric data of ripple bedform topography and orthoimages to train a machine learning algorithm to map transverse aeolian ridges (TARs) in planetary remote sensing data of Mars.

Diniega S. Hansen C. J.
Tracking Gully Activity Within the North Polar Erg, Mars **[#8027]**
Sand flows; gully forms. / Is frost involved, Or just winds? / Hard to say, it's dark.

Dinwiddie C. L. Hooper D. M.
Parameterization of Finite-Element Cryo-Hydrologic Sand Dune Model to Constrain Debris-Flow-Initiating Subsurface Temperatures and Pore-Water Pressures, Great Kobuk Sand Dunes, Alaska **[#8018]**
To explain how debris flows form at subfreezing air temperatures, we present meteorology-driven, numerical simulation-derived subsurface temperature and pore-water pressure profiles in the Great Kobuk Sand Dunes of Alaska, for incipient flow events.

Anderson W. Blois G. Christensen K. T. Best J. Kocurek G. A.
Attributes of Flow Structures During Turbulence Extrema in Close Proximity to Dunes **[#8002]**
Conditional averaging based on pre-defined criteria in the flow close to dunes is used during simulations and experiments. This averaging procedure offers a unique perspective on flow structures present during intermittent, elevated erosion.

Smith I. B. Spiga A. Tyler D. Ewing R. C.
Wind at the North Pole of Mars: Comparisons of Modeling and Observations **[#8013]**
We simulate the winds at the north pole above 75° N at mesoscale resolution throughout a spring and summer season. The wind vectors extracted from our simulations agree with observations at these locations and provide a two-way feedback to compare.

Johnson M. B. Zimbelman J. R.
Mapping Winds over Martian Sand Dunes from Ripples and Digital Terrain Models **[#8015]**
Sand dunes preserve wind flow patterns in their ripple formations. DTMs can be used with wind modeling software to simulate wind speed and direction over these dunes. Results can be compared and together offer a more complete picture of recent wind.

Vaz D. A. Sarmento P. T. K. Silvestro S. Cardinale M.
Ripple Pattern Analysis in Herschel Crater **[#8044]**
We present the analysis of a dataset that integrates several ripple pattern characteristics for a dune field located in Herschel crater. Our aim is to use this source of information to understand ripple pattern variations.

Fenton L. K. Michaels T. I. Chojnacki M.
The Sediment State of Meridiani Planum, Mars **[#8020]**
Meridiani: / winds strengthen, new ripples form, / then the winds die down.

Fernandez-Cascales L. Lucas A. Rodriguez S. Narteau C. Allemand P. Spiga A.
Courrech du Pont S. Garcia A.
Tow Modes for Dune Orientation on Mars **[#8041]**
Do the two modes of dune orientation exist on Mars and can we know more precisely the climate from them ?

Kerber L. Hamilton C. W. Scheidt S. P.
The Aerodynamic Roughness of Mars-Like Surfaces **[#8033]**
A field study was conducted to measure aerodynamic roughness lengths over under-characterized, Mars-like terrains in Hawai'i for the purpose of improving Mars climate models.

Van Kooten S. J. Putzig N. E. Fenton L. K.
Investigating the Poleward Trend of Southern Dune Field Stabilization on Mars Using Thermophysical Observations **[#8052]**
We hypothesize that dune fields near Mars' south pole are stabilized by shallow ground ice, a linkage that would make dune morphology a tracer for local climate. We investigate with thermal inertia measurements and thermal models and find surprises.

Charles H. R. Titus T. N.
Mineral Abundance Estimates and Distribution Derived from Mars Dune Field #2938-497 **[#8014]**
The goal of this analysis was to determine the presence or absence of feldspar and examine its distribution if present in dune field #2938-497. We deconvolved thermal emissivity data from TES to identify mineral abundances in the dune field.

Titus T. N. Hayward R. K. Bogle R. Zimbelman J.
Sediment Flux Measurements at a Mars Analog Site **[#8006]**
The goal of the Grand Falls project was to measure sediment flux at a Mars analog site and to field test whether hysteresis can be responsible for the flux rate observed on Mars.

Hayward R. K. Titus T. N. Zimbelman J. R.
Mars Aeolian Analog: Instrument Evaluation **[#8007]**
As part of a study of flux rates at a Mars analog site, we installed an experimental sediment collector equipped with a time-lapse camera. We will evaluate the suitability of the experimental instrument for sediment flux studies on Mars.

Wishard C. A. Zimbelman J. R.
Wind Patterns on the Southern End of the Bruneau Dunes Compared to Remote Automatic Weather Station Data from Mountain Home, Idaho **[#8016]**
This study compared remote automatic weather data to data collected from an on site camera in order to study the wind patterns affecting the Bruneau sand dune.

Cornwall C. Jackson D. W. T. Bourke M. C. Cooper J. A. G.
Investigation of Martian Aeolian Dynamics Using Terrestrial Dune Analogues and Airflow Modelling **[#8050]**
We combine field observations, 3D computational fluid dynamics modeling and remote sensing data from Mars to constrain grain flow events that occur on lee slopes of dunes to improve estimates of dune field migration and sediment flux on Mars.

Wednesday, May 20, 2015
BRUNEAU DUNES FIELD TRIP
7:30 a.m. Towne Place Suites Parking Lot

The workshop will include a full-day field trip to Bruneau Dunes State Park, May 20, 2014. The field trip will be led by Dr. James Zimbelman, who is conducting active field research studies in this location. Participants will depart at 7:30 a.m. from the TownePlace Suites parking lot at 1455 South Capitol Boulevard, Boise ID 83706-3012.

We expect the return time to be about 5:00 p.m.

This field trip is self-organized (e.g. no chartered bus or catered box lunches), so we will be depending on volunteers to drive their vehicles. Coordination of vehicles, drivers, and passengers will be conducted on Tuesday, May 19, 2015, to reduce the size of the convoy and to ensure everyone has a ride. At sign-in we will collect names of drivers and the number of people they can take in that vehicle. Also, each vehicle will need to pay a $5 day use fee upon entering the park.

NOTE: Attendees that elect to voluntarily go on the field trip must sign the liability waiver form and turn it in on the morning of the field trip.

Thursday, May 21, 2015
DUNE MIGRATION AND TRANSPORT
8:30 a.m. Lookout Room

Investigation dune migration and transport on Mar sand Titan.

Chairs: **James Zimbelman**
Kristen Bennett

8:30 a.m. Bridges N. T. * Ehlmann B. L. Conrad P. Ewing R. Ayoub F. Day M. de la Torre M. Fisk M. Fraeman A. Hardgrove C. Herkenhoff K. E. Johnson J. Lapotre M. Lewis K. Kocurek G. Le Mouélic S. Martin-Torres J. Newman C. Newsome H. Rubin D. Sullivan R. Zorzano M. -P.
Investigation of the Bagnold Dunes by the Curiosity Rover: Plans for the First Study of an Active Dune Field on Another Planet **[#8028]**
We describe plans for MSL investigations of the Bagnold Dune Field in Gale Crater.

9:00 a.m. Banks M. E. * Geissler P. E. Bridges N. T. Russell P. Silvestro S. Chojnacki M. Zimbelman J. R. Delamere W. A.
Emerging Global Trends in Aeolian Bedform Mobility on Mars **[#8036]**
Emerging global trends in the mobility of martian bedforms in relation to their general location, albedo, surrounding surface slope, and elevation.

9:30 a.m. Bennett K. A. * Fenton L. Bell J. F. III
Correlating Albedo with Dune Movement on Mars **[#8038]**
In this study we propose a method to estimate dune activity by calculating changes in dune field albedos.

10:00 a.m. BREAK

10:15 a.m. Chojnacki M. * Michaels T. I. Fenton L. K. Banks M. E.
Widespread Dune Migration in Meridiani Planum, Mars **[#8030]**
Here we describe the migration rates, volumetric sediment fluxes, and turnover times of sand dunes across Meridiani Planum. Results suggest high rates of sediment transport and youthful ages for large dark dunes across the region.

10:45 a.m. MacKenzie S. M. * Barnes J. W.
The Lake-Dune Donnection: Investigating Titan's Sand Sources **[#8029]**
To address how Titan's sand particles become large enough to saltate, we investigate the feasibility of flocculation and evaporite-derivation, especially with respect to possible equatorial sites of formation.

11:15 a.m. Barnes J. W. *
Global Connectivity and Transport within Titan's Sand Sea **[#8040]**
Global sand river, / Dunes like a Mobius strip: / Xanadu, the twist.

11:45 a.m. DISCUSSION

Thursday, May 21, 2015
SEDIMENT FLUX AND COMPOSITION
1:00 p.m. Lookout Room

Sediment Flux and Composition from Mars and Earth, as Determined from Remote Sensing, In-Situ Studies, and Numerical Modeling.

Chairs: **Christy Swann**
Shannon MacKenzie

1:00 p.m. Lucas A. * Narteau C. Rodriguez S. Courrech du Pont S. Rozier O. Spiga A. Callot Y. Garcia A.
Estimation of Sand Flux from Linear Dunes Using High-Precision Satellite Measurements and Numerical Modelling **[#8025]**
We present here high-resolution satellite imagery analysis coupled with numerical modelling in order to assess sand fluxes at the crest of linear dunes. We will then discuss the implication in terms of landscape dynamics and climatic conditions.

1:30 p.m. Runyon K. D. * Bridges N. T.
Internal Boundary Layer Control for Sediment Flux in Herschel Crater, Mars **[#8021]**
Flux predictions compared against flux measurements from HiRISE change detection campaign.

2:00 p.m. Swann C. M. * Ewing R. C. Sherman D. J.
Wind-Blown Sand on Mars: Preliminary Results of Transport Intermittency and Thresholds from Wind-Tunnel Simulations **[#8056]**
This research presents thresholds for surface creep and saltation movement in a simulated martian environment.

2:30 p.m. BREAK

3:00 p.m. Redsteer M. H. * Hayward R. K.
A Field Comparison of Basalt vs. Quartz Sediment Transport in the Grand Falls Dune Field, Northeastern Arizona, USA **[#8019]**
We describe the distribution and sorting of sediment in the Grand Falls Dune field, and provide field measurements of transport rates for vesicular basaltic ash vs. fine grained quartz, as well as size and spacing of quartz-rich vs basaltic dunes.

3:30 p.m. Fenton L. K. * Bishop J. L. King S. Lafuente B.
Dunes Creating an Abrupt Increase in Gypsum Grain Concentration Along a Transport Pathway at White Sands National Monument, NM, USA **[#8017]**
Gypsum is so light;/ Strong winds make granules saltate. / Heavies can't keep up!

4:00 p.m. Horgan B. * Seelos F.
Using Mineralogy to Trace Sand Sources and Transport Histories in the North Polar Sand Sea, Mars **[#8054]**
Minerals and glass / Over three billion years of / Blowing in the wind.

4:30 p.m. DISCUSSION

Friday, May 22, 2015
RIPPLES AND LIDAR
8:30 a.m. Lookout Room

A Short Session with a Focus on Ripples and a Concluding Discussion from the Great Sand Dunes.

Chairs: **Serina Diniega**
Heather Charles

8:30 a.m. Yizhaq H. * Schmerler E. Katra I. Tsoar H. Kok J.
Experimental and Numerical Study of Sharp's Shadow Zone Hypothesis on Sand Ripples Spacing and Implication for Martian Sand Ripples **[#8012]**
We show by wind tunnel experiments and numerical simulations that the impact angle of saltation grains decreases with wind velocity. This relationship can explain the increase in ripple wavelength with wind speed as was suggested by Sharp (1963).

9:00 a.m. Silvestro S. * Vaz D. A. Popa C. Esposito F.
Longitudinal Aeolian Depositional Features on Mars? **[#8049]**
We show evidence of potential longitudinal sand ribbon patterns and longitudinal ripples on Mars.

9:30 a.m. Valdez A. D. *
Using Lidar Data has Helped Improve the Understanding and Interpretation of Resources at Great Sand Dunes National Park and Preserve, Colorado, U.S.A. **[#8026]**
In 2011 Great Sand Dunes National Park, Colorado, was mapped using airborne lidar. The lidar dataset has been used by the National Park Service to measure resource properties and as a landform visualization tool. Examples will be presented.

10:00 a.m. DISCUSSION

WORKSHOP DISCUSSION AND WRAP-UP
10:15 a.m. Lookout Room

The Workshop Discussion and Wrap-Up Includes Identifying the Highlights from each Session.
These Highlights will Become part of a Meeting Proceedings Article that will be Submitted to EOS.
Future Plans will also be Discussed, such as a Special Issue.

Chairs: **Timothy Titus**
Lori Fenton

10:15 a.m. Session Chairs *
Session Highlights

10:45 a.m. *Workshop Discussion*

11:15 a.m. *Special Issue*

11:30 a.m. *Next Workshop*

Friday, May 22, 2015
COSI-CORR TUTORIAL
11:45 a.m. Lookout Room

An Optional Session for Those Who Want to Use Remote Sensing Data to Identify Change Detection and Dune Migration.

Chair: Nathan Bridges

11:45 a.m. Ayoub F. * Leprince S. Avouac J. P. Bridges N. T.
COSI-Corr: A Software to Monitor Ground Surface Deformation from Satellite Imagery **[#8008]**
COSI-Corr is a software allowing precise co-registration of time-series of images and sub-pixel measurement of ground surface deformation. This presentation is a tutorial about COSI-Corr capability and use, with emphasis HiRISE imagery.

Attributes of Flow Structures During Turbulence Extrema in Close Proximity to Dunes

William Anderson[1], G. Blois[2], Kenneth T. Christensen[2], Jim Best[3], Gary Kocurek[4]

[1]The University of Texas at Dallas
[2]The University of Notre Dame
[3]The University of Illinois at Urbana-Champaign
[4]The University of Texas at Austin

Summary: Conditional averaging based on pre-defined events in the flow field close to dunes has been used during numerical simulations and experiments. This averaging procedure provides a unique means to characterize flow structures present during intermittent periods of elevated erosion.

Abstract: Erosion of bedform sediment via aeolian or alluvial processes is induced (and sustained) by kinetic energy fluxes transported by the above fluid (winds in the atmospheric surface layer or water in river beds). Conceptual models typically indicate that sediment flux, q (via saltation or drift), scales with imposed aero-/hydro-dynamic (basal) stress raised to some exponent, n, where $n > 1$. Since basal stress (in fully rough, inertia-dominated flows) scales with the incoming velocity squared, u^2, it follows that $q \sim u^{2n}$ (where u is some relevant component of the above flow field, $\boldsymbol{u}(\boldsymbol{x},t)$). Thus, even small (turbulent) deviations of u from its time-averaged value may play an enormously important role in geomorphic evolution of bedforms. The importance of this argument is further augmented given that turbulence in the fluid within one to two dune heights above the bedform exhibits non-Gaussian statistics (intermittent, large fluctuations). In order to illustrate the importance of these fluctuations, we have used conditional averaging predicated on turbulence extrema in close proximity to the dunes. This averaging procedure provides an ensemble-mean visualization of flow structures responsible for erosion `events'. The conditional averaging has been performed on results obtained during large-eddy simulations and high-fidelity experiments using a refractive index matching environment.

COSI-CORR: A SOFTWARE TO MONITOR GROUND SURFACE DEFORMATION FROM SATELLITE IMAGERY. F. Ayoub[1], S. Leprince[1], J.P Avouac[1], and N.T. Bridges[2], [1]Caltech GPS, 1200 East California Blvd, Pasadena, CA91125 (fayoub@gps.caltech.edu), [2]Johns Hopkins University Applied Physics Laboratory, 11100 Johns Hopkins Road, Laurel, MD 20723.

Introduction: COSI-Corr is a software developed at the California Institute of Technology for the accurate geometrical processing of optical satellite and aerial imagery. The software allows precise co-registration of time-series of images and sub-pixel measurement of ground surface deformation.

Released to the academic community in 2007, COSI-Corr is used in Earth Sciences to monitor surface processes such as co-seimic deformation, glacier flow, landslide, sand dune migration. The method has recently been applied on Mars using HiRISE imagery to monitor sand ripple displacement on the Nili Patera dune field [1,2]. Complete HiRISE and CTX imagery support was released to the community in October 2014.

Tutorial: This presentation is in essence a tutorial about COSI-Corr, with emphasis on the processing of HiRISE imagery. After a few illustrations of the software capability, a detailed presentation of the software use will be presented: software installation and resources, description of the standard processing steps, HiRISE specificities, and post-processing tools. The objective is to provide enough information to the audience for it to be aware of the software capability and be able to process Martian (or Earth) imagery.

COSI-Corr (an ENVI plugin) is available at:
http://www.tectonics.caltech.edu/slip_history/spot_coseis/

References: [1] Bridges N.T. et al. (2012) *Nature 485,* 339-342. [2] Ayoub F. et al. (2014) *Nature Communications* 5:5096 doi: 10.1038/ncomms6096

EMERGING GLOBAL TRENDS IN AEOLIAN BEDFORM MOBILITY ON MARS. M. E. Banks[1], P. E. Geissler[2], N. T. Bridges[3], P. Russell[4], S. Silvestro[5,6], M. Chojnacki[7], J. R. Zimbelman[4], and W. A. Delamere[8]. [1]Planetary Science Institute, Tucson, AZ, banks@psi.edu. [2] US Geological Survey, Flagstaff AZ. [3]Johns Hopkins University, Applied Physics Laboratory, Laurel, MD. [4]Center for Earth and Planetary Studies, Smithsonian Air and Space Museum, Washington, DC, [5]INAF Osservatorio Astronomico di Capodimonte, Napoli (Italy). [6]Carl Sagan Center, SETI Institute, CA, [7]Lunar and Planetary Lab, U.A., Tucson, AZ, [8]Delamere Space Sciences, Boulder, CO.

Introduction: Until relatively recently, it was not clear as to whether fields of sand dunes on Mars were actively evolving in the present martian climate [1–4]. When wind velocity exceeds the threshold speed, sand particles are mobilized. However, due to Mars' thin atmosphere, the threshold friction speed for movement of fine sand is several times greater than on Earth [e.g., 1]. The High Resolution Imaging Science Experiment (HiRISE) on Mars Reconnaissance Orbiter (MRO) has acquired sets of images covering aeolian features at resolutions up to 25 cm/pixel, and with consistent lighting conditions, at intervals of 1 or more martian years. Analysis of these repeat image sets has led to the detection of changes and the migration of aeolian bedforms (dunes and ripples) in about 70% of the locations investigated (excluding locations between 70-90° N latitude where the detection of movement was 100%), with other locations not yet revealing detectable changes or movement (Fig. 1) [e.g. 5–12].

While such imaging currently exists in only a limited number of locations, preliminary results hint at possible trends in the global distributions of active and inactive bedforms, and provide potential insight into local and regional conditions most conducive to bedform mobilization on the martian surface. Here we investigate possible emerging trends in the mobility of bedforms in relation to their general location, albedo, surrounding surface slope, and elevation.

Results and Discussion: *Spatial distribution.* Figure 1 shows the locations of bedforms analyzed for changes. Locations of transverse aeolian ridges (TARs) have not been included due to the lack of evidence for activity in current martian atmospheric conditions [e.g., 13]. The majority of observations in the northern hemisphere indicate movement. This is especially apparent in the high northern latitudes (polar erg) where all of the image pairs investigated indicated movement. Observations in the southern hemisphere show a more even distribution of results with roughly half the locations exhibiting movement and half with no detectable changes. Movement detected in the high northern latitudes may be associated with strong katabatic winds from the high elevation polar cap [14–15] and possibly with the presence of seasonal volatiles [6–7,9,14]. Bedforms at high southern latitudes may be stabilized by agents such as ground ice acting over a longer period of time in comparison to the north polar region [16].

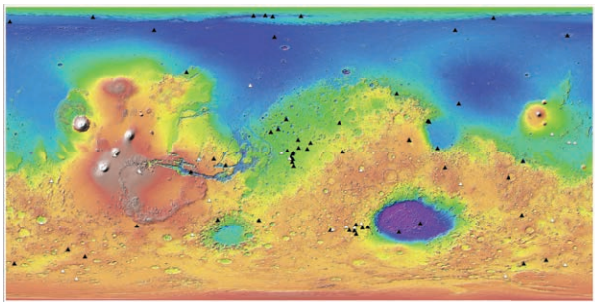

Figure 1: Locations of bedforms where movement has been detected (black triangles) and where no movement has been detected (white triangles) overlaid on Mars Orbiter Laser Altimeter topography. TARs are not included.

Bedform albedo and dust coverage. For both active and inactive bedforms, and for TARs, mean DN values were determined over small areas of representative dune surfaces with low surface slopes using HiRISE RED (570-830 nm) images. The mean DN was translated into the radiance factor (*I/F*; *I/F* = (DN * Scaling Factor) + Offset), and divided by the cosine of the solar incidence angle [17]. Images were also assessed as to the dust content of the atmosphere at the time of acquisition and outliers (i.e. offset values >0.9) were eliminated. Figure 2 shows the average albedo

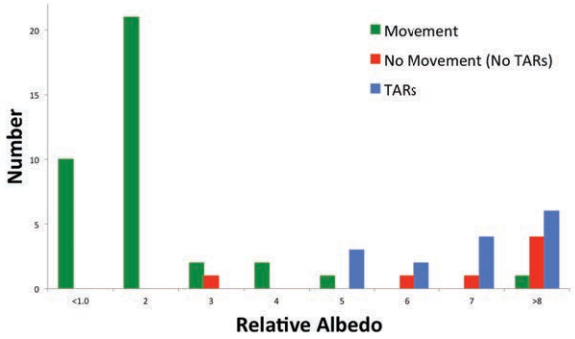

Figure 2. Average albedo signatures for different dune fields relative to the average albedo for the dunes in Nili Patera.

signature for different dune fields relative to the that of the well documented active bedforms in Nili Patera [e.g. 5]. Initial results indicate that active bedforms generally have low albedos, or dark and presumably fresh surfaces. In contrast, bedforms with no detectable movement (including TARs) generally have higher albedos. These relatively bright surfaces may be the

result of a number of processes that cause an initial mobile bedform to become immobile, such as anchoring by a coarse creep grain population or a decline in wind intensity, that then allows dust to accumulate, resulting in further stabilization [e.g., 1, 9].

Surrounding surface slopes: Average kilometer-scale surface slopes of the dune fields and immediately surrounding surfaces were calculated from profiles derived from the MOLA global base map in JMARS. Slopes associated with both active and inactive bedforms ranged from ~0.05-6°, with ~80% of the slopes ≤1°. Thus local surface slopes do not generally appear to differ for active versus inactive bedforms and likely do not play an significant role in influencing bedform mobility (with the exception of the steep slopes and high elevations in the far northern latitudes associated katabatic winds)

Dune fields located in impact craters. Roughly 70% of the dune fields located within craters exhibit detectable movement, the same percentage obtained for the dune locations analyzed outside of craters (excluding locations between 70-90° N latitude). Thus while craters serve as excellent traps for sediments, the topography associated with craters (tens of kilometers in diameter or larger) does not appear to be crucial for creating conditions conducive to bedform mobilization. However, for the craters investigated so far, a general trend is emerging in the location of active dune fields versus inactive dune fields on the crater floor. Using dune slipface orientations to derive paleowind directions, roughly 75% of inactive dune fields are centrally located or located within the upwind portion of crater floors. In contrast, 80% of the active dune fields are located in the downwind half of the crater floors, often right at the downwind crater wall (consistent with observations discussed in [18]). The significance and implications of this initial trend is unclear but may be related to the age of the dune field or maturity or duration of development.

Elevation. An estimated elevation of the dune field and immediate surrounding area was obtained from the label file for the associated HiRISE image pair (Fig. 3 and 4). The majority of the bedforms located at low elevations (-1 km and lower) are active, while the majority of bedforms at high elevations (3 km and higher) appear to be inactive. At the highest elevations in this data set (≥4 km), no observations of bedforms showed evidence of movement (Fig. 3). Higher rates of migration are also more commonly observed at lower elevations and may suggest that bedforms at higher elevations are simply migrating so slowly we are not yet able to observe the movement (Fig. 4). The slightly higher atmospheric pressure associated with lower elevations may enable bedforms to move more frequently in the denser atmosphere; threshold friction speed is inversely proportional to the square root of atmospheric density [1,8,19-21]. In the same way, the general difference in elevation of the northern lowlands/global dichotomy and the southern highlands may contribute to the greater number of active bedform detections in the northern hemisphere.

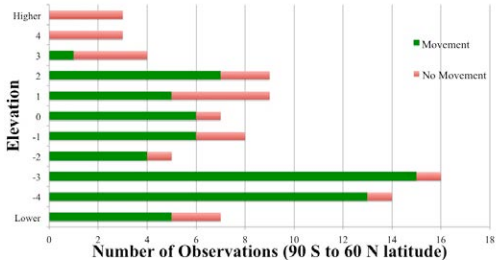

Figure 3: Number of observations per kilometer of elevation, (expressed as kilometers above the 6 mbar datum) showing movement (green) and no detectable movement (red).

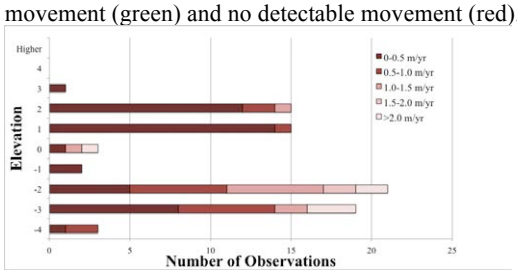

Figure 4: Distribution of rates of migration (in meters/Earth year) by elevation.

Acknowledgments: This research is supported by NASA MDAP Grant NNX14AO96G.

References: [1] Greeley R. and Iverson J. D. (1985) *Wind as a Geologic Process*, *Cambridge University Press*, 333pp. [2] Zimbelman, J. R. (2000) *GRL*, doi:10.1029/ 1999GL008399. [3] Malin, M. C., and Edgett, K. S. (2001), *JGR*, doi:10.1029/2000JE001455. [4] Bourke, M. C. et al. (2008), *Geomorph*, 94, 247-255. [5] Silvestro S. et al., (2010), *GRL*, *37*, doi:10.1029/2010GL044743. [6] Silvestro S. et al. (2011), *GRL*, *38*, doi:10.1029/ 2011GL048955. [7] Hansen, C. J. et al. (2011), *Science*, *331*, 575–578. [8] Bridges, N. T. (2012), *Geology*, *40*, 31–34. [9] Bridges, N. T., et al (2013), *Aeolian Research*, *9*, 133–151. [10] Chojnacki et al. (2011) JGR, doi:10.1029/2010JE003675, 2011 [11] Chojnacki M. et al. (2015) *This Conference*. [12] Banks et al. (2014) *LPSC*, #2857. [13] Sullivan, R. et al. (2005), *Nature*, *435*, 58–61. [14] Horgan, B. H. N. and Bell, J. F. (2012), *GRL*, *39*, doi:10.1029/ 2012GL051329. [15] Ewing, R. C. et al. (2010), *JGR*, *115*, doi:10.1029/2009JE003526. [16] Fenton, L. K. and Hayward, R. K. (2009), *Geomorphology*, *121*, 98–121. [17] Delamere, W. A. et al. (2010), *Icarus 205*, 38–52, doi:10.1016/j.icarus.2009.03.012. [18] Hayward, R. et al. (2007), *JGR*, doi:10.1029/2007JE002943 [19] Lorenz et al. (2014), *Icarus*, *230*, 77-80. [20] Chojnacki et al. (2014), *Icarus*, *230*, 96-142. [21] Hess, S. L. et al. (1980), *GRL*, *7*, 197–200.

Global Connectivity and Transport within Titan's Sand Sea

Jason W. Barnes, Department of Physics, University of Idaho, Moscow, Idaho, USA (jwbarnes@uidaho.edu)

Meta-Abstract Haiku

Global sand river,
dunes like a Möbius strip:
Xanadu, the twist.

Figure 1: Kuiseb River stopping the dunes, as seen from the air. Here we show that the longitudinal dunes of the Namib Sand Sea (visible as red-orange near the horizon to the south) do not continue past the Kuiseb river despite sand transport in the south-to-north direction. The dark material is vegetation that lives in the channel bottom even though the river flows only a few tens of days per year on average. The nearfield desert north of the riverbed is devoid of sand cover. The Gobabeb Desert Research Station is visible at the right, near the river.

Abstract

I propose that Titan's extensive equatorial dune fields represent a single interconnected sand sea. Individual sand seas such as Belet and Shangri-La all have connections to their west, from which they import sediment, and to their east, to which they export sediment. Titan's sand may therefore represent an ancient, continuous conveyor belt flowing from west to east. The only break in the chain is the continent-sized badlands of Xanadu in the middle of the leading hemisphere. To bypass Xanadu, dune sands may form fast-moving sub-pixel barchan chains to the north, eventually arriving in northern Fensal near Menrva. The sharp boundary between Shangri-La's dunes and Xanadu at the south end may be due to fluvial activity. Mountains can detain or divert dunes, but have difficulty stopping them unless their height is comparable to that of the atmospheric boundary layer. Liquid rivers, on the other hand, can stop dunes cold by transporting their sediment downstream. I will show the rationale behind my suggestions and then explore the consequences of this idea for global sediment sources and sinks. Such an integrated global system also implies that Titan's sand seas are geologically old and that its present atmospheric regime is not of recent construction.

2

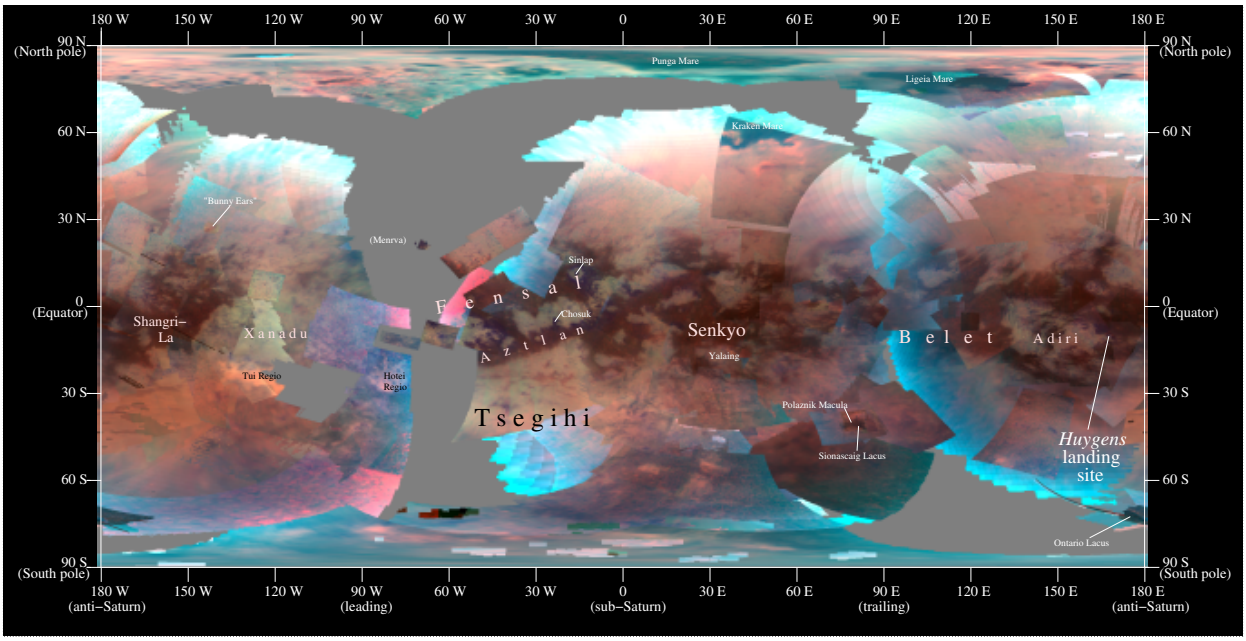

Figure 2: Global VIMS color mosaic of Titan. We used an empirical atmospheric correction for Titan's atmospheric windows at 1.08 μm, 1.28 μm, 1.6 μm, 2 μm, and 2.8 μm, and a single-scattering atmospheric model for 5 μm. The map uses the best views of each area, but we remove pixels with incidence, emission, or phase angles above $80°$. Those removed pixels are grey in the map. The correction works best at longer wavelengths; hence some residual haze becomes prominent in blue given our color mapping of R=5 μm, G=2 μm, B=1.28 μm. The bright pink areas represent overcorrections of the 5-μmwindow and are thus artifacts.

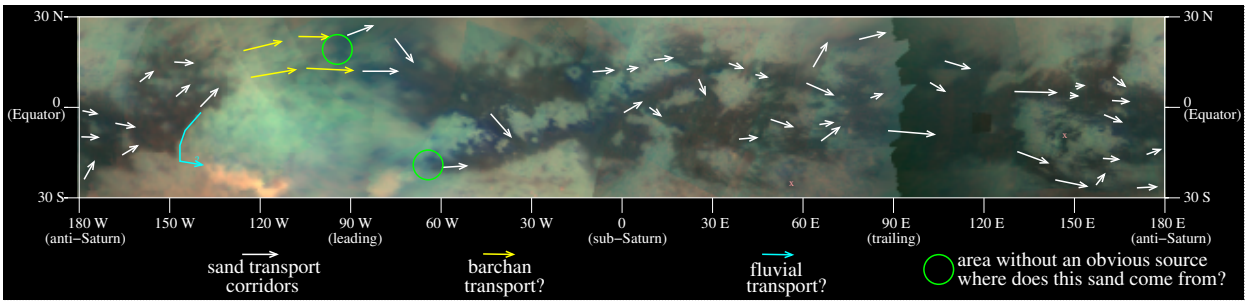

Figure 3: Notional sand transport map with VIMS R=5 μm, G=2 μm, B=1.3 μm of Titan's equatorial region in cylindrical projection. The annotations on the map show that each major sand sea or dune field has sand corridors from the west from which new sand can arrive and sand corridors to the east for it to exit. Two possible exceptions are indicated as pink 'x's: small dunefields within Adiri and some east of Yalaing Terra. The major obstacle to global sand transport then is Xanadu, for which we propose two possible mechanisms for the sand to bridge the gap (see text), fast-moving barchan dunes and fluvial sediment transport in river channels. These particular sand transport corridors are hypothetical, though consistent with both topography and observed sand transport directions .

Correlating Albedo with Dune Movement on Mars K. A. Bennett[1], L. Fenton[2], and J. F. Bell III[1], [1]School of Earth and Space Exploration, Arizona State University, Tempe, AZ, [2]Carl Sagan Center at the SETI Institute. (primary contact: Kristen.A.Bennett@asu.edu)

Introduction: Aeolian activity is the primary geologic agent currently influencing the surface of Mars. Now that high resolution cameras have been orbiting Mars for decades, evidence of aeolian activity in the form of mobile dunes has been identified [1-4]. As it is not possible to take multiple high resolution images over many years at every dune field on Mars, we propose a method to estimate dune activity by calculating changes in dune field albedos.

Background: The hypothesis that albedo could correlate to dune movement has been previously proposed. Edgett [5] hypothesized that transverse aeolian ridges (TARs) had higher albedo than other dune fields because the TARs were less active. This is because in active dunes, grains of a certain size will saltate. Once these particles impact the surface, they will hit any dust that has settled on the top of the dune and cause the dust to be suspended. Any dust that settles on top of sand dunes will be removed more efficiently by dunes with higher activity. [6,7]

Chojnacki *et al*. [8] observed variations in albedo with time at the dune fields in Meridiani Planum. They attributed this to deposition and removal of dust.

In a study using THEMIS-VIS color images at Gale crater, Bennett *et al*. [9] showed that dune fields within the crater have different colors. We hypothesize that these color differences are due to the different levels of dust cover on each dune. This in turn, can be used to infer how active each dune field is.

Methods: We selected several dune fields with various levels of activity that had been previously identified [1-4]. We obtained Mars Odyssey Thermal Emission Imaging System, Visible Imaging Subsystem [10; THEMIS-VIS] images and MRO Context Camera [11; CTX] images taken over each dune field. We converted both datasets to Lambert albedo values and conservatively estimated the error at 4% for THEMIS VIS and 20% for CTX [10,12]. We investigated how the albedo at each site changed with time and how the albedo of fast moving dunes compared to the albedo of slower moving dunes. In three out of four cases (Nili Patera, Gale crater, and Ganges Chasma), we analyzed pixels from the exact dunes used in each earlier study that identified the dunes were mobile. At the fourth site (Becquerel) we took an average of several dunes.

In this study, we assume that all dunes on Mars have a similar composition and the albedo of dust-free dunes are the same. While this is not always the case, most dunes exhibit low albedos and are dominated by pyroxene [13] so to first order this assumption is valid.

Results: Figure 1 shows how the CTX albedo of dunes varies with time at two of our sites (Gale crater and Nili Patera). At the Gale crater dunes, the albedo varies roughly from 0.12 to 0.2. In Nili Patera, it varies roughly from 0.1 to 0.15. In general, the highest albedos for each site occurred after 180° solar longitude. There was no CTX coverage of the Becquerel or Ganges dunes after Ls 180°.

Figure 2a shows the CTX albedo of each site plotted against the measured rate of movement of the dune ripples. Figure 2b shows the THEMIS VIS albedo of three sites plotted against the measured rate of movement of the dune ripples.

Discussion: Large-scale Martian dust storms occur after Ls 180° [14], which explains why the albedos of dunes increase after Ls 180°. During dust storms, dust is deposited on top of dunes. Afterwards, as sand particles continue to saltate, the dunes "clean" themselves of dust.

THEMIS-VIS has less coverage than CTX. The limited data points available with THEMIS-VIS show that the Band 4 (749 nm) albedo inversely correlates with dune movement. This preliminary study suggests that THEMIS-VIS albedo may potentially be used to estimate dune activity.

CTX albedo is less straightforward to interpret. Since there are no images after Ls 180° at two of the sites, we should only compare data at Ls < 180°. There does not appear to be a simple inverse relationship between albedo and dune movement. The minimum albedo at three locations was roughly 0.1.

One possible issue with these data is that at Becquerel we were not able to obtain the albedo from the exact dunes that had been previously determined to be moving at 0.33 m/Earth year [1]. It is possible that the dunes we used in this study were moving at a different rate. If this is the case, we should not consider the Becquerel dunes in this study. In the future, we will include more sites and have better statistics which will enable us to reevaluate whether to include Becquerel.

Excluding Becquerel, Figure 2a shows that the slower moving dunes at Gale (0.66 m/ Earth year) [3] have a higher albedo than the faster moving dunes in Ganges Chasma (2.9 m/Earth year) [4] and Nili Patera (9.1 m/Earth year) [2]. However, the relationship does not appear linear. Instead, it is possible that there is a rate where dunes will "clean" off all the dust before the next year's dust storms and the albedo will reach a minimum value that represents a dust-free dune. In this scenario, if the minimum albedo is roughly 0.1, then it

meets a minimum threshold of activity required to completely "clean" the dune before the next dust season.

Future Work: We plan to extend this work to additional dune fields and visible datasets such as HRSC and HiRISE. Each visible dataset is at a slightly different wavelength and band width. By looking at dunes in each dataset, we can determine which dataset is the most useful in detecting albedo variations at dune fields. We can also compare in-situ data from each rover to our orbital observations. MER-A, MER-B, and MSL all have observed dunes. We can use MARCI data (though at coarser spatial resolution) to tie variations in albedo with time for larger dune fields to individual dust events. Finally, we will compare these results to wind models at our study sites to test whether the albedo of dunes can be used as a first order estimate of the local wind regime.

References:

[1] Bridges, N. T. *et al.* (2012) *Geology*, 40, 31-34. [2] Silvestro, S. *et al.* (2010) *JGR*, 37. [3] Silvestro, S. *et al.* (2013) *Geology*, 41, 483-486. [4] Fenton, L. K. *et al.* (2014) *Icarus*. 230. 47-63. [5] Edgett, K. (1997) *Icarus*, 130, 96-114. [6] Bagnold, R. A. (1941) Methuen, London. [7] McEwan, I. K. *et al.* (1992) *Sedimentology*. 39, 6. [8] Chojnacki M. *et al.* (2014) *Icarus*. [9] Bennett, K. A. *et al.* (2014) *8th Int. Mars Conf.*, #1029. [10] McConnochie, T. *et al.* (2006) *JGR*, 111, E6. [11] Malin, M. C. *et al.* (2007) *JGR*, 112, E5. [12] Bell, J. F. III *et al.* (2013) *Mars*, 8, 1-14. [13] Tirsch, D. *et al.* (2011) *JGR*, 116, E3. [14] Wang, H. and M. I. Richardson (2013) *Icarus*.

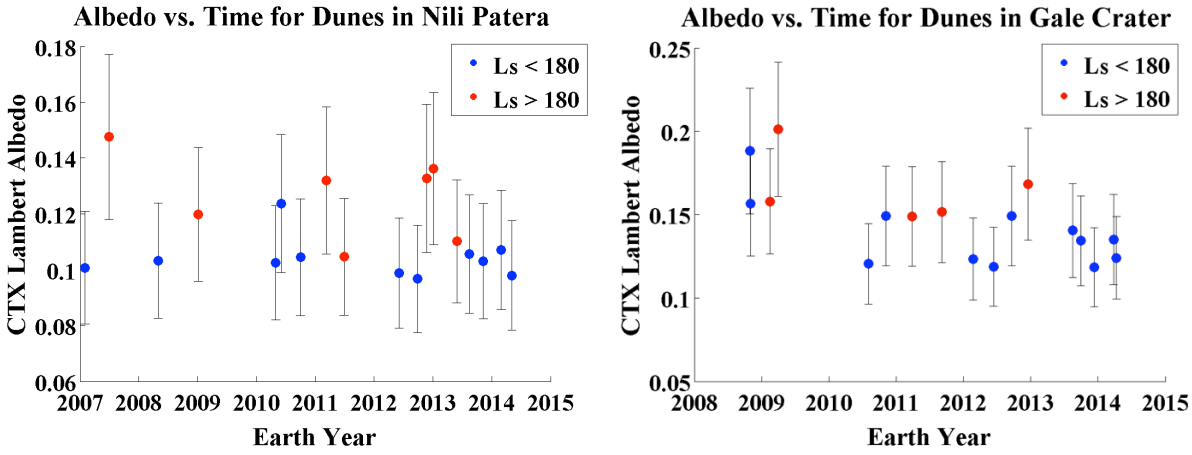

Figure 1: This figure shows how the CTX albedo of dunes varies with time at (left) Nili Patera and (right) Gale crater. We use a conservative error estimate of 20% [12]. In general, the highest albedos at each site occur during Ls > 180° when large dust storms are most common.

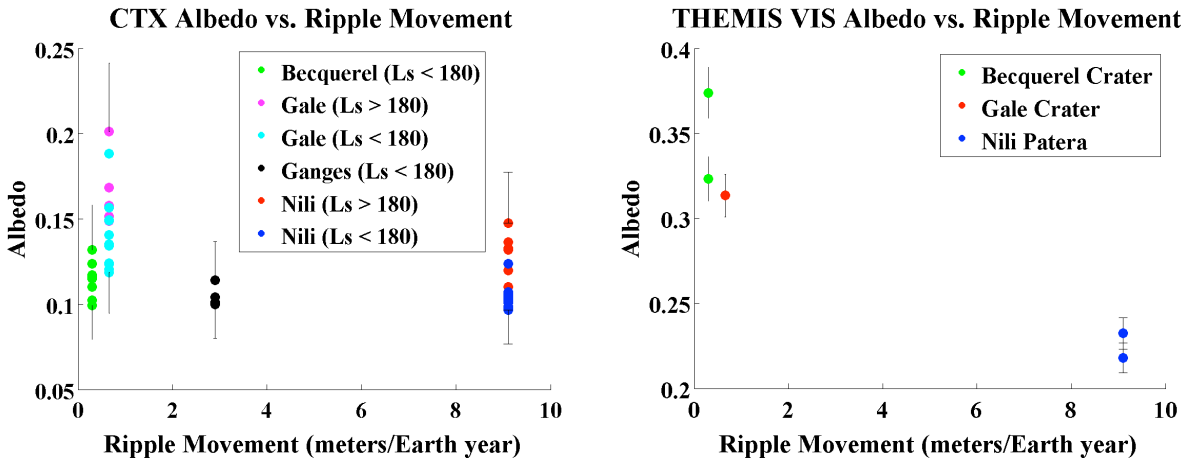

Figure 2: a) (left) The CTX albedo of each dune field plotted against the measured ripple movement. There were no CTX images taken at Ls > 180° for the Becquerel and Ganges dune fields. Error bars of 20% are included only for the minimum and maximum albedos at each site. b) (right) The THEMIS-VIS albedo of three of the dune fields plotted against the measured ripple movement. We use an error estimate of 4% [10]. There was one image that covered the Ganges Chasma dunes, but there was an instrument artifact over the dunes of interest.

GEOGRAPHIC POSITION OF DUNES RELATIVE TO THE BELET SAND SEA MARGINS AND CORRELATION WITH DUNE WIDTH AND SPACING. B. Bishop[1], J. Radebaugh[1], E. H Christiansen[1], R.C. Lewis[1]. [1]Brigham Young University, Department of Geological Sciences, Provo, UT 84602, *b.radleybish87@gmail.com*.

Introduction: Eolian dune fields found within Titan's equatorial region between ±30° latitude cover approximately 15-17% of the moon's surface [1]. These dominantly linear dunes are similar in form, size, and radar reflectivity to the large dunes of the Namib, Saharan, Saudi Arabian, and Australian deserts [2, 3]. Earth analog studies indicate that the presence of linear dunes suggests adequate sediment supply, sufficient wind, and minimal sediment loss through transport or trapping by liquids [2, 4, 5]. Analysis of parameters such as dune width and spacing has revealed important aspects of dune-forming processes, regional conditions and relative ages for Earth [7], Mars [13] and Titan [8]. These studies may also help us better understand the interplay between the surface and atmosphere, and to ultimately discover potential sediment sources and further constrain global transport pathways [7, 13, 8].

Within Titan's dune fields, initial studies of dune parameters utilizing a broad, global approach have shown that greater dune width tends to correlate with low latitudes [3, 8]. The relationship between dune width/spacing with sediment supply and distance from sand sea margins, however, is not as well understood on Titan [9]. In this study, we discuss results from new width and spacing data gathered from Cassini's Synthetic Aperture Radar (SAR), and implications of the geomorphological variation throughout one of Titan's major sand seas, Belet.

To help constrain the nature of Titan's sediment transport, we analyzed results from previous studies on dune width and spacing from Earth analogs, in particular the Namib and Australian deserts. In the Namib Sand Sea, the greatest dune width, and additionally sediment accumulation, is located near the center [10]. The same is true for the linear dunefields of the Strzelecki and Tirari Deserts of Australia [11]. Common to both these analogs is greater sediment volume towards the middle of the sand seas, which is also postulated for Titan, based on an increase in SAR-dark, and therefore sandy, interdunes in the sand sea centers [12]. Detailed analyses of width and spacing across the sand seas will help us determine the relationship between Titan's sand seas and the Earth analogues.

Approach: Our current study focuses on the Belet Sand Sea located on Titan's trailing hemisphere between -30° and 25° latitude, and 65° and 150° W longitude. [3] and [12] describe Belet as the largest sand sea on Titan with an estimated area of 3.3 + 0.6 million km^2 and a sand volume of 610,000-1,270,000 km^3, double the size of the Arabian sand seas on Earth. The dune forms in Belet appear to be tightly spaced, exceptionally straight and long and with SAR-dark, sand-rich interdunes in the center of the sand sea [5, 2, 3]. We analyzed the relationship between approximately 2,470 measurements of dune width and spacing with their associated distance from the sand sea margins [8] (Fig. 1).

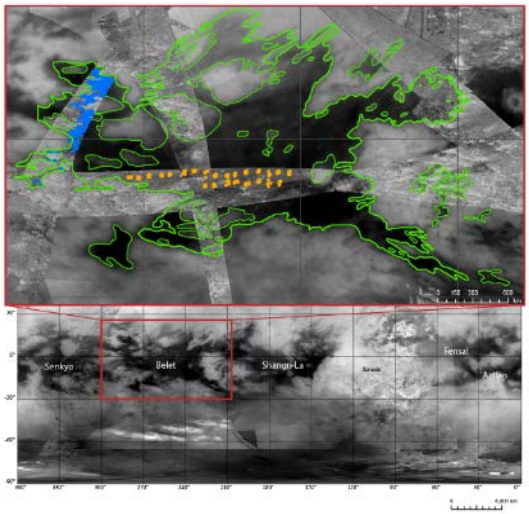

Fig. 1 Dune width and spacing locations shown on Cassini SAR swath relative to the maximum extent of the Belet dune field. *Blue points were measured from swath T21, 12 Dec, 2006 [8]. Orange points measured from swath T08 28 Oct, 2005[9].*

Sand Sea boundaries were previously mapped by defining a correlation of dune covered regions in SAR to near-infrared images from the Cassini Imaging Science Subsystem (ISS) [12]. Dune width and spacing measurements were obtained in discrete locations across Belet, 90 km^2 each in area (Orange markers in Fig. 1) [8]. The average width/spacing values associated with these areas were then compared to the distance measured from the nearest none-dune material, which in some cases included relatively small, bright obstacles scattered within the defined sand sea [8, 9]. That study revealed a slight correlation between dune width and the distance to obstacles and/or the sand sea margin [9].

We continued to investigate the relationship between dune width and spacing with the distance to the sand sea margin through increasing the sample size and

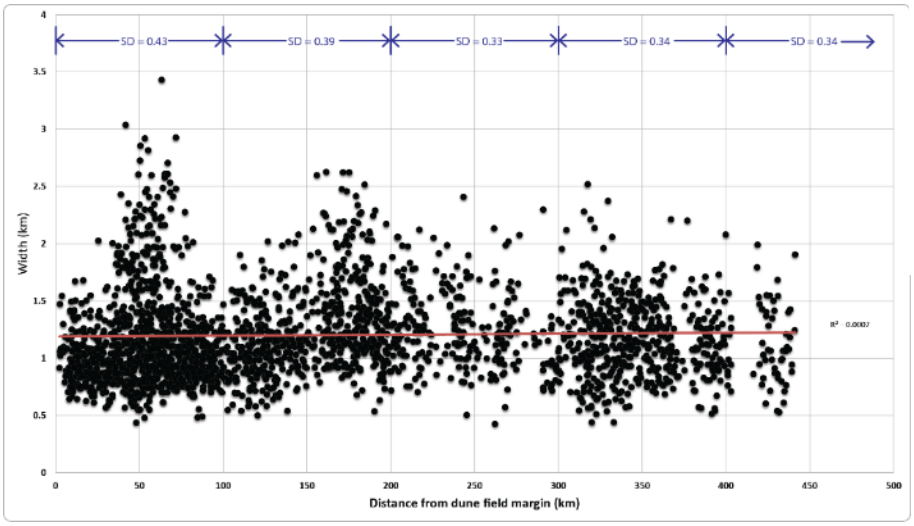

Fig.2 Graph shows high variability of dune width throughout Belet. Width variability tends to decrease with increasing distance from Belet's sand sea margins. Standard deviations are shown in blue for 100 km distance intervals.

redefining the sand sea boundaries to account for size variations of obstacles. Instead of using the average width and spacing values for the 90 km^2 areas, we incorporated all the measurements in our analyses. Using the near analysis proximity tool in ESRI's ArcMap 10.1, we calculated the shortest path to the sand sea margin from the locations of width/spacing measurements.

Results and Discussion: Dune width verses the distance to the nearest sand sea margin is shown in Fig. 2. This shows that dunes of all widths can be found at all distances from the margins. Separating the width data into distinct groups at 100 km intervals from the sand sea margin showed a decreasing standard deviation with increasing distance from the margin. One explanation for this is that as distance from the margin increases, the variability of input parameters for dune formation likely decreases, whereas the longer-term morphological stability of dunes increases. The distribution of all recorded width data in Fig. 3. The average width is comparable to widths of linear dunes

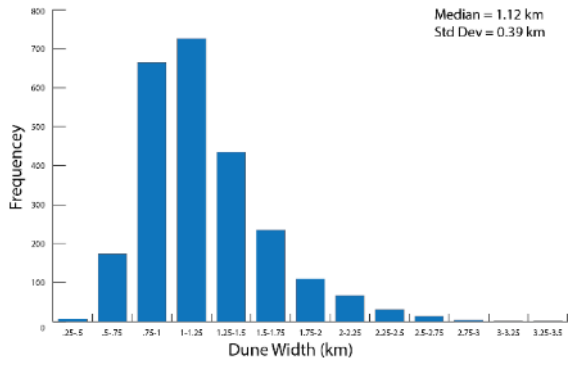

Fig. 3 Positively skewed histogram shows dune width frequencies across Belet's sand sea (n= 2,470). Average dune width is 1.2 km, the median is 1.1 km, and the standard deviation is 0.4 km.

on Earth [8]. We are currently considering how dune forms are affected by their position and distance relative to obstacles within the sand sea. These obstacles will likely have a greater impact, compared to the smaller ones, on sediment supply, wind variation and velocity, and the adjacent basin topography. The different dune morphologies within Earth's dune fields represent particular interactions between the surface and the atmosphere.

Conclusions: While the correlation between dune width and spacing with latitude has been demonstrated [3, 8], we have yet to see a strong correlation of dune width with distance from the sand sea margin. We have shown that measuring the distance from the nearest edge of obstacles found within the dune field yields only a weak relationship to dune width and spacing [8]. Likewise, there appears to be a faint correlation, if any, when the interior obstacles are removed and distances are measured from the outermost edge of the sand sea. We will continue to investigate these obstacles and their relationship to dune patterns and sediment transport pathways. Ultimately, we seek to describe with confidence the interplay of atmospheric processes with Titan's surface.

References: [1] Rodriguez et al., (2014) *Icarus 230*, 168-179. [2] Lorenz, R.D. et al., (2006) *Science 312*,724-727. [3] Le Gall, A. et al., (2011) *Icarus 213*, 608-624. [4] Radebaugh, J. (2013) *Aeolian Res 11*, 23-41. [5] Radebaugh J. et al., (2008) *Icarus 194*, 690-703. [6] Kok, J.F. et al., (2012) *Rep. Prog. Phys. 75*, 106901. [7] Ewing, R.C., et al., (2006) *Earth Surface Processes and Landforms 31*, 1176-1191. [8] Savage, C.J. et al., (2014) *Icarus 230*, 180-190. [9] Williams and Radebaugh, J. (2014) *DPS Abstracts.* [10] Lancaster, N. (1989) *A.A. Balkema Rotterdam Brookfield.* [11] Fitzsimmons (2007) *Geomorph 91*, 146-160. [12] Arnold K. 2014 *MS Thesis, BYU.* [13] Ewing and Kocurek (2010) *Geomorph* 175-187. [14] Lancaster (1995) *Routledge.*

INVESTIGATION OF THE BAGNOLD DUNES BY THE CURIOSITY ROVER: PLANS FOR THE FIRST STUDY OF AN ACTIVE DUNE FIELD ON ANOTHER PLANET

N.T Bridges[1], B.L. Ehlmann[2,3], P. Conrad[4], R. Ewing[5], F. Ayoub[2], M. Day[6], M. de la Torre[3], M. Fisk[7], A. Fraeman[2], C. Hardgrove[8], K.E. Herkenhoff[9], J. Johnson[1], M. Lapotre[2], K. Lewis[10], G. Kocurek[6], S. Le Mouélic[11], J. Martin-Torres[12], C. Newman[13], H. Newsom[14], D. Rubin[15], R. Sullivan[16], and M-P. Zorzano[17]; [1]Johns Hopkins University Applied Physics Laboratory, Laurel, MD 20723 (nathan.bridges@jhuapl.edu); [2]Jet Propulsion Laboratory, Pasadena, CA 91109; [3]California Institute of Technology, Pasadena, CA 91125; [4]Goddard Space Flight Center, Greenbelt, MD 20771; [5]Texas A&M Univ., College Station, TX 77843; [6]Univ. Texas, Austin, TX 78712; [7]Oregon State Univ., Corvallis, OR 97331; [8]Arizona State Univ., Tempe, AZ 85287; [9]U.S. Geological Survey, Flagstaff, AZ 86011; [10]Johns Hopkins Univ., Baltimore, MD 21218; [11]Université de Nantes, 44035 Nantes Cedex 1, France; [12]CSIC-UGR, Granada, Spain; [13]Ashima Research, Pasadena, CA 91106; [14]U.N.M., Albuquerque, NM 87131; [15]U.C. Santa Cruz, Santa Cruz, CA 95064; [16]Cornell Univ., Ithaca, NY 14853; [17]INTA-CSIC, Madrid, Spain

Introduction: For much of Mars' history the dominant geomorphic processes have been due to wind, with resultant effects on landscape modification through burial, exhumation, and abrasion. Initial orbital studies showed that bedforms ranging in scale from enigmatic "transverse aeolian ridges" (TARs) to dunes were common on the surface, although the level of activity could not be gauged due to limitations in image resolution and temporal observation baselines. Hints of dune dynamics from the Mars Orbiter Camera [1-3] and Mars Exploration Rover (MER) surface observations [4-6] were confirmed with increasingly sophisticated data and studies using the High Resolution Imaging Science Experiment (HiRISE) [7-10]. These results showed that many dark dunes and ripples on the planet were active, with displacements and sand fluxes comparable to those on Earth [10]. Surface investigations from the MERs and later the Mars Science Laboratory (MSL) Curiosity rover have investigated, in situ, ripples, sand shadows, and megaripples/TARs, but an active dune field on Mars (or any planetary body besides Earth) has never been studied up close despite the fact that sandstones make up a significant component of the Martian stratigraphic record [11,12]

Of the seven sites so far visited by landed spacecraft, the MSL traverse region in Gale Crater is the only location where large, active dunes are accessible for in situ investigation. HiRISE time series images show that this dune field is in an active state of migration, with dune migration rates of 0.4 m per Earth year [13]. Although not a primary goal of the MSL mission, the planned traverse path passes through the informally-named Bagnold Dunes, offering a unique opportunity, for the first time, to investigate an extraterrestrial active dune field. Here we describe plans for the campaign, which is expected to provide important information on Martian sedimentary processes, dune mineralogy/chemistry, aeolian transport rates, sandstone genesis/stratigraphy, and possibly even habitability.

The MSL payload is well suited for studying active dunes. The rover mast cameras, Navcam [14], Mastcam [15], and the ChemCam remote microimager (RMI) [16,17] provide images of varying coverage and spatial scale. The Mars Hand Lens Imager (MAHLI), located on the rover arm, can achieve a pixel scale of 14.5 μm at a working distance of 22 mm [18]. The Rover Environmental Monitoring Station (REMS) measures wind speed and direction, pressure, relative humidity (RH), air temperature, ground temperature, and ultraviolet radiation, with 1 Hz sampling for ~5 min every hour and extended hour-long observations typically several times per sol [19]. ChemCam LIBS (laser-induced breakdown spectroscopy) remotely measures major and many minor elements within a spot size less than 0.5 mm [16,20]. The Alpha Particle X-ray Spectrometer (APXS) provides in situ elemental abundance for $Z \geq 11$ (Na) in a ~1.7 cm diameter spot size [21]. The Dynamic Albedo of Neutrons (DAN) instrument detects hydrogen beneath the surface to depths of ~60 cm [22]. The rover Sample Acquisition, Processing, and Handling (SA/SPaH) system uses a scoop and rotary-percussion drill to acquire soil and rock samples, which can be sieved to size fractions of <150 μm and < 1 mm [23]. The samples can then be delivered to the CheMin [24] and Sample Analysis at Mars (SAM) [25] instruments for detailed mineralogical and elemental/isotopic measurements, respectively. In addition, the rover wheels can "scuff" soils and sand, revealing sub-surface structure in the exposed walls.

Science Goals and Objectives: The MSL Bagnold dune campaign addresses four broad science goals: 1) Understanding current Martian dune processes and rates, including differences between dunes and other bedforms, 2) deciphering dune processes, rates, and geochemical pathways in the past (e.g., consider Bagnold as an unaltered Mt. Sharp [Aeolus Mons] sandstone protolith), 3) determining dune material provenance, and 4) assessing the dunes as traps for interplanetary dust particles (IDPs) and water. These goals are met by achieving the following objectives:

1. *Determine dune mineralogy and chemistry* (ChemCam, APXS, CheMin, SAM) (Goals 1, 2, 3, 4) a. Measure mineralogy and chemistry as a function of location on the dunes and dune ripples, both on the surface and in the interior. b. Relate mineralogy/chemistry to dune dynamics, infrared spectral and photometric properties, and development of sedimentary structures.

2. *Determine grain size and sorting as a function of mineralogy, and contributions of atmospheric dust* (ChemCam, MAHLI, AXS, CheMin, SAM) (G1,2,3) a. See how grain chemical, mineralogical, and physical properties vary as a function of location on dunes and

dune ripples, both on the surface and in the interior. b. Relate the level of activity to grain properties and dust content. c. Relate to spectral/photometric properties which can then serve as a calibration for remotely sensed data elsewhere on Mars

3. *Determine modern aeolian transport rates* (Mastcam, ChemCam RMI, REMS) (G1, 2) a. Measure movement of dune slip faces and ripples at a range of spatial scales and temporal baselines, with simultaneous wind measurements. b. Measure size of dune ripples to calibrate contributions to sand flux. c. Measure saltation fluid and impact threshold speeds and provide better estimates of reptation and saltation fluxes on Mars.

4. *Determine dune stratification and structure* (G1,2) (Mastcam, ChemCam RMI, MAHLI) a. Measure size, shape, and volumes of wind ripple, grain fall, grain flow, and interdune deposits. b. Look at stratification and structure within dune and dune ripple scuffs.

5. *Determine if dunes trap IDPs and sequester water* (G4) (DAN, REMS HS, SAM) a. Use DAN to measure hydrogen and thereby infer the presence of water at depth, and SAM to measure H_2O and other volatiles released in sampled materials. b. Have REMS measure surface and atmospheric temperature, pressure, and relative humidity with extended hours at night to determine if there are changes in the local water volume mixing ratio over dunes. c. Use SAM to search for the presence of organic matter, either within mafic grains [e.g., 26] or as IDPs by characterizing the amount and type of reduced carbon as well as its mineral/chemical associations.

Planned Campaign: The exact path that MSL will take to approach and then sample the Bagnold Dunes has not yet been decided, although notional traverses have been proposed. The dunes that could be investigated are barchan-barchanoid to longitudinal in morphology. The distance over which the rover may drive on the dunes is also uncertain; short drives along the stoss or near the lateral edges may be possible but there is risk of getting stuck in the sand.

With these caveats in mind, the overall plan is to investigate at least two dune locations, each being distinct in the level of aeolian activity as determined from HiRISE data and infrared spectral properties determined from CRISM. Prior to reaching the dunes, MSL will image the same locations at similar times of day to document any changes. As the rover closes in, increasingly finer scale changes, such as ripple migration at shorter temporal baselines, are expected. During the approach, the plan is to "calibrate" REMS wind speed measurements by orienting the rover in 120° increments for a full sol each to sample the wind field with the one working wind sensor.

Each dune stop is expected to last at least 6-7 sols, with the following planned activities (described in very generalized form here, without contingencies, and with recognition that early measurements may inform upon and change subsequent plans and rover operational constraints and consumables must be considered):

Sols 0-1: 1) Approach dune, 2) Mastcam and ChemCam remote sensing, 3) MAHLI goniometer and Mastcam multiple time of day sequences for photometric characterization, 4) short drive on to dune with DAN in active mode to detect possible sub-surface hydrogen, 5) scuff edge of dune, with Mastcam imaging

Sols 2-4: 1) Scoop and deliver <150 μm fraction to SAM, 2) Mastcam and ChemCam remote sensing of scuff, 3) MAHLI and APXS on dune surface and scuff, 4) SAM EGA/TLS/GCMS analysis, 4) deliver sample to CheMin, 5) Dump sieved and sieved-rejected materials, followed by remote sensing of piles, 6) CheMin overnight analysis, 7) MAHLI and APXS on dump piles, 8) CheMin overnight and SAM preconditioning.

Sols 5-6: 1) Scoop and process < 1mm portion and deliver to SAM (there may be a possibility of segregating to a 150 μm – 1 mm size, but this must be tested), 2) SAM EGA/TLS/GCMS, 3) Dump sieved and sieved-rejected materials, followed by remote sensing of piles, 4) CheMin overnight.

Sol 7+: Drive to next dune location

Expected Outcome: At the conclusion of the Bagnold Dune campaign we will have investigated, in situ and for the first time, an active dune field on Mars. We expect to significantly expand our understanding of current and past aeolian processes, sand provenance, and other questions that, until now, have been addressed solely from remote orbital observations, models, or partial analogs. This campaign should result in significant advancements in Martian and aeolian science.

References

[1] Malin, M.C. and K.S. Edgett (2001), *JGR, 106*, doi:10.1029/2000JE001455. [2] Fenton, L.K. (2006), *GRL, 33*, doi: 10.1029/2006GL027133. [3] Bourke et al. (2008), *Geomorph., 94*, doi: 10.1016/j.geomorph.2007.05.012. [4] Geissler, P.E. et al., *JGR,* doi: 10.1029/2008JE003102. [5] Sullivan, R. et al. (2008), *JGR, 113*, doi: 10.1029/2008JE003101. [6] Geissler, P.E. et al (2010), *JGR, 115*, doi: 10.1029/2008JE003102. [7] Silvestro, S. et al. (2010), *GRL, 37*, L20203. [8] Chojnacki, M. et al. (2011), *JGR, 116*, E00F19. [9] Hansen, C.J. et al. (2011), *Science, 331*, 575-578. [10] Bridges, N.T. et al. (2012), *Nature*, doi: 10.1038/nature11022. [11] Grotzinger, J. et al. (2011), *The Sed. Record, 9*, doi: 10.2110/sedred.2011.2 [12] Milliken, R.E. et al. (2014) *GRL, 41-4*, 1149-1154. [13] Silvestro, S. et al. (2013), *Geology,* doi: 10.1130/G34162.1. [14] Maki, J. et al. (2011), *Space Sci. Rev., 170*, 77-93. [15] Malin, M.C. et al. (2010), *Lun. Planet. Sci., XLI*, 1123. [16] Maurice, S. et al. (2012), *Space Sci. Rev., 170*, doi:10.1007/s11214-012-9912-2. [17] Le Mouélic, S. et al. (2015), *Icarus, 249*, 108-128. [18] Edgett, K.S. et al. (2009), *Lunar Planet. Sci., XL*, 1197. [19] Gomez-Elvira, J. et al. (2011), *4th Internat. Wkshp. Mars. Atm.* [20] Wiens, R.C. et al. (2012), *Space Sci. Rev.,, 170*, 167-227. [21] Schimdt, M.E. et al. (2014), *JGR, 119,* doi: 10.1002/2013JE004481. [22] Mitrofanov, I.G. et al. (2012), *Space Sci. Rev., 170*, 559-582. [23] Anderson, R.C. et al. (2012), *Space Sci. Rev., 170*, 55-75. [24] Zimmerman, W. et al. (2013), *IEEE Aerospace Conf.* [25] Mahaffy, P.R. et al. (2012), *Space Sci. Rev., 170*, 401-478. [26] Steele A et al. (2012), *Science*, *337*, 212.

MINERAL ABUNDANCE ESTIMATES AND DISTRIBUTION DERIVED FROM MARS DUNE FIELD #2938-497. H. R. Charles[1] and T. N. Titus[2], [1]Northern Arizona University, Flagstaff, AZ 86001 (hc383@nau.edu), [2]U.S.G.S. Astrogeology Science Center, 2255 N. Gemini Dr., Flagstaff, AZ 86001.

Introduction: The surface of Mars is a dynamic and evolving environment where aeolian processes play an influential role. Dunes are one of the most common aeolian features on Mars. The processes which form dune fields are indicators of interactions between the atmosphere and the surface, and are related to both climatic and sedimentary mechanisms [1]. While less than the volume of terrestrial sand, the Mars Global Digital Dune Database (MGD[3]) estimates the total volume of sand in dune fields included in the database between 65 and -65 N latitude to be from 3618.54 to 15169.16 km^3 [1]. As ubiquitous features found over many different types of topographical regions, understanding the mineral composition of dune fields is important to studying planetary processes [1].

Dune field composition is dependent on a number of factors, including the parent material mineralogy, grain size selection due to wind speed, and the different minerals' reaction and resistance to mechanical and chemical weathering [2]. These variables can potentially cause a non-uniform distribution of minerals within the dune field. Terrestrial analogs, such as the dunes in Grand Falls, AZ [3] exhibit visible segregration of minerals. It is known that Mars' crust is primarily mafic [e.g. 4] which weathers into basaltic sand. On Earth basaltic grains are considered compositionally immature as they are more susceptible to chemical weathering [5]. However, due to significantly slower chemical weathering on Mars than on Earth, basaltic minerals, such as olivine, are being considered as possible sediment maturity indices [5]. Refining our techniques for analyzing mineral composition and studying possible trends in the distribution of various minerals within a dune field will allow us to better understand the geological history of Mars.

Background: A previous study by Ahrens et al. [6] selected a dune field identified as 2938-497 in the MGD[3] [1], which is in Mars' southern hemisphere on the far western edge of Argyre Planitia. The mineral composition of the dune field was analyzed using thermal emissivity data from the Thermal Emissivity Spectrometer (TES) aboard the Mars Global Surveyor (MGS) [7]. This dune field was considered a good candidate for analysis because the available dataset contained multiple and overlapping orbital tracks. The proximity of the tracks to each other over two regions of the dune field allowed for the examination of trends in mineral abundances from west to east.

In the Ahrens study [6], it was noted that feldspar was either not present or had a non-uniform distribution across the dune field. The goal of this analysis was to determine the presence or absence of feldspar, examine its distribution if present, and identify any trends in other minerals present in the dune field.

Methods: For this study, we used the TES layer in the Java Mission-planning and Analysis for Remote Sensing (JMARS) [8] to obtain the emissivity data. The data was restricted to orbital tracks 1583 to 7000. The 1583 represents the beginning of the mapping phase for TES [7]. Above 7000, a noise anomaly of unknown origin (most likely related to spacecraft vibration) begins to appear [9]. Within this sampling of the TES dataset, eight orbits crossed the interior of dune field 2938-497. From west to east, these were orbits 3615, 5514, 4030, 5187, 3703, 5602, 5929, and 5275. Only TES observations within the boundaries of the dune field were selected from each orbital track.

We used the Davinci programming environment developed by Arizona State University (ASU) [10] to spectrally deconvolve the emissivity data. The spectral mixing analysis (SMA) function was first used to separate the atmospheric component (caused by airborne dust and aerosols) from the surface spectra. The SMA function was used a second time to determine the mineral abundances from the surface spectra alone. We used the spectral library developed by Deanne Rogers in a previous study of Mars sediments [11]. This is the same spectral library used in the Ahrens study [6], consisting of 44 minerals from 8 mineral groups (Table 1). Spectral deconvolution was conducted using two versons of the library, one that included the feldspar mineral group and one without.

Table 1: The mineral groups and spectral endmembers from the mineral library [11].

MINERAL GROUP	ENDMEMBER	MINERAL GROUP	ENDMEMBER
Feldspar	Microcline	Sulfate	Anhydrate
	Albite		Gypsum
	Oligoclase		Kieserite
	Andesine	Carbonate	Calcite
	Labradorite		Dolomite
	Bytownite	Olivine	Forsterite
	Anorthite		Fayalite
	Shocked Anorthite (6 types)		KI (4 types)
High-Phase Silica	Illite	Quartz	Quartz
	Montmorillonite	Hematite	Martian Hematite
	Saponite	Pyroxene	Bronzite
	Na-Montmorillonite		Enstatite
	K-rich glass		Hypersthene
	SiO_2 glass		Lindsley Pigeonite
	Opal A		Diopside
	Aluminous Opal		Augite (2 types
	Heulandite		Hedenbergite
	Stilbite		

Results: Of the eight mineral groups, only four (pyroxene, sulfate, feldspar, and silica) appeared in abundances of over 5%. The results for the other four (carbonate, hematite, quartz, and olivine) with one exception were below the detection limit [12].

Olivine has been identified as having a low minimum detection limit on Mars and can be detected at abundances of 5% and possibly lower, whereas most minerals have a minimum detection limit of 5-10% [12]. In half the orbital tracks removing feldspar increased olivine to as much as 7% mineral abundance.

Removing feldspar caused slight changes in the abundances for pyroxene, sulfate, and silica, but all variations were less than the estimated uncertainties. Carbonate, olivine, and hematite all saw increases when feldspar was excluded. Even with the increase, the carbonates and hematite remained under 5% abundance.

When graphed as a function of longitude, the trend in abundances for pyroxene and sulfate appeared to be loosely correlated (both with and without feldspar). There also appeared to be a correlation between the trends for feldspar and silica, which in turn were inversely related to pyroxene and sulfate [Figure 1].

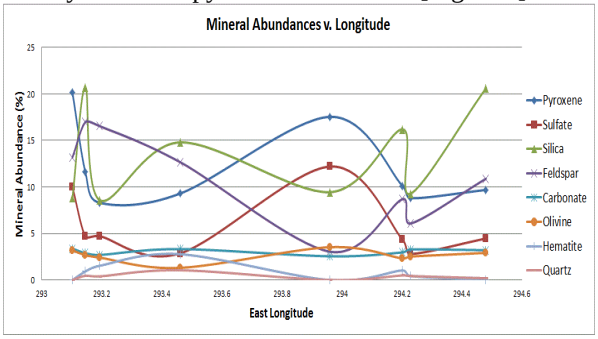

Figure 1: Mineral abundances for the eight mineral groups across the dune field. Figure 2 contains error bars for feldspar, which are representative of the error for the other seven.

Feldspar was examined in greater detail as the Ahrens study indicated that it might not be present. Figure 2 shows feldspar abundances graphed as a function of longitude. With error, feldspar could be uniform in the western half of the dune field, but in the east central section the abundance drops to a level arguably below the minimum detection limit [12] and below the error bars in the west. Further east, the abundance rises to just above the detection limit.

Conclusion: Feldspar abundances are above the minimum detection limit over most of the dune field but the abundance does drop below the detection limit in the east central portion of the dune field. Analyses in both the Ahrens study and this one show a significantly high variance in feldspar abundances between orbits. However removing feldspar from the spectral library worsens the variance, increases the RMS values, and increases abundances in minerals originally falling below minimum detection limits. Feldspar appears to be present and a non-uniform distribution may be causing the variance. Pyroxene, sulfate, and silica all appear to follow similar trends in abundance and may also be non-uniformly distributed.

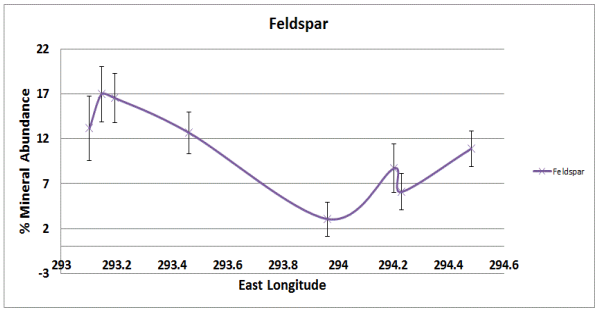

Figure 2: Feldspar abundances as a function of longitude.

Future Study: To better understand the nature of this dune field's composition THEMIS and CRISM data are being examined and will be discussed. The mineral composition results from these instruments will be compared to the TES mineral abundances.

Acknowledgements: We would like to thank R. Hayward for her knowledge of this dune field and assistance with Davinci coding. We would also like to thank C. Edwards for his help in troubleshooting Davinci and with understanding THEMIS and CRISM data. We would also like to thank L. Kestay for his insightful comments that greatly improved this abstract.

References: [1] Hayward, R. K. et al., 2007, *JGR*, **112**, E11007. [2] Titus, T. N. et al., 2014, 8th Internat. Conf. on Mars, #1091. [3] Hayward, R. K. et al., 2014, 8th Internat. Conf. on Mars, #1009. [4] Toulmin, P., III, et al., 1977, *JGR*, **82**, 4625 [5] Cornwall, C. & Schreiber, C., 2014, 8th Internat. Conf. on Mars, #1011. [6] Ahrens, C. A. & Titus, T. N., 2014, 8th Internat. Conf. on Mars, #1012 [7] Christensen, P. R., et al., 2001, *JGR*, **106**, 23,823. [8] JMARS, Ariz. St. Univ., <http://jmars.asu.edu/>. [9] Bandfield, J. L., 2002, *JGR*, **107**, JE001510. [10] Davinci, Ariz. St. Univ., <http://davinci.asu.edu>. [11] Rogers, A.D., and Fergason, R.L., 2011, *JGR*, **116**, EO8005. [12] Koeppen, W.C. & Hamilton, V.E., 2008, *JGR*, **113**, E05001.

Methane storms as a driver of Titan's dune orientation.

B. Charnay[1,2]. E. Barth[3], S. Rafki[3], C. Narteau[4], S. Lebonnois[2], S. Rodriguez[5], S. Courrech du Pont[6], and A. Lucas[5]

[1]Virtual Planetary Laboratory, University of Washington, Seattle, USA (benjamin.charnay@lmd.jussieu.fr), [2]Laboratoire de Météorologie Dynamique, UPMC, Paris, France, [3]Southwest Research Institute, Boulder, USA, [4]Institu de Physique du Globe de Paris, Université Paris-Diderot, Paris, France, [5]Laboratoire AIM, Université Paris 7, Gif/Yvette, France, [6]Laboratoire Matièreet Systèems Complexes, Université Paris Diderot, Paris, France

Titan's equatorial regions are covered by eastward oriented linear dunes. This direction is opposite to mean surface winds simulated by Global Climate Models (GCMs) at these latitudes, oriented westward as trade winds on Earth [1, 2].

Here, we propose that Titan's dune orientation is actually determined by equinoctial tropical methane storms producing a coupling with superrotation and dune formation [3].

Using meso-scale simulations of convective methane clouds [4] with a GCM wind profile featuring the superrotation [5, 6], we show that Titan's storms should produce fast eastward gust fronts above the surface (see Figure 1). Such gusts dominate the aeolian transport. Using GCM wind calculations and analogies with terrestrial dune fields [7], we show that Titan's dune propagation occurs eastward under these conditions (see Figure 2).

Finally, this scenario combining global circulation winds and methane storms can explain other major features of Titan's dunes as the divergence from the equator or the dune size and spacing. It also implies an equatorial origin of Titan's dune sand and a possible occurence of dust storms.

References: :[1] Lorenz et al. (2006), *Science,* 312, 724-727. [2] Lorenz & Radebaugh (2009), *Geophysical Research Letter,* 36, 3202. [3] Charnay et al. (2015), *Nature Geoscience* (in press). [4] Barth & Rafkin. (2007), *Geophysical Research Letter,* 34, 3203. [5] Charnay & Lebonnois (2012), *Nature Geoscience,* 5, 106–109. [6] Lebonnois et al. (2012), *Icarus,* 205, 719–721. [7] Courrech du Pont, Narteau & Gao (2014), *Geology,* 42, 743–746.

Figures:

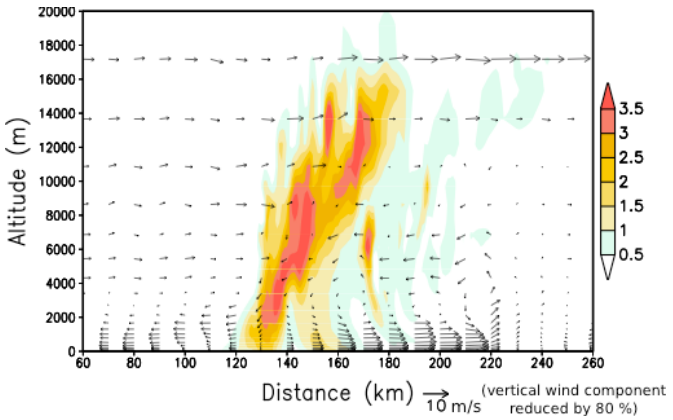

Figure 1: 2D simulation of a methane storm developping under the wind shear produced by the supperotation. Colors correspond to the mixing ratio of condensed methane and vectors to wind direction and speed. A gust front appears in front of the storm and propagates eastward.

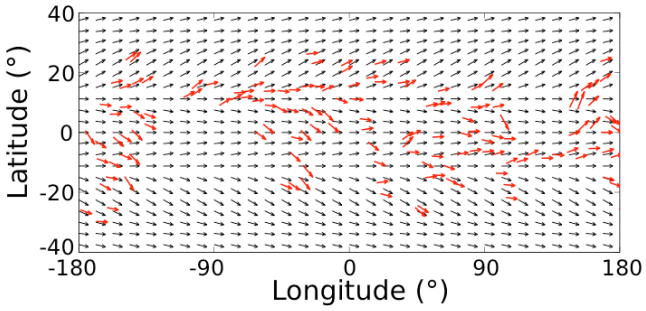

Figure 2: Map of dune orientation observed with Cassini's Radar (red vectors) and predicted by the GCM including the effect of storms (black vectors)

WIDESPREAD DUNE MIGRATION IN MERIDIANI PLANUM, MARS. M. Chojnacki[1], T. I. Michaels[2], L. K. Fenton[2], and M. E. Banks[3]. [1]Lunar and Planetary Lab, U.A., Tucson, AZ (chojan1@pirl.lpl.arizona.edu), [2]Carl Sagan Center at the SETI Institute, Mountain View, CA, [3]Planetary Science Institute, Tucson, AZ.

Introduction and Motivation: It is now known unambiguously that wind-driven bedform activity is occurring at scattered sites across Mars today [for a review see 1]. However, many of these reports are only based on a few sets of observations separated by 1–2 Mars-year-intervals, yielding preliminary but incomplete information. Moreover, volumetric sand fluxes, which are independent of dune size, have only been documented for a few sites.

The Noachian-aged Meridiani Planum-Arabia Terra region is host to abundant intracrater low-albedo dark and light streaks, sand patches, and dune fields [for a review see 2]. All of these landforms are present in the vicinity of the Opportunity rover, now located on the edge of Endeavour crater. Bedforms within Endeavour crater have produced ample evidence for intracrater aeolian change [3, 4], but may not be representative for the region.

Here we investigate and quantify dune activity across central Meridiani. Related questions include: What are the regional variations of aeolian bedform transport rates, migration directions, and volumetric sediment fluxes? Similarly, are there substantial spatial differences in dune construction times (or turnover times) and do those point to variations in climate?

Data Sets and Methods: To estimate dune migration rates, bedform displacements were measured using repeat fine-scale (25 cm/pix) images from the High Resolution Imaging Science Experiment (HiRISE) [5]. Dune heights (for sediment flux estimates) can be obtained using a slip face length height technique [6] and equation (1):

$$H = L_s \times \mathrm{Tan}\theta, \quad (1)$$

where L_s is the measured adjacent slip face length, θ is the assumed angle of repose, yielding dune relief (H). A slip face angle of 33° was used, as this value is a common average value for terrestrial [7] and martian [8] dunes. In addition, Endeavour crater possesses one HiRISE Digital Terrain Model (DTM) (at 1 m post spacing) constructed from a stereo pair [4]. Slip face height measurements were within ~8% of those measured with DTMs in one trial (typically +/-1 m).

Results: Thirteen dune field sites were examined with repeat HiRISE observations separated by one-half to three Mars years. Sites were classified into three categories: confirmed bedform migration (6), bedform change (4), and no detection (3) (Fig. 1). Locations with migrating dunes include, Endeavour, east Firsoff, and several unnamed craters. At some sites clear changes had occurred but bulk dune migration was ambiguous, showed evidence for ripple movement, bedform deflation, or dune border modification (e.g., Xainza crater). The remaining sites showed no detectable changes.

Meridiani barchan, barchanoid, and dome dunes were detected translating 1–6 meters between images, resulting in migration rates of 0.1–5 m/Earth-year (0.2–11 m/Mars-year) (Fig. 2; time periods are in Earth years unless explicitly stated). The observed sediment transport direction was dominantly to the south-to-southeast, consistent with a regional northwesterly wind regime. Dune crest relief ranged from one to forty meters in height.

Volumetric sand flux at the crests of dunes can be obtained from the product of the bedform height and associated migration rate [9]. This metric is useful for comparison to other planetary dune fields and can be related to erosion rates [10]. Meridiani dune fluxes ranged from 1 to 20 $m^3\ m^{-1}\ yr^{-1}$ and can span an order of magnitude for a given site (Table 1; Fig. 2). The largest crest fluxes correspond with tall but slowly-advancing barchan dunes (e.g., Fig. 3) – alternatively, large fluxes were also observed for small but extremely fast-translating dome dunes [4].

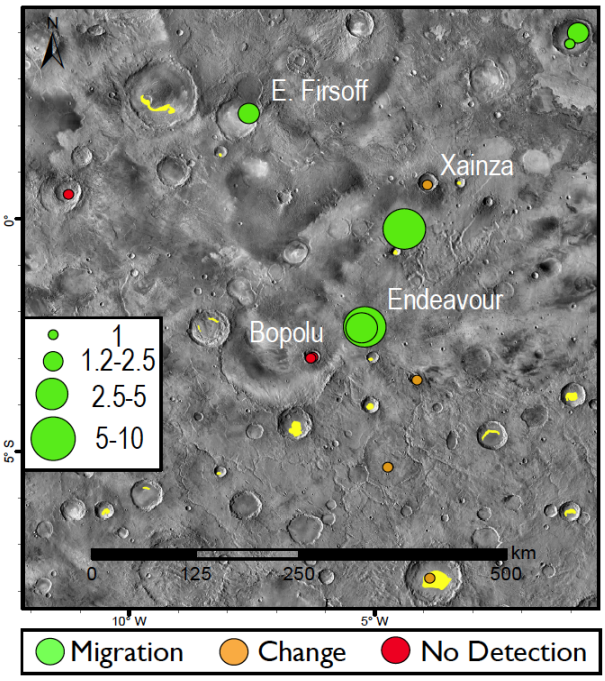

Figure 1. Meridiani dune activity classifications shown on a THEMIS day infrared mosaic. Average dune sand flux estimates of HiRISE monitored sites are provided (green circles in units of $m^3\ m^{-1}\ yr^{-1}$). Dune fields are mapped in yellow.

Table 1. Average values for migrating dune sites[a].

Dune Field ID and Coordinates[b]	Rate (m yr^{-1})	Crest Flux (m^3 m^{-1} yr^{-1})	Turnover Time (yr)
3524+023	0.3	2.3	680
3556-023	0.4	9.5	773
3590+037	0.1	1.2	1346
3592+040	0.2	1.6	668
3548-024	0.5	2.9	410
3548-023	3.7	6.8	23

[a] All time periods are in Earth years.
[b] See [12] for naming convention.

All bedforms possess a characteristic time period referred to as the turnover time, which is the period a bedform takes to travel its own stoss-to-lee length in the downwind direction [11]. Given dune migration rates and lengths along the direction of transport (50–350 m), turnover times span from 10–1500 Earth-years (5–800 Mars-years).

Discussion and Summary: The majority of dune sites in the study area with sufficient HiRISE data clearly showed aeolian activity, if not bulk bedform migration. Sites with no detections had particularly large, contiguous dark dunes (e.g., Bopolu crater), or only possessed images with a small temporal separation, making analysis difficult. Migration rates of most Meridiani dunes are near the averages from global studies (~1 m yr^{-1}) [1, 13], but several outliers exist that showed evidence for rapid sediment transport in short periods of time [4, 14]. Some of these detections are likely due to short-term diurnal and seasonal winds. Mesoscale atmospheric modeling can provide more detailed insight into such wind patterns [15].

Dune crest fluxes also showed substantial variation across the study area and per site (Fig. 2) For comparison, Nili Patera barchan dunes have reported values ranging from 1–5 m^3 m^{-1} yr^{-1} [10]. Relatively slow terrestrial dunes in Mauritania [9] and Antarctica [16] show comparable fluxes (Fig. 2); but those of active barchans on Earth are an order of magnitude higher. Nevertheless, dune sand fluxes described herein and at other locations on Mars (e.g., Herschel crater, Nili Patera [10, 14, 17]) demonstrate the potential for high rates of aeolian sediment transport and the potential for prolonged landscape modification of Mars.

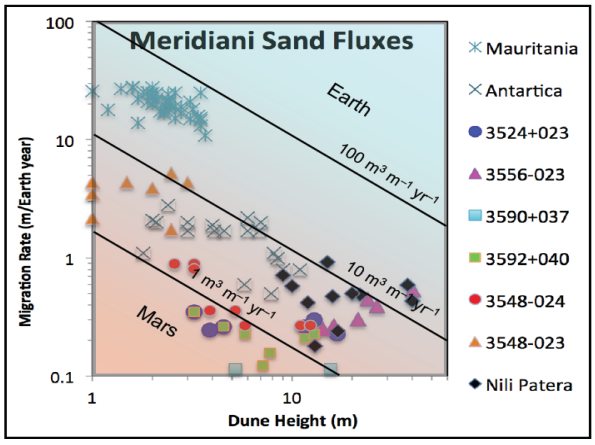

Figure 2. Log-log plot comparison of dune migration rates vs. heights for martian and terrestrial dunes. Diagonal lines are isopleths of sand flux. Other sites include: Nili Patera [10], Mauritania [9], Antarctica [19].

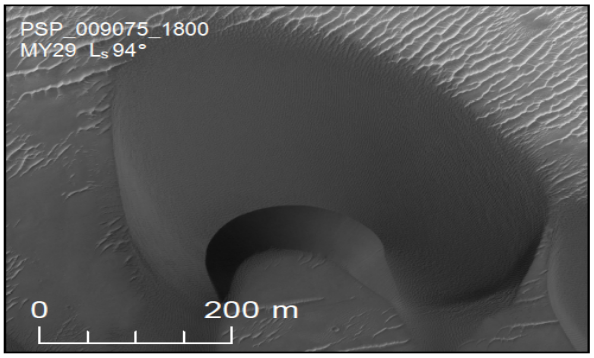

Figure 3. The largest migrating dune detected (40-m-tall), which translated 0.5 m in the 3 Mars years between images. Site 3556-023, just north of Endeavour.

The turnover time of aeolian bedforms is a measure of how long it takes to respond to major (~90°) changes in wind patterns. Estimated turnover times for the six sites with migrating dunes (Table 1) are significantly shorter than modeled martian obliquity cycles of 100,000–200,000 Earth years [18]. This result implies that it is not necessary to invoke paleoclimate wind regimes to explain morphologies of large dark dunes and demonstrates dunes here are capable of being constructed by the modern climate of Mars. This is not thought to be the case for many Meridiani aeolian features (e.g., plains ripples, transverse aeolian ridges), which, based on their morphology and superpositional relationships, appear to be relic landforms last shaped by ancient (50 ka to >>200 ka) wind regimes [2].

Acknowledgments: This research was supported in part by NASA MDAP Grant NNX13AK68G and the HiRISE/MRO mission.

References: [1] Bridges N. et al. (2013) *Aeolian Res., 9,* 133–151. [2] Fenton L. et al. (2015) *Aeolian Res., 16*, 75–99. [3] Chojnacki M. et al. (2011) *JGR Plan., 116,* E003675. [4] Chojnacki M. et al. (2015) *Icarus, in print*. [5] McEwen A. et al. (2007) *JGR Plan., 112,* E05S02. [6] Bourke M. et al. (2006) *Geomorph. 81*, 440–452. [7] Pye K. and H. Tsoar (1999) *Aeolian sand and sand dunes*, Unwin Hyman, London. [8] Atwood-Stone C. and A. McEwen (2013) *Geophys. Res. Lett., 40*, 2929–2934. [9] Ould Ahmedou D. et al. (2007) *JGR Earth Surf., 112*, F02016. [10] Bridges N. et al. (2012) *Nature*, *485*, 339–342. [11] Allen J. (1974) *Earth Sci. Reviews, 10,* 263–342. [12] Hayward R. et al. (2007) *JGR Plan., 112*, E002943. [13] Banks M. et al. (2014) *LPS XLV,* Abstract #2857. [14] Ayoub F. et al. (2014) *Nat Commun*., *5*, 10.1038/ncomms6096. [15] Michaels T. (2014) *LPS XLV,* Abstract #2897. [16] Bourke M. et al. (2009) *Geomorph*., *109*, 148–160. [17] Runyon K. et al. (2015) *LPS XLVI,* Abstract #1999. [18] Laskar J. et al. (2004) *Icarus*., *170,* 343–364.

Investigation of Martian Aeolian Dynamics Using Terrestrial Dune Analogues and Airflow Modelling. C. Cornwall[1], D. W. T. Jackson[1], and M. C. Bourke[2], and J. A. G. Cooper[1], [1]Ulster University (Cromore Road, Coleraine, BT52 1SA, United Kingdom, cornwall-c@email.ulster.ac.uk), [2]Trinity College, Dublin

Introduction: Wind measurements from lander missions, as well as mesoscale and global circulation modeling indicate that Mars' low-density atmosphere rarely exceeds the threshold speed necessary to facilitate sediment saltation [e.g. 1, 2, 3, 4, 5, 6]. However, the surface of Mars is dominated by aeolian features and recent studies involving high resolution images have shown that there are many locations on Mars where ripple and dune modification have occurred over the past few years [e.g. 4, 6, 7, 8, 9, 10, 11, 12, 13, 14] with a few of the sediment fluxes comparable to some terrestrial dunes [15]. Although these observations seem contradictory to circulation modeling, it has been suggested that aeolian modification may be due to strong localized winds generated by topographic obstacles [16], such as craters. Localized winds are complex and cannot be resolved at the resolution of mesoscale and global circulation models.

One of the leading goals in investigating aeolian processes on Mars is to explore the boundary conditions of sediment transport, accumulation, and dune morphology in relation to wind regime as well as to quantify migration rates and sediment flux [17]. This study aims to investigate complex local wind patterns on terrestrial and martian dunes that shape the morphology of aeolian deposits as well as investigate the relationship between flow patterns and slipface activity. Through this analysis, it will be possible to improve constraints and details of sediment flux on Mars including rate, timing and volume which will ultimately lead to a better understanding of sediment source material and dune migration.

Methodology: This study combines terrestrial field observations, three-dimensional computational fluid dynamics (CFD) modeling and remote sensing data from Mars to better constrain grain flow magnitudes and frequencies that occur on slipface slopes of dunes in order to improve estimates of martian dune field migration and sediment flux related to wind velocity and flow patterns.

The chosen study site for the terrestrial dune analog is located in the Maspalomas dune field in Gran Canaria, Spain. This location was chosen due to the aridity of the area, making it a reasonable analog for Martian aeolian systems. Ground-based, high-resolution laser scans collected in the field will be used to generate three-dimensional surface topography and quantify change on a slipface [Fig. 1]. These scans will also be incorporated into a computational fluid dynamics model to investigate interaction with wind velocity, flow patterns and sediment transport.

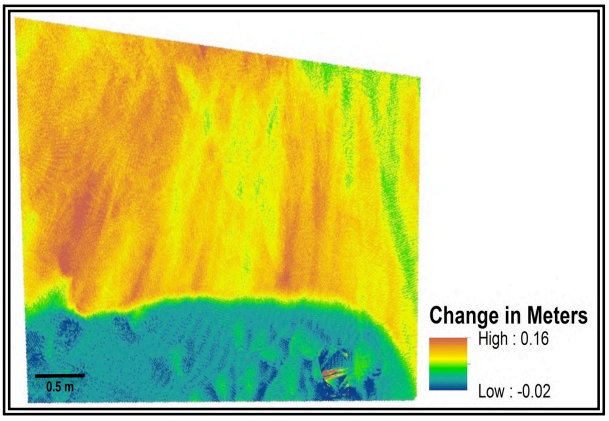

Figure 1. Difference map depicting change in meters on a dune slipface in Maspalomas dune field, Gran Canaria, Spain. This map was created by subtracting two 3D laser scans taken 55 minutes apart. The image shows horizontal dune advancement due to individual avalanche events with little change at the base of the slipface.

This technique will also provide a way to investigate potential triggers for processes on slipface slopes of dunes including, grainflows, formation of alcoves and advancement of the slipface.

Following the investigation of air flow patterns and slipface processes on Maspalomas dunes, remote sensing data of martian dunes will be collected and compared to the results of the Maspalomas dunes. Images from the High Resolution Imaging Science Experiment (HiRISE) on board the Mars Reconnaissance Orbiter (MRO) and photogrammetry will be used to create three-dimensional digital terrain surfaces. The latter will be used with the computational fluid dynamic model OpenFoam in a process similar to the three-dimensional surface topography generated by laser scans of the chosen terrestrial dunes. HiRISE provides the resolution necessary to resolve smaller scale ripples and quantify sediment flux as well as rate and timing of sediment transport of ripples and dunes in conjunction with airflow modeling [Fig. 2; 19].

The project will investigate a variety of dune morphologies on Mars, including transverse ridges, barchanoids, and domes. The chosen dunes will be located in a wide range of latitudes and environments in order to compare differences between aeolian systems. Wind patterns will be analyzed using computational fluid dynamics and surface flow vectors will be superimposed onto three-dimensional HiRISE images with a spatial resolution of 30-60 cm/pixel, which will allow for a direct comparison with local bedforms.

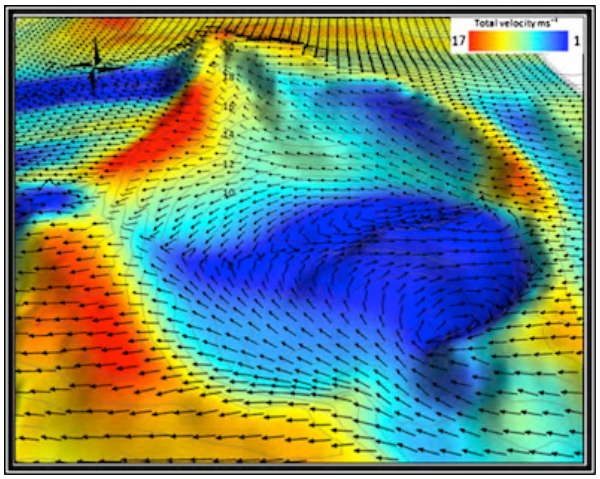

Figure 2. An example of CFD modeling results showing air flow 1 meter above the surface of a dune blow out feature, Ireland. Taken from [20].

Details of sediment flux will be estimated based on terrestrial observations and changes in dune location and evidence of slipface activity which can be identified using repeat coverage of HiRISE images taken inter annually and at various times throughout the martian year.

Significance: This study has valuable application to martian surface geology and evolution as well as terrestrial systems. The results that will be produced can be used for local circulation modeling, especially in locations where wind flow, sediment deposition and dune morphologies are complicated by small-scale topography [4]. A better understanding of the effects of small scale topography on the local wind regime as well as the timing, location and frequency of slipface processes on terrestrial dunes will be provided which will also improve estimates of sediment flux and interpretation of aeolian systems on Mars and other planetary bodies using remote sensing data. For example, many martian dune fields have smaller bedform features superimposed on their surfaces, suggesting a complex wind regime that may be composed of varied magnitude and multidirectional winds influenced by local topography and seasonal changes. In addition to studying local wind regime and slipface processes, constraining the rate, timing, and volume of sediment flux will also lead to a better understanding of the nature and location of the source material for martian dunes and can support future studies focused on recent aeolian activity on Mars including dune migration and morphological changes.

This project has significant implications for studies focused on the processes that form a variety of aeolian deposits with similar morphologies, such as Transverse Aeolian Ridges (TARs), sand ripples, gravel ripples, and mega ripples. Knowledge of localized wind flow patterns will ultimately lead to a better understanding of the conditions in which these morphologies formed and evolve today.

References:

[1] Zurek, R. W. et al. (1992) In Mars, 799-817. [2] Sullivan, R. et al. (2000) JGR, 105, 24547-62. [3] Haberle, R. M. (2003) Icarus, 161, 66-89. [4] Fenton et al. (2005) JGR, 110, doi:10.1029/2004JE002309. [5] Holstein-Rathlou, C. et al. (2010) JGR, 115, doi:10.1029/2009JE003411. [6] Chojnacki, M. et al. (2011) JGR, 116, doi: 10.1029/2010JE003675. [7] Fenton, L. K. et al. (2006) GRL, 33, L20201. [8] Greeley, R. et al. (2006) JGR, 111, E02S09. [9] Bridges, N. T. et al. (2007) GRL, GRL, 34, doi:10.1029/2007GL031445. [10] Bourke, M. C. et al. (2008) Geomorph., 94, 247-255. [11] Sullivan et al. (2008) JGR, 113, E06S07. [12] Silvestro, S. (2010a) GRL, 37, doi:10.1029/2010GL044743. [13] Silvestro, S. et al. (2010b) 2nd Int'l Dunes Workshop, abs. #2003. [14] Silvestro, S. et al. (2012) 3rd Int'l Dunes Workshop, abs. #7036. [15] Bridges, N. T. et al. (2012) Nature, 485, 339-342. [16] Fenton, L. K. and T. I. Michaels (2010) In Mars, 5, 159-171. [17] Fenton, L. K. et al. (2013) Aeolian Res., 8, 29-38. [18] Jackson, D. W. T. et al. (2013) J. Coastal Res., 65, 1301-1306. [19] Jackson, D. W. T. et al. (2012) 3rd Int'l Dunes Workshop, abs. #7018. [20] Smyth et al. (2012) Geomorphology, 177, 62-73.

Tracking Gully Activity Within the North Polar Erg, Mars. S. Diniega[1], C.J. Hansen[2], [1]Jet Propulsion Laboratory, California Institute of Technology (4800 Oak Grove, Pasadena, CA 91109; serina.diniega@jpl.nasa.gov), [2]Planetary Science Institute.

Introduction

Analyses of high-resolution observations have shown that the dunes within the Martian North Polar Erg (AKA Olympia Undae) are currently very active on seasonal and yearly timescales. Over 40% of the dunes sampled within the North Polar Erg show dune brinks that seem to erode each year with small alcoves [1] (Figure 1). Sometimes these avalanche features also contain a large, but thin, depositional fan (Figure 1) that may reflect a mechanism for dune advancement [1]. Additionally, many of these degraded brinks are then "restored" to a crisp and continuous edge. When considering these dunes in aggregate, it has been proposed that present-day conditions result in a net equilibrium between erosion and restoration processes [1], although interannual variation has been observed [2]. However, it has not yet been determined exactly which processes are reshaping these dunes, or at what rates this activity occurs.

This project seeks to conclusively distinguish between a general aeolian versus a seasonal frost process origin of the gullies observed to form annually on these dunes. An initial study found that these features formed during the spring season and proposed that sublimation activity could destabilize the dune slopes and overlying seasonal CO_2 frost [1]. A subsequent study showed that many of the "new" alcoves seen in the spring were present and visible beneath the frost [3]. Thus, they proposed that alcove formation may occur before CO_2 accumulation and is due to aeolian processes in the mid- to late-summer. A third study reinforced the evidence for seasonal frost-driven processes, but acknowledged difficulties with detecting a gully (and thus identifying when it first appears) due to effects of frost and lighting changes [2].

These three studies [1-3], along with studies of dune gullies formed in the southern hemisphere [e.g., 4-6], have shown that a clear identification of when the gully first appeared is a key factor when considering activity under current environmental conditions. This project aims to definitively determine the timing and nature of gully formation within the North Polar Erg by carefully examining seven sites, dispersed around the pole, over four Mars years. We also aim to investigate any subset(s) of gullies that appears distinct in morphology aspects or other gully characteristics, and to connect those variations to environmental conditions or process specific to a locale or season. This will greatly aid geomorphological interpretation of HiRISE images of the North Polar Erg.

This presentation

Preliminary results, examining gully formation within at least one location, will be presented. Observed trends and patterns will be discussed, especially with regards to location of the gullies on gully slopes, slope orientation, and gully size and shape (average and variation). Methodology will be also discussed, along with issues encountered. In particular, this study is complicated by the fact that during winter – when gullies are perhaps forming on these dunes – is when images are not taken within the polar region as it is too dark (Figure 2). Comments will be welcome.

Significance for dune studies

In addition to identifying the gully formation mechanism, this project also aims to measure the rate of gully formation and dune restoration. Doing so will allow estimation of the volume of sediment transport occurring through each activity. Estimates of sediment flux are valuable constraints for most studies of present-day Martian surface modification as aeolian processes play a large role in both material redistribution and erosion. Finally, consideration and measurement of the effects of both seasonal and aeolian processes on the north polar dunes will form a much more complete picture of present-day conditions and activity within this extensive region that plays an important role in the global climate. Our results will help promote a better local, regional, and global understanding of seasonal and aeolian processes active on Mars.

References: [1] Hansen et al., 2011, Seasonal erosion and restoration of Mars' northern polar dunes, *Science* **331**, 575-578. [2] Hansen et al., 2015, Agents of change on Mars' northern dunes: CO2 ice and wind, *Icarus*, in-press. [3] Horgan and Bell, 2012, Seasonally active slipface avalanches in the north polar sand sea of Mars: Evidence for a wind-related origin, *Geophys. Res. Lett.* **39**, L09201. [4] Diniega et al., 2010, Seasonality of present-day Martian dune-gully activity, *Geology* **38**, 1047–1050. [5] Dundas et al., 2012, Seasonal activity and morphological changes in Martian gullies, *Icarus* **220**, 124-143. [6] Treiman, 2008, Wind and the origin of Martian gullies: A local and regional test in Cimmeria, *Workshop on Martian Gullies: Theories and Tests*, Ab. 8020.

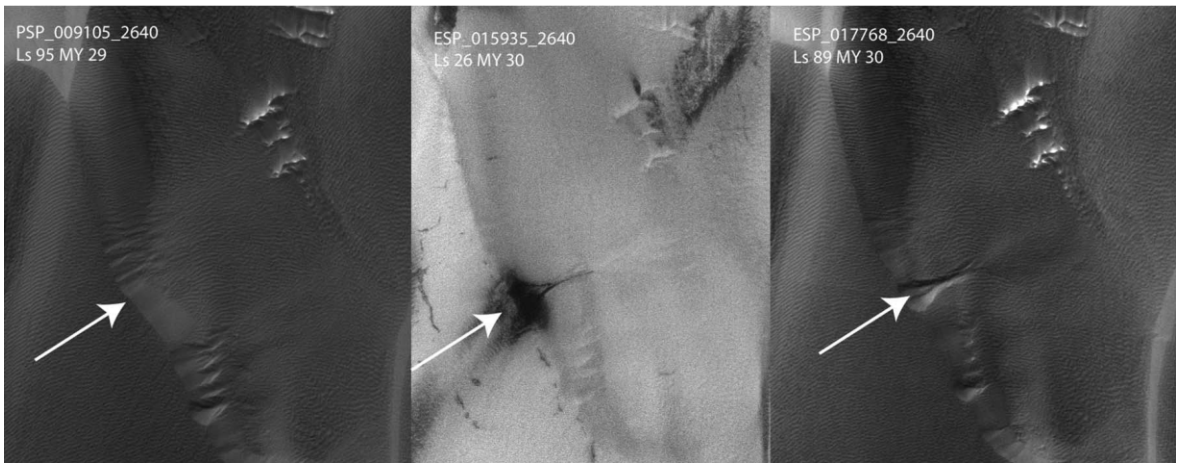

Figure 1. Alcove formation on a dune slope (at 84°N, 233°E) within the North Polar Erg. The white arrows point to a location on the brink of this dune that had no alcove in MY29 and experienced sublimation activity (middle), which resulted in the new alcove and fan (with total length of 120 m) in MY30. The layer of new material forming the apron is very thin and does not obscure pre-existing ripples. Restoration of the dune slope (or degradation of the gully) then also occurs, with alcoves being filled in on either side of the highlighted feature and new ripples forming across all surfaces. Image taken from [1].

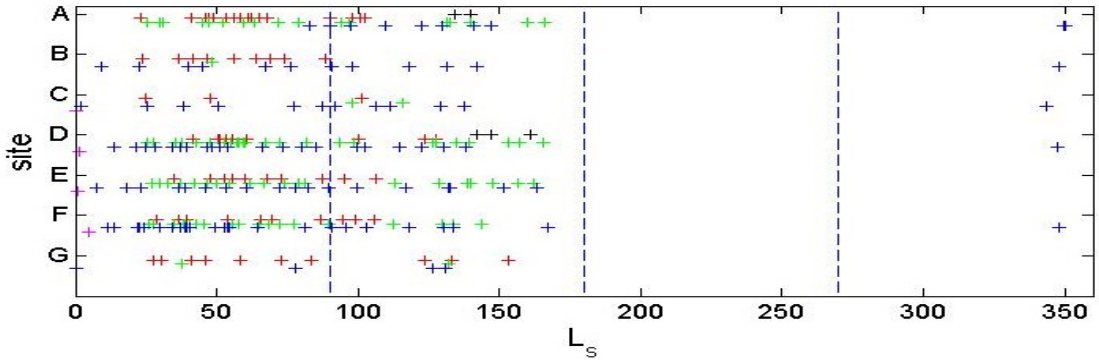

Figure 2. Plot of all publically-available images (as of Summer 2014) taken over seven sites dispersed around the pole (spanning latitudes 76-85°N and longitudes 0-334°E; locations will be shown in presentation). L_s is solar longitude – in the northern hemisphere, spring = L_s 0-90, summer = L_s 90-180, autumn = L_s 180-270, and winter = L_s 270-360. Black markers = MY28, red = MY29, green = MY30, blue = MY31, and magenta = MY32. The only non-spring or summer images were taken at the end of MY31 (A-D, F) and a few sites (C-F) have MY32 images available. [1] tracked changes within Sites A/F over MY 29-30. [2] tracked changes in Site A over MY29-30.

PARAMETERIZATION OF FINITE-ELEMENT CRYO-HYDROLOGIC SAND DUNE MODEL TO CONSTRAIN DEBRIS-FLOW-INITIATING SUBSURFACE TEMPERATURES AND PORE-WATER PRESSURES, GREAT KOBUK SAND DUNES, ALASKA. C. L. Dinwiddie (cdinwiddie@swri.org) and D. M. Hooper (dhooper@swri.org), Southwest Research Institute®, San Antonio, Texas.

Introduction: We published field observations of debris flows (**Fig. 1**) that formed in March 2010 on two sunward, southwestward-facing lee slopes of the Great Kobuk Sand Dunes, Alaska [1], on late-winter days when ambient air temperatures measured onsite were continuously subfreezing [2].

To better understand how debris flows fed by liquid water form at subfreezing air temperatures, we are undertaking meteorology-driven, cryo-hydrologic numerical modeling using a commercial geotechnical engineering finite-element code—the VADOSE/W variably saturated porous media flow module of GeoStudio 2012 by GEO-SLOPE, v.8.14.1.10087 [3]. This is a fully coupled energy and mass balance model using adaptive time-stepping, which calculates evaporation, sublimation, net infiltration, change in storage, and runoff as part of the overall water balance.

Model Domain and Grid: A 1-m^2-area, 5-m-thick 1D column model domain was constructed to extend beneath the seasonally freezing and thawing active layer of the dune sands [4]. Where large vertical gradients are expected in the very near surface, element thickness is on the order of 1-mm; generally, the mesh consists of 2.5-cm-thick elements, 256 in total. VADOSE/W "surface layers" are directly influenced by meteorology and are extended here to 4.5 m below ground level.

Material Properties: The initial model domain is constructed of GKSD sand [5], which ultimately will be variably saturated with meteoric water in both solid and liquid phases. Air–water soil moisture characteristic and hydraulic conductivity functions of volumetric water content (**Fig. 2**) were derived from grain size analysis and knowledge of typical sandy soil field capacities and saturated hydraulic conductivities. With additional funding, these properties and their variability will be directly assessed through laboratory testing of available samples. The ice–water soil moisture characteristic is calculated internally by VADOSE/W and is not included as input. The thermal conductivity function of volumetric water content was developed by scaling the low-sand function of [6] using our heat-dissipation values of oven-dried GKSD sand thermal conductivity (**Fig. 3**). The volumetric heat capacity function of water content was estimated using the method of [7], based on our dual-probe heat-pulse values of oven-dried GKSD sand volumetric heat capacity (**Fig. 3**). With additional funding, available samples will undergo thermal testing in the laboratory at variable water contents to confirm the validity of the derived functions and their variability. VADOSE/W internally accounts for the thermal properties of liquid water, water ice, and accumulated snow.

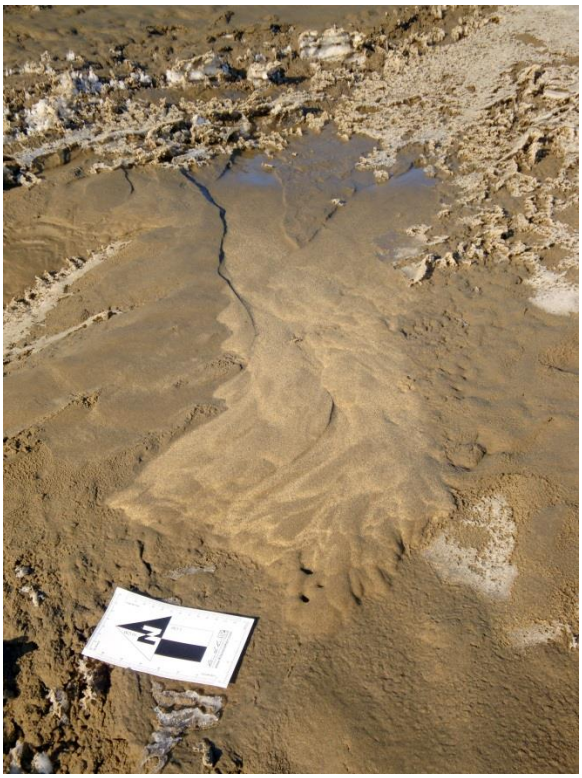

Fig. 1. GKSD debris flow, 25 March 2010. Scale is 10 cm.

Boundary Conditions: Atmospheric boundary conditions were developed based on 22+ years of Kavet Creek Remote Automated Weather Station (RAWS) data [8] and augmented with Bettles Field SNOTEL station solid precipitation data [9]. VADOSE/W ingests meteorological data records for: (i) daily maximum and minimum air temperatures; (ii) daily maximum and minimum relative humidities; (iii) daily mean wind speed, (iv) daily total precipitation; (v) optionally, it ingests daily net solar radiation; otherwise, it internally calculates daily net solar radiation based upon site latitude. The Kavet Creek RAWS data record includes only liquid precipitation, so a hybridized precipitation record (**Fig. 4**) was developed using Kavet Creek RAWS liquid precipitation [8] and appropriately scaled values of solid precipitation measured at the Bettles Field SNOTEL station [9].

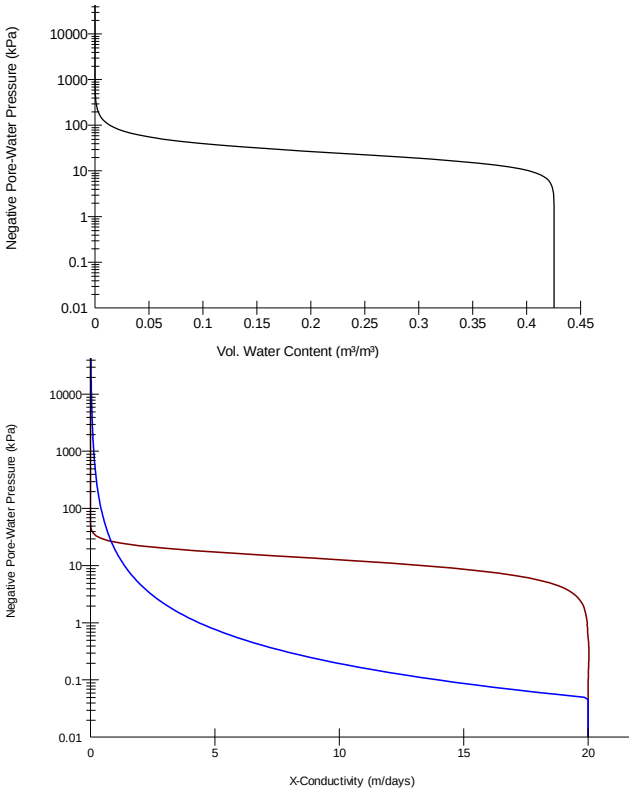

Fig. 2. GKSD sand hydraulic material properties (**black:** air–water soil moisture characteristic function; **red:** hydraulic conductivity function; **blue:** relaxed hydraulic conductivity function only used within upper 4 cm of sand to aid model convergence. Note that mean GKSD sand porosity is 42.5 percent.

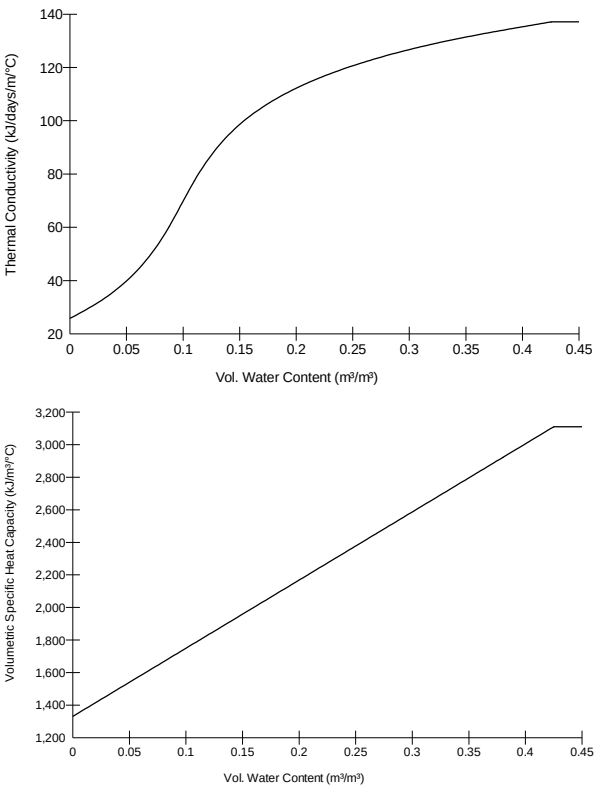

Fig. 3. GKSD sand thermal material properties.

At the base of the model, unit hydraulic gradient and constant −0.2 °C thermal boundary conditions are applied, based on geophysical interpretations of [4].

Modeling Approach: A minimum sequence of four simulations will be run, with results from the former providing initial conditions for the next:

1. Develop steady-state pore-water pressure profile given constant 0.1 mm/yr input flux at dune surface.

2. Spinup subsurface equilibrium response to variable Kobuk Valley climate (22-yr simulation).

3. Simulate cryo-hydrologic response to climate from June 1992 until March 2010 (17-yr simulation).

4. Simulate March 2010 cryo-hydrologic precursor conditions incipient to debris flow events with high temporal resolution (~1-mo simulation).

Simulation results, analyses, and interpretations will be presented at the *4th International Planetary Dunes Workshop*.

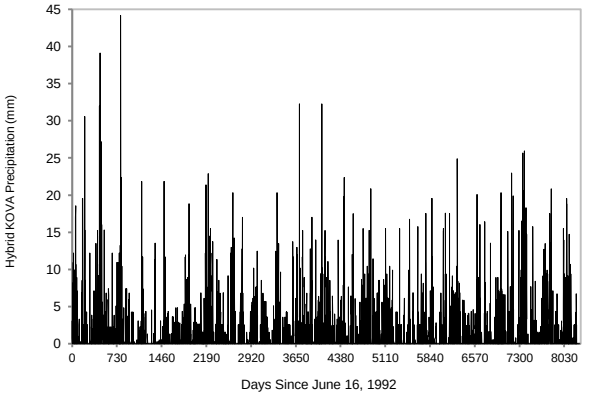

Fig. 4. Hybrid precipitation record for Kobuk Valley.

References: [1] Hooper D. M. and Dinwiddie C. L. (2013) *Icarus, 230,* 15–28. [2] Dinwiddie C. L. et al. (2012) *3rd Int'l Planet. Dunes Wkshp, LPI Contribution No. 1673,* Abstract #7034. [3] GEO-SLOPE International Ltd. (2012) *Vadose Zone Modeling with VADOSE/W: An Engineering Methodology.* Calgary, Alberta, Canada. [4] Dinwiddie C. L. (2014) *8th Int'l Conf on Mars,* Abstract #1256. [5] Dinwiddie C. L. et al. (2011) *LPS XLII,* Abstract #2501 [6] Becker B. R. et al. (1992) *Int'l Com in Heat and Mass Transfer, 19,* 59–68 [7] de Vries D. A. (1963) *Physics of Plant Environment.* Amsterdam, Netherlands: North Holland Publishing Co., 210–235. [8] Western Regional Climate Center (2015) www.raws.dri.edu/cgi-bin/rawMAIN.pl?akAKAV. [9] Natural Resources Conservation Service (2015) www.wcc.nrcs.usda.gov/nwcc/site?sitenum=1182.

DUNES CREATING AN ABRUPT INCREASE IN GYPSUM GRAIN CONCENTRATION ALONG A TRANSPORT PATHWAY AT WHITE SANDS NATIONAL MONUMENT, NM, USA. L. K. Fenton[1] , J. L. Bishop[1], S. King[2], B. Lafuente[3], [1]SETI Institute (189 Bernardo Ave., Ste. 100, Mountain View, CA, 94043, USA, lfenton@seti.org), [2]California State University, Sacramento, CA, USA, [3]University of Arizona, Tucson, AZ, USA.

Introduction: In 2005, a large quantity of the mineral gypsum was unexpectedly identified on Mars in the high latitude dune sands of Olympia Undae (Langevin et al., 2005). Because gypsum is formed in the presence of liquid water, the discovery of this extensive deposit has important implications for the climatic and sedimentary history of the currently cold and dry north polar regions of Mars. CRISM data indicate that gypsum sand grains appear to concentrate at dune crests [1-3], but the significance of this pattern is not clear.

The intent of our work is to investigate how aeolian processes distribute soft and hard sand grains (e.g., gypsum and other minerals, respectively) across active dunes. We performed a field investigation at White Sands National Monument (WSNM) in New Mexico, USA, selecting sites for their likely contamination by non-gypsum grains. Field samples from these dunes have been separated by grain size and apparent color, and mineralogical analysis has been done with the combined use of X-ray diffraction (XRD), visible and near-infrared (VNIR) spectroscopy, Raman spectroscopy, and Fourier Transform infrared (FTIR) spectroscopy. This presentation focuses on the compositional variation of coarse grains found at the study site.

Study Area: The White Sands Dune Field is located in the Tularosa Basin in New Mexico, USA. The southern portion of the dune field is contained in the WSNM (see Fig. 1a). The dune sand is derived from sediment eroded from lake beds located immediately upwind (on Alkali Flat, to the west) [4-7].

The study area is a barchanoid dune located at the western edge of the dune field, along the northern border of WSNM (see Fig. 1b). The area was chosen for a transport pathway of dolomite grains that are present, among the more plentiful gypsum grains, upwind on Alkali Flat. Samples from this area were collected along one main streamwise traverse (locations 1 through 9), the upper slip face (SF), and two coarse-grained ripples (Ripples 1 and 2).

Ripple 1 is located 224 m WSW and upwind of the study dune brink. Its component grains reflect the transport pathway that has carried dolomite, gypsum, and other minerals from Alkali Flat to the main dune field. The crest of Ripple 1 was covered in 1-4 mm grains, and the sample scoop disturbed the surface layer, producing rafts of cohesive clods.

Ripple 2 is located in a local low between two barchanoid dunes south of the study dune. These grains have traveled up a portion of the stoss face; their components may reflect transport on the dunes in addition to that along the transport pathway. The crest of Ripple 2 was covered by 1-2 mm grains, and lacked both the larger grains and the cohesion found at Ripple 1.

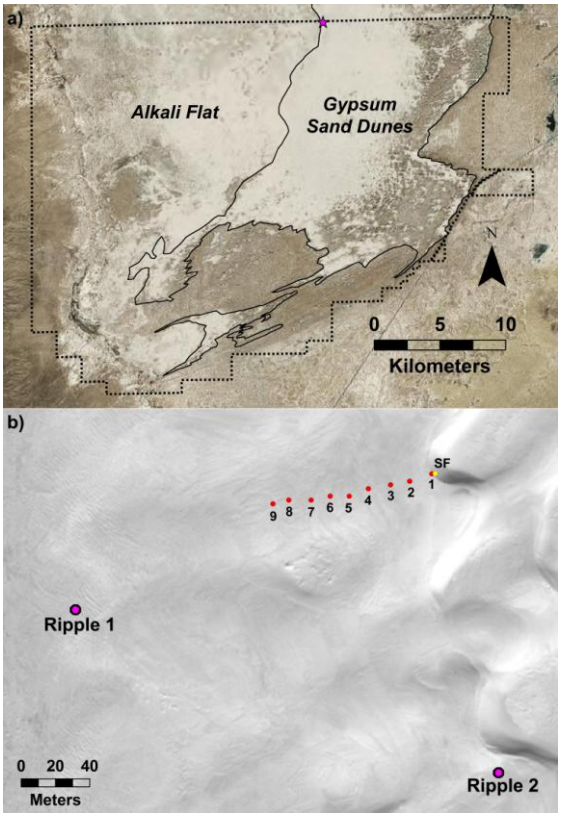

Figure 1. The study area, including a) its location inside WSNM (magenta star) and b) sampling locations. Note that Ripple 1 is upwind of the main dune field and Ripple 2 is near the crest of a dune.

VNIR, XRD, and Raman Spectroscopy: Gypsum dominated all samples at all grain sizes smaller than 1mm. However, this was not the case for coarse grains (>1 mm). Coarse grains from the crests of Ripples 1 and 2 were isolated and manually sorted by apparent color. Ripple 1 coarse grains were separated into white, beige, brown, translucent, pink, green, and dark grains. Ripple 2 coarse grains were separated into white and dark grains.

Ripple 1. Figure 2 shows VNIR spectra of seven different grain color groups found in the Ripple 1 crest. White and beige grains contained gypsum and dolomite; translucent grains contained quartz; pink grains

contained hematite, calcite, and microcline; green grains contained the clays beidellite and prehnite; and the dark grains contained a yet undetermined mafic component.

Ripple 2. In contrast, the coarse grains of Ripple 2 contained mainly white and dark fractions, which appear similar to the white and dark components of Ripple 1 (i.e., they are dominted by gypsum).

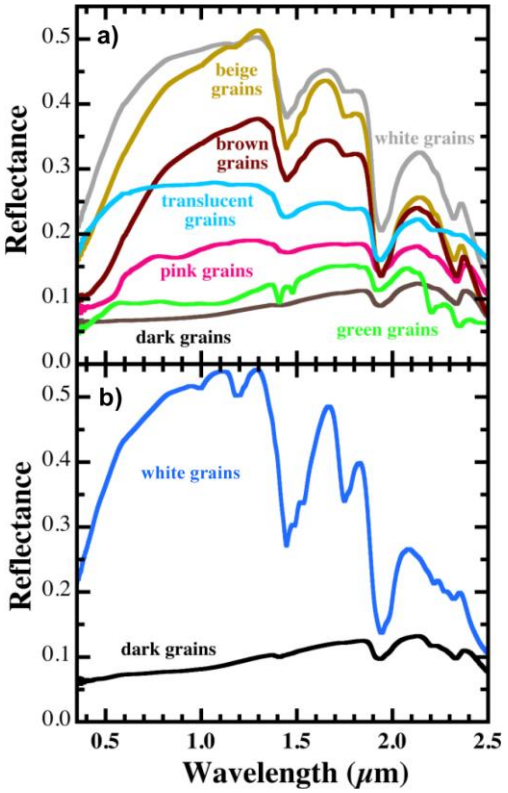

Figure 2. VNIR spectra of >1mm grains from a) Ripple 1 and b) Ripple 2. Note the great variety of mineralogies in Ripple 1 relative to Ripple 2.

Discussion: In the distance from Ripple 1 to Ripple 2, the coarse grain population changed considerably. Larger grains (>2 mm) were lost, as was the wide variety of multicolored grains. This shift was likely caused by differences in grain transport.

Creep. Coarse grains commonly travel in creep, pushed along the ground by saltating grains. A creep flux model [8,9] predicts that the creep flux q_c is inversely proportional to the grain density ρ_g. In this case, the mass flux of creeping grains relative to that of gypsum q_{c_gypsum} is simply ρ_{gypsum}/ρ_g. Figure 3 shows that the relative creep fluxes of minerals found at WSNM have a slight dependence on grain density, but it is not significant enough to explain the sharp dropoff of heavy minerals on the dune stoss slope.

Saltation. The wind can blow strongly enough to saltate 1 mm grains at WSNM [10]. Using threshold friction velocities u_{*t} estimated from [11] and the WSNM formative friction velocity u_* of 0.39 m/s of [12] accelerated 1.4x by flow acceleration up a dune stoss side [13], the steady state saltation mass flux can be estimated from [14]. Figure 3 shows the mass flux q relative to that of gypsum grains q_{gypsum} for both 400 μm (the median size at WSNM [11]) and 1 mm grains (Fig. 3). At 400 μm, saltation has little dependence on grain density. However, 1 mm gypsum grains would outmass 1 mm dolomite grains by 5x.

Conclusions: Saltation of coarse grains (>1 mm) explains an observed increase in grain sorting and decrease in mineralogical variation in the coarse grain population along the upwind edge of the WSNM dune field. This work demonstrates that sorting by transport is another process that should be considered when investigating the mineralogical maturity of a dune field, although this process may be unique to dune fields rich in evaporitic sediments.

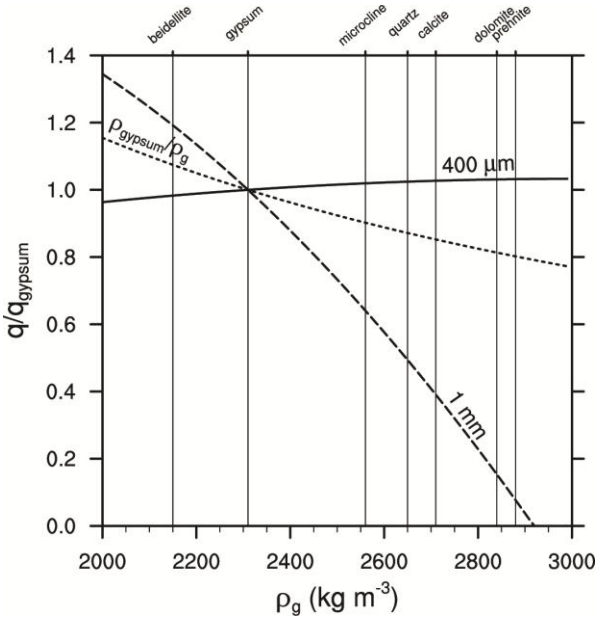

Figure 3. The saltation mass flux of 400 μm (solid line) and 1 mm (dashed line) grains relative to gypsum grains of the same size. The dotted line shows the creep mass flux relative to gypsum grains. Grains in saltation segregate by density much more strongly than those in creep.

References:

[1] Calvin et al. (2009) doi:10.1029/2009JE003348.
[2] Horgan et al. (2009) doi:10.1029/2008JE003187.
[3] Murchie et al. (2009) doi:10.1029/2009JE003342.
[4] Fryberger (2001) http://tinyurl.com/Fryberger2001WSNM.
[5] Langford (2003) doi:10.1016/S1040-6182(02)00133-7.
[6] Kocurek et al. (2007) doi:10.1016/j.sedgeo.2006.10.00.
[7] Szynkiewicz et al. (2010) doi:10.1016/j.geomorph.2009.02.017.
[8] Wang and Zheng (2004) doi:10.1016/j.powtec.2003.11.001.
[9] Dong et al. (2002) doi:10.1016/S0169-555X(02)00170-8.
[10] Eastwood et al. (2012), doi:10.1029/2012JF002368.
[11] Shao and Lu (2001) doi:10.1029/2000JD900304.
[12] Jerolmack et al. (2011) doi:10.1029/2010JF001821.
[13] Jackson and Hunt (1975) doi:10.1002/qj.4971014.
[14] Sørensen (2004) doi:10.1016/j.geomorph.2003.09.005.

THE SEDIMENT STATE OF MERIDIANI PLANUM, MARS. L. K. Fenton[1], T. I. Michaels[1], and M. Chojnacki[2], [1]SETI Institute (189 Bernardo Ave, Ste. 100, Mountain View, CA 94043, USA, lfenton@seti.org), [2]Lunar and Planetary Lab (University of Arizona, Tucson, AZ 85721, USA).

Introduction and Background: A fundamental control of bedform field accumulation is the sediment state, which is governed by three factors: the sediment supply, the sediment availability, and the transport capacity of the wind [1]. The sediment supply is defined as the volumetric influx rate of source material into an aeolian system (e.g., river sediments, volcanic ash). Sediment availability is the degree to which the sediment supply's is inhibited (e.g., it is reduced when the sand is cemented, vegetated, or buried). The wind's transport capacity is its sediment-carrying capacity (e.g., a strong wind transports more sand than a weak wind). The ***sediment state*** at any point in an aeolian system's history is determined by 1) which of these three components limits aeolian sediment flux and 2) whether the sediment supply is/was contemporaneous (e.g., actively eroding from a lakebed), lagged (e.g., reworked from older bedforms), or both.

Making some assumptions about bedform development in Meridiani Planum, it is possible to qualitatively determine the sediment state of the plains during the Late Amazonian, to the extent revealed by the visible bedforms [2]. This analysis does not include dark intracrater dune fields (e.g., [3,4]). These dunes represented a sediment state different from that on the plains; they are modified by a wind regime heavily influenced by the crater topography (affecting the wind transport capacity) and are likely less indurated than the plains bedforms (affecting sediment availability).

Bedform construction: The following describes three sets of superposed bedforms found on the plains and on the floors of small (<200 m) craters.

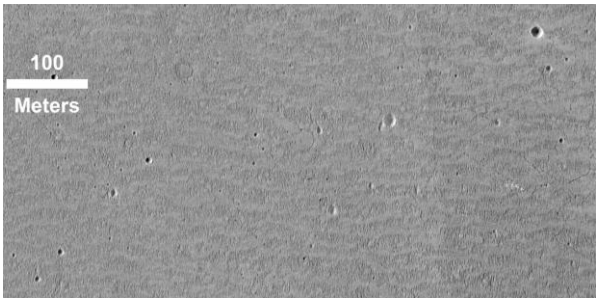

Figure 1. E-W bedforms first identified by [5]. These are the oldest known bedforms on the plains.

E-W bedforms. Figure 1 shows a set of ~15-m-wavelength structures on the plains that are aligned east-to-west (E-W). Because they are sub-parallel, have positive relief (~1-1.5 m), and often terminate in Y-junctions, they were interpreted as bedforms [5]. Little is known about these features, but they are superposed by plains ripples, and therefore they must at minimum predate the last known plains ripple migration, dated to 50-200 ka by [6].

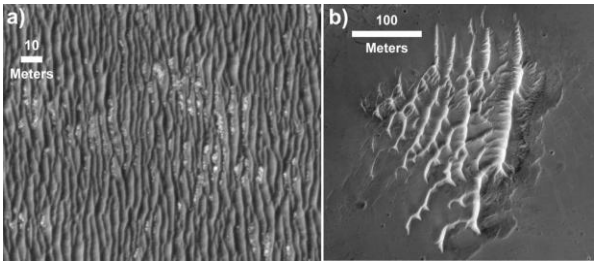

Figure 2. N-S bedforms, including a) plains ripples and b) some elements of intracrater TAR fields.

N-S bedforms. North-to-south (N-S) aligned plains ripples (Fig. 2a) and west-oriented ripple streaks [2, 7] were formed by a strong (u_* = 2.5-3.5 m/s [8]) unimodal easterly wind (~092.5º) that was directionally uniform throughout the study area. One of two modal intracrater Transverse Aeolian Ridge (TAR) crestline sets is also oriented N-S (Fig. 2b), which suggests that the TARs and plains ripples may be coeval. Atmospheric modeling and observations of present-day activity suggest this easterly wind no longer dominates sediment transport in the region [9,11].

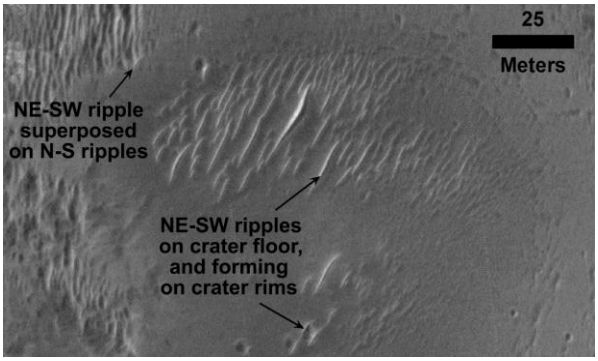

Figure 3. NE-SW bedforms, which are always found superposed on other surface features.

NE-SW bedforms. A number of relatively young bedforms are aligned northeast-to-southwest (NE-SW). This includes ~3-5-m-wavelength ripples found on the floors of small (<200 m) craters (Fig. 3), the second of two modal intracrater TAR crestline sets (Fig. 2b), and relatively young ripples superposed on the plains ripples traversed by Opportunity [10]. These bedforms overlie other features in Meridiani Planum, including N-S plains ripples and crater ejecta from an 0.84 km crater dated by [6] to 50-200 ka.

Modern aeolian landforms. Mobile sand streaks, dust streaks, and sand dunes (not shown) indicate that present-day sand transport is dominated by both northwesterly and southeasterly winds [3,4,8,10,11,12]. Although sand can be transported by these winds, it is not strong enough to mobilize the N-S plains ripples, nor does it match the NE-SW superposed ripples.

Sediment state:

Sediment supply. Basaltic sand and hematite granules on the plains consist of both contemporaneous grains (those slowly eroding from the Burns Fm.) and lagged grains (those currently stored inside inactive bedforms and crater fill). Figure 4 shows that the sediment supply (red line) is constant but very low, representing the slow erosion of the plains. [5] proposed the plains sand was derived from an overlying sand-rich layer that has since eroded away; in that case the sediment supply would instead be represented as a flux pulse predating the E-W bedforms >>~200 ka.

Sediment availability. Both coarse grains [8] and particle cohesion [10,13] limit sediment mobility. These factors are unlikely to change over time, unless winds become strong enough to overcome the higher stress thresholds required to transport larger grains and destroy cohesive crusts. Figure 4 shows sediment availability (green dotted line) as lower than the sediment supply, except in the rare cases in which the wind transport capacity exceeds the transport threshold.

Wind transport capacity. Wind stresses are thought to vary with orbital cycles [14]. Extended periods of high wind stress are required to construct the observed bedforms, with larger bedforms typically requiring longer or more extreme windy conditions. Figure 4 shows a proposed wind transport capacity history (black dashed line), with three episodes of decreasing intensity that correspond to the construction of the E-W, N-S, and NE-SW bedforms. Not included in Fig. 4 is the (perhaps ongoing) construction of the intracrater dune fields.

Conclusions: The preserved surface record from the Late Amazonian in Meridiani Planum consists of four potential periods of bedform construction. The most recent three periods can be represented by an easterly wind gradually giving way to a relative strengthening of northwesterly and southeasterly winds. Based on observations, we propose a scenario describing the sediment state of the plains with conditions alternating between transport-limited contemporaneous and lagged sediment influx (CLI_{TL}, gray in Fig. 4), during which bedforms are constructed, and relatively long periods (including the present-day) of availability-limited contemporaneous sediment influx (CI_{AL}, light green in Fig. 4).

Acknowledgements: This research was supported by NASA MDAP grant NNX13AK68G.

References: [1] Kocurek and Lancaster (1999), doi:10.1046/j.1365-3091.1999.00227.x. [2] Fenton et al. (2015) doi:10.1016/j.aeolia.2014.11.004. [3] Chojnacki et al. (2015) doi:10.1016/ j.icarus.2014.04.044. [4] Chojnacki et al. (2015), this mtg. [5]. Silvestro et al. (2014) *8th Int'l. Mars Conf.* http://www.hou.usra.edu/meetings/8thmars2014/eposter/1193.pdf. [6] Golombek et al. (2010) doi:10.1029/2010JE003628. [7] Silvestro et al. (2014) *XLV LPSC*, Abst. #1887. [8] Jerolmack et al. (2006) doi:10.1029/2005JE002544. [9] Chojnacki et al. (2011) doi:10.1029/2010JE003675. [10] Sullivan et al. (2005) doi:10.1038/nature03641. [11] Michaels et al. (2015), this mtg. [12] Geissler et al. (2010) doi:10.1029/2010JE003674. [13] Sullivan et al. (2008) doi:10.1029/2008JE003101. [14] Haberle et al. (2003) doi:10.1016/S0019-1035(02)00017-9.

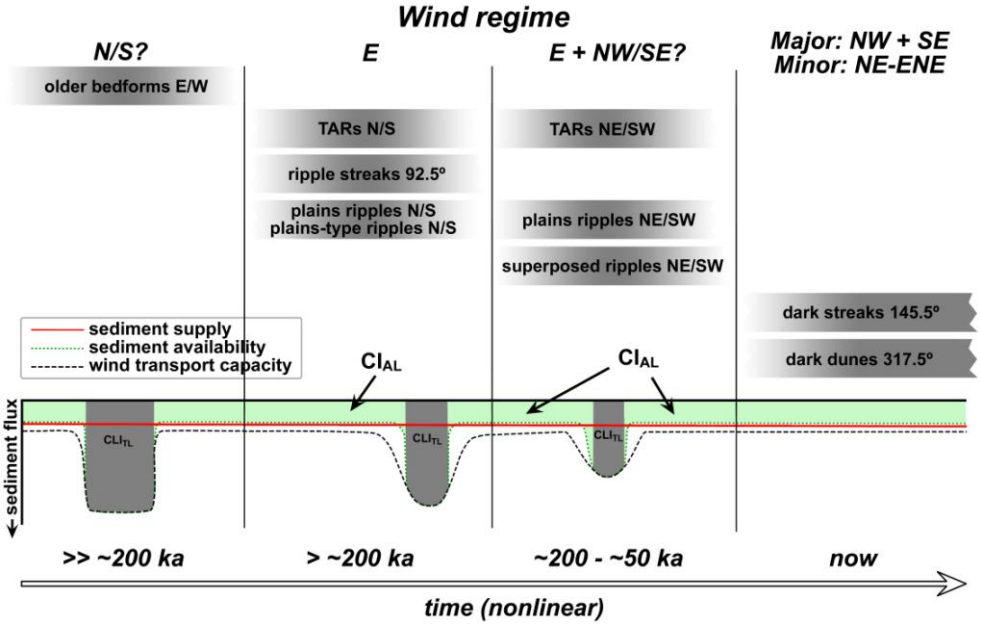

Figure 4. Proposed sediment state of Meridiani Planum

TWO MODES FOR DUNE ORIENTATION ON MARS. L. Fernandez-Cascales[1], A. Lucas[2], S. Rodriguez[2], C. Narteau[1], P. Allemand[3], A. Spiga[4], S. Courrech du Pont[5], A. Garcia[2]. [1]Institut de Physique du Globe de Paris, Sorbonne Paris Cité, University Paris Diderot, UMR 7154 CNRS, Paris, France, [2] Laboratoire AIM - Université Paris 7, Planetology, Gif/Yvette, France, [4] LMD IPSL, Paris, France, [3] Laboratoire Sciences de la Terre, UMR 5570, CNRS Université Claude Bernard Lyon 1, Lyon, France, [4] LMD IPSL, Paris, France, [5] Laboratoire Matière et Systèmes Complexes, Sorbonne Paris Cité, Université Paris Diderot, CNRS UMR 7057, Paris, France.

Introduction: Recent numerical simulations [1], laboratory experiments [2], and field measurements [2-4] show that, under the same multidirectional wind regime, dune crests can have two different orientations depending on sediment availability. In zones of high sand availability (i.e., mobilizable sediment in the inter-dune areas), dunes can grow in height following the orientation for which the sum of the normal to crest components of transport is maximum [5], henceforth referred to as the *"bed instability mode"*. In zones of low sand availability (i.e., non-mobilizable bed in the inter-dune areas), dunes elongate in the direction of the resultant sand flux by deposition of the sediment which is transported along the crest, henceforth referred to as the *"fingering mode"*. Thus, sediment availability is a key parameter that selects the dune growth mechanism and controls the subsequent dune orientation.

From wind data to dune orientation and vice-versa: A more complete forward model to predict dune orientation from the winds has been developed by [2], now taking into account the two growth mechanisms. This may significantly refines the inverse method commonly used to derive wind regime from dune orientation.

The direct model has been used in terrestrial deserts and has shown an excellent ability for predicting dune orientation for a great variety of environmental conditions [2,9]. We recently considered these two modes on other planetary bodies where dune fields have been observed. On Titan, the fingering mode coupled with the predictions of Global Circulation Models has proven to be the only one able to reconcile all the observations and conjointly explain the actual shape, orientation, direction of propagation and equatorial confinement of the dunes [8].

Exploring the two modes for dune orientation on Mars: Our aim is now to test the occurrence of both dune growth mechanisms on Mars, selecting regions where the bed instability and fingering modes seem to be explicitly expressed. First, dune orientations are extracted from CTX images using an automatic linear segment detection method (Figures 1 and 2). Second, dune orientation are derived from Martian General Circulation Models (GCM), which have been developed using different climatic scenarios. Then, we can directly compare the prediction of the models to the orientation measured from the satellite images to distinguish among the different climatic scenarios. In addition, looking at the inverse problem and assuming a limited number of dominant winds, we can try to reconstruct the family of wind regimes that can satisfy such observations. So we hope to contribute to the improvement of the GCM and provide new constraints on the past winds regimes.

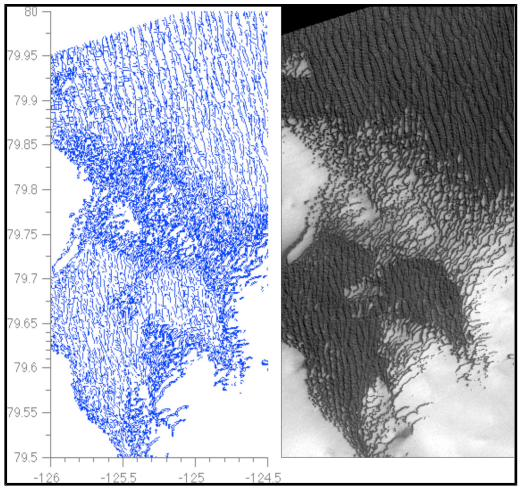

***Figure 1** : Crest orientation (left) obtained from linear segment detection method (see [8]) applied on a CTX image (right).*

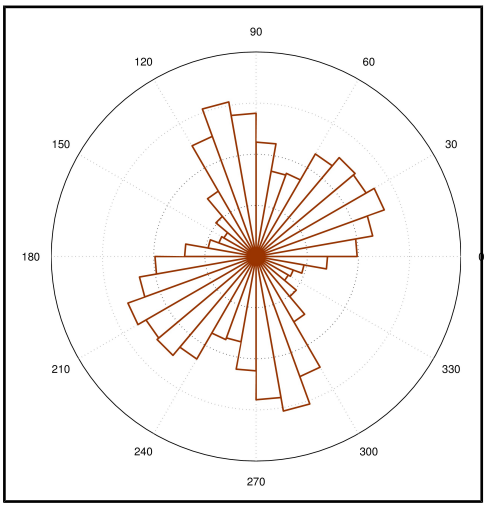

***Figure 2** : Crest orientation distribution from linear segment detection method (see Figure 1 and [8]). More tham 3.410^4 segments are obtained. Two orientations are detected: i) 28º and -75º from East.*

References: [1] Zhang D. et al. (2012), *Nat. Geosci., 5(7), 463–467*. [2] Courrech du Pont S. (2014), *Geology, 42, no. 9, 743-746*. [3] Ping L. et al. (2014), *Nat. Geosci., 7(2), 99–103*. [4] Lancaster N. and G. McCarley-Holder (2013), *Geomorphology, 181, 281–291*. [5] Rubin D. M. and R. E. Hunter (1987), *Science, 237, 276–278*. [6] Reffet E. et al. (2010), *Geology, 38, 491–494*. [7] Fenton L. K., et al. (2014), *Icarus, 230, 5–14*. [8] Lucas et al. (2014), *Geophys. Res. Lett., 41, doi:10.1002/2014GL060971*. [9] Lucas et al., this issue

Genesis of dune fields under unidirectional wind with sand input flux control: an experimental approach

A. Garcia[1], S. Courrech du Pont[2], S. Rodriguez[1], A. Valance[3], C. Narteau[4], X. Gao[4], A. Lucas[1]
[1]Laboratoire AIM, Université Paris-Diderot – CEA-SACLAY/Paris 7, 91191 Gif sur Yvette, France (amandine.garcia@cea.fr); [3]Laboratoire Matière et Systèmes Complexes, Université Paris Diderot, France, Institut de Physique de Rennes, France ; [4]Institut de Physique du Globe de Paris, Laboratoire de Dynamique des Fluides Geologiques, France ;

Introduction: Earth deserts show a rich variety of dune shapes from transverse to barchan, including star and linear dunes, depending on the history of wind regimes (strength and variability) and sand availability [1]. In desert, exposed to one wind direction, dunes perpendicular to the wind direction are found to be transverse or barchan, only sand availability plays a major role on their formation and evolution. However, the evolution time scale of such structures (about several years) limits our investigation of their morphogenesis and morphodynamics. We use here, a laboratory experiment able to considerably reduce space and time scales by reproducing millimeter to centimeter subaqueous dunes, and allowing the control of environmental parameters such as the wind regime (multi-winds, unidirectional wind, [2,3]) and recently, amount of sediment. This set up allows us to characterize more precisely the different modes of dune formation and long-term evolution, and to constrain the physics behind the morphogenesis and dynamics of dunes fields. Indeed, the formation, evolution and transition between the different dune morphologies are better understood and quantified thanks to a new experimental setting constitued by a remote continuous source of sediment (closer to what happens in sand desert): a sand distributor that enables a fine control of the input sand flux. In unimodal wind condition, we will monitor and quantify the transition between stable transverse dunes to barchan's field by modifying the sand supply.

Methods: Our experimental setup allows reproducing subaqueous dunes by controlling environmental parameters, the wind regime (number of winds, frequency, strength…). It consists of a water tank with inside, a disk covered by sand over a plate. The quick translatation moving of the plate (with a speed greater thatn the transport threshold) in one direction triggers a unidirectional wind on the opposite direction of its motion. Then, the plate goes back on it initial position by a slow motion able to prevent grain motion. This movement of roundtrip is called a period. If needed, the rotating disk can reproduce the different direction of the wind to reproduce more complex dunes by multi-winds. The sand bed evolution is followed by a camera top setting and the topography of features is retrieved by a scanner (laser sheet) that acquired profiles at given time points. This set up has already been used successfully by Hersen [2] and Reffet [3], where they studied formation and evolution of barchan, transverse and longitudinal dunes.

Here, in the aim to improve the constraint and the characterization of the transition between transverse and barchan dune fields by the control of input flux sediment, we set a sand distributor able to continuously feed our system in sand. By a translation movement and the rotation of an endless screw, the sand distributor can deposit a sand line just at the entrance of the disk.

We are now able to control the input mass flow of sand per unit length, Qin (mm2/T), and thus to precisely explore different input sand flux by modifying only the frequency of the sand line deposition on the disk (fig. 1). We ran the sand distributor experiment between 0.01 (low) and 0.82 mm2/T (to high sand supply, greater than the saturation flux of our experiment).

Results: We observed three dune morphology domains (Fig. 2):

1. For a low sand availability: the stable "barchans dune fields" domain: The sand line gets the time to decay into barchans before the deposit of the following line. In final, by feeding constantly the system, we observed the formation of a stable field of barchans.

2. For an intermediate sand availability: a transverse dune is created where barchans are continuously ejected. More collisions are counted compared to the low sediment availability morphology domain and superimposed patterns are observed on the transverse dune. The transverse is initially quite flat, and gets bigger over time and input sand flux to tends to a final mature shape. This second regime is defined as the "barchanoïd ridge" domain.

3. For a high sand availability, no more ejections of barchans are observed and a big transverse dune is present with an abrupt avalanche face. This domain is called "the transverse dune stable" domain.

A summary of results is shown with the "phase diagram" in figure 3. This latter contains a description of the three morphologies domains and a 3D scan analysis for domains 2 and 3. The plot corresponds to an estimation of the time necessary to reach a certain value of sand ejected per unit area from the front of the transverse dune, function of imposed experimental Qin. This time is normalized by the period of the sand line deposition of the sand distributor (T_{dist}). It demon

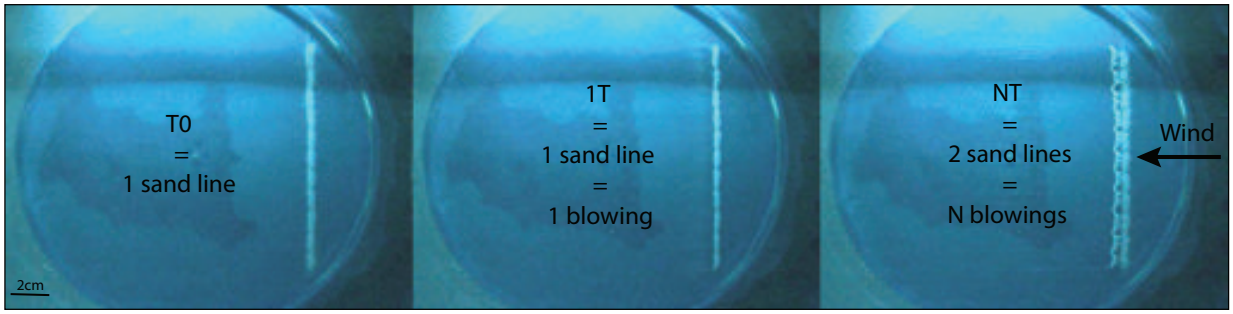

Figure 1: Principle of sand deposit on the disk by the sand distributor after one and n periods of the tray

Figure 2: Dune field morphologies under unidirectional wind depending on sand supply – Right to left: low sand availability (Qin 0.017mm^2/T, barchans fields), medium availability (Qin 0.11mm^2/T, barchnoid ridge), high sand availability (Qin 0.24mm^2/T, transverse dune)

strates that the time necessary to reach a certain value of sand ejected gets bigger with the increasing of input sand. It reflects the fact that, as we feed our dune field with more and more sand, we counter the destabilization of the deposited sand line into barchans and allow it to grow in size and aspect ratio, to a point that it finally forms a mature transverse dune with an abrupt avalanche face that traps the sand. At this moment, the big transverse dune does not eject barchans any more.

Moreover, barchnoid ridge seems the most common morphology on earth desert. This morphology is often found along the beach's coasts, area that offers a linear source of sediment [5], very close to our experimental conditions. We thus related this experimental study with a terristrial area (The Maroc south coast) that presents the same condition and the same different type of dunes morphologies due to local difference in availability of sediments.

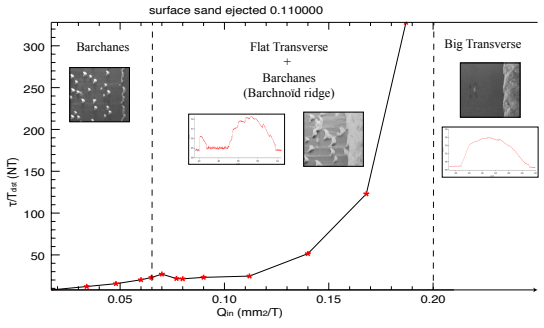

Figure 3: Time necessary to reach a certain value of surface sand ejected over Qin

Connclusion: The running of a set of experiments under an unidirectional wind, and the control of the input sand flux revealed the formation of three morphological domains for dune fields: barchan dune field, barchnoid ridge and a big transverse dune. It appears in presence of a sand input flux, the dunes can growth and spread over time by stability. Inspired by analytical model of [4] about the physic processes of the growth and migration of a dune fields, we would like in a near future to improve our physic understanding of the behavior of dune morphologies and their respective migration speeds in the three domains of stability identified. Also, the next step will be to perform experiments under bimodal wind conditions in order to better constrain the formation mode of linear dunes, depending only on the input sand flux [6]. These kind of studies can farther help us to explain more precisely in different wind history and sand supply, these patterns state that should emerge and, by applying the relevant scale law, to apply this laboratory work to terrestrial and planetary (Venus, Mars and Titan) desert dynamics.

References: [1] Bagnold R.A. The physics of blown sand and desert dunes (1941). [2] Hersen P., Morphogénèse et dynamique des barchans (2004). [3] Reffet E., Interaction Surface-Atmosphère en planetology compare: application à la formation des dunes (2010). [4] Guignier L. et al., Sand dunes as migrating strings, PRE (2013). [5] Eastwood E. et al., Modeling controls on Aeolian dune-field pattern evolution, Sedimentology (2011). [6] Courrech Du Pont S. et al., Two modes for dunes orientation, geology (2014).

ANTIDUNES ON MARS? P.E. Geissler[1] and J.T. Wilgus[2], [1]Astrogeology Science Center, U.S. Geological Survey, Flagstaff, AZ 86001 USA (pgeissler@usgs.gov) [2]Northern Arizona University, Flagstaff, AZ 86001 USA

Introduction: The decameter-scale bright bedforms that are common in the tropics of Mars were given the non-genetic name "transverse aeolian ridges" or TARs because their origin is unknown [1]. First seen in Viking [2,3] and MOC [4,5] images, the genesis of these features remains a mystery to this day. They are distinctly different from sand dunes and may have formed by an entirely different process.

We are beginning a project to test a recently proposed hypothesis that TARs are sediments deposited by dusty turbidity currents in the martian atmosphere, in a manner similar to features formed by fluvial processes on Earth [6].

Background: This hypothesis supposes that dust is transported across the surface of Mars in turbulent winds with suspended aerosols concentrated close to the surface, similar to turbidity currents on Earth. Stationary gravity waves in these shallow flows could produce the semi-regular, periodic spacing of martian TARs.

On Earth, stationary waves in shallow fluid flows generate "antidunes" [7], sedimentary structures that are common in higher energy terrestrial fluvial deposits. The characteristic wavelength of antidunes is given by Equation 1 [8]:

$$\lambda = \frac{2\pi V^2}{g}$$

and the condition for critical flow needed to form stationary waves is given by Equation 2:

$$\frac{V}{\sqrt{gd}} = 1$$

where λ is the wavelength, V is the flow velocity, g is the gravitational acceleration on Mars, and d is the depth of the flow. The left hand side of equation 2 is known as the Froude number, and is simply the ratio of the flow velocity to the propagation speed of surface gravity waves in a shallow flow. Stationary waves form when the flow velocity matches the wave propagation velocity. Putting numbers into these equations for Mars' gravity and a 50 m wavelength gives a flow velocity of 5.4 ms^{-1}, corresponding to a flow depth of 7.9 m.

These equations are valid for the current-driven case of windblown dust that is flowing at a velocity that depends mainly upon the wind speed. However, even in the absence of wind, turbulent dust clouds should continue to cascade downslope under gravity because they are denser than the atmosphere, similar to the behavior of turbidity currents and base surges on Earth. In this gravity-driven case, antidunes form according to Equations 1 and 2 with a reduced gravity g' used to account for sediment buoyancy [9] (Equation 3):

$$g' = g\frac{\Delta\rho}{\rho_a}$$

where ρ_a is the ambient fluid density and $\Delta\rho$ is the density contrast between the current and the ambient density. The flow velocity of gravity-driven density currents depends on the square root of the surface slope (sin α) [9], so the wavelength of gravity-driven antidunes is predicted by Equation 1 to be directly proportional to the sine of the slope angle. Gravity cancels out of the ratio of flow depth to antidune wavelength, which remains $1/2\pi$ whether the antidunes are current-driven or gravity-driven.

Approach: We are examining the detailed morphology of martian TARs in order to determine how well this theory fits the observations. We are using publicly released digital terrain models (DTMs) produced from MRO HiRISE observations to measure the orientations, heights and spacings of TARs and the local slopes of the settings in which they are found. Regional slopes are also being measured at 10 km and 100 km scales from MOC MOLA elevation data. More than 140 study sites are being considered by this survey, all places where HiRISE DTMs captured and resolved TARs even though the DTMs were targeted at other features such as rock outcrops and craters. The features of interest to us are taller than 1 m and spaced more than 10 m apart, but smaller ripples are also noted and their orientations and spacings recorded.

Our goals are to test several predictions of the antidune hypothesis and learn more about how and when TARs formed on Mars. We assume that TARs cannot grow taller than the depth of the dusty turbidity current, so the maximum TAR height to wavelength ratio should be no more than $1/2\pi$, a prediction that we can test with our measurements.

We can learn whether the TARs were formed by winds or by gravity by determining the correlation between TAR spacing and surface slope. A closer correlation between wavelength and local slope would indicate that the dust was cascading downhill under gravity, whereas a closer correlation with regional slope

would suggest that the dust was blown by (katabatic) winds.

Results: Figure 1 shows an example of this approach applied to unusual TARs in Syria Planum that are thought to be actively forming today [6]. The HiRISE DTMs have post spacings of 1-2 m and vertical precision in the tens of centimeters and easily resolve these bright dune-like features, which have heights of up to 4 m.

Our global survey of TARs has just begun but has already revealed many surprises, including TARs that are much taller than previously reported (up to 14 m in Kaiser crater) and TARs that are found at higher latitudes than previously reported. Much more work is needed to establish global trends and reach a conclusion about the origin of TARs.

References: [1] Bourke, M et al. LPSC 34, 2003 [2] Thomas, P et al. Icarus, 45, 124–153, 1981; [3] Zimbelman, J., Icarus 71, 257-267, 1987 [4] Thomas, P et al. Nature 397, 592-594, 1999; [5] Malin, M and Edgett, K, J. Geophys. Res., 106, 23429, 2001 [6] Geissler, P. E., J. Geophys. Res. Planets, 119, 2014. [7] Gilbert, G.K. 1914. US Geological Survey Professional Paper No. 86. [8] Kennedy, J.F., 1960. Ph.D. thesis, Cal Tech. [9] Kneller, B. and Buckee, C. 2000, Sedimentology, 47 (Supp. 1), 62-94.

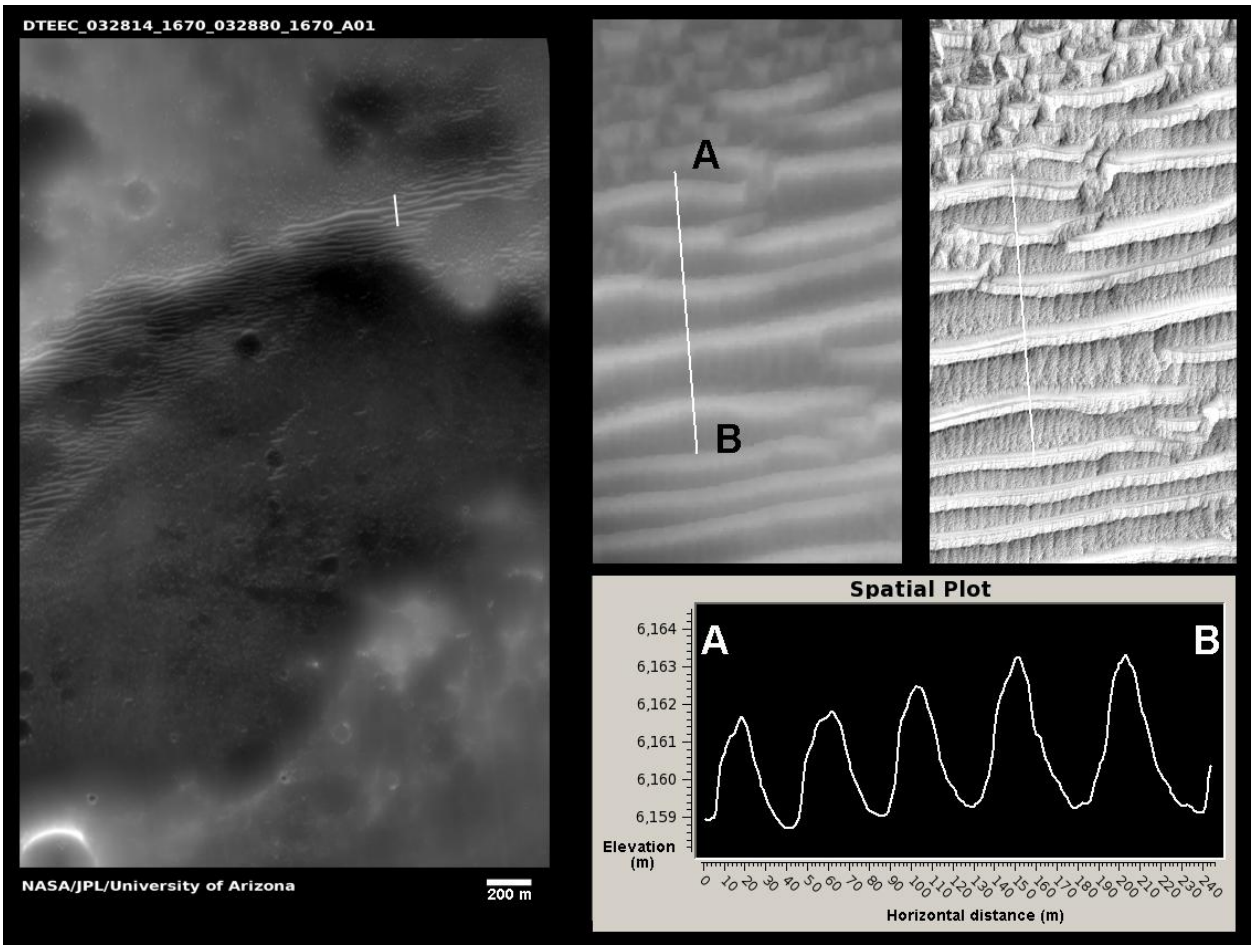

Figure 1. Elevation and topographic expression of dust deposits in Syria Planum. (Left) Cutout of digital elevation model DTEEC_032814_1670_032880_1670 showing bright dune-like features resolved along the north rim of a shallow canyon. Elevations portrayed here range from 6148 m (black) to 6182 m (white) above datum. A line shows the location of profile A-B. (Middle) Cutout of digital elevation model showing traverse from A to B. (Right) cutout of geometrically corrected (orthorectified) HiRISE image ESP_032814_1670 showing traverse. (Bottom) Topography along traverse from A to B. These bright dune-like features reach heights of up to 4 m and have slopes of up to 15°.

MARS AEOLIAN ANALOG: INSTRUMENT EVALUATION. R. K. Hayward[1], T. N. Titus[1], and J. R. Zimbelman[2], [1]U.S.G.S., Astrogeology Science Center, 2255 N. Gemini Dr., Flagstaff, AZ 86001, rhayward@usgs.gov. [2]CEPS/NASM, MRC 315, Smithsonian Institution, Washington, D.C. 20013-7012.

Introduction: Understanding how the surface and atmosphere interact on Mars today is important to the safety of landing missions and to understanding climate evolution and the potential for past life on Mars. Martian dunes record the interaction of the surface and atmosphere. Recent studies have demonstrated that dunes are surprisingly active in the current climate regime [e.g. 1,2,3,4,5]. Sand flux rates measured by Bridges et al. [6] show that flux rates at some places on Mars are similar to flux rates on Earth. This is surprising because both atmospheric modeling and *in situ* meteorological measurements on Mars suggest that winds are seldom above the saltation threshold [7,8,9,10]. Direct evidence of how sediment moves on Mars is needed, thus instrumentation capable of observing and measuring sediment flux should be part of future missions to Mars. Adapting time-proven terrestrial methods of sediment flux measurement for the challenges presented by Mars is a needed step.

Research Objective: As part of our study of flux rates at a Mars analog site, we installed an experimental sediment collector (referred to as the "Mars BSNE"). It is equipped with a time-lapse camera so that we can compare a visual record of sediment accumulation to results from traditional sediment collectors. Why use visual documentation? In addition to measuring sediment flux, visual documentation can potentially be used to determine the size and other physical characteristics of the mobile grains. We will discuss and evaluate the suitability of the Mars BSNE for measuring sediment flux on Mars.

Grand Falls, AZ as Analog: The Grand Falls (GF) dune field is located ~70 km NE of Flagstaff, AZ, 2 km east of Grand Falls, and just north of the Little Colorado River (LCR). The dune field consists of barchans, smaller dunes/ripples, and bare interdunes with indurated surfaces, all features commonly found on the Martian surface. A brief discussion of other characteristics that support GF as a Mars analog follows.

Dune Field Size and Setting. The size of the dune field (~1.5 x 1 km) and its location within a topographic trap, combine to make the GF dune field similar to ~900 dune fields that occur within craters and valleys on Mars [e.g. 11,12].

Dune Composition and Relationship to Source: Most of the dune sand on Mars is likely of basaltic composition [e.g.,13]. Basalt sand is present in significant amounts at GF, originating as ash and lapilli-fall from local volcanic eruptions. Flash floods may have washed additional ash and lapilli deposits into the LCR, making more basalt available to the dune field. The episodic availability of a local source of sand is analogous to Mars, where unconsolidated sand may become locally and episodically available (e.g., through excavation by erosion or impact).

Equipment: We measure sediment flux using a Sensit saltation sensor and a set of three Big Spring Number Eight (BSNE) passive sediment samplers, at 20, 50, and 100 cm (#1, 2 and 3, respectively) above ground level (AGL). The samplers are "weighing BSNEs" that automatically weigh and log accumulated sediment weight. The Sensit and BSNE data, as well as wind data collected from a set of three anemometers (installed at the same heights as the weighing BSNEs), are taken once per second, then averaged and logged at one minute intervals. BSNEs are emptied monthly. The contents are weighed in the laboratory to calibrate weight logs. We began data collection in November 2013. Equipment is shown in Figure 1.

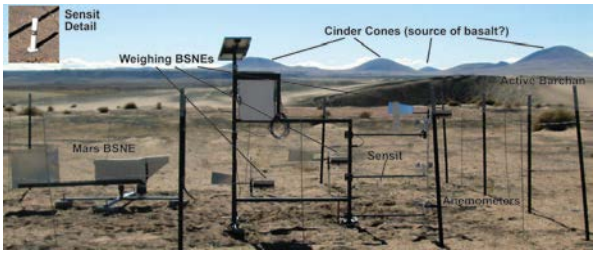

Figure 1. Instruments showing location relative to upwind barchan and cinder cones.

The Mars BSNE (details shown in Figure 2), designed and built by the maker of the weighing BSNEs, passively collects sediment at ~50 cm AGL and records data as time-lapse photos of the collection chamber taken at 15 minute intervals. The Mars BSNE is emptied monthly. Its contents are weighed and compared to photo-based weight estimates to evaluate the accuracy of this method.

Our instruments were originally positioned ~120 m downwind from an active barchan that migrates ~30 m/year. This ensures ample sand supply and multiple years of data collection.

Results: We are interested in two aspects of visual documentation: 1) accuracy of Mars BSNE volume/weight estimates, and 2) potential for analysis of grain size and other grain characteristics (e.g. sphericity, porosity, and composition). It is beyond the budget and scope of our study at GF to purchase a high-

resolution camera and have grain-size analyses performed. Literature research [14] and tests with a low-cost camera suggest that if instrument design could allow for sufficient light inside the collection chamber, images could be used to measure physical characteristics of grains as they accumulate.

Figure 2. Mars BSNE detail showing camera, transparent calibrated panel, top view of collection chamber, and their locations within instrument.

Figure 3 shows plot of the calibrated mass of sediment collecting in weighing BSNE #2 and images of the Mars BSNE transparent calibrated panel as it appeared at selected times during the wind event.

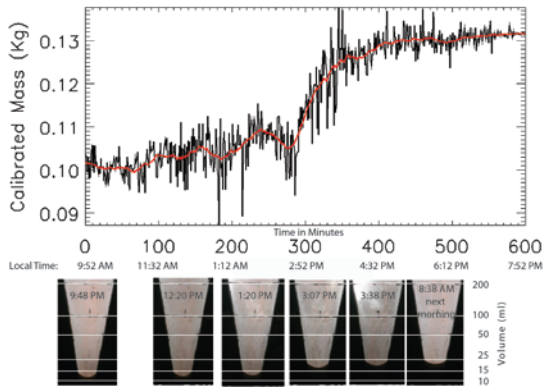

Figure 3. Calibrated mass of sediment in weighing BSNE #2 plotted for ten-hour wind event that began February 27, 2014. Black line represents unsmoothed data logged at one minute intervals. Red line represents smoothed data. Below graph, Mars BSNE images visually document accumulation.

The estimated mass of sediment collected in the Mars BSNE during the wind event is less than expected, based on the mass of the sediment collected in BSNE #2. It is possible that the Mars BSNE responds more slowly to wind direction changes, thus it may not collect sediment efficiently if wind direction shifts during the wind event.

Summary/Conclusion: Accurately estimating the volume and mass of sediment collected using Mars BSNE images is an ongoing challenge. The challenge is to some degree offset by having an independent visual record of sediment as it collects; the record is a valuable aid that helps determine the cause of anomalous weighing BSNE results. Design improvements to the Mars BSNE that would enhance its performance include modifying the collection chamber shape so that small amounts of sediment could be estimated more accurately. A high-resolution camera is needed as are more transparent parts in the instrument for better daytime images and a flash to allow night images. The instrument should have multiple collection heights because we are not certain of saltation height on Mars. Multiple layers would also allow calculation of sediment flux profile. *Should Mars BSNE go to Mars?* A weighing BSNE would measure the amount of sediment collected with greater accuracy, but an improved Mars BSNE would enable us to monitor the size, composition, and other characteristics of grains as they accumulate.

References: [1] Bourke, M.C. et al. (2008) Geomorphology, 94, 247-255, doi:10.1016/j.geomorph.2007.05.012. [2] Silvestro, S. et al. (2010) Geophys. Res. Lett., 37, L20203, doi:10.1029/2010GL044743. [3] Chojnacki, M. et al. (2011) JGR 116, E00F19, doi:10.1029/2010JE003675. [4] Geissler, P. E. et al. (2011) LPS XLII, #2537. [5] Hansen, C. J. et al (2011) Science, Vol. 331 no. 6017 pp. 575-578 DOI: 10.1126/science.1197636. [6] Bridges, N. T. et al. (2012) Nature, 485, 339-342, doi:10.1038/ nature11022. [7] Sullivan, R. et al. (2005) Nature 436, doi: 10.1038/nature03641. [8] Greeley, R. et al. (1980) GRL v. 7, no. 2, 121-124. [9] Hess S.L. et al. (1977) JGR 82:4559–74. [10] Kok, J. (2012) Nature, doi:10.1038/nature11193. [11] Hayward, R. K., et al. (2007), JGR, *112*, E11007, doi:10.1029/ 2007JE002943. [12] Fenton L. K. and Hayward R. K. (2009), Geomorph doi: 10.1016/j.geomorph.2009. 11.006. [13] Herkenhoff K. E. and Vasavada A.R. (1999) JGR 104(E7), 16,487–16,500, doi:10.1029/1998JE000589. [14] Buscombe, D. (2008) Sed. Geol., *210*.

Additional Information: This research is funded by the NASA Moon and Mars Analog Missions Activities (MMAMA) program, project #NNH13AV781.

USING MINERALOGY TO TRACE SAND SOURCES AND TRANSPORT HISTORIES IN THE NORTH POLAR SAND SEA, MARS. B. Horgan[1] and F. Seelos[2], [1]Department of Earth, Atmospheric, and Planetary Sciences, Purdue University, West Lafayette, IN (briony@purdue.edu), [2]JHU/Applied Physics Laboratory, Laurel, MD.

Introduction: The north polar sand sea is the largest sand sea on Mars, and encircles the north polar plateau, Planum Boreum (PB) [1]. The deposits within and around PB record diverse sedimentary and aqueous processes that likely reflect those that have been ongoing in the northern lowlands since the Hesperian [2-9]. In this study, we show that dune fields within the north polar sand sea of diverse mineralogies are directly sourced from specific layers within PB, and that these mineralogies also correspond to more extensive units within the northern lowlands. Thus, we hypothesize that the sediments that currently supply the sand sea were originally sourced from these larger units, and emplaced within PB via impact and aeolian processes.

Data Sets: We have used near-infrared spectra (~0.3-2.5 μm) from the Mars Express OMEGA and MRO CRISM imaging spectrometers. Initial interpretations were completed using calibrated summer OMEGA observations mosaicked into a 1 km/pxl polar stereographic mosaic above 70°N [9]. We are also constructing a new ~200 m/pxl CRISM multispectral mosaic [7] above 75°N with enhanced calibration techniques to investigate terrains near scarps and troughs that are compromised in OMEGA observations by mixing with plateau ice and slope-related phase effects. Finally, we are conducting a detailed investigation of PB scarps with full-resolution (18 m/pixel) CRISM enhanced MTRDR products [10].

Mineral detection methods: Hydrated minerals are mapped using the 1.9 μm band depth, modified to account for the presence of ice [6]. Water ice is mapped using the 1.5 μm band depth [4]. Iron-bearing minerals are detected based on the position and shape of the ~1 μm iron absorption band. Band position alone can be used to broadly differentiate minerals: iron oxides and low-Ca pyroxene (LCP) usually exhibit band centers between 0.88-0.94 μm, high-Ca pyroxene (HCP) 1.00-1.05 μm, olivine 1.04-1.09 μm, and iron-bearing glass 1.10-1.18 μm [11]. When these minerals mix, the band centers and shapes vary in predictable ways, and thus these parameters can be used to identify even small abundances of Fe-minerals and glass in mixtures [12].

Sand mineralogy: Based on our low-resolution OMEGA map, we have identified three major spectral endmembers in north polar sediments. *(1) Gypsum*: strong hydration and other diagnostic gypsum signatures throughout the Olympia Undae dune field [4], as well as weaker signatures on PB [6,13] associated with the north polar veneers [14]. *(2) HCP:* strong 1.01 and 2.10 μm iron bands in western Olympia Undae and

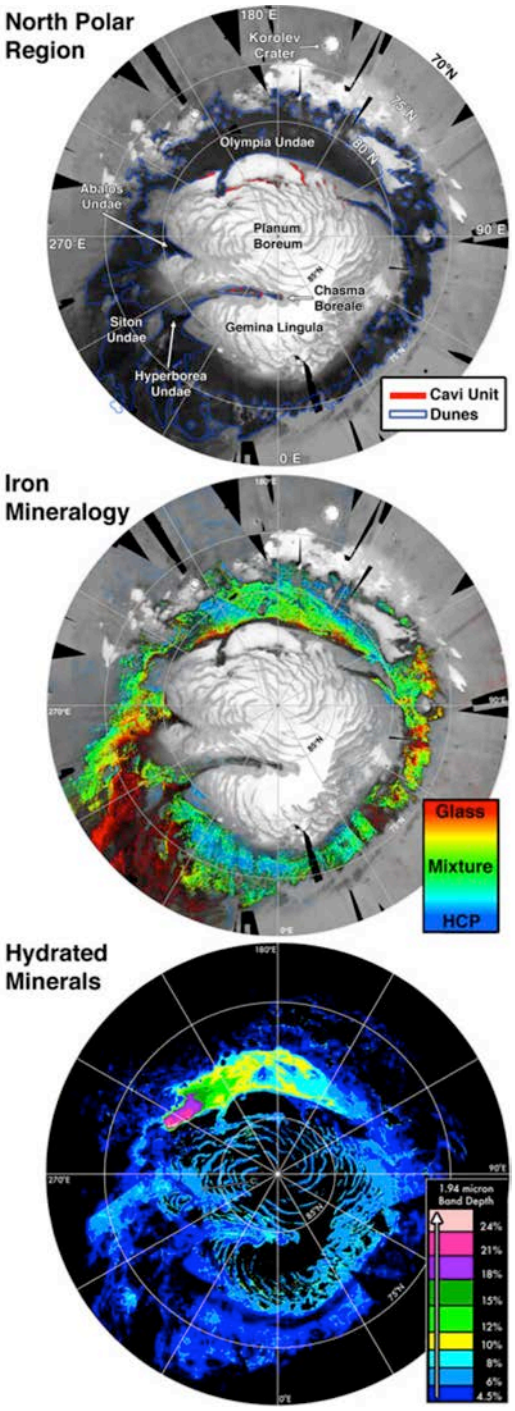

Figure 1: *OMEGA maps of north polar region. Top: major features on 1 μm albedo. Middle: Iron mineralogy derived from 1 μm band center. Bottom: 1.9 μm hydration band depth, mostly indicating gypsum.*

weaker signatures on and near PB associated with the veneers. *(3) Weathered iron-bearing glass:* weak 1.10-1.15 μm iron bands and a concave up spectral slope from 0.7-1.5 μm consistent with weathered glass in dune fields 260-300°N, far eastern Olympia Undae, and many of the chasmata [9].

Glass sources: Our analysis suggests that the bulk of the sand sea is composed of weathered glass. Glass-rich dunes demark apparent transport pathways that lead back to exposures of the PB cavi unit, an ancient ice-indurated dune field that comprises up to 1.5 km of the PB basal unit [15]. Similar weathered glass surficial deposits cover much of Acidalia and Utopia Planitiae [9], so we hypothesize that the cavi unit sands were created via deflation and aeolian transport of these units sometime after the Late Hesperian or Early Amazonian, based on the age of underlying PB units [5].

Pyroxene sources: Strong HCP signatures appear in dunes adjacent to and apparently sourced from within the icy outliers to the south of Olympia Undae, which may contain a similar set of units to the upper layers of PB [16]. HCP is also detected within the north polar veneers that drape PB and emanate from the PB 2 unit [14], a lithic unit located between the upper and lower NPLD. It has been proposed that these sediments are a dusty sublimation lag [15]; however, this is inconsistent with their HCP mineralogy. An aeolian origin is also unlikely on top of the plateau. We propose that these sediments may instead be a layer of impact ejecta [17], which is consistent with our observations of HCP in some impact ejecta elsewhere in the northern plains. HCP from the veneers is also incorporated into dunes near 0°E, where the dark veneers partially obscure the underlying terrain below the ice cap.

Gypsum sources: There is at least one obvious source of gypsum in the north polar region: the concentrated gypsum deposit sourced from far eastern Olympia Undae and transported via wind throughout that dune field [4]. However, hydrated minerals, usually identifiable as gypsum, appear to also be present at lower abundances in all aeolian source units – both the veneers and cavi unit [6,13,17]. This is reflected in the low abundance of gypsum present throughout the north polar dune sea, and may suggest that some process of aqueous alteration has been common in this region during the Amazonian.

CRISM hi-res analysis: Preliminary analysis of CRISM MTRDR observations over the Chasma Boreale scarp appears to generally support the inferences made from the lower resolution OMEGA map. The cavi unit exhibits spectral signatures similar to that of the OMEGA weathered glass unit, and the north polar veneers exhibit HCP-like signatures. Interestingly, the strongest hydration signatures at this location are associated with sand dunes on the chasma floor, potentially sourced from the cavi unit. More detailed analysis with methods like those used on the OMEGA map will help to confirm the hypotheses discussed above.

References: [1] Hayward, R. (2011) *ESPL* 36, 1967-1972. [2] Byrne, S. & B. Murray (2002) *JGR*, 107, doi: 10.1029/2001JE001615. [3] Tanaka, K. (2005) Nature, 437, 991-994. [4] Langevin, Y. *et al* (2005), Science, 307, 1584. [5] Tanaka, K. *et al*. (2008) Icarus, 196, 318-358. [6] Horgan, B. *et al*. (2009) *JGR*, 114, doi:10.1029/2008JE003187. [7] Calvin, W. *et al*. (2009) *JGR*, 114, doi:10.1029/2009 JE003348. [8] Poulet, F. *et al.* (2007) *JGR, 112,* doi: 10.1029/2006JE002840. [9] Horgan, B. and J.F. Bell III (2012) Geology, 40, 391–394. [10] Seelos, F. *et al*. (2012) Planet. Data Users Wkshp. [11] Adams, J. (1974), *JGR*, *79*, 4829. [12] Horgan, B. *et al*. (2014) Icarus, 234, 132-154. [13] Masse, M. *et al*. (2010) Icarus, 209, 434–451. [14] Rodriguez, A. *et al*. (2007) Mars, 1, 15, doi:10.1555/mars.2005 .1.0. [15] Masse M. *et al*. (2012) EPSL, 317-318, 1–12, doi: 10.1016/j.epsl.2011.11.035. [16] Tanaka, K. & Fortezzo, C. (2012) USGS SIM 3177. [17] Horgan, B. & Seelos, F. (2014) LPSC 44, #2158.

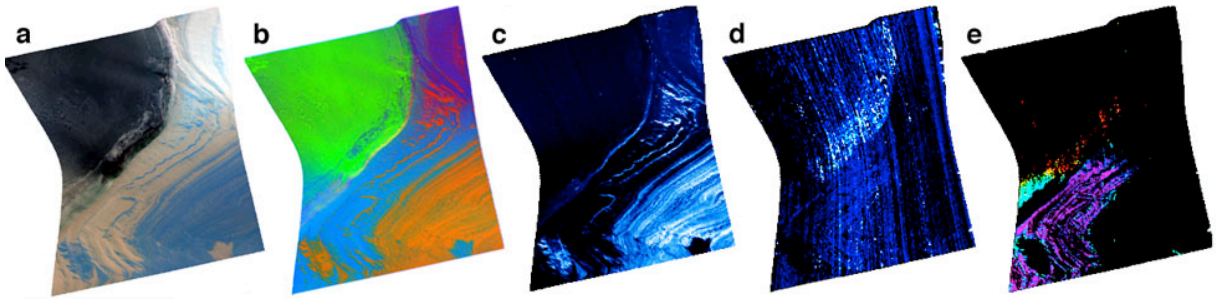

Figure 2: *CRISM FRT0000C093 at the head scarp of Chasma Boreale, with the plateau to the bottom right and floor to the upper left, separated by an exposure of the lower PLD and the cavi unit. (a-b) False color RGB composites of VNIR and IR parameters (a: 2.5/1.3/0.77μm; b: BD1500/BDI1000VIS/RBR), only possible with joined MTRDR data [10]. (c) 1.5 μm ice band depth [6] showing ice on plateau. (d) 1.9 μm band depth (corrected for ice), indicating hydrated minerals on chasma floor. (e) Concavity [9], low values (purple/blue) indicate pyroxene on the plateau, high values (green/red) indicate weathered glass in the cavi unit.*

TARs on Mars: A study of the spatial variability and physical characteristics of Martian Transverse Aeolian Ridges. A.D. Jessar[1], J.R. Zimbelman[2], and L.A. Hennig[3]; [1,3]Astronomy and Astrophysics Research Laboratory, Thomas Jefferson High School for Science and Technology, Alexandria, VA 22312; [1]2015ajessar@tjhsst.edu, [3]LAHennig@fcps.edu; [2]CEPS/NASM MRC 315, Smithsonian Institution, Washington, D.C. 20013-7012; zimbelmanj@si.edu

Introduction: Transverse Aeolian Ridges (TARs) are wavelike formations of sediment, similar in appearance to terrestrial ripples, which form in groups across the Martian surface. TARs resemble Martian dunes and ripples but have not been studied as extensively as some other aeolian bedforms. It is generally recognized that TARs are smaller than dunes and larger than ripples. However, previous studies have determined that there are different types of TARs, and some of them resemble dunes, while others resemble ripples [1, 2]. Research to date has focused on the spatial variability of TARs (that is, how TAR concentration varies across the Martian surface) and, more generally, on the factors hypothesized to influence TAR formation, including latitude, elevation, and local geology [3]. Such research helps to develop an understanding of TARs in Martian geology, specifically with respect to dunes and ripples.

In this study of images taken by the High Resolution Imaging Science Experiment (HiRISE), we confirmed that, as previous studies have indicated, TARs come in various shapes and sizes and with differing degrees of topographic dependence [1, 2]. Although too few images had been analyzed at the time of this writing to warrant conclusions based on numerical data, we expected to find latitude as a major determinant of TAR concentration. Over the course of this study, new methods of image analysis were developed that should allow for more quantitative studies of the spatial variability and diverse physical characteristics of TARs.

Data Collection: This study focused on HiRISE images from the longitudinal swath extending from 70°E to 80°E, a region selected because it includes part of the Hellas impact basin. This depression is the site of the lowest elevations on Mars and is an appropriate choice for examining how altitude and local terrain affect TAR concentration. Thumbnails of the HiRISE images were accessed online through Arizona State University's map of HiRISE images. The full-resolution images were downloaded into the HiVIEW analysis program from the University of Arizona's HiRISE website.

Once an image was opened in HiVIEW, the zoom function was used to examine the surface in greater detail. The total TAR coverage, defined here as the percentage of a given image covered by TARs, was then estimated. The coverage estimate was entered into an Excel spreadsheet, along with the latitude and longitude of the center of the image and next to qualitative notes about the physical characteristics of the TARs in the image.

After analysis of about 90 images, a sampling technique was developed to avoid the unnecessary analysis of many similar images within small surface areas. The sampling was governed by selecting one image from each 1° x 1° (lat. - long.) square in a grid superimposed on the surface (part of the grid is illustrated in Figure 1).

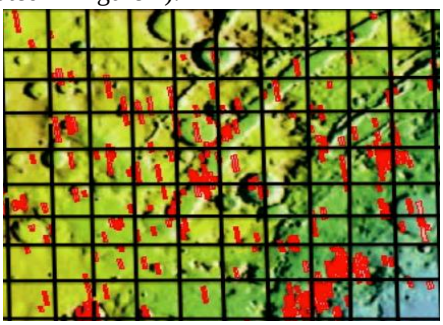

Figure 1: Part of the sampling grid. Squares run from 70°E to 80°E and about 17°N to 25°N. Red dashes represent HiRISE images on Arizona State University's HiRISE Camera Image Map.

After analysis of about 100 images, the TARs were divided in all of the ensuing images into three categories (based on their physical characteristics) that seemed representative of all the TARs observed in the first 100 images. These TAR types were designated as "patchy" TARs, "well-defined" TARs, and "superimposed" TARs (see "Analysis" section below for a description of these kinds of TARs). For a given image, the percent coverage of each of the three TAR types present in the image was estimated, so that each image was associated with four estimates instead of just one (the three specific estimates and the total coverage estimate). By definition, the three "type concentrations" added up to the total coverage estimate of the image. Estimates of the type concentrations were made more consistent with the HiVIEW "distance tool," which was used to circle TAR deposits of a given type and calculate their areas. These areas were added together to get the total area covered by a TAR type. The total area was divided by the area of the entire image and multiplied

by 100% to give the type concentration. This numerical approach reduced dependence on a solely visual estimation method. The type concentration technique offered a new way to analyze physical characteristics and spatial variability of TARs at the same time, since it enabled differentiation between TARs throughout the swath.

Analysis: The names "patchy," "well-defined," and "superimposed" were devised based on observations of TARs' physical characteristics, which were recorded in the Excel spreadsheet. "Patchy" TARs are formations that form in large groups and cover significant surface area. "Well-defined" TARs are high-albedo formations that often form in craters and valleys. "Superimposed" TARs are more spread out relative to one another and seem to lie on top of local terrain. Figure 2 shows examples of the three types of TARs.

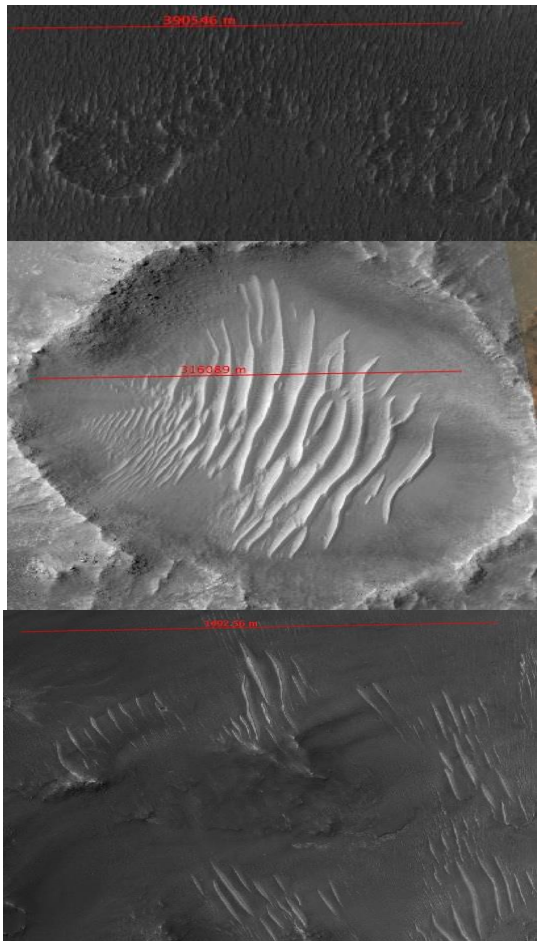

Figure 2: The top image shows "patchy" TARs (the scale indicated by the red distance tool is 390546 meters). The second image shows "well-defined" TARs within a crater (the distance reading is 316089 meters). The third image shows "superimposed" TARs (the distance reading is 1492.56 meters).

The average total TAR coverage was calculated and recorded for each 10° latitudinal zone within the swath. For each of these zones a histogram of all coverage estimates was constructed. These calculations were repeated for the type concentrations ("patchy, well-defined, and superimposed") in each zone except the 10°N-20°N region (which had already been examined before the decision to divide total estimates into estimates based on TAR type). The only difference in this second set of calculations was that three averages and three histograms were produced for each zone, instead of one average and one histogram (since there were three types of TARs).

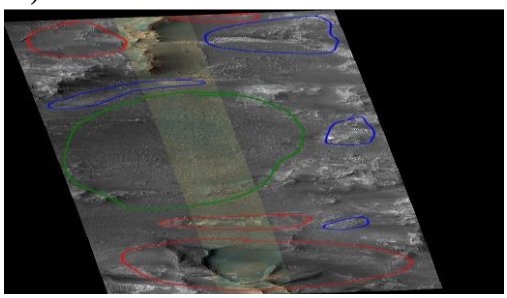

Figure 3: TARs circled by red, blue, and green ovals are "patchy," "well-defined," and "superimposed" TARs, respectively. The horizontal edge of the image is approximately 5300 meters long. The side is approximately 14300 meters long.

Conclusions: At the time of this writing, only the 10°N-20°N had been completed. Thus, conclusions were not yet formulated, but they will be presented at the workshop. Preliminarily, we expected to find that the latitudinal zones closest to the equator would have the highest average total coverages, since previous research found that TARs were most prevalent at low latitudes [3]. We also expected to find high TAR concentrations in the Hellas impact basin, since earlier studies also found that TARs were most concentrated at low elevations [3]. Analysis of more images over the swath should determine whether these expectations were well-founded. The coverage estimate data and qualitative notes from this study should be a valuable addition to the developing science techniques of studying Martian TARs.

References: [1] Balme, M., Berman, et al. (2008). Transverse Aeolian Ridges (TARs) on Mars. Geomorphology, (101), 703-720. [2] Zimbelman, J. R. (2010). Transverse Aeolian Ridges on Mars: First results from HiRISE images. Geomorphology, (121), 22-29. [3] Ebinger, E. K., & Zimbelman, J. R. (2015). Geospatial classification of Transverse Aeolian Ridges on Mars. *LPS 46*. (retrieved from http://www.hou.usra.edu/meetings/lpsc2015/pdf/1137.pdf)

MAPPING WINDS OVER MARTIAN SAND DUNES FROM RIPPLES AND DIGITAL TERRAIN MODELS. M. B. Johnson[1] and J. R. Zimbelman[1], [1]Center for Earth and Planetary Studies, Smithsonian Institution, Independence Ave and Sixth St SW, Washington, D.C. (JohnsonMB@SI.edu; ZimbelmanJ@SI.edu)

Introduction: Sand dunes have been shown to preserve wind flow patterns in their ripple formations on both Earth [1] and Mars [2]. By documenting ripple orientations shown in High Resolution Imaging Science Experiment (HiRISE) images of sand dunes at widely distributed sites across Mars, we can begin to identify the most recent wind directions at these locations [3]. However, we must also consider the effects of form flow and slope deflection on these wind patterns [4]. These considerations reinforce the value of DTMs for comparing ripple measurements to elevation and slope information. DTMs can also be used with wind modeling software to create raster maps of simulated wind speed and direction. Together, documented ripples, DTMs, and wind models can offer a more complete picture of recent wind flow patterns on Mars.

Ripple Mapping: Using GIS, lines were drawn perpendicular to ripple crests across three adjacent ripples in order to document ripple wavelength from line length and inferred wind direction from azimuth. Because it is not possible in most areas to infer a unique wind direction from the ripples alone, line orientations have a 180 degree ambiguity. Actual orientations can be defines after further study. Measurements are made about 40 meters apart, though this number may decrease in areas where ripples quickly change wavelength or orientation, and increase where ripple patterns are obscured or complex. Figure 1 is an example of these lines.

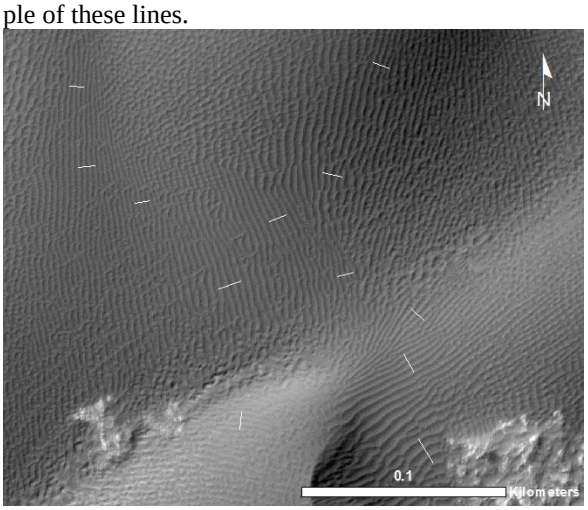

Figure 1: Ripple mapping in a subscene of HiRISE frame ESP_025645_1455. Note that areas with clear ripple definition for tens of meters contain measurements while areas with over-lapping patterns have been intentionally avoided.

DTMs: DTM creation software uses two stereo images along with absolute height reference points to create an elevation map for the overlapping area. The Soft Copy Exploitation Toolkit (SOCET SET) used by the USGS in Flagstaff can create a DTM with 1 meter post spacing from 25 cm/pixel resolution HiRISE images and MOLA track data [5]. To ensure the best quality product without artifacts, the images should be taken close together in time and have minimal untextured areas. Further manual editing, such as editing by interpolation in selected areas, may alter the product quality.

Wind Modeling: Though it has been shown that surface slopes on a sand dune can deflect ripple orientation with respect to the incident wind [4], we have found this effect to be not large in our study sites when slip faces are avoided, and when the dunes lack great vertical relief [6, 7]. DTMs can therefore be used to predict reasonable form flow deviations. To do this, we have begun to explore open source software that simulates spatially varying winds dependent on DTM data, starting with OpenFOAM and WindNinja. OpenFOAM has been compared to WindNinja for dune sites which include large obstacles on both Earth and Titan. OpenFOAM was found to be superior, but was also more complicated and more difficult to use [8, 9]. WindNinja can be used in three modes: with model data from the US National Weather Service, with one or more surface wind measurements, or a user-specified average surface wind speed and direction. Because of its ease of use and multiple run options, we chose to first explore WindNinja for Mars DTMs.

Using WindNinja:

Methods: We used a subset of the DTM DTEED_016907_1330_016973_1330_U01 (seen partially in Figure 2), which covers a large dune within Kaiser Crater. The DTM data were loaded into WindNinja along with an average incident wind direction of 80° (cw from N), based on the shape of this barchan dune. Separate runs with an average wind speed of 20, 30, 40, and 50 mph (1 m/s = 2.2 mph) were used to evaluate the effect of differing speeds. Because of the nature of the program, we then chose constraints closest to our situation (e.g., 'grassy' for the terrain type). A domain average wind model was used because we lack wind data for this location. The WindNinja output for this DTM is shown in Figure 3.

Results: For each of the simulated regimes (20, 30, 40, and 50 mph average wind speed, each with 80 de-

grees average wind direction and 1 meter above the ground), the wind direction output was the same at corresponding points. For each run, the directional summary information was an 80° average wind direction with a standard deviation of 3.5°. Changing the average wind speed for each run showed that both the standard deviation and range of wind speed measurements (highest value-lowest value) increased. Specifically, standard deviation increased by 1.3° and range increased by 20 with each change in speed (10 mph).

When the assumed height of the wind measurements increased to 3m above the ground, the wind direction output was identical to those at a 1m height, but the average wind speed output decreased.

Summary: DTMs, though sometimes difficult to create, are necessary in order to evaluate wind flow over a dune or dune field, in order to aid in the interpretation of documented ripple measurements. DTMs can be used with circulation models in order to simulate possible winds for comparison to documented ripples. WindNinja is a fast and easy way to create a raster map of simulated wind directions, but can be relatively low resolution (less than 70 m is usually not recommended) and is sometimes trivial. Further work will include using WindNinja with additional DTMs of dunes with ripples, and including data from global or regional circulation models as tie points for the WindNinja simulations.

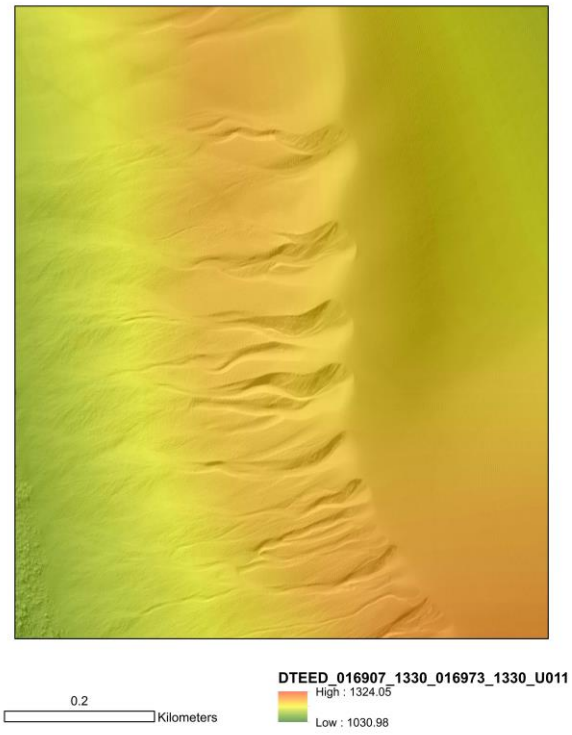

Figure 2: Small subscene of HiRISE DTM DTEED_01607_1330_16973_1330_U011 showing the dune crestline and gullies, which may affect wind flow.

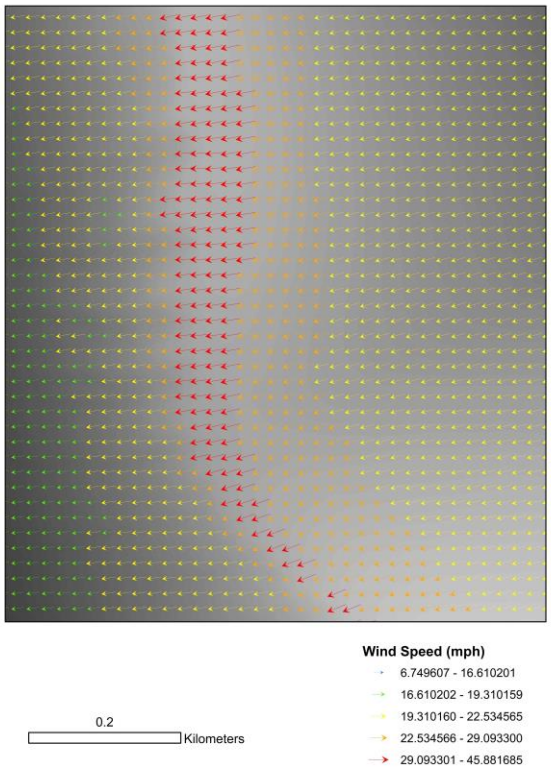

Figure 3: WindNinja output for the same subscene shown in Figure 2, using an average wind direction from 80 degrees, average wind speed of 20 mph, and wind height of 1 m above the ground. The fastest speeds are observed at the crest of the dune, consistent with likely form flow effects. The largest change in wind direction occurs where the crest changes direction.

References: [1] Neilson J. and Kocurek G. (1987) *Geol. Soc. Am. Bull., 99,* 177-186. [2] Ewing R. C. et al. (2010) *J. Geophys. Res., 115,* E8. [3] Johnson M. B. and Zimbelman J. R. (2013-2015) LPSC abstracts 2111, 1518, 1539. [4] Howard A. D. (1977) *Geol. Soc. Am. Bull., 88,* 853-856. [5] USGS (2013) *Photogrammetric Processing of Planetary Stereo Images Using ISIS3 and SOCET SET*, http://astrogeology.usgs.gov/search /details/Docs/Photogrammetry/Primer/docx. [6] Johnson M. B. and Zimbelman J. R. (2014) *Geol. Soc. of America* meeting abstract 329-11. [7] Zimbelman J. R. and Johnson M. B. (2014) *Am. Geophys. Union*, Fall meeting abstract EP43B-3564. [8] Cisneros *Am. Geophys. Union*, Fall meeting abstract EP43B-3570. [9] Cisneros J. (2015) LPSC abstract 2683.

THE AERODYNAMIC ROUGHNESS OF MARS-LIKE SURFACES. L. Kerber[1], C. W. Hamilton[2], S. P. Scheidt[2]. [1]Jet Propulsion Laboratory, California Institute of Technology, Pasadena, CA 91109, kerber@jpl.nasa.gov, [2]Lunar and Planetary Laboratory, University of Arizona Tucson, AZ, 85721.

Introduction: Accurate knowledge of near-surface winds is important for understanding many atmospheric and geologic processes. In the case of dunes, high-resolution surface winds are needed—sometimes down to the scale of an individual valley or crater—to determine how the dunes were shaped and whether or not they are active in the present era [1]. Knowledge of the surface wind environment on Mars is vital for many other scientific and engineering concerns as well, including the entry, descent, and landing of martian probes; the understanding of dust storm initiation; the characterization of wind-induced vibrations; and the study of landscape modification through aeolian erosion. However, despite the importance of surface winds, they remain the least well characterized winds on Mars [2]. For most applications, both scientists and engineers rely upon the results of atmospheric models such as global circulation models, mesoscale climate models, and large eddy simulations for information about the surface winds [e.g., 1].

One of the major variables affecting the character of the surface wind is the terrain roughness at the air/land boundary, which is parameterized by an "aerodynamic roughness length" [3]. On the Earth, roughness lengths are measured experimentally over various terrains (e.g., tundra, grasslands, corn fields, suburbs, forest, etc.). On Mars, volcanic terrains constitute over a third of the planet's surface, yet their areodynamic roughness properties have not been thoroughly characterized. In 1976, wind profiles over an alluvial plain were compared to those over a rough volcanic surface, and it was found that the wind changes significantly because of the change in surface roughness [4]. Due to a lack of measurements, however, these effects are not reflected in Martian wind modeling studies. For example, in present martian climate models, a single roughness value is often chosen to represent the entire planet. In some cases surface roughness is based on rock abundance data, but such an approach neglects the effects of the local-scale topography, which falls between the scale of rocks and the orographic-scale [5].

A pilot study investigating the relationship between aerodynamic roughness and volcanic terrain type was conducted on the Kīlauea Volcano in Hawai'i (**Fig. 1**) from May 6th to May 27th, 2014. During this this time, wind profiles were recorded over Mars-like volcanic landscapes, including fresh 'a'ā lava, platy lava, slabby pāhoehoe lava, weathered 'a'ā lava infilled with sand, and a tumuli field (**Fig. 2**). Each represents a different kind of surface roughness which is seen on Mars.

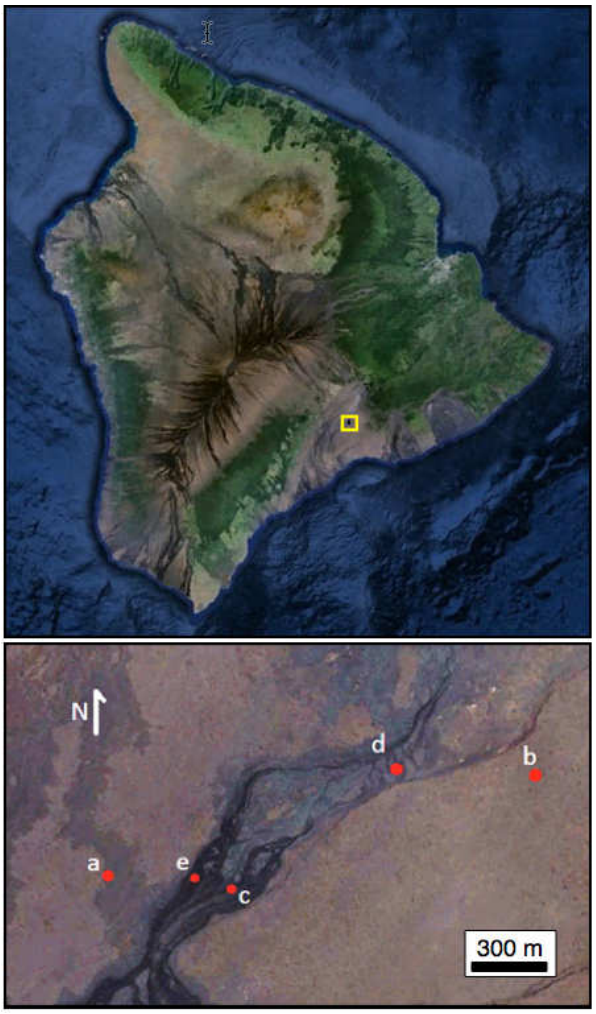

Fig. 1. Location of the field site on the main island of Hawai'i (top). Image from Google Earth. Data SIO, NOAA, U.S. Navy, NGA, GEBCO, MBARI, Landsat, LDEO-Columbia, NSF, NOAA. Close up of the December 1974 flow and roughness measurement locations (bottom). (a) sediment-covered 'a'ā, (b) tumuli field, (c) slabby pāhoehoe, (d) fresh 'a'ā, (e) lava plates. Image from Google Earth; data from Digital Globe, 2015.

Methods: The apparatus used to make measurements consisted of a 7.64-m mast instrumented with anemometers spaced at logarithmic heights (**Fig. 3**). Simulaneous wind speed measurements were recorded at five heights, at increments of 30 seconds. The mast was left at each site for several days (**Fig. 4**). From the

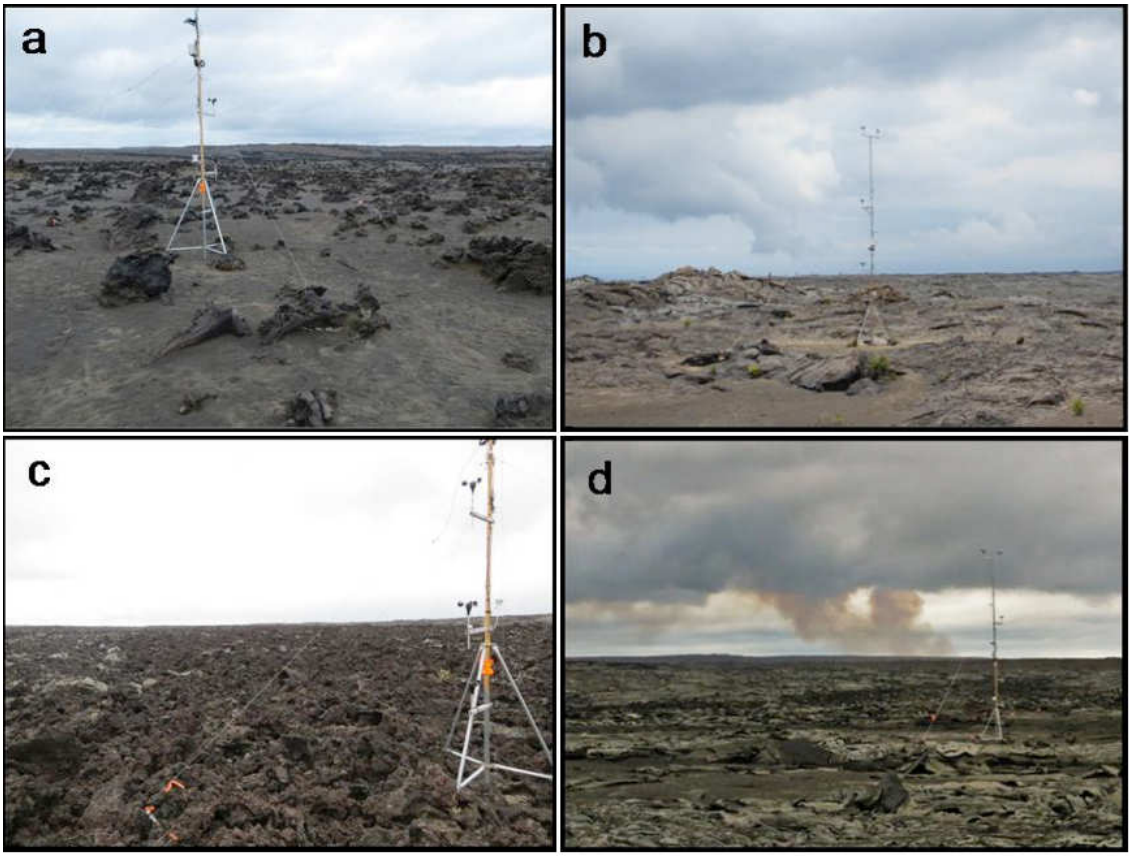

Fig. 2 Aerodynamic roughness measurement sites. (a) sediment-covered ʻaʻā, (b) tumuli field, (c) slabby pāhoehoe, (d) fresh ʻaʻā, (d) lava plates. Fresh ʻaʻā from **Fig 1e.** is not shown.

Fig. 3. Anemometer mast, instrumented with five anemometers, a wind vane, and temperature sensors at the top and bottom to measure atmospheric stability.

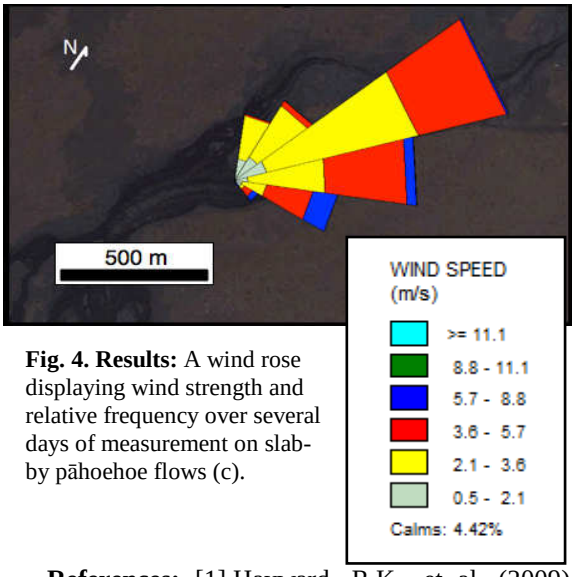

Fig. 4. Results: A wind rose displaying wind strength and relative frequency over several days of measurement on slabby pāhoehoe flows (c).

resulting logarithmic profiles, the aerodynamic roughness constant can be calculated as the height above the surface at which the wind's velocity goes to zero [3].

Acknowledgments: We would like to thank Patrick Whelley, Andy Ryan, Brent Garey, Cecilia Leung Lo, Ali Bramson, Tiffany Kataria, and especially Jodi Fox for assistance in the field.

References: [1] Hayward, R.K., et al. (2009) *JGR, 114*, E11012. [2] Lenoir, B. et al. (2011) *J. Atm. Oceanic Tech.*, 28, 210–218 [3] Bagnold, R.A. (1941) *The Physics of Blown Sand and Desert Dunes*. Dover Pub., NY. [4] Greeley, R., and Iversen, J.D. (1986) *Physics of Desertification*, 290–317. [5] Hébrard, E., et al. (2012) *JGR 117*, E04008.

AEOLIAN BEDFORMS ASSOCIATED WITH RADAR-DARK DIFFUSE FEATURES ON VENUS.
Mikhail A. Kreslavsky[1] and ***Nataliya V. Bondarenko***[1,2], [1]Earth and Planetary Sciences, University of California - Santa Cruz, 1156 High Street, Santa Cruz, CA, 95064, USA (nbondar@ucsc.edu; mkreslav@ucsc.edu), [2]IRE, NAS of Ukraine, 12 Ak.Proskury, Kharkov, 61085, Ukraine.

Introduction: Data about the surface of Venus are rather scarce. Magellan radar images with resolution ~120 m have revealed only two dune fields [1,2]. Indirect indications of small-scale, unresolved aeolian bedforms came from azimuthal anisotropy of radar backscattering. The only reasonable explanation for such anisotropy is unresolved decameter-scale asymmetric topography, and in many geological settings aeolian bedforms are the only possible explanation for such asymmetric topography. A few areas of strikingly strong anisotropy have been interpreted as dense fields of microdunes [1,2] with steep slip faces [3]. Two different radar remote sensing techniques show independently that weak backscattering anisotropy is ubiquitous [3-5]. This fact was interpreted as ubiquity of decameter-scale aeolian bedforms without steep slip faces and/or sparse surface coverage [3, 5]. Here we report on some typical geological settings where such deposits systematically do and do not occur, and discuss possible implications.

Areas of weak backscattering anisotropy associated with the extended crater-related features. Many craters on Venus have specific associated extended deposits; they appear as diffuse dark areas in Magellan radar images and are dubbed dark diffuse features (DDFs) [6]. They are thought to form by particulate material ejected by crater-forming impacts and slowly descending through the atmosphere [7]. There are two kinds of DDF planforms: parabolas and halos. Parabolas are forming due to transport of descending particles by superrotating atmosphere [7]. Halos were thought to be a result of degradation of older parabolas [8], although it cannot be completely excluded that the halos were formed during an epoch without the atmospheric superrotation.

We analyzed microwave (12 cm wavelength, Magellan data) remote sensing signatures related to DDF. The data included: (1) radar *images*, spatial distribution of radar cross-section under oblique radar incidence at moderately high spatial resolution (~120m); (2) microwave *emissivity* at low resolution (~10 km); (3) Hagfors' *roughness* parameter derived from nadir-looking radar altimeter echo; this parameter characterizes typical slopes at meter and longer baselines; (4) *Doppler centroid* shift of the radar altimeter echo [4,5] that quantifies asymmetry between north- and south-facing slopes at meter and longer baselines and thus characterizes the presence of asymmetric aeolian bedforms.

Although there are many individual peculiarities in microwave signatures of the largest and the most pronounced DDFs, there is prominent similarity schematically depicted in **Fig. 1**. There are two distinctive units associated with DDFs. Dark parabola or halo (unit **A**) is characterized by low radar cross-section (dark in radar images), low roughness, uniform microwave emissivity and zero Doppler centroid (isotropic meter-scale topography). Surrounding area (unit **B**) is characterized by regular radar-cross-section (the boundary with parabola is diffuse), regular or slightly decreased roughness, the same microwave emissivity as unit A, and consistently high Doppler centroid, typically positive in the N hemisphere and negative in the S hemisphere.

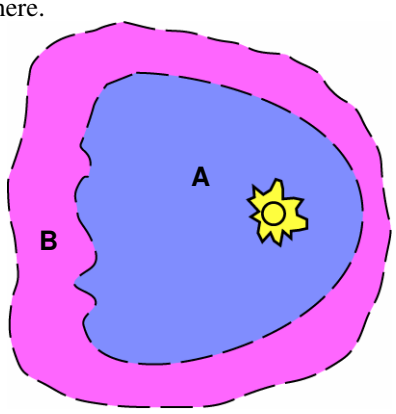

Fig.1

The remote sensing signature and diffuse boundary of unit A indicates that the surface of the deposit is flat, and particles forming the deposit are millimeters in size or smaller. The emissivity signature of unit B indicates that the surface is covered with the same material that forms unit A, but this cover is thinner (decimeters) [9].

The Doppler centroid signature indicates that unit B is covered with anisotropic aeolian bedforms, while unit A made of the same material and exposed to the same winds has flat surface.

Discussion. The density of the Venus' atmosphere is a factor of ~50 higher than terrestrial air density and a factor of ~15 lower than water density. In a sense, venusian air is more similar to water than to terrestrial air. Given that the gravity is very similar to terrestrial, it is reasonable to expect that aeolian bedforms on Venus are rather similar to terrestrial sub-aqueous deep water bedforms. Recently, the observed morphologies

of such bedforms have been systematically correlated against grain size and free-flow velocity [10]. **Fig. 2** is a result diagram from that work. Although classic barchan dunes do form under deep water, they occupy a very limited domain in the grain size - flow velocity space. Small gentle ripples with characteristic wavelength of centimeters and amplitude of millimeters are typical for sub-aqueous sand sheets. Such ripples would be indistinguishable from flat surfaces in microwave data.

Wind tunnel experiments with the same air density as on Venus [11] also revealed that microdunes are typical for only a small domain in the same parameter space. Therefore it is possible that saltation of sand-size particles on Venus do not produce bedforms with any distinguishable microwave signatures.

Thus, one of possible explanations for our observations is the following. Within unit A saltation does occur, the bedforms do form, however, they are too small and gentle to be indirectly detected with 12 cm wavelength remote observations. Within unit B decimeter-scale roughness elements protruding through smooth crater-related deposit cause bedforms to be taller, which results in the observed signature.

Another possible explanation is that all sand-size particles are already removed from unit A, and only well-sorted few-millimeter-size granules that are too large to be moved by saltation form the deposit. Time needed to remove all sand fraction from the deposit is scaled as $(H\,L)\,/\,(s\,f\,h\,v)$, where L ~ 100s km is a typical spatial scale of the DDF, H ~ 1 m is the sand thickness, v ~ 1 m/s is a typical saltation velocity, h ~ 2 mm is saltation height [12], $f << 1$ is a poorly constrained factor describing filling of the saltation layer with saltating particles, our terrestrial-experience-based guess is $f \sim 10^{-4}$, and $s \leq 1$ is a fraction of time, when winds exceed saltation threshold; for the dense atmosphere of slowly rotating Venus we assume stable winds and s ~ 1. These give ~1 Ma for the time scale of sand removal, which would mean that all DDFs except only a few may be already sand-free. A few DDFs with sand remaining are consistent with only a few DDFs having distinctive microdune signatures [2]. Under this scenario decimeter-scale topographic obstacles in unit B are responsible for catching sand and preserving bedforms.

If the bedforms in unit B were lee dunes (aka shadow dunes), the observed Doppler centroid signature would imply poleward dominant winds in both hemispheres, while the global wind streak pattern [1] is consistent with Hadley-cell-driven equatorward winds. This discrepancy requires some additional complications in both proposed explanations.

Reerences [1] Greeley R. et al. (1997) In *Venus II*, Univ. of Ariz. Press, 547– 590. [2] Weitz C. M. et al. (1994) *Icarus.,112,* 282–295. [3] Kreslavsky M. A. and Vdovichenko R. V. (1999) *Solar System Res.*, *33*, 110 – 119. [4] Tyler G. L.et al. (1992) *JGR*, *97*, 13115 – 13139. [5] Bondarenko N. V.et al. (2006) *JGR*, *109*, E09004. [6] Campbell D. B. et al. (1992) *JGR*, *97*, 16249. [7] Vervack R. J. and Melosh H. J. (1992) *GRL*, *19*, 525. [8] Basilevsky et al. (2004) *JGR*, *109*, E12003. [9] Bondarenko N V. and Head J. W. (2004) *JGR*, *109*, E09004. [10] Stow D.A.V. et al. (2009) *Geology*, *37*, 327. [11] Marshall J. R. and Greeley R. (1992) *JGR*, *97*, 1007. [12] Kok J. F. (2012) *Rep. Prog. Phys.*, *75*, 106901.

Fig.2

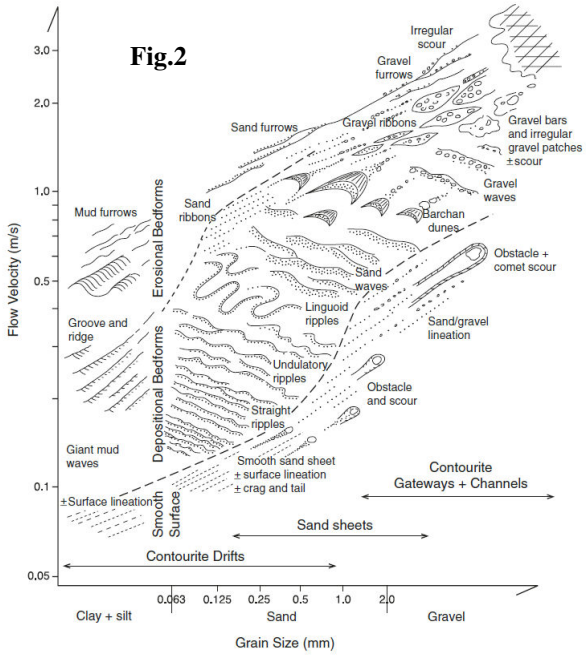

HEIGHTS OF FORTUNA-MESHKNET DUNES (AL-UZZA UNDAE), VENUS, FROM MAGELLAN RADARCLINOMETRY

R. D. Lorenz, Space Exploration Sector, Johns Hopkins University Applied Physics Laboratory, Laurel, MD 20723, USA. (Ralph.lorenz@jhuapl.edu).

Abstract

We apply radarclinometric methods, first used for dune height estimation on Titan with Cassini data, to archive Magellan imaging of dunes. Estimates of ~40m height are obtained, suggesting the dunes are not 'fully-grown' perhaps due to sand supply limitations. The need for new, higher-resolution radar observations on Venus is noted.

1. Introduction

As discussed in [1,2,3] Venus has relatively few known Aeolian bedforms, in part perhaps due to a lack of sand-sized particles, and in part due to the limited spatial resolution of Magellan data. In Venus' dense atmosphere, saltation speeds are rather low, and thus one might expect Aeolian features to be present. It has been suggested [4] that widespread areas have small unresolved bedforms ('microdunes'), indicated by anisotropy in radar backscatter.

There are two major dunefields known [1,2,3]. The most prominent dunes are perhaps those in the Algaonice dunefield (Menat Undae) at 25°S, 340°E cover some 1300 km^2 at the end of the ejecta outflow channel from the Algaonice impact crater. The dunes are 0.5-5km in length and are quite bright, likely because there are slip faces oriented towards the radar illumination, which was at an incidence of 35°**.** However, their shape is rather hard to determine and they are not considered further here.

The more northern dune field, Fortuna-Meshkenet, lies at 67°N, 91°E in a valley between Ishtar Terra and Meshkenet Tessera (the dunes are formally named Al-Uzza Undae). The dunes are 0.5-10km long, 0.2-0.5km wide and spaced by an average of 0.5km. They appear (figure 1) to be transverse dunes, in that there are several bright wind streaks visible in the region, which seem generally orthogonal to the dunes. Glints are not observed strongly on these dunes, although here the incidence angle of the radar observation was 22-25°.

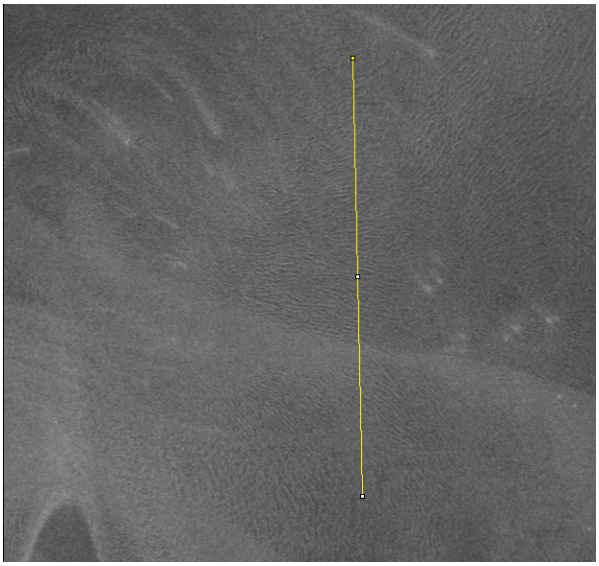

Figure 1. Dunes in the Fortuna dunefield (Al-Uzza Undae). Wind-streaks are prominent in the image, the dunes less so. Yellow line (36km long) is the profile examined in figures 2 and 3. Part of F-MIDR fr61n090.

2. Magellan Data

In contrast to typical Earth-observing radars, Magellan was in a highly elliptical orbit, and the range to Venus' surface, the incidence angle, and the image quality (SNR, resolution, etc.) are all functions of latitude (varying geometry is an even more prominent challenge for Cassini). Although the archive products are sampled at 75m spacing, the actual radar resolution at 25S is 135x120m (range x azimuth)with 7 looks and ~170x120m with 10 looks at 67N [5].

Examining the Muhleman function used to normalize the image, we find over the incidence angle range of interest, the backscatter variation with slope for 'typical Venus' is about 0.3 dB per degree. Thus we can convert the backscatter (fig.2) into a local slope estimate, and integrate along a profile to develop a height estimate. This approach was used to estimate the height of dunes on Titan when they were discovered [6], and has since been validated in Earth satellite observations of the Namib sand sea [7].

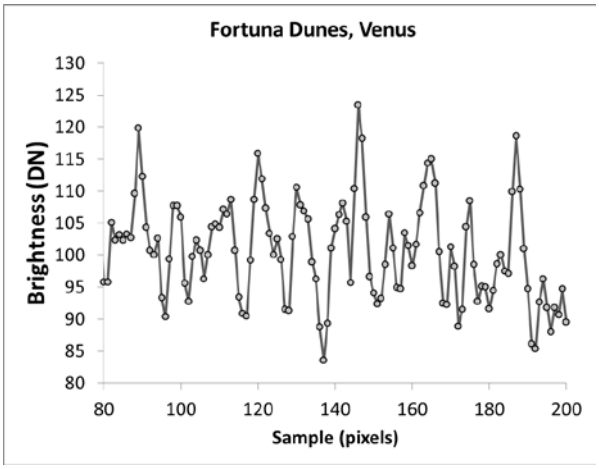

Figure 2. Magellan data product. The archived product is radar reflectivity relative to an assumed backscatter function

An example result is shown in figure 3. It can be seen that this small example has a dune wavelength of 1-1.5km and heights of 20-60m. (For comparison, Titan's dunes [6,7] have a spacing of 2-3km, and heights reaching 150m).

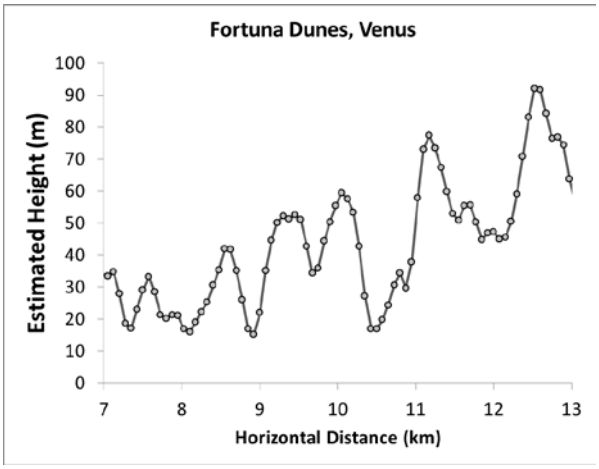

Figure 3. A radarclinometric profile.

3. Discussion

This aspect ratio (wavelength/height) of 20-50 is not as large as mature 'fully-grown' dunes which tend to reach ratios of about 12 [8,9], wherein the dune wavelength approaches the thickness of the atmospheric boundary layer. (We may note here that no in-situ measurements are presently available to define the thickness of the atmospheric boundary layer, but if maximum dune spacing is an indication, as it seems to be on Earth and Titan [8,9] , it may be 1~1.5km thick at this location.) It is possible the example shown does not capture the largest dunes in the field, but another interpretation is that these dunes are sand-supply-limited. That is of course consistent with Venus overall, where sediment-generating processes are suspected to be limited [2,3].

4. Conclusions

Clearly much work remains in the study of Venus dunes, but must await future radar observations with higher spatial resolution. Interferometric observations would be of interest to assess whether the dunes (or at least ripples/microdunes on them) are active. Although relatively comfortable for spacecraft landings, dunefields are unlikely to be prime targets for future missions (a question which might be reconsidered!). Future high-resolution in-situ temperature measurements during probe descents are also needed to define the atmospheric boundary layer thickness.

References: [1] Greeley, R.,et al, 1992. Aeolian Features on Venus: Preliminary Magellan results, Journal of Geophysical Research, 97, 13,319-13,345 [2] Weitz, C. M., J. I. Plaut, R. Greeley and R. S. Saunders, 1994. Dunes and Microdunes on Venus: Why were so few found in the Magellan Data?, Icarus, 112, 282-285. [3] Lorenz, R and J. Zimbelman, Dune Worlds, How Wind-Blown Sand Shapes Planetary Landscapes, Springer, 2014 [4]. Kreslavsky, M. A.; Vdovichenko, R. V. 1998,Microdunes on Venus: Are They Ubiquitous? 29th LPSC, 1998, Houston, TX, abstract no. 1166. [5] Pettengill, G. P. G. Ford, W. T. K. Johnson, R. K. Raney and L. A. Soderblom, 1991. Magellan: Radar Performance and Data Products, Science, 252, 260-265 [6] Lorenz et al. 2006. The Sand Seas of Titan : Cassini Radar observations of Longitudinal Dunes, Science, 312, 724-727, 2006 [7] Neish, C., R. Lorenz, R. Kirk and L. Wye, 2010. Radarclinometry of the sand seas of Africa's Namibia and Saturn's moon Titan, Icarus, 208, 385-394 [8] Andreotti, B., Fourriere, A., Ould-Kaddour, F., Murray, B., Claudin, P., 2009. Size ofgiant aeolian dunes limited by the average depth of the atmospheric boundary layer. Nature 457, 1120–1123. [9] Lorenz, R. D., P. Claudin, J. Radebaugh, T. Tokano and B. Andreotti, A 3km boundary layer on Titan indicated by Dune Spacing and Huygens Data, Icarus , 205, 719–721, 2010

Acknowledgements. This work was supported by the Applied Physics Laboratory.

Giant Linear Dunes as the Formation Pathway to Megabarchan Chains : Titan and the Rub 'Al Khali.

Ralph D. Lorenz[1] and Jani Radebaugh[2]. [1] Space Exploration Sector, JHU Applied Physics Laboratory, Laurel, MD 20723, USA. (Ralph.lorenz@jhuapl.edu) [2] Dept. Geological Sciences, Brigham Young University, Provo, UT, USA.

Introduction: The term megabarchans, referring to large crescentic forms, might be thought to suggest a link to common barchans. However, the spatial arrangement of megabarchans, such as those at Liwa in the United Arab Emirates (fig.1) is quite distinct from that found in barchan corridors, and the mechanism by which winds in a unidirectional regime might accumulate to such large sizes is not at all obvious.

Instead, we suggest that the accumulation to large size, and the regular arrangement of megabarchans, results from their prior formation as large linear dunes in a bidirectional wind regime, where the frequency or intensity of one of the wind directions has diminished.

In the case of the Liwa dunes, the growth as linears (which are seen to the west) results from the North-Westerly Shamal wind and the southerly monsoon. During the Last Glacial Maximum, the monsoon is thought to have penetrated further north than it presently does, so the central areas of the Arabian desert would have seen bimodal winds, whereas now they are more predominantly exposed to the Shamal. This more unidirectional flow results in the formation of slip faces on the southern flanks of the dunes, and a slow advance to the south.

We suggest [1,2] a similar evolution may be taking place on Titan where megabarchan forms have been noted [3] amid the equatorial sand seas of linear dunes.

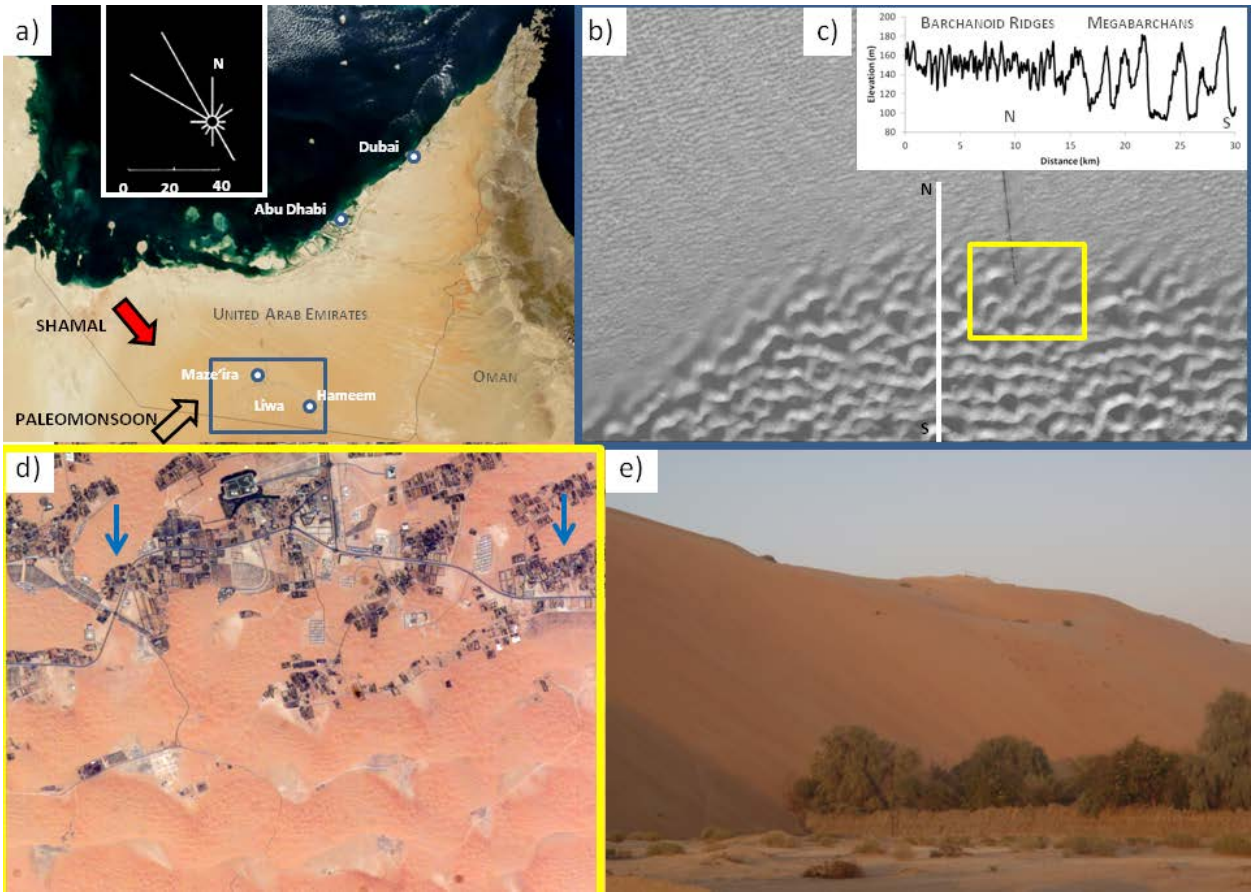

Figure 1. (a) Regional satellite image (MODIS) of the UAE : the oasis arc is visible inside the blue box which defines area in fig. 1b. Red arrow shows dominant Shamal winds which lead to observed Abu Dhabi wind rose in yellow box [Bristow]; open arrow denotes possible monsoon winds which were likely necessary to allow the Liwa megadunes to grow. (b) Enlarged area with ASTER topography showing the abrupt morphological transition from small ridges in the north to megabarchans in the south. (c) North-South ASTER profile (at white line in fig. 1b) showing transition and dune height. (d) Astronaut digital image of Mezeira region (yellow box in fig.1b) showing megabarchan geometry with sabkhas and oasis plantations between. Note the superposed small barchanoid forms, and the sharp edges of the plantations defined by the advancing dune slip faces (blue arrows). (e) ~20m megabarchan slipface (dune apex is rather higher but hidden here) advancing onto trees near Mez'eira.

2. Titan While linears are by far the predominant detectable duneform [1,2], recent denoised Cassini radar images [3, fig 2] show what appear to large crescentic dunes arranged in a linear trend, consistent with the E-W trend in the dunes overall [4]. This has been interpreted to indicate a change in wind regime. Morphologically these appear very similar to the Liwa megabarchans, which are also of a similar size.

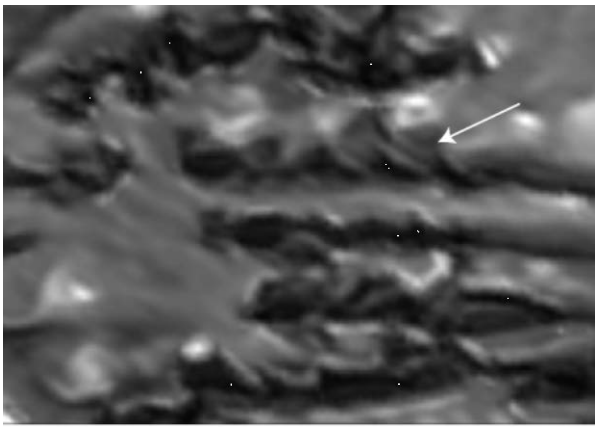

Figure 2. Crescent dunes on Titan (arrowed) from [3]. Dunes are 2-3km apart, a rather similar scale to those at Liwa

3. Morphodynamics at Liwa

To our knowledge, no estimate of the migration rate of the Liwa dunes has been published : since the dunes are large, they would be expected to be slow-moving. Even on high-resolution satellite images, movement is rather small and difficult to quantify, but field observation [1] suggests, from the overrunning of healthy date palms (fig. 1e), that a rate of~0.1 meter per year is about right. Given the ~50m slip face height (fig.1c), such a migration rate implies a sand transport rate of ~5 m3/m/yr (fig.3), somewhat consistent with estimates from the Resultant Drift Potential computed from wind data [1]. The transport is furthermore consistent with the migration of small dome and barchan dunes near the horns of the megabarchans [1.5]. It is perhaps not coincidental that the re-orientation timescale (~wavelength/migration rate) of 10-20,000 yrs coincides with the time since the wind regime may have changed.

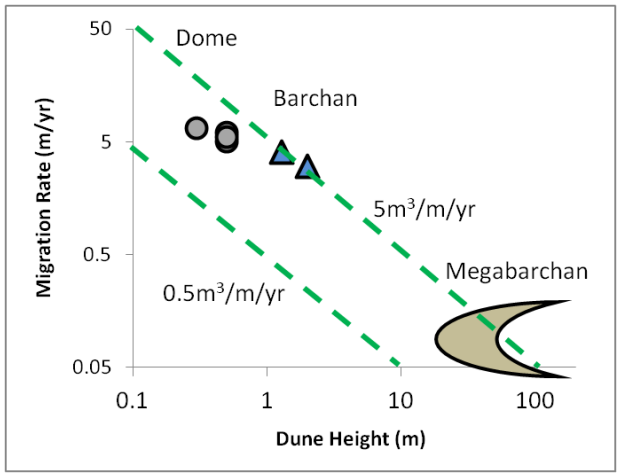

Figure 3. Migration rates of megabarchans and small dome and barchans at Liwa [1,5]

4. Implications

The availability of readily-studied analogs to Titan dunes allows these remarkable landforms to be better-understood. Not only do they serve to calibrate paleoclimate interpretations of Titan dune morphology, but the paradigm suggested here (that megabarchans are merely evolved linears) may have application on Earth. A worthwhile next step would be the exploration of this growth/re-orientation process with numerical models.

References :[1] Lorenz, R. and J. Radebaugh, Morphodynamics of the Liwa Megabarchans : Reworking of Giant Linear Dunes by Unidirectional Winds, GeoResJ, submitted [2] Radebaugh, J., R. Lorenz, T. Farr, P. Paillou, C. Savage, C. Spencer, Linear Dunes on Titan and Earth: Initial Remote Sensing Comparisons, Geomorphology, 121, 122-132, 2010 [3] Ewing, R., A. Hayes and A. Lucas, Sand Dune patterns on Titan controlled by long-term climate cycles, Nature Geoscience, DOI: 10.1038/NGEO2323 [4] Lorenz, R. D. and J. Radebaugh, Global Pattern of Titan's Dunes : Radar Survey from the Cassini Prime Mission, Geophysical Research Letters, 36, L03202 [5] Lorenz, R. and J. Zimbelman, Dune Worlds, Springer 2014

Acknowledgement: This work is supported by NASA Grant NNX13AH14G via the Cassini project.

The Tallest Dunes in the Solar System ? Dune Heights on Earth, Mars, Titan and Venus

Ralph D. Lorenz[1], Lori Fenton[2] and Nick Lancaster3 [1] Space Exploration Sector, JHU Applied Physics Laboratory, Laurel, MD 20723, USA. (Ralph.lorenz@jhuapl.edu) [2] SETI Institute, Mountain View, CA, USA. [3]Desert Research Institute, Reno, NV, USA.

Introduction

We initiated this study, to consider what are the tallest dunes on each planetary body, largely out of curiosity given that a somewhat unified perspective on dune morphology and its relationship to planetary circumstances has emerged [1,2]. However, the exercise raises interesting questions about sand supply and dune growth and ultimate limits on dune size. The search for a superlative is always a work in progress: we have attempted only a preliminary survey here and we welcome suggestions of yet larger dunes.

Mars

While Mars is often thought to be dune-covered (an impression reinforced by ripples and drifts commonly seen by rovers and landers), in fact the area coverage fraction of Mars by dunes is rather small, with most dunes, apart from the circumpolar Olympia Undae, confined in sand traps such as crater basins [3]. Dunes in some locations have been measured via stereo imaging, or in a few cases by laser altimetry, to be ~200m high, with most dunes only a few tens of meters tall (e.g. [3,4]). A prominent exception (Fig.1) is the large crescent-shaped dune in Russell Crater, which stereo data (Fig.2) shows to be 450m – 600m tall, depending on the assumed base level (a challenge common to estimating dune heights elsewhere).

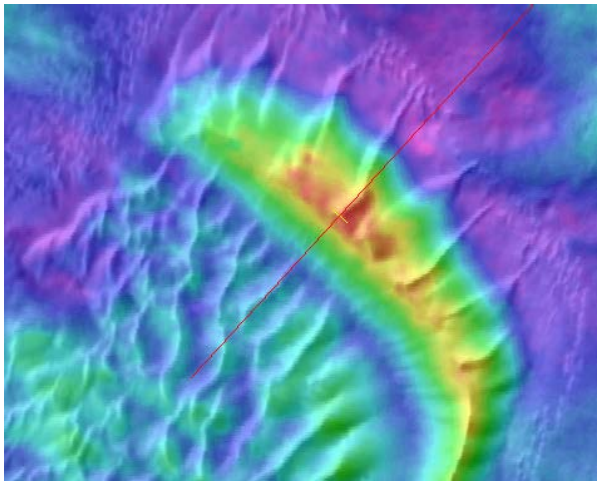

Figure 1. The tallest dune on Mars? A DEM (H2247_0000_DT4) of the large dune in Russell Crater acquired by HRSC superpimposed on a THEMIS daytime IR map. The red line denotes the profile in figure 2. Note that the base level is different on the two sides of the dune.

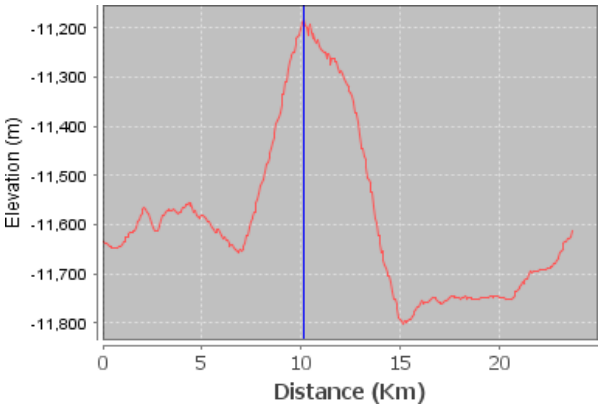

Figure 2. Topographic profile from figure 1, indicating a height of at least ~450m.

Titan

Titan is in fact the most dune-covered planetary body known [1,2] (roughly 15% of its land area is dune-covered, compared with ~2% for Earth), and the discovery of its giant equatorial fields of linear dunes was enabled by their large size, making them recognizable even in the rather coarse (~350m+) resolution radar data from Cassini [4]. Radarclinometry [5], altimetry, and near-infrared photoclinometry have been applied to Titan's dunes, but the tallest appear to be the first ones recognized, in the Belet sand sea. These have heights determined to be 100-175m tall.

Venus

Venus has very few dunes resolvable in Magellan data. Only recently [6] has one height determination been made, using radarclinometric methods. That sudy suggested the Fortuna-Meshkenet dunes (Al-Uzza Undae) may have heights of 40-80m.

Earth

The dunes on our own planet are likely to be the most contentious in terms of superlative claims: we report here only claims in the literature. As for Mars and elsewhere, it is important to distinguish between large free-standing dunes, dunes that mantle bedrock topography, and dunes that form large accumulations of sand (e.g. Great Sand Dunes, Colorado), which have a thickness of 100-180 m [7].

Dunes (mostly of complex linear form) with a height of 150 – 200 m are widespread in sand seas in Namibia and Arabia. Much larger dunes (height > 200 m) are commonly of complex star or reversing form and ap-

pear to be associated with areas of multi-directional and/or opposed wind directions, as well as topographic obstacles. Such dunes are common in the Lut Sand Sea of Iran [8], Grand Erg Oriental, Issaouane-N-Irarraren, and other northern Saharan sand seas.

Dunes with a height of 300 – 400 m are known from the Sossus Vlei area of the Namib Sand Sea [9]; the Badain Jaran sand sea of China [10] and the small Erg Guidi and Erg Tihodaine in the central Sahara [11].

Dunes exceeding 400 m height have been identified in the Badain Jaran [10]; the Grand Erg Oriental [12] and Issaouane-N-Irarraren of Algeria [11]. These appear to be the tallest dunes reported on Earth: the global topography datasets from SRTM and ASTER would now permit a systematic survey.

Implications:

It has been suggested [14] that dunes may grow until they reach a height of ~H/12, where H is the thickness of the planetary boundary layer (PBL): coincidentally, the dune spacing then tends to ~H. At this point, the flow over the dune becomes constricted (much like at an obstacle in shallow water) and the shear at the crest suppresses further growth. This concept appears to describe the Namib sand sea, where the PBL grows from ~300m near the coast to ~3km inland: it is possible that the PBL thickness may be higher in continental interiors, especially at the somewhat high elevations of the Badain Jaran . This PBL thickness argument appears to be consistent with dune heights on Titan [15]. The Venus PBL has not been characterized – it may be that dune heights can at least establish a lower limit on its depth. On Mars, the PBL can be 10km thick, allowing (in principle) dunes some ~1km high, but none near this size are observed. Presumably either there is simply not enough sand, or the winds have not operated in a constant regime for long enough to allow sand accumulation at this scale. On Earth, and perhaps Titan too [16], large (100m+) dunes retain some memory of the last Croll-Milankovich climate cycle: 400m+ dunes on Mars require longer than a ~100kyr cyle to grow.

Conclusions: Mars appears to have the tallest dune known (~450-600m), consistent with it also having the thickest PBL, although most Martian dunes are much smaller, either due to local PBL suppression [17], or due to incomplete growth since climate cycles established the present wind regime, or to limited sand supply. The largest terrestrial dunes appear to be about 400m tall. Titan's dunes appear to have a mature pattern, with few dislocations, suggesting they may have reached a limiting height of ~175m, although the Titan heights have not been widely-surveyed. Venus' sparse dunes have only been measured to be 40-80m: in all probability, the same issue that limits the number of dunes on Venus (restricted sand supply) may also limit their height. The simple-sounding question posed in the title of this abstract illuminates interesting differences between dune worlds.

References :[1] Fenton, L. K., et al., Extraterrestrial Aeolian Landscapes, in Treatise on Geomorphology, pp.287-312 in vol. 11 Aeolian Geomorphology, pp, edited by J. Shroder et al., Elsevier, 2013 [2] Lorenz, R. and J. Zimbelman, Dune Worlds, Springer 2014 [3] Hayward, R. K., L. K. Fenton, and T. N. Titus (2014), Mars Global Digital Dune Database (MGD3): Global dune distribution and wind pattern observations, Icarus, 230, 38–46, [4] Bourke, M. C., et al. (2006), A comparison of methods used to estimate the height of sand dunes on Mars, Geomorphology, 81(3-4), 440–452 [5] Lorenz, R. D. et al., The Sand Seas of Titan : Cassini RADAR observations of Longitudinal Dunes, Science, 312, 724-727, 2006 [6] Neish, C. D. et al., Radarclinometry of the sand seas of Namibia and Saturn's Moon Titan, Icarus, 208, 385-394, 2011 [7] Lorenz, this meeting [8] Andrews, S., 1981. Sedimentology of Great Sand Dunes, Colorado. In: F.P. Ethridge, R.M. Flores (Eds.), Recent and Ancient Non Marine Depositional Environments: models for exploration. The Society of Economic Paleontologists and Mineralogists, Tulsa, OK, pp. 279-291. [9] Gabriel, A., 1938. The Southern Lut and Iranian Baluchistan. The Geographical Journal, 92(3), 193-208. [10] Lancaster, N., 1989. The Namib Sand Sea: Dune forms, processes, and sediments. A.A. Balkema, Rotterdam. [11] Yang, X. et al. , 2011. Formation of the highest sand dunes on Earth. Geomorphology, 135, 108-116. [12] Wilson, I.G., 1973. Ergs. Sedimentary Geology, 10, 77-106. [13] Mainguet, M., Chemin, M.-C., 1984. Les dunes pyramidales du Grand Erg Oriental. Travaux de l'Institut de Géographie de Reims, 59-60, 49-60. [14] Andreotti, B., et al (2009), Giant aeolian dune size determined by the average depth of the atmospheric boundary layer., *Nature*, *457*(7233), 1120–3 [15] Lorenz, R. D.,et al (2010), A 3km atmospheric boundary layer on Titan indicated by dune spacing and Huygens data, *Icarus*, *205*(2), 719–721 [15] Hinson, D. P. et al., (2008), The depth of the convective boundary layer on Mars, *Icarus*, *198*(1), 57–66, , [16] Ewing, R. C., Hayes, A. G., & Lucas, A. (2015). Sand dune patterns on Titan controlled by long-term climate cycles. Nature Geoscience, 8(1), 15-19. [17] Tyler, D., and J. R. Barnes (2013), Mesoscale Modeling of the Circulation in the Gale Crater Region : An Investigation into the Complex Forcing of Convective Boundary Layer Depths, Mars, 8, 58–77

Acknowledgement: This work is supported in part by NASA Grant NNX13AH14G via the Cassini project.

ESTIMATION OF SAND FLUX FROM LINEAR DUNES USING HIGH-PRECISION SATELLITE MEASUREMENTS AND NUMERICAL MODELLING. A. Lucas[1], C. Narteau[2], S. Rodriguez[1], S. Courrech du Pont[3], O. Rozier[2], A. Spiga[4], Y. Callot[5], A. Garcia[1]. [1]AIM, LADP, Université Paris-Diderot, CEA-Saclay, Gif/Yvette, France (dralucas@astrogeophysx.net), [2]IPGP, Sorbonne Paris Cité, Université Paris Diderot, [3]MSC, Sorbonne Paris Cité, Université Paris Diderot, [4]LMD, IPSL, UPMC, Paris, France, [5]Archéorient, Université Lumière Lyon 2, France.

Introduction: Although linear dunes are the most common dune type on Earth and Mars [5], estimation of sand flux relies essentially on the migration speed of barchan dunes [1–4]. In addition to problems associated to multi-directional winds, this is mainly due to the lack of a complete understanding regarding linear dune growth, either by extension of lateral migration [6, 7]. In a topographic induced dune field on Earth, we present here high-resolution satellite imagery analysis in order to assess sand fluxes at the crest of linear dunes. We will then discuss the implication in terms of landscape dynamics and climatic conditions that occur at present day in different places of the Solar System including Mars and to some extent Titan, the largest Saturn's moon.

Methodology: High-resolution aerial and/or satellite imagery allow assessing the planetary dune morphodynamics over time at length scales of dune fields. If these images have been extensively used on Mars [8], they have not been fully exploited on Earth. To tackle this problem, stereo acquisitions have been used to retrieve by photogrammetry the morphologies of linear dunes in remote places of Niger with a precision of 0.7 m. Using temporal sequences of images, sediment fluxes can then be derived from dune growth using the precise shape of dunes. We compare these new measurements with the growth rate predicted by [9] accounting for local wind measurements and/or the output of global atmospheric reanalysis models. In addition, we introduce similar flow conditions in numerical simulations to investigate the conditions under which these linear dunes may nucleate and develop.

Results: Accounting for more than 50 years of observations in the erg of Fachi-Bilma (Ténéré desert, Niger), we demonstrate that linear dunes elongate in the direction of the resultant sand flux with no lateral migration. Extending away from topographic obstacles in a zone of low sediment availability experiencing bimodal winds conditions, these finger-like structures are ideal to isolate for quantifying sand flux parallel to the crests [9]. From the pure elongation of linear dunes in the field (Figure 1) and the fine dune shape derived from the high-resolution satellite imagery, we can also estimate the loss of sediment at the dune tip as well as the sand flux in the inter-dune area. In addition, our numerical simulations show how deposition downstream of any topographic obstacles (hills, vegetation…) provides the fix source of sediment that stabilizes the dune (Figure 2). The whole evolution sequence is identified from nucleation to silk's segmentation and barchan ejection.

Discussion and conclusion: Together with sand fluxes perpendicular to the barchan dune crests, this study indicates that sediment flux parallel to the crest of linear dunes can now be used to infer the local wind regimes. We started to apply this methodology on Mars as well as on Titan accounting for the available data set and GCM predictions [10]. We will discuss the implied sediment fluxes and their implications concerning changes in climatic forcing and landscape dynamics.

References: [1] Long & Sharp, (1964), *Geophys. Soc. America, 75, 149–169.* [2] Hastenrath (1967), *Zeitschrift fur Geomorphologie, 11, 300–331.* [3] Ahmedou et al., (2007), *J. Geophys. Res. 112.* [4] Elbelrhiti et al., (2008), *J. Geophys. Res. 113.* [5] Livingstone & Warren (1996), *Aeolian geomophology.* [6] Tsoar et al, (2004), *Geomorphology 57,293–302*. [7] Telfer, (2011) *Earth Surface Processes and Landforms, 36, 1125–1135*. [8] Bridges et al., (2012) Nature, *485, 339*. [9] Courrech du Pont S. (2014), *Geology, 42, no. 9, 743-746*. [10] Lucas et al. (2014), *Geophys. Res. Lett., 41.*

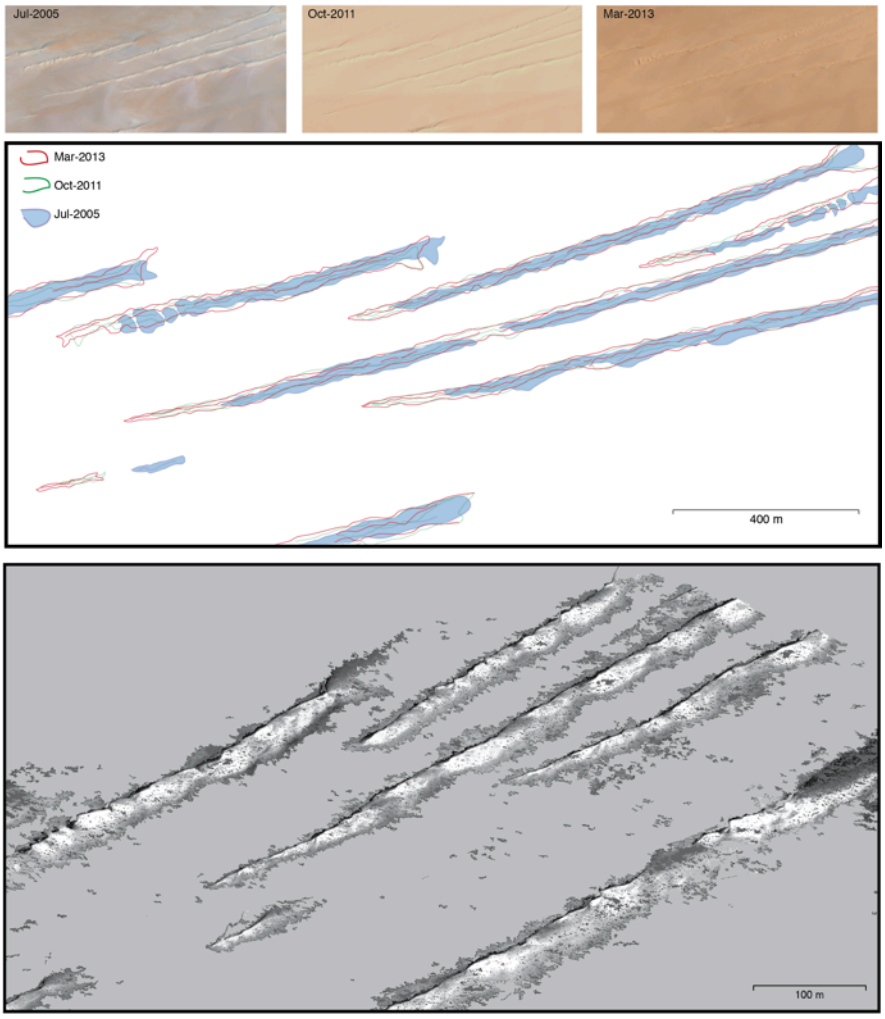

Figure 1 – (Top) High-resolution optical imagery (from Global View) from July 2005 to March 2013 over linear dunes observed in the Fachi-Bilma Erg, Niger. (Middle) Mapping of the elongation of the linear dunes. (Bottom) Perspective view of a 3D point cloud textured and derived from a Pleiades stereo pair.

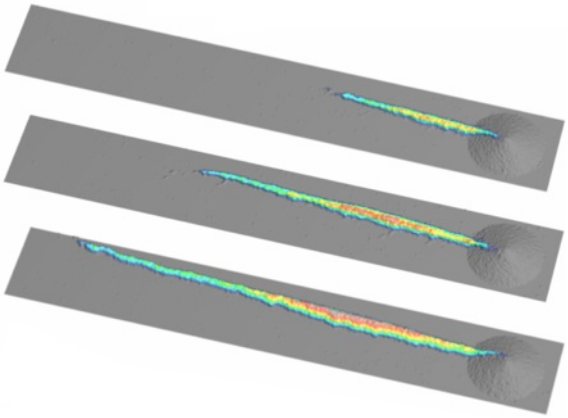

Figure 2 – Morphodynamics of finger dunes away from a topographic obstacle using numerical model and a bimodal wind regime.

GROWTH MECHANISM AND DUNE ORIENTATION ON TITAN. A. Lucas[1], S. Rodriguez[1], C. Narteau[2], B. Charnay[3], S. Courrech du Pont[4], T. Tokano[5], A. Garcia[1], M. Thiriet[1], A.G. Hayes[6], R.D. Lorenz[7] and O. Aharonson[8].

[1] Laboratoire AIM - Université Paris 7, Planetology, Gif/Yvette, France (sebastien.rodriguez@cea.fr), [2] Institut de Physique du Globe de Paris, Sorbonne Paris Cité, University Paris Diderot, UMR 7154 CNRS, Paris, France, [3] LMD IPSL, Paris, France, [4] Laboratoire Matière et Systèmes Complexes, Sorbonne Paris Cité, Université Paris Diderot, CNRS UMR 7057, Paris, France, [5] Institut für Geophysik und Meteorologie Universität zu Köln, Cologne, Germany, [6] Astronomy Division, Cornell University, Ithaca, New York, USA, [7] Johns Hopkins University Applied Physics Lab, Laurel, Maryland, USA, [8] Weizmann Institute of Science, Rehovot, Israel.

Dune fields on Titan cover more than 17 % of the moon's surface, constituting the largest known surface reservoir of organics [1,2]. Their confinement to the equatorial belt, shape, and eastward direction of propagation offer crucial information regarding both the wind regime and sediment supply.

Herein, we present a comprehensive analysis of Titan's dune orientations [3] using automated detection techniques on non-local denoised Cassini radar images [4]. By coupling a new dune growth mechanism [5] with actual wind fields generated by climate modelling [6], we find that Titan's dunes grow by elongation on a non-mobile substratum.

To be fully consistent with both the local crestline orientations and the eastward propagation of Titan's dunes, the sediment should be predominantly transported by strong eastward winds, most likely generated by equinoctial storms [6] or occasional fast westerly gusts [7].

Additionally, convergence of the meridional transport predicted in models can explain why Titan's dunes are confined within plus or minus 30° latitudes, where sediment fluxes converge.

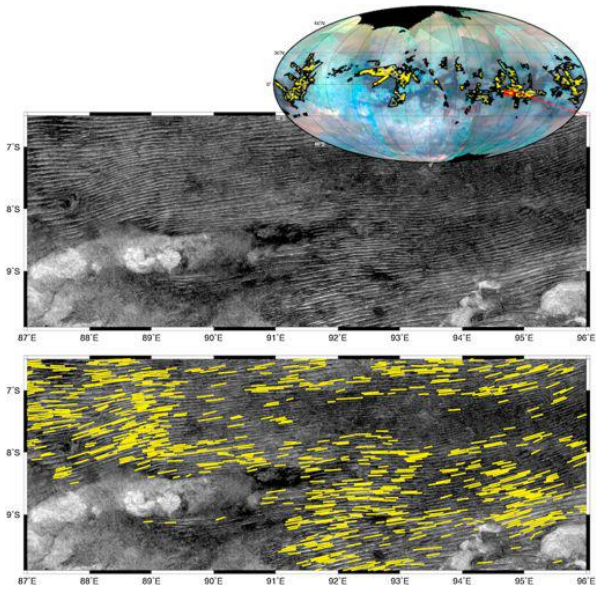

Figure: Linear segment detection over Titan's dune fields. (Inset) Visual and infrared mapping spectrometer (VIMS) global map with extracted segments in yellow. Black polygons contour the dune fields mapped from SAR images (including TA through T92). The red box indicates the location of the close-up of NLDSAR release of T8 shown below with and without the segment overlays (yellow lines). Note that as dunes can extend in some cases hundreds of kilometers continuously, they can incorporate multiple individual segments.

References: [1] Lorenz R.D. et al. (2006), *Science, 312, 724–727*. [2] Rodriguez S. et al. (2014), *Icarus, 230, 168–179*. [3] Lucas et al. (2014), *Geophys. Res. Lett., 41, doi:10.1002/2014GL060971*. [4] Lucas et al. (2014), *J. Geoph. Res.: Planets, 119, Issue 10, 2149–2166*. [5] Courrech du Pont S. (2014), *Geology, 42, no. 9, 743-746*. [6] Charnay et al. (2015), *Nat. Geosci., in press*. [7] Tokano et al. (2012), *Aeolian Res., 2(2-3), 113–127*.

Raked Linear Dunes as An Example of The Coexistence of Two Modes of Crest Orientation. P. Lv [1], C. Narteau[2], and Z. B. Dong[1], [1] Key Laboratory of Desert and Desertification, Cold and Arid Regions Environmental and Engineering Research Institute, Chinese Academy of Sciences, 320 West Donggang Road, Lanzhou, 730000, Gansu, China (lvping@lzb.ac.cn), [2]Institut de Physique du Globe de Paris, Sorbonne Paris Cité, Univ Paris Diderot, UMR 7154 CNRS, 1 rue Jussieu, 75238, Paris Cedex 05, France (narteau@ipgp.fr).

Raked linear dunes exhibit a marked asymmetry with a perpendicular pattern of secondary ridges on one side and a smooth sinuous slope on the other. Although these dunes occur in multidirectional wind regimes, they resemble barchans connecting to each other with the same arm. Here we show that this specific dune morphology results from the coexistence of two dune growth mechanisms. The main linear ridges result from the extension of a finger dune in the mean sand flux direction. Secondary ridges are superimposed bedforms associated to the development of a transverse bed instability. These two modes for dune orientation are not perfectly perpendicular and the bed instability grows preferentially on the leeward side of the linear dune according to the prevailing wind direction. This explains the asymmetry as well as the relationship between the crest-to-crest wavelength of the secondary ridges and dune height. All these characteristics are observed and measured in modern sand seas but also in a numerical model to analyze the influence of sand availability, the period of wind directionality and wind strength**.**

THE LAKE-DUNE CONNECTION: INVESTIGATING TITAN'S SAND SOURCES.

S.M. MacKenzie[1] and J. W. Barnes[1], [1]University of Idaho Department of Physics

Abstract: Titan, Saturn's largest moon, is host to a sand sea in its equatorial region (between 30° N to 30° S). This indeed seems to be a global sea as corridors connect sandy regions across almost all longitudes, interrupted only by Xanadu [1]. The predominantly linear dunes that make up the sand sea have been spatially resolved by the Huygens probe [2], Cassini's Visual and Infrared Mapping Spectrometer [3], and, more extensively, the RADAR mapper [e.g. 4-7]. Theoretical calculations [8] and recent wind-tunnel experiments [9] estimate typical sand sizes based on saltation thresholds necessary to create Titanian dunes to be a few hundred microns.

If the sand material is organic (indicated by the water-ice poor infrared spectra described in [3] and microwave properties described in [10]) and the source of such organic material is a gentle haze fall out of particles a few microns in size [11], then the question remains: how do sand particles become large enough to saltate? By considering sand formation mechanisms observed here on Earth, [1] summarized several hypotheses for production of sand on Titan. In this work, we investigate the feasibility of two of the proposed origin stories for Titan's sand: flocculation and evaporite formation.

In the flocculation scenario, organic particles in a turbulent Titan sea or lake could conglomerate under the frequent interactions driven by moving substrate to form larger and larger clusters. If the liquid is subsequently removed, the clumps would be left behind, free to saltate.

Evaporite, on the other hand, is created when organics in solution precipitate out when the liquid is removed via evaporation. On Earth, the resulting deposits can form at a variety of scales, but erosion or redissolution/deposition cycles can either break down material that is too large or too small to saltate. Figure 1 (from Figure 2 of [1]) shows a satellite view of White Sands New Mexico where gypsum evaporite from Lake Lucero makes up the white dunes.

In both scenarios, it may be difficult to move sand produced at polar lakes or seas to the equatorial region as the sand would be travelling not only a long distance, but uphill. We thus also explore the equatorial basins of Tui and Hotei (shown in Figure 2) as potential sites of either production process as they have been proposed to be fossil seas by [12, 13].

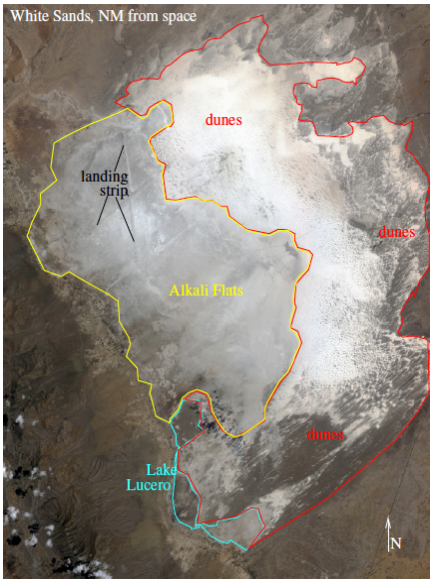

Figure 1: Lake Lucero and the white sand dunes made up of its gypsum evaporite (from Figure 2 of [1]).

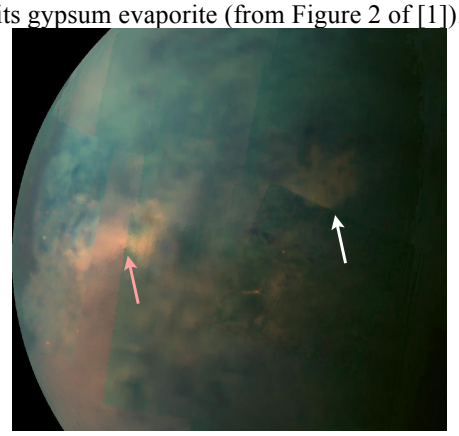

Figure 2: Tui (pink arrow) and Hotei (white arrow) Regio, proposed fossil-seas of Titan's equatorial region, as seen by VIMS in T49.

References: [1] Barnes, J.W. et al. in press *Planetary Science* [2] Lunine, J.I. et al. (2008) *Icarus* 195, 414-433 [3] Barnes J.W. et al. (2008) *Icarus*, 195:400 [4] Lorenz R.D. et al. (2006) *Science*, 312:724-727 [5] Radebaugh J. et al. (2008) *Icarus*, 194:690-703 [6] Neish, C.D. et al. (2010) *Icarus*, 208, 385-394 [7] Lavas, A. et al. (2014) *JGR Planets,* 119, 2149 [8] Lorenz R.D. (2014) *Icarus*, 230:162-167 [9] Burr D.M. et al. (2015) *Nature*, 517:60-63 [10] Le Gall A. et al. (2011) *Icarus*, 213:608-624 [11] Tomasko M.G. et al. (2008) *Planet. Space Sci.*, 56:669-707 [12] Moore J.M. and Howard A.D. (2010) *Geophys. Res. Lett.*, 37:L22205 [13] MacKenzie S. M. et al. (2014) *Icarus* 243, 191–20

A TALE OF TWO WIND PARADIGMS: UNRAVELING A PARADOX IN MERIDIANI PLANUM, MARS.
T. I. Michaels[1] and L. K. Fenton[1], [1]SETI Institute, Mountain View, California, USA (tmichaels@seti.org).

Introduction: Meridiani Planum has been a focus of Mars research since at least the late 1990s when the Thermal Emission Spectrometer (TES; on the Mars Global Surveyor spacecraft) found a strong hematite signature there. It was rigorously vetted as a Mars Exploration Rover (MER) landing site using the Mars Orbiter Camera (MOC), the Thermal Emission Imaging System (THEMIS), and other instruments. In 2004 the MER Opportunity began its *in situ* exploration of a small portion of the region (that continues to this day). More recently, imagery from the High Resolution Imaging Science Experiment (HiRISE) and the Context Camera (CTX) aboard the Mars Reconnaissance Orbiter has greatly added to our ability to both perceive details and detect change on the surface.

Evidence for present-day aeolian activity within Meridiani Planum was observed by the MER Opportunity in the form of the deposition and erosion of basaltic sand in a dark streak at Victoria Crater [1]. Further such evidence from orbit was discovered in very high-resolution imagery (HiRISE, CTX, and/or MOC Narrow-Angle) of Endeavour crater, the current location of the Opportunity rover [2,3]. Present-day aeolian transport has also been detected elsewhere in and near Meridiani Planum, *e.g.*, [4,5,6].

Observationally-Inferred Wind Paradigms: The morphology and migration of intracrater large dark dunes (LDDs) implies net sand transport towards the southeast by NW winds (*e.g.*, [2,3,6]; see Fig. 1). However, these observations lie in stark contrast to dark sand transport on the plains. Orientations of dark streaks indicate that transport of dark sand from small craters (diameter <200 m) in Meridiani Planum is currently dominated by a SE wind (*e.g.*, [6]; see Fig. 2). Many craters smaller than a few kilometers in diameter have dark sand accumulations on the north side of the crater floor, which often appears to be a source of the dark streaks (*e.g.*, [1]). Although this SE wind does blow sand off the Endeavour crater dunes during southern hemisphere winter (L_s=85-180°), it does not influence migration rates of larger dunes or dominate dune morphology [3].

Paradox: In this limited region, winds with a significant northerly component dominate the LDD morphology (within larger craters), while winds with a significant southerly component dominate aeolian processes in the wake of smaller craters (diameter <~3 km). How can one reconcile the presence of opposing dominant winds in a tropical region of Mars, both of which are known to be currently moving sediment, but that appear to significantly act only on separate features and/or scales?

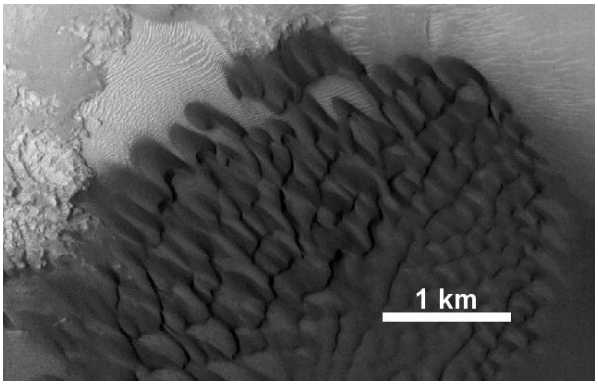

Figure 1. Barchans and barchanoid dunes in Bopolu crater. The morphology and migration of Meridiani Planum intracrater LDDs is dominated by a NW wind.

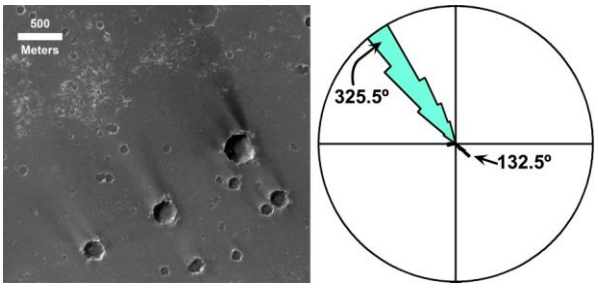

Figure 2. Dark sand streaks and their measured orientations in Meridiani Planum, most of which were formed by a SE wind (from [6]).

Towards Understanding: Does the key to understanding this riddle lie in a crater's dimensions (and implicitly, its particular interaction with winds)? A crater depth-to-diameter ratio (d/D) dependence on the placement (relative to the inferred formative wind) of intracrater sand accumulations was determined by [7]. However, in central Meridiani Planum (at least) that dependence is only partially consistent with observed intracrater features [6]. Perhaps [7] implicitly assumed a simplified interaction with the atmosphere versus what is occurring in Meridiani Planum?

MRAMS [8,9,10] mesoscale atmospheric modeling of Meridiani Planum has previously been performed at lower spatial resolutions (and only 4 seasons) [2] and now at higher spatial (<1 km, resolving the larger craters) and seasonal resolution (12 seasons). Figure 3 (resampled to ~2 km gridspacing for better clarity) illustrates that the larger craters (larger than few km in

diameter) selectively enhance the northerly winds, apparently to magnitudes that do significant aeolian work. This was pointed out for Endeavour crater in [2], but new model results suggest that it holds for all larger craters in the region. The simple assumption that the winds are relatively uniform (speed and direction) everywhere in the region (both on the plains *and* inside craters) appears to be invalid within Meridiani Planum.

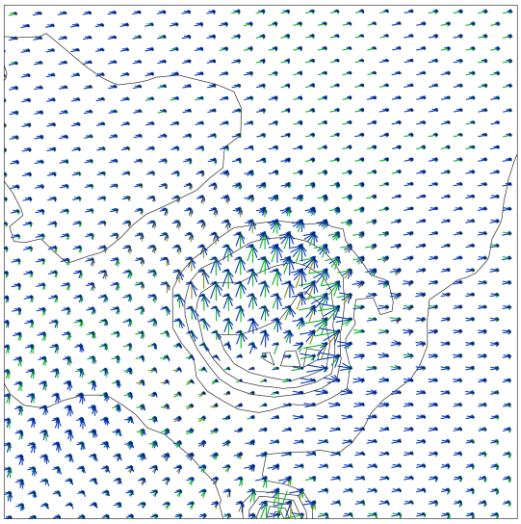

Figure 3: Example MRAMS results for Endeavour Crater (center) and its immediate surroundings (bottom: Iazu crater) at L_s~240°. Model topography (black contours) with each impulse representing winds in one of 20 equally-spaced directions at each gridpoint during each sol (length = maximum daily wind speed, color = relative frequency of that wind direction). Note that the strong (northerly) winds only appear to occur inside the craters.

Broader Implications: Topographic interactions with the atmosphere/wind are often of the "obstacle" variety (quasi-2D and fairly intuitive), but more complex interactions exist (3D and much less intuitive) that likely occur on Mars (*e.g.*, in the larger craters of Meridiani Planum). Future use of aeolian features/change as remotely-determined "wind vanes" should not summarily assume that a wind speed or magnitude in a local topographic region (such as a crater or plain) can be accurately extrapolated outside those features. Inferring a broad regional wind that affects all "non-sheltered" sand regardless of its topographic (and therefore wind-modulating) context is unwise. It may coincidentally work in certain locations on Mars, but not for locales with more subtle and/or complex wind regimes.

Acknowledgements: This research was supported by NASA MDAP grant NNX13AK68G.

References:

[1] Geissler P. et al. (2008) *JGR, 113,* E12S31. [2] Chojnacki M. et al. (2011) *JGR*, *116*, E003675. [3] Chojnacki M. et al. (2014) *Icarus*, in press, doi:10.1016/j.icarus.2014.04.044 [4] Silvestro S. et al. (2011) *GRL*, *38*, doi:10.1029/2011GL048955 [5] Geissler P. et al. (2012) *Earth Surf. Process. Landforms*, doi:10.1002/esp.3331 [6] Fenton L. et al. (2015) *Aeolian Res.*, *16*, 75-99, doi:10.1016/j.aeolia.2014.11.04 [7] Kienenberger R. and Greeley R. (2012) *Plan. Space Sci.*, *68*, 25-33. [8] Rafkin et al. (2001) *Icarus, 151*, 228-256. [9] Michaels T. and Rafkin S. (2008) *J. Geophys. Res.*, *113*, doi:10.1029/2007JE003013

Boundary conditions and the aeolian sediment state of the Olympia Undae Dune Field, Mars. W. Middlebrook[1], R.C. Ewing[1], F. Ayoub[2], N. T. Bridges[3], I. Smith[4], A. Spiga[5]. [1]Texas A&M University, 3115 TAMU, College Station, TX 77843 (rce@tamu.edu), [2] California Institute of Technology, Pasadena, CA 91125; [3]Johns Hopkins Applied Physics Laboratory, Laurel, MD 20723), [4]Southwest Research Institute, Boulder, CO, [5]Laboratoire de Meteorologie Dynamique, Paris, France.

Introduction: The dominant geomorphic process on Mars today is the transport of particles by wind, which exerts a primary control on planetary resurfacing rates. Detemining sediment fluxes is a primary means to constrain these rates. In the equatorial region of Mars, sediment fluxes comparable to those on Earth have been measured over barchan dunes [1]. However, as on Earth, sediment fluxes should vary with environmental boundary conditions, such as sediment supply, sediment availability and wind transport capacity [2, 3]. In the north polar region of Mars within the Olympia Undae Dune Field, for example, seasonally varying CO_2 frost covers the dune fields for part of the year. Are fluxes in the north polar region of Mars similar to those in the equatorial regions? What boundary conditions affect sand transport in the polar region of Mars? How do these boundary conditions vary spatially and temporally?

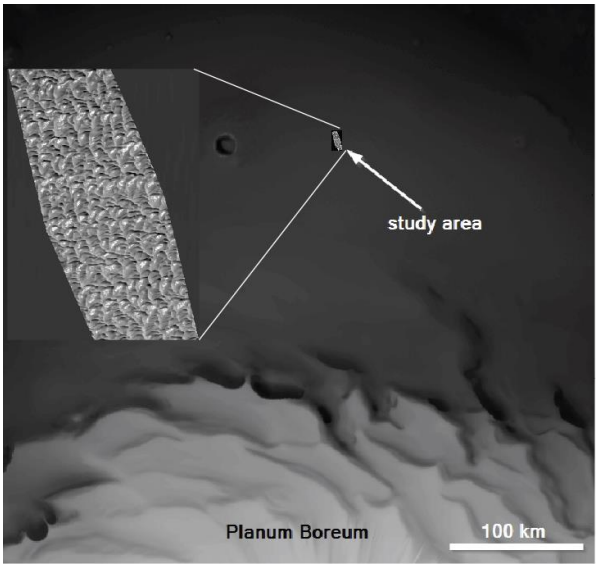

Figure 1. Study area in Olympia Undae

Here we evaluate the boundary conditions in Olympia Undae that affect sand flux. We document variations in seasonal CO_2 cover on dune field patterns, map two and three dimensional dune parameters from two locations proximal and distal to Planum Boreum and constrain sediment fluxes. We compare our results with a mesoscale atmospheric model in order show how topographic driven winds and seasonal variability in wind patterns influence dunes mobility. We develop a sediment state model for Olympia Undae for annual changes in sediment supply, sediment availability and wind transport capacity.

Methods: Repeated High Resolution Imaging Science Experiment (HiRISE) images and digital terrain models (DTMs) were used from two locations to study seasonal changes in the dune field patterns. Two and three dimensional dune parameters such as crest length, crest spacing, dune height and meter-scale slope were measured using the DTMs. Repeated imagery was processed using Co-registration of Optically Sensed Images and Correlation (COSI-Corr)[4], which uses sub-pixel image correlation to measure horizontal surface displacements. Ripple displacement is tracked by this method and provides a measure of sediment flux [1] (Fig. 2). Where dune migration could be measured, flux measurements were constrained by mapping crest line migration. Mesoscale atmospheric model simulations were run at resolutions of 18 km per grid point for three days every 5° or 10° of L_s with increased fre-

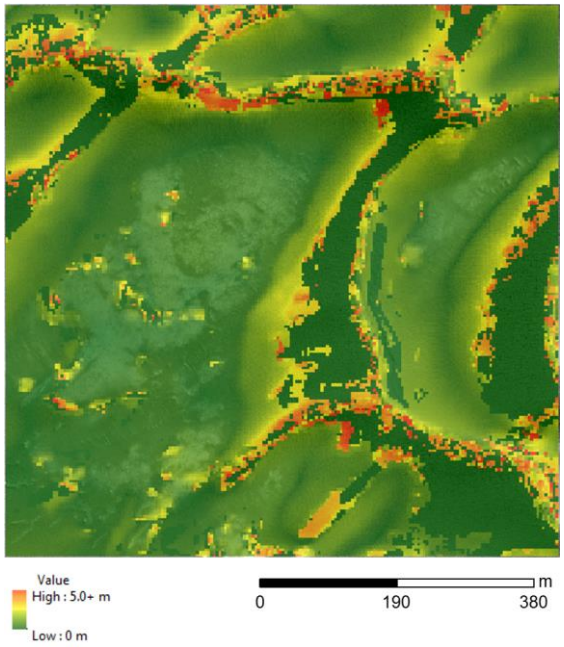

Figure 2. Ripple displacement magnitude map of study area 1 from My 30, Ls 135 to My 31, Ls 130 (677 Earth days). 95th percentile of ripple displacement on primary and secondary dunes is 1.23 m ± .25 mean interdunal displacement error per Earth year. The average ripple displacement is 0.6 meters per year. Colors indicate meters per Mars year.

quency near the summer solstice (See also Smith *et al.*, from this conference) [7,8].

Results: Multi-temporal HiRise images show no dune and ripple activity during the frost covered time of year. Transport during this period is limited to wind blown frost movement, slumping and cryoventing [5]. Dunes in both localities were fully defrosted by L_s 90. Dune and ripple movement occurred during the time period in which the dunes were defrosted.

Variations in dune morphology between localities are controlled by local dune field boundary conditions. Adjacent to the cavi escarpment, dune morphology is dominated by a line source area of sediment. Dunes emerge from a line-source area [6], develop into proto-dunes, increase in height and spacing downwind and decrease in defect density downwind. Dune migration rates near the escarpment range up to two meters per Mars year and are greatest at the most upwind margin where dunes are a few meters in height. Maximum downwind dune heights are 20 meters. Crest line orientations adjacent to the escarpment are transverse to the local orientation of the escarpment and nearly perpendicular to modeled winds (Fig. 3).

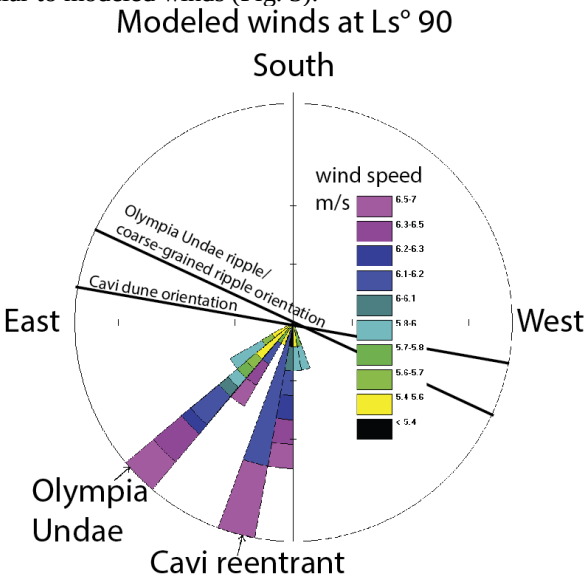

Figure 3. Rose diagram showing wind speed and direction for study locations near the cavi escarpment and in the core of Olympia Undae Dune Field.

In the core of the Olympia Undae Dune Field dunes are controlled by a multi-modal wind regime and a transition to availability limited conditions. Two trends of crestlines intersect non-orthogonally. Primary crestlines dominate the pattern and trend NNE-SSW. Secondary dunes lacking slipfaces trend WSW-ENE. Modeled winds are oblique to both crest lines. Dune heights range up to 40 meters from the interdune surface. Dune migration rates are not measureable at this location over the temporal scale of the imagery, but ripple migration on the dunes ranges up to 2.5 meters per Earth year and average around 0.6 m per year (Fig. 1). Ripple orientation is nearly orthogonal to the modeled winds, but dune orientations are oblique to the dominant modeled wind mode.

Discussion: In the polar region, seasonal differences in CO_2 ice cover act to limit sediment supply, sediment availability and wind transport capacity. Supply is limited because CO_2 covers surfaces subject to deflation by aeolian processes. Sediment availability is limited because the CO_2 ice covers and freezes the majority of ripples and dunes in place, preventing the transport of the sand grains by wind. Model results indicate that wind transport capacity varies seasonally with peak winds occurring during the retreat and onset of the CO_2 cap [7], in late spring leading up to L_s 90.

Non-orthogonal, intersecting crest lines within Olympia Undae are thought to be the result of the superposition of different generations of crestlines [8] generated by an influx of sediment from the cavi reentrant. This is supported by the break-up of the larger crests by smaller crests. An alternative hypothesis, is that the crest lines are forming simultaneiously under the influence of two winds, but affected by spatial changes in sediment availability. This could be support ed by the general trend from transport- to availablility-limited dunes from the east to west side of Olympia Undae denoted by east-to-west increase in the exposure of the interdune areas and a change from orthogonally intersecting crestlines to non-orthogonally intersecting crestlines. In this scenario, the dunes on the western side of the dune field could be transitioning to a fingering-mode of dune orientation [9], in which the crest line orients to the resultant sand flux direction rather than gross-bedform normal transport [10].

References: [1] Bridges et al. (2012) Nature 385, 339-342. [2] Kocurek, G. and Lancaster, N. (1999) Sedimentology 46, 505-515. [3] Kocurek, G. and Ewing, R.C. (2012) SEPM 11, 151-168 [4] Leprince, S. et al. (2007) IEEE, 45, 6. [5] Hensen, C.J. et al (2011) Science 331, 575-578. [6] Ewing, R.C. and Kocurek, G. Geomorphology (2010) 114, 175-187. [7] Smith, I. *et al.* This conference. [8] Spiga et al. (2011) Icarus 212, 504-519. [9] Ewing, R.C. et al. (2010) 115, 1-25. [10] Courrech du Pont, S. et al. (2014) Geology 9, 743-746. [11] Rubin, D. and Hunter, R. (1987) Science 237, 276-278.

TWO INDEPENDENT DUNE GROWTH MECHANISMS IN LABORATORY AND LANDSCAPE-SCALE EXPERIMENTS. C. Narteau[1], S. Courrech du Pont[2], P. Lü[3], Z. Dong[3], S. Rodriguez[4] and L. Fernandez-Cascales[1], [1]Institut de Physique du Globe de Paris, Sorbonne Paris Cité, University Paris Diderot, UMR 7154 CNRS, Paris, France (narteau@ipgp.fr), [2] Laboratoire Matière et Systèmes Complexes, Sorbonne Paris Cité, Université Paris Diderot, CNRS UMR 7057, Paris, France, [3] Key Laboratory of Desert and Desertification, Cold and Arid Regions Environmental and Engineering Research Institute, Chinese Academy of Sciences, 320 West Donggang Road, Lanzhou 730000, Gansu, China, [4]Laboratoire AIM - Université Paris 7, Planetology, Gif sur Yvette, France.

Introduction: Dunes in many environments on Earth and other planetary bodies (e.g., Mars, Titan) are shaped by varying flow conditions over time scales that are too long to be constrained by direct measurements. Hence, a major issue in planetary science is to establish precise relationships between the flow regime and both dune shape and alignment. These relationships are obviously essential for reconstruction of terrestrial wind regimes, past and present, but also for verification of global circulation models on Mars and Titan. Here, we identify two independent dune growth mechanisms in laboratory and landscape-scale experiments that can together provide less uncertainties on the estimation of the wind regime that have been responsible for the development of bedforms.

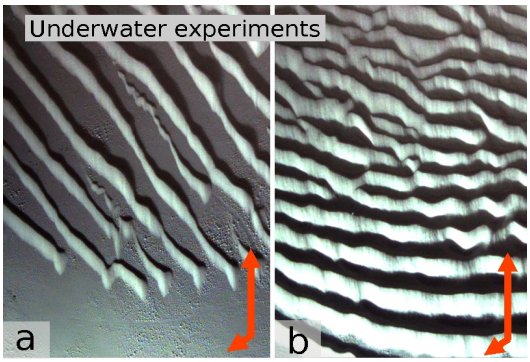

Figure 1: *Two modes of dune orientation in underwater experiments: (a) dunes in a zone of low sand availability; (b) dunes in a zone of high sand availability. Both experiments are conducted using the same asymmetric bimodal flow regime (red arrows).*

Two modes of dune orientation in laboratory experiments: Using underwater experiments, we show that a single bidirectional flow regime can lead to two different dune orientations depending on sediment availability [1]. We find that dunes in zones of high sand availability grow in height selecting an orientation that maximizes the normal to crest components of transport (Fig. 1b), a result consistent with the rule of maximum gross bedform-normal transport [2]. In zones of low sand availability, dunes extend on a non-erodible bed away from a sand source in the direction of the resultant sand flux at the crest (Fig. 1a). These two dune growth mechanisms and the subsequent orientations may coexist, especially where linear dunes growing by extension are large enough to exhibit superimposed bedforms.

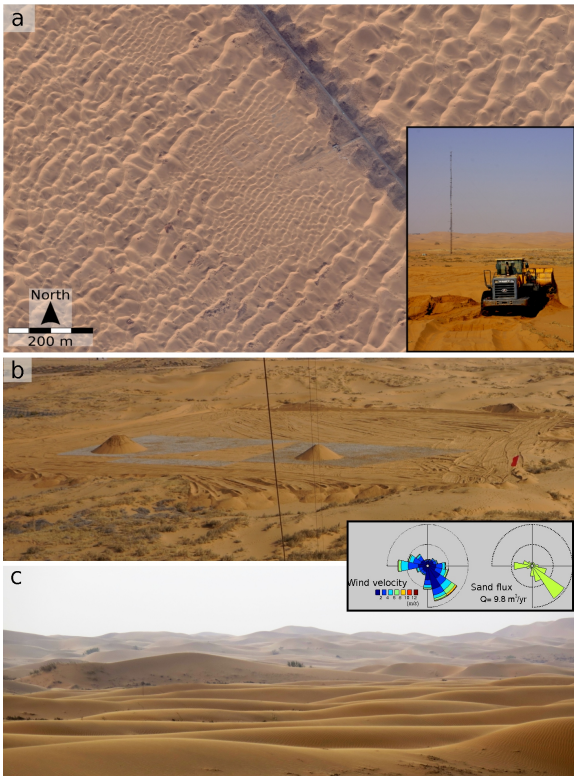

Figure 2: *Two modes of dune orientation in landscape-scale experiments: (a) Global view of the experimental site in Inner Mongolia, China. (b) Original sand piles on a gravel bed to investigate the development of linear dunes from a localized source of sediment; (b) Dunes in a zone of high sand availability five years after complete flattening of the area. The inset shows the local wind and sand flux roses of this part of the Tengger desert.*

Dune growth in landscape-scale experiments: Laboratory results have been used to develop a new set of landscape-scale experiments in the Tengger desert in Inner Mongolia, China (Fig. 2a). Exposed to bimodal winds, this site is unique because it allows multiparametric analysis of dune morphodynamics in a natural environment (16 hectares) under well-controlled initial and boundary conditions. The orientation of dunes as a function of the wind regime and the coupling between flow and topography are currently investigated in two experiments that provide empirical support for the coexistence of two independent dune growth mechanisms. The first experiment consists in regularly supplying sand to an initial sand pile located on a non-erodible bed (Fig. 2b) to mimic the development of dunes from a localized sand source in zones of low sand availability. The second experiment is to flatten a sand bed to observe and quantify the development of the bed instability (Fig. 2c). In this case, for more than 4 years of data, we find that crests are oriented in a direction that combines the normal contributions of the two dominant winds to form an angle of 50° with the resultant sand flux [3]. This rare evidence on the formation of aeolian oblique dunes in a natural environment suggests that the climatic forcing can be derived from the alignment of bedforms.

Conclusion: The two modes of dune orientation and the corresponding dune growth mechanisms can be used to quantitatively predict the orientation of primary and secondary dune patterns from any given wind regime [1]. Thus, they may explain many of the controversial dune features observed in modern terrestrial sand seas but also on Mars and Titan. The challenge is now to differentiate between these various types of dunes and to classify them, not only with respect to their shape and orientation, but also according to the underlying dune growth mechanism.

References: [1] Courrech du Pont S. (2014), *Geology, 42, no. 9, 743-746*. [2] Rubin D. M. and R. E. Hunter (1987), *Science, 237, 276–278*. [3] Ping L. et al. (2014), *Nat. Geosci., 7(2), 99–103*.

TERRESTRIAL ANALOGS FOR VENUSIAN DUNES: SUB-AQUEOUS, SEAFLOOR DUNE FIELDS

L.D.V. Neakrase[1], [1]Department of Astronomy, New Mexico State University, Las Cruces, New Mexico, P.O.Box 30001, 88003-8001, USA. lneakras@nmsu.edu

Introduction. Saltating sand grains on Venus have long been the subject of debate including a wealth of wind tunnel experiments and a handful of observations from the Venera landers. Since the probable identification of dune fields on Venus from Magellan radar data, there have been few terrestrial analogs for comparison to the high-pressure, high-temperature surface conditions present on Venus. One possibly over-looked environment that could help constrain formation, propagation, and evolution of dune forms on Venus could be sub-aqueous dunes found at the bottom of the ocean on Earth. Seafloor dunes form in a higher-pressure environment more analogous to the surface pressures of Venus.

Venusian surface pressures measured by Venera 9 and 10 averaged about 90 bar with measured wind speeds 0.4 – 1.3 m s^{-1} [1]. Surface images from the Venera landers (9,10,13,14) showed fine-grained material at some of the sites suggesting the presence of potential sand to dust-sized sediment capable of being moved through aeolian processes [2,3].

Laboratory experiments [4,5] tested near-Venus-like conditions for a range of particle sizes (30-650 μm, silica) and free-stream velocities (0.4-4 m s^{-1}). Threshold conditions yielded an optimal grain size of 75 μm for movement by the lowest wind speeds. Experiments suggested that grains can be mobilized under venusian conditions, but rock abrasion by sand impact is probably limited because of low particle velocities once grains are mobile.

One possible analog that has not been extensively studied is dunes at the bottom of the ocean on Earth. Given the high density of the venusian atmosphere, sand transport necessary for dune formation might better be represented by sub-aqueous, oceanic currents found at the seafloor. Typical current speeds near the seafloor tend to be ~0.1-1.0 m s^{-1} and produce dunes and ripples in seafloor fines (sand) at these velocities in areas where flow can be confined by topography (e.g., [6,7]). Perhaps dune fields discovered in Magellan radar images on Venus could form and evolve in similar ways to that of sub-aqueous seafloor dune fields on Earth.

Venusian Dune Fields. Dune fields on Venus were first described after acquisition of Magellan synthetic aperture radar (SAR) data [8,9,10]. Numerous features were identified that could be attributed to aeolian processes including possible dunes, windstreaks, and yardangs. [9] identifies the most common aeolian features on Venus as wind streaks. Dunes, though present and identified in two main locations, are relatively rare.

The dune fields are similar to each other in appearance and constrained by topography with possible source material being reworked crater ejecta lag deposits. The original studies used radar bright wind streaks as indicators of prevailing winds arguing that the dune fields are aligned transverse to the wind direction.

The Agloanice dune field (centered 25°S, 340°E) is situated ~100 km north of the impact crater Aglaonice covers an area ~1290 km^2 with individual dunes estimated to be between 0.5 to 5 km in length but spacing is not clear because of specular returns from the radar images. Orientation of the dunes and the wind streaks suggest wind direction to the west.

The Fortuna-Meshkenet dune field to the north (centered 67°N, 91°E) is situated in a valley between Ishtar Terra and Meshkenet Tessera. This field covers roughly 17,120 km^2. As was the case with Aglaonice, this dune field is marked with dunes and wind streaks that correspond to what are assumed as the prevailing wind directions; southeast-northwest flow in the southern part of the field and westward flow in the northern part. Most of the wind streaks in the Fortuna-Meshkenet field seem to originate from small cone-like features. Source material for this dune field is suggested to be from the surrounding complex terrain associated with tectonics of the tessera.

Backscatter effects seen in radar data show differences in dielectric coefficients, which do not necessarily denote changes in composition, but could also represent changes in particle size or changes in reflection orientation. This fact is part of the reason radar images are so hard to interpret for geologic context. Comparison to terrestrial dunes observed by radar systems (reviewed by [9,10]) suggest that viewing limitations for the Magellan SAR prevent ubiquitous detection of dunes in any orientation and may account for the paucity of dunes in other regions on Venus. [11] showed that with Seasat viewing dunes on Earth, these viewing effects are important for understanding the orientation and composite grain sizes of the observed dune forms.

A different approach to compare to the radar images from dune fields on Earth and Venus is to examine side-scanning sonar studies of dunes on Earth's ocean floors. A similar remote sensing technique to synthetic aperture radar, side-scanning sonar together with visible images of the seafloor

dunes can yield other potentially useful constraints for venusian dune studies.

Terrestrial Seafloor Dunes. Sand dunes found on the seafloor have been studied since the 1960s and are typically found in areas confined by topography where oceanic sedimentation transitions from pelagic to current-driven [6]. The important part of this description is the dependence on ocean currents to transport various sediments along the seafloor. This flow dependency is capable of producing meter-sized to centimeter ripples along local regional slopes culminating in larger dune forms. Estimates of the flow velocities (ocean current velocity) over the seafloor features are measured at 0.3 to 2 m s^{-1}, but these estimates could be lower bounds not including higher energy events such as benthic storms, analogous to surface storm events causing bursts of dune activity over a short time.

Seafloor dunes are typically classified as crescentic (abyssal barchans) or transverse dunes. Sizes can range from 10 to 100+ m in length. Transverse dunes in most areas seem to be due to coalescence of strings of barchans [6,7]. [7] described tightly spaced barchans from the Faroe-Shetland Channel as having the appearance of a speckled backscatter signal in the side-scanning sonar. This effect made tightly spaced barchans nearly indistinguishable from transverse dunes. Higher-resolution photographs of the same area clearly separated barchanoid shapes. In almost all cases asymmetric barchanoids also had ripple patterns on the stoss slopes at centimeter to meter scales, typical of arid desert dunes.

Application to Venus. Seafloor dune studies potentially provide another source of study beyond traditional surface dune studies for comparison to environments with very thick atmospheres. Seafloor currents are of the same order as Venus wind tunnel experiments under near-venusian atmospheric viscosities suggesting a possible analog in the types of bedforms that are produced in both environments. In places where observations are limited to radar images with limited surface resolution, seafloor studies with side-scanning sonar and complementary photos could bridge the gap of the orbital resolution limitations.

Venusian dunes are presently limited to the Aglaonice and Fortuna-Meshkenet dune fields and many more indications of wind streaks planet-wide. There has been no indication of barchanoid dune forms in the venusian environment. The paucity of other identified dune fields and specifically barchan dune morphologies is most likely the limitation of the viewing angle effects of the SAR and lack of high enough resolution to resolve individual dunes. Instead the venusian dune fields appear to be collections of transverse dunes. [10] also noted that the viewing effects of the Magellan radar data also probably limited dune detection to dunes situated in N-S configurations potentially neglecting any other configuration suggesting that different orbital parameters for a space-borne radar platform would have the potential to detect many more aeolian features not presently accounted for in the Magellan data.

Future Work. Continued study of features on seafloor dunes and more specifically the scale and slipface orientations might aid in determination of the expected features for future higher-resolution radar studies of the venusian surface.

Another planetary surface that might also benefit from examination of the marine literature is potentially Saturn's moon Titan, where long systems of linear duneforms have been identified similarly to Venus. Titan's atmosphere presents its own challenges but is still thicker than Earth's with potentially higher viscosity similar to certain depths within the terrestrial ocean.

Clearly this is preliminary work and should benefit from further examination of the marine literature. It would be useful to create some sort of database of terrestial sub-aqueous seafloor dunes for comparison to similar areas on Venus and Titan in the future. Flow velocities and dissecting the individual parameters that influence the bottom currents in the ocean need to be more carefully compared to what is known about the venusian surface environment; specifically the atmospheric density and viscosity. Wind streaks and dune forms on Venus that are not associated with domes or other topographic sources should be considered candidates for future high-resolution radar studies if possible. These features (as they have been) can be considered diagnostic of prevailing wind directions but the sub-meter to tens-of-meter scale will be more important when diagnosing the capabilities of the venusian atmosphere to move sediment.

References.[1] Keldysh, M.Y. (1977), *Icarus* 30, 605-625; [2] Florensky et al. (1977), *Geol. Soc. Am. Bull.* 88, 1537-1545; [3] Garvin et al. (1984), *JGR* 89, 3381-3399; [4] Greeley et al. (1984), *Icarus* 57, 112-124; [5] Greeley and Iversen (1985) *Wind as a Geologic Process*; [6] Lonsdale and Malfait (1974), *Geol. Soc. Am. Bull.* 85, 1697-1712; [7] Wynn et al. (2002), *Marine Geol.* 192, 309-319; [8] Arvidson et al. (1991), *Science* 252, 270-275; [9] Greeley et al. (1992), *JGR* 97, 13,319-13,345; [10] Weitz et al. (1994), *Icarus* 112, 282-295; [11] Blom and Elachi (1981), *JGR* 86, B4, 3061-3073.

WINDS AND AEOLIAN ACTIVITY IN GALE CRATER ON MARS: MODEL RESULTS AND COMPARISON WITH OBSERVATIONS. C. E. Newman[1], M.I. Richardson,[1] N. T. Bridges[2], K. W. Lewis[3], J. Gómez-Elvira[4], S. Navarro[4] and M. Marín Jiménez[4]; [1]Ashima Research, 600 S. Lake Ave., Pasadena, CA 91106 (claire@ashimaresearch.com); [2]Johns Hopkins University Applied Physics Laboratory, Laurel, MD 20723; [3]Johns Hopkins University, Baltimore, MD 21218; [4]Centro de Astrobiología, INTA, 28850 Torrejón de Ardoz, Madrid, Spain.

Introduction: The Mars Science Laboratory (MSL) Curiosity rover, has been operating in Gale Crater on Mars since August 2012. MSL carries a meteorology package (the Rover Environmental Monitoring Station, REMS [1]), as well as cameras capable of imaging aeolian features at a range of scales (Navcam [2], Mastcam [3], the ChemCam remote microimager, RMI [4], and the Mars Hand Lens Imager, MAHLI, on the rover arm [5]), and other instruments able to provide information on their surface and internal composition. The region of Gale being explored during the mission contains abundant aeolian features, from small-scale ripples and ventifacts to large-scale, active dune fields. Although some information can be obtained about the largest features from orbit [6,7], MSL observations provide invaluable structural and compositional information at far higher resolution. Also, unlike any previous rover mission, MSL measurements of the wind environment provide vital constraints on the aeolian processes behind these features' formation.

Types of study: There are numerous ways in which MSL's suite of instruments can be used to improve our understanding of Mars aeolian processes. Examples specifically related to simultanous measurements of aeolian features and winds include: (a) Measuring the diurnally- and seasonally-varying wind field (directions and speeds) throughout the mission. This dataset can (i) be used directly to understand the aeolian features observed by MSL along its traverse, but can also (ii) be used to constrain and validate models of Gale's wind field, which can then be applied to investigate aeolian features in other parts of the crater; (b) Measuring the wind field in the vicinity of large, active dunes that have been fully characterized by the suite of MSL instruments. A dune campaign, including comprehensive characterization of the wind field, is planned for MSL's closest approach to dunes on its way up Aeolis Mons; (c) Measuring upper or lower limits on the saltation threshold *in situ*, using the ambient winds and observations of particle motion (or lack thereof) for different surface types, grain sizes, etc.

Difficulties with the wind dataset: Because the two REMS wind sensor booms are located on the remote sensing mast (RSM) – the diameter of which is similar to the length of each boom – the wind reaching them from behind is strongly perturbed by the RSM. This motivated flying two booms with different orientation directions, and the original wind calibration/retrieval method began by selecting the least affected boom. However, one of the booms was damaged during landing, leaving only the forward-facing boom able to measure winds. This presents some difficulties in interpreting and analyzing the REMS wind data, as the wind sensor is largely 'blind' to winds from the rear of the rover in any given orientation. This problem can be mitigated by combining wind data with the rover facing in different directions, and we will demonstrate some of the process involved here.

Results to be presented: We will present observations of the measured wind field in Gale Crater at selected seasons, and show comparisons with Gale wind predictions from the MarsWRF multiscale atmospheric model [8-10]. We will examine how the measured wind field relates to aeolian features already examined along MSL's path. We will also use the model – constrained by existing meteorological data – to predict aeolian features (e.g. dune orientations) over the rest of Gale, focusing on the active dune fields now being approached by the rover. Figure 1 shows an example of dune predictions for two different assumed saltation thresholds. We will also look at the predicted seasonal change in dune transport rates based on the model, and where possible relate this to ground-based and remote observations of the Gale dunes.

References:

[1] Gómez-Elvira, J. et al. (2014), *J. Geophys. Res. Planets*, *119*, 1680–1688. [2] Maki, J. et al. (2011), *Space Sci. Rev., 170*, 77-93. [3] Malin, M.C. et al. (2010), *LPSC, XLI*, 1123. [4] Le Mouélic, S. et al. (2015), *Icarus, 249*, 108-128. [5] Edgett, K.S. et al. (2009), *LPSC, XL*, 1197. [6] Silvestro, S. et al. (2010), *GRL, 37*, L20203. [7] Chojnacki, M. et al. (2011), *JGR, 116*, E00F19. [8] Richardson et al., *J. Geophys. Res. Planets*, *112*, E09001. [9] Toigo et al. (2012), *Icarus*, *221*, 1, 276-288. [10] Ayoub et al. (2014), *Nature Comm.*, 5, 5096. [11] Rubin D.M. and R.E. Hunter (1987), *Science*, *237* (4812), 276-278.

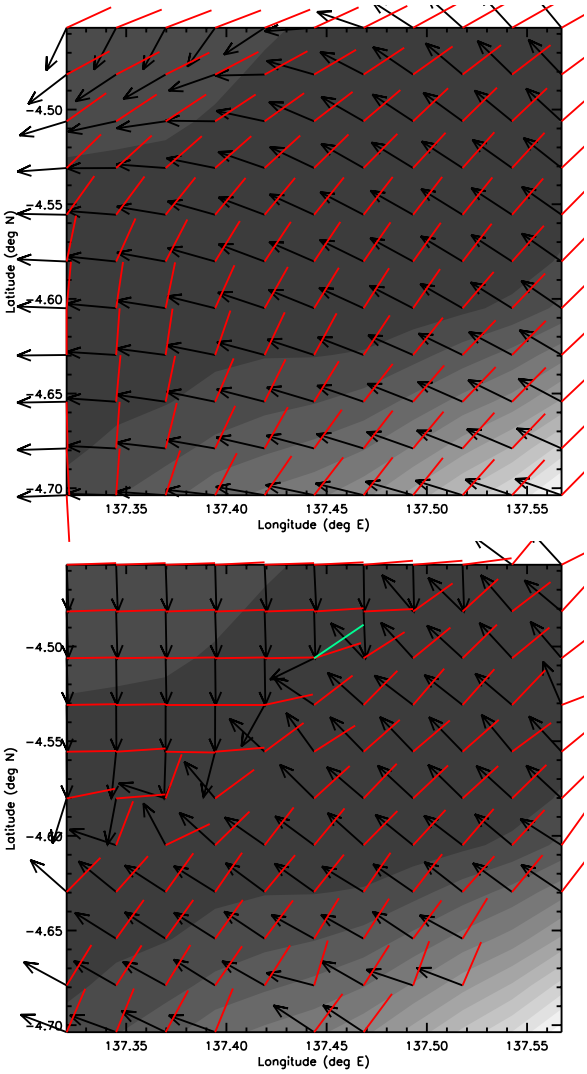

Figure 1: Resultant transport direction (black arrows) and dune crest orientations predicted using the Gross Bedform-Normal Transport model [11] (red and green lines) for a region of Gale Crater including the MSL landing site, using MarsWRF winds. The background shading is topography, and shows the slope from the crater floor (darkest color) up the side of Aeolis Mons (colors lightening at the bottom right). The upper plot shows predictions for a saltation threshold of zero, whereas the lower plot shows predictions for a saltation threshold of 0.05 Pa.

COMPARATIVE ANALYSIS OF YARDANG MORPHOLOGIES IN CHINA. D. Northrup[1], J. Radebaugh[1], R.D. Lorenz[2], B. Bishop[1], R.C. Lewis[1] and E. H Christiansen. [1]Brigham Young University, S-389 ESC, Provo, UT USA 84602, [2]Johns Hopkins Applied Physics Laboratory, Laurel, MD, USA, northrup.dustin@gmail.com.

Introduction: Relatively straight, elongate ridges that form as wind and other mechanisms erode sediment and rock are known as yardangs [1,2,3,4]. These can be found in many deserts on Earth [1], Mars [5,6], and perhaps Venus [7] and Titan [8]. They generally form in soft sediments such as lakebed clays [10] and volcanic ash [9], but can form in resistant layers [11] or microcrystalline basement rock. Yardangs typically form in regions where there are arid conditions, a lack of vegetation, and a persistent, unidirectional wind, oriented in the direction of the long axis of the yardang [1].

A study of yardang characteristics, including morphologies, lengths, widths, spacings and sinuosity, and other factors may help distinguish similar landforms on planetary surfaces from dunes as well as shed light on the requirements for their formation [6,9]. We describe characteristics of a yardang field on Earth, in China, and discuss how a study of morphology can reveal aspects of the erosional history. We also discuss how our methods may be applied to studies of other yardangs on Earth and other planets.

Yardangs of Western China: Our study area is in the Dunhuang Yardang field of western China, east of the Taklamikan desert. Erodable lakebed sediments at 40°30' N, 93°06' E form a series of discontinuous, linear features that are highly parallel and generally straight (Fig. 1). Yardangs are oriented N-S in the northern portion of the field and E-W in the eastern portion of the field. There is a set of NE-SW oriented linear dunes between the yardang fields, further evidence of the action of NS and EW winds in the region. Yardangs are generally more discontinuous, longer and more widely spaced in the eastern field than in the northern field.

A closeup view of the upwind margin (Fig 2) reveals a blunt morphology and streamlining of wind blown deposits around the steep hills which may be as much as 40 m high (Fig. 3). A grey limestone gravel lag deposit surrounds the yardangs; the clasts are 0.5-1.0 cm and form large ripples (0.5 m), indicative of high wind speeds or reptation, as seen in gravel ripples in the Altiplano [12].

Yardang Measurement Methods: We made measurements of the yardangs using images acquired from ESRI World Imagery which were taken by the IKONOS satellite. The image resolution is approximately 1 m (Fig. 4). Measurements were made initially on the NE portion of the northern yardang field, and similar methods will be employed across the remaining yardangs in the region.

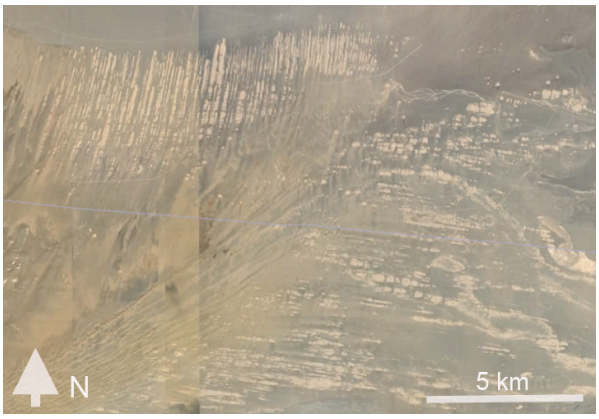

Fig. 1. The Dunhuang Yardang Park, China. Yardangs trend NS and EW, with a set of NE-SW trending linear dunes between them. Fig. 2, Fig. 4 and the study area are at the top center of the image.

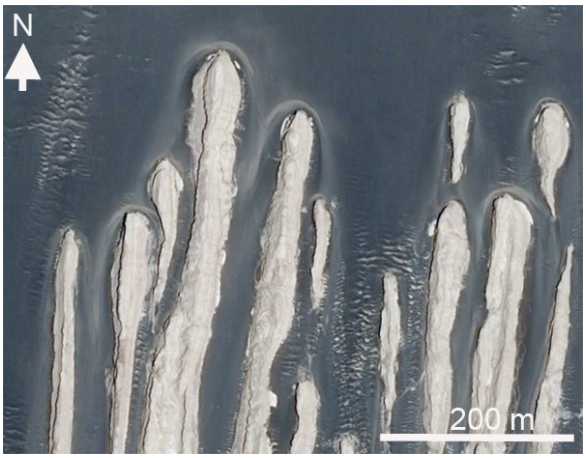

Fig. 2. Dunhuang yardangs are made of light-colored clays while substrate is grey lag gravel with large gravel ripples.

Yardang length was measured as a straight line from one end to the other through the center of the yardang, which can be seen as light-colored sediments in Figs 1, 2 and 4. Yardang spacing was obtained by measuring from the line running through the center of the yardang perpendicular to the line running through the adjacent yardang, in three separate places along each yardang. These were averaged to obtain the average spacing between each yardang. Sinuosity of the yardangs was obtained by drawing a curve along the

Fig. 3. Dunhuang yardang study area viewed from the north (winds blow to the south). Low gravel ripples are apparent in the forground.

yardang crest and then ratioing this curve to the length of the straight line measurements.

Yardang Measurement Results, NE Dunhuang Yardang Field: Yardang length in the NE field ranged from 340 m to 2120 m, with an average length of 1260 m from the start of the yardang to its final termination with a SD of 560 m. The yardang spacing ranged from 52 m to 377 m, with an average spacing of 131 m and SD of 67 m. The sinuosity ranged from 1.00 to 1.06 with an average sinuosity of 1.01 and SD of 0.01.

Discussion: The yardangs in the NE portion of the Dunhuang yardang field display a great deal of variability in length and a very low degree of sinuosity. They have moderately variable spacings, are relatively continuous along their lengths, with a high yardang density per area. Variability in length could result from a regional change in materials available for yardang formation. The low value for sinuosity corroborates their generally straight appearance. By comparision, the yardangs in the southeastern portion of the field trend east-west, display a large degree of discontinuity in yardang material along their lengths, and have a low yardang density per area in comparison with the northern field. This may have resulted when winds changed direction from east-west to north-south, which exposed the yardangs to cross-feature erosion. Further analysis is expected to yield a greater understanding of yardang morphology and their formative processes. This work may also be used to help distinguish between yardangs and dunes on other celestial bodies.

References: [1] Goudie A.S. (2007) *Geography Compass 1*, 65-81. [2] Cooke R., Warren A. and Goudie A.S. (1993) *Desert geomorphology*, UCL Press. [3] Goudie A.S. (1999) in *Aeolian environments, Sediments and Landforms*, 167-180. [4] Mainguet M. (1972) *Le modele des gres*, Paris. [5] Ward A.W. (1979) *Jour Geophys Res 84*, 8147-8166. [6] Zimbelman J. et al. (2010) *Icarus 205*, 198-210. [7] Greeley R. (1999) *Technical Report*, ASU. [8] Paillou et al., Icarus in progress (2015). [9] de Silva S. et al. (2010) *PSS 58*, 459-471. [10] Bristow C. et al. (2009) *Geomorphology 105*, 50-58. [11] Bridges N. et al. (2007) GRL. [12] Bridges et al. Altiplano 2015.

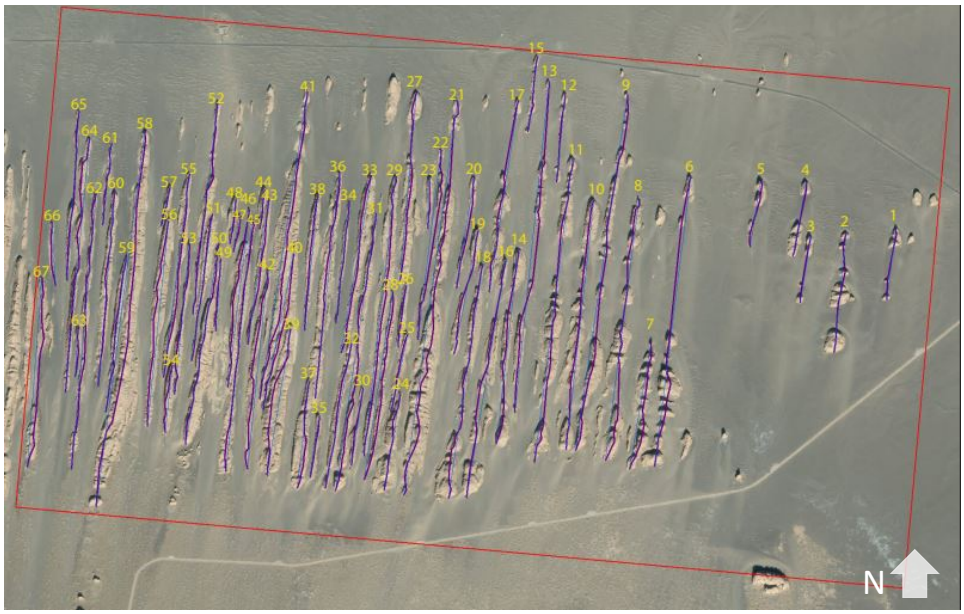

Fig. 4. Measurements of yardangs in the NE portion of the Dunhuang Yardang Field. Lines show the trace along each yardang length, to compare with a straight, end-to-end segment to determine sinuosity.

MORPHOLOGIES, MORPHOMETRIES AND SAR BRIGHTNESSES OF YARDANGS AND DUNES ON EARTH AND TITAN. J. Radebaugh[1] R.D. Lorenz[2], P. Paillou[3] and D. Northrup[1]. [1]Brigham Young University, S-389 ESC, Provo, UT USA 84602, janirad@byu.edu, [2]Johns Hopkins Applied Physics Laboratory, Laurel, MD, USA, [3]Universite de Bordeaux, Floriac, France.

Introduction: Wind-erosional landscapes on planetary surfaces are often dominated by yardangs, which are created by the stripping of surface materials by winds. They are long, narrow, parallel ridges having steep slopes, streamlined shapes and blunt upwind margins [1,2]. There are many similarities in their basic morphology to linear dunes, which are also long, narrow and generally parallel [3]. Yet, there is something about their shape that makes it known they are yardangs and not dunes. We seek to describe general differences between yardangs and dunes in terms of basic morphology, and then to quantify these differences through analyses of length, width, spacing, discontinuousness of form and sinuosity, the latter two factors being perhaps most discriminating. In addition, analysis of radar response can help reveal material differences.

If we can define the similarities and differences between dunes and yardangs on Earth, then we can apply these factors to possible yardangs on other planets [4,5]. This will be especially useful where resolutions are poor, such as on Titan [6] and Venus [7]. The study of and discrimination between dunes and yardangs can reveal wind direction and strength, the presence and condition of sediments, the nature and erodability of the substrate and regional climate [1].

Yardangs of China and Iran and Dunes of Egypt: Yardangs are found in many deserts on Earth. Yardangs in Dunhuang, western China, at 40°30' N, 93°06' E (Fig. 1) have an average length in this portion of the field of ~2.5 km. They are generally straight, are highly discontinuous, and have large variability in width. They range in width from ~30-165 m, with an average of ~60 m, for a roughly average length:width relationship of 40:1, slightly higher than determined for other yardang fields on Earth [8,9].

The Lut Desert of Iran is home to one of the largest yardang fields on Earth, at 30°24' N, 58°22' E. Yardang spacing is very dense and interyardang width small. The yardangs are discontinuous and the forms feather into each other in a mosaic pattern (Fig. 2). Yardangs here can reach 120 km, and while width and spacing are difficult to measure (this is underway), a very rough average width in the center of ~600 m yields a rough length:width of 200:1.

Linear dunes in the Egyptian Great Sand Sea, by comparison, are also long, narrow and straight. These dunes rest on a sand-free substrate, near an oasis in this location at 26°02' N, 26°48' E. They are generally wider and with a greater spacing (mean spacing here is 3.5 km) than the yardangs of China and Iran, and they are overall more continuous. The crestline of the dunes is apparent, while no such crestline is apparent in yardangs, and their tops are typically flat [6].

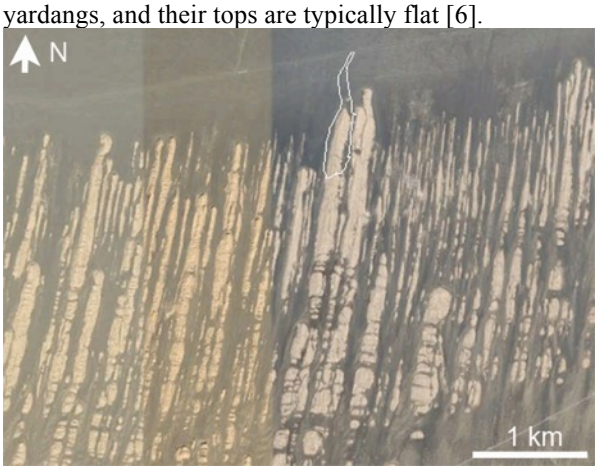

Fig. 1. A portion of Dunhuang Yardang Park, China.

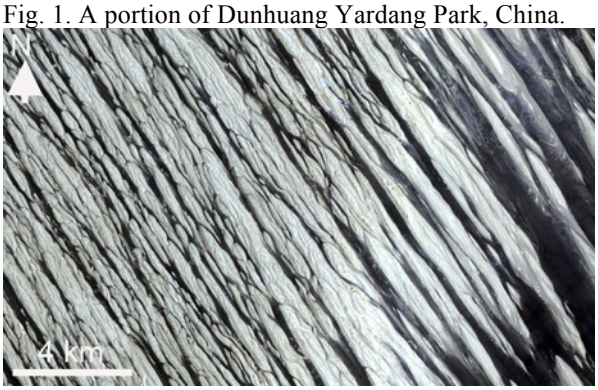

Fig. 2. Yardangs of the Lut desert, Iran. ASTER image.

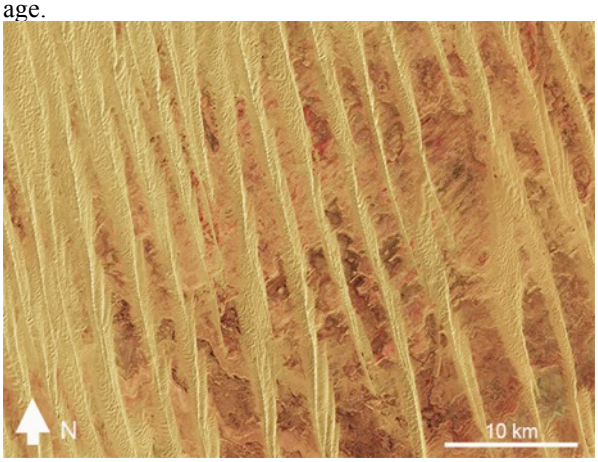

Fig. 3. Linear dunes of Egypt, Landsat ETM+.

Dunes and Yardangs of Titan: Titan has extensive linear dune fields that are similar in size, shape, and radar response to large, linear sand dunes on Earth, such as those seen in Fig. 3 of Egypt (Fig. 4) [10,6]. Two other locations at Titan's northern midlatitudes have landforms resembling yardangs (Fig. 5).

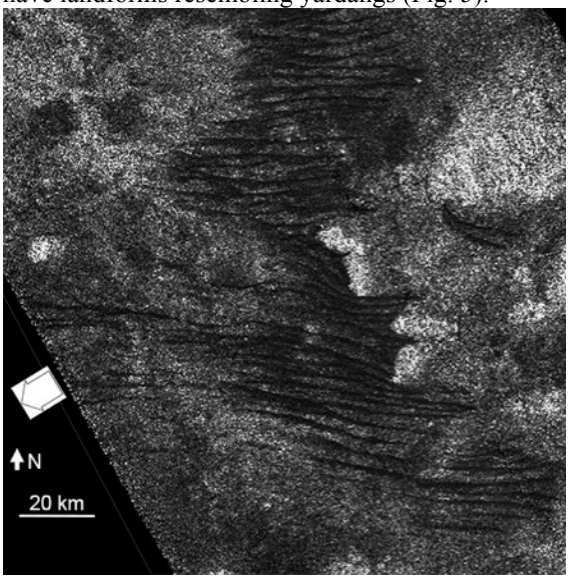

Fig. 4. SAR image of a field of short linear dunes on Titan, T23, 9.7° N, 357.5° W, similar scale to Fig. 5.

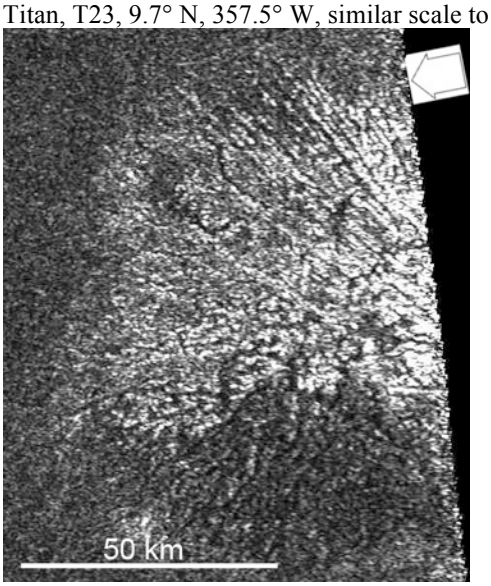

Fig. 5. Possible yardangs on Titan at 41°N, 210°W, from Cassini SAR swath T64, 12/09.

Dunes in Fig. 4 have an average length of 32 km, width of 940 m and spacing of 2.9 km, for a length:width of 34:1. The features of Fig. 5 appear to be more straight and closely spaced than the dunes, and they have an average length of 28 km. They have a mean width of 660 m (SD=230 m) resulting in a length:width of 40:1. Similar landforms seen just 10° to the E in T83 have a mean length of 20 km and a mean width of 740 m (SD=280 m), yielding a length:width of 27:1.

One significant difference between dunes and possible yardangs on Titan is their SAR brightness. A small sample of each region reveals dunes are darker to SAR (Fig. 6), similar to [8]. This is also true for yardangs on Earth [8], and reveals a fundamental difference in material roughness at 2.17cm wavelengths.

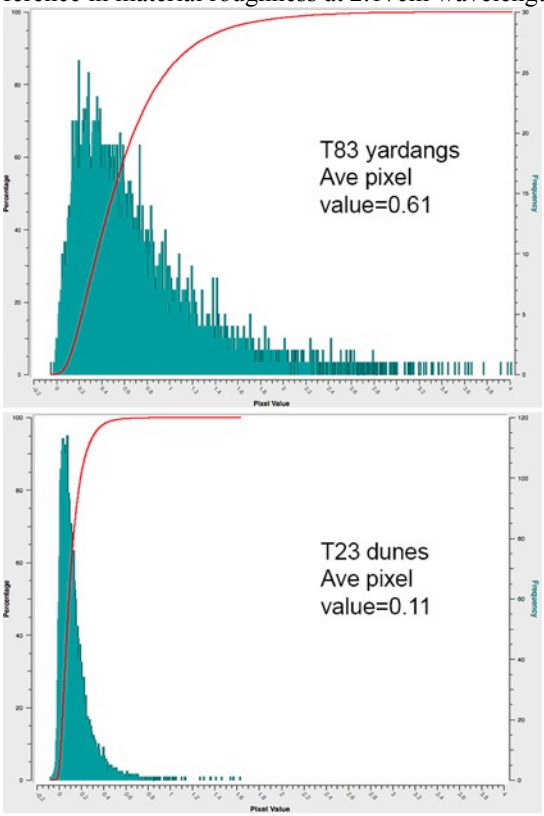

Discussion: Yardangs and linear dunes on Earth and Titan have broad similarities, but some key differences. Dunes in our study areas are generally wider than yardangs, though length:width does not seem to discriminate. Straightness and discontinuousness, currently not quantified, may be key discriminators. SAR brightnesses may be the most significant factors in determining differences between the two landforms.

References: [1] Goudie A.S. (2007) *Geography Compass 1*, 65-81. [2] Cooke R., Warren A. and Goudie A.S. (1993) *Desert geomorphology*, UCL Press. [3] Lancaster, N., Geomorphology of desert dunes (1995). [4] Ward A.W. (1979) *Jour Geophys Res 84*, 8147-8166. [5] Zimbelman J. et al. (2010) *Icarus 205*, 198-210. [6] Paillou et al., Icarus in progress (2015). [7] Greeley R. (1999) *Technical Report*, ASU. [8] Goudie A.S. (1999) in *Aeolian environments, Sediments and Landforms*, 167-180. [9] Bristow C. et al. (2009) *Geomorphology 105*, 50-58. [10] Lorenz R. et al. (2006) *Science 312*, 724-727.

A field comparison of basalt vs. quartz sediment transport in the Grand Falls Dune Field, northeastern Arizona, USA

M.H. Redsteer[1], R. K.. Hayward[2]
[1,2] U.S Geological Survey, 2255 N. Gemini Dr. Flagstaff AZ 86001 [1]mhiza@usgs.gov, [2]rhayward@usgs.gov

Introduction: The Grand Falls dune field, located in semi-arid to arid northeastern Arizona, consists of source bordering dunes downwind of the Little Colorado River (LCR), near Grand Falls, on the northeastern margin of the San Francisco Volcanic Field. Individual dunes are primarily barchans, with a small number of zibars and coppice dunes on the leading edge of the dune field. Collectively the dunes form a mega-barchan complex of small and rapidly migrating dunes (Bogle et al. 2015). Dunes are typically from 500 m^2 to 4000 m^2 and 1 to 5 m high at the crest. Migration rates have been as high as 35 m/yr in recent years, and the dunefield itself has grown in areal extent by more than 70% since 1992 (Redsteer et al. 2011).

The dune deposits consist of fine-grained quartz sand abundant in Little Colorado River deposits and local sandstones, and medium to coarse-grained basalt sand derived from local ash deposits of the San Francisco volcanic field. Dunes become progressively higher in quartz sediment, smaller in size, and more closely spaced downwind (Figure 1.) The mixed source characteristics of sediment transported in the dune field offers an opportunity to conduct a field comparison of the transport characteristics of vesicular basaltic ash vs. well-rounded quartz sand (Figure 2).

Methods: Dune sediment was sampled from four dunes distributed across the dunefield, with samples taken from the crest, toe and limbs of the barchan dunes (Figures 1, 3 and 4). Additional quartz sediment was also sampled from the LCR riverbed for comparison. The density of quartz and basalt sediment samples were estimated by weighing samples and estimating their volume by the amount of water displaced in a graduated cylinder.

To examine the distribution, sorting and transport of basalt vs. quartz sediment across the entire dune field, additional sediment was collected from dunes along a transect, bisecting the dune field, and parallel to the predominant direction of the wind. In addition, passive-sampling Big Spring Number Eight (BSNE) sediment trap samplers [*Fryrear*, 1986] were deployed from the upwind to downwind sides of the dune field to examine sediment transport rates. Windblown sand was collected in three traps mounted on a vertical pole, with sand-trap orifices 0.25, 0.5, and 1.0 m above the ground.

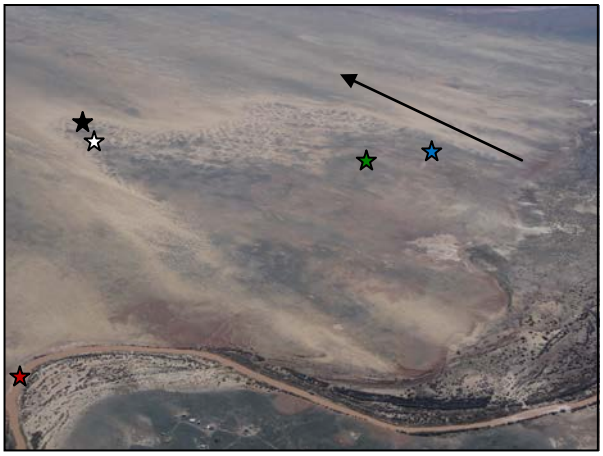

Figure 1. Oblique aerial view of the Grand Falls Dune Field looking east, showing overall dunefield organization with larger, more widely spaced dunes upwind (with higher amounts of basalt sediment) and smaller, more closely spaced dunes downwind (lighter in color, with higher amounts of quartz sand). Stars designate sample locations for data in PSA graphs, with colors corresponding to Figure 3. Arrow indicates predominant direction of wind.

Preliminary Results: There are significant differences in the particle size distributions of the basalt and quartz sediments, with a 300 μm median diameter of quartz river sediment and 1000 μm median diameter of basaltic ash in the dunefield (Figures 2 and 3). Some basaltic ash that is transported and trapped in BSNEs on the upwind side of the dunefield is very coarse (> 2mm, at 1 m height). There are also differences in sediment density, with the fine-grained quartz being somewhat less dense (2.4 g/cm^3) than the vesicular basalt (2.8 g/cm^3). We hypothesize that these differences have led to differentiation of sediment transport populations, so that the coarser, denser basalt grains are transported during the high wind events, whereas, the quartz sand is transported more frequently (with a lower velocity threshold).

Additional work is underway to examine the threshold velocity and transport rates for coarse-grained, vesicular basaltic ash in the Grand Falls dunefield.

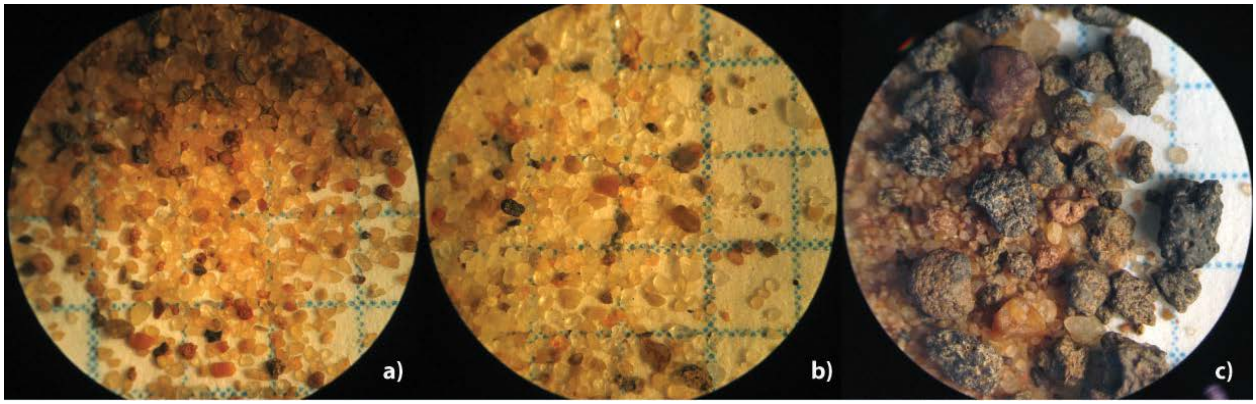

Figure 2. Microphotographs of samples from the Grand Falls dunefield study area: a) barchan slip face b) LCR alluvial deposit c) interdune ripple crest. Grid behind photos is 1.3 mm. (Photo courtesy of Jim Zimbleman.)

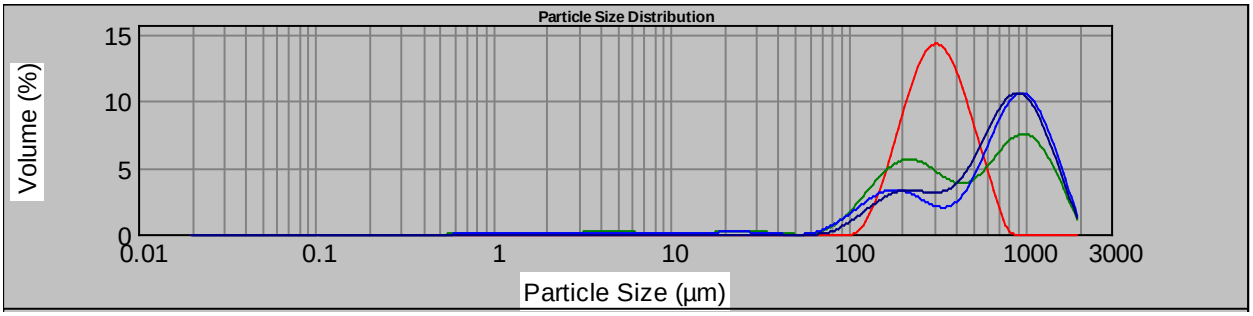

Figure 3. Particle size analysis for predominantly quartz river sediment (red) and for three dune samples of mixed quartz and basalt sand (dune crest of dune on downwind side of field (black) and from two basaltic dunes on upwind side of dune field (green and blue). Sample locations shown as stars on oblique photo of dune field, with same color designations.)

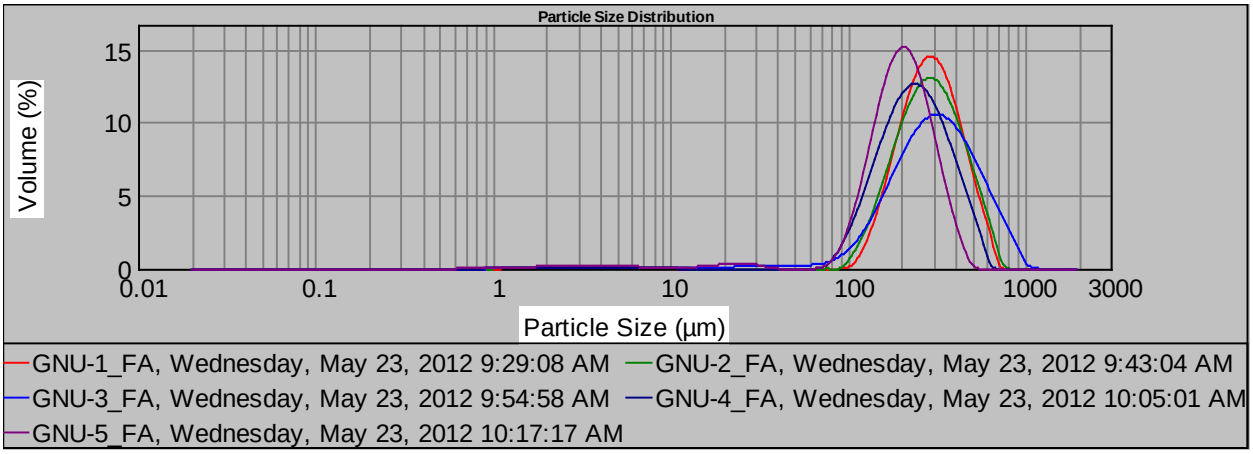

Figure 4. Particle size analysis for dune on western, downwind side of dunefield (location approximated with white star on photo). Dune sediment is prediminantly quartz with 10% basalt sand (visually estimated). Red designates sediment from dune crest, green- dune toe, purple- west limb of barchan, light blue and dark blue are from mid-way points between crest, toe, and limbs.

References

Bogle, R., Redsteer, MH. And Vogel, J. 2015, Field measurements and analysis of climatic factors affecting dune mobility in the Grand Falls area of the Navajo Nation of the Colorado Plateau, southwestern United States; Journal of Geomorphology, vol. 228, p. 41-51.

Redsteer, M.Hiza, Bogle, R.C. and Vogel J.M., 2011, Monitoring and Analysis of Sand Dune Movement and Growth on the Navajo Nation, Southwestern United States; U.S. Geological Survey Fact Sheet 2011-3085. http://pubs.usgs.gov/fs/2011/3085/

INTERNAL BOUNDARY LAYER CONTROL FOR SEDIMENT FLUX IN HERSCHEL CRATER, MARS.

K. D. Runyon[1] and N. T. Bridges[1,2], [1]Johns Hopkins University Dept. of Earth & Planetary Sciences, Baltimore, MD, USA (kirby.runyon@jhuapl.edu). [2]Johns Hopkins University Applied Physics Laboratory (APL), Laurel, MD, USA (nathan.bridges@jhuapl.edu).

Introduction: As wind blows over a landscape, increases in surface roughness can act as a sink for the wind's momentum; this retardation diffuses upward creating an internal boundary layer (IBL). Since terrestrial work [1] has shown that IBL formation can easily explain the observed decreasing sand flux profile in a barchan and crescent dune field at White Sand, NM, we are testing the hypothesis that IBL formation can also largely explain measured flux profiles in Martian aeolian settings.

Two distinct modes of sand flux [2] potentially affected by IBLs are saltation and reptation, which together make up the bulk of all sand transport. Saltation is primarily a fluid mechanical phenomenon whereas reptation is largely ballistic. Saltation is the main contributor to the formation and movement of dunes whereas reptation is responsible for the formation and movement of ripples. Tracking dune slip face advancement provides an estimate of total flux (saltation + reptation) whereas tracking ripples (via the semi-automated COSI-Corr method [3]) provides a measure of reptation flux [4].

IBL theory has yet to be tested on Martian sand sheets. These wide-spread sand sheets lack slip faces and have diffuse margins; the only precise means of tracking sand flux via remote sensing is to track ripple migration. Then, assuming a flux partition ratio derived from ripple and slip face studies of dunes, the total flux can be estimated. With such an estimate for total flux, we can compare measured and estimated flux values with those predicted from the formation of an IBL.

Case Study: Herschel Crater is a 300 km diameter Noachian-aged [5] peak-ring impact basin featuring extensive dune and sand sheet fields. The HiRISE camera (High Resolution Imaging Science Experiment) has sufficiently imaged two sites within Herschel (termed Herschel West and Center) in order to produce digital elevation models (DEMs) and to measure changes. Herschel West aeolian morphology grades downwind from barchans, to barchanoids, to barchans together with dome dunes, to sand sheets (Figure 1). Herschel Center only features sand sheets.

Measurements on Herschel West's dunes and sand sheets allows partitioning flux between saltation and reptation; this partition is then used to estimate total flux from the reptation-only measurements in Herschel Center's sand sheets.

Flux Measurements & Partition: *Total Flux:* Co-registered, HiRISE orthoimages reveal advancing slip faces in repeat imaging. Manual mapping of the advancement area and slip face arc length, together with the time between the images, gives an average value for dune advancement rate. Multiplying this rate by the dune height—measured from HiRISE DEMs—yields dune crest volumetric flux.

Reptation Flux: Two co-registered HiRISE orthoimages taken at different times allows measurement of ripple rate and, when multiplied by the average ripple height (taken as the half-height of a representative ripple) yields reptation flux. Ripple heights are below the resolution of the HiRISE-derived DEM and so must be assumed as some fraction of the ripple crest-to-crest wavelength spacing. Using ground-truthed data from the Mars Exploration Rover Spirit [6], the wavelength/ripple height ratio is 0.1-0.15. For Herschel West the mean ripple spacing is 2.6 m and we take the characteristic half-height to be 0.13-0.20 m.

Figure 1. Moving downwind in Herschel West, the dune morphology evolves from discrete barchan to barchanoid, to a mix of barchan and dome dunes, and finally to sand sheets. This change in morphology correlates with a change in flux (Figure 2). Each square frame is 500 m x 500 m. HiRISE/UA PSP_002860_1650.

Fluxes: The mean measured total flux for Herschel West dunes is 1.412 m^3/m/yr; for the same dune population the mean reptation flux is 0.316 m^3/m/yr yielding a total flux/reptation flux ratio of 4.5 (saltation/reptation ratio of 3.5). This ratio is similar to the value of 5 found by [4] in Nili Patera using identical methods. For comparison, dunes in Victoria Valley, Antarctica have volumetric fluxes ~10x higher [4 & references therein].

IBL Comparison with Observed Fluxes: [1] present a relation of predicted flux

versus downwind distance assuming the flux is controlled by IBL development:

$$\langle q_s \rangle = 0.055 I \frac{\rho_{\text{air}}}{\rho_{\text{solid}}} \frac{C}{g} \sqrt{\frac{D}{D_0}} U^3 \left(\frac{\nu}{U z_{0L}^{1/5}} \right)^{3/8} x^{-3/10}$$

where the variables are defined in Table 1 alphabetically.

Herschel West Dunes: Figure 2 shows flux predictions (thin colored curves) assuming a range in wind intermittency (Table 1) and is compared against total flux measurements in Herschel West. While the IBL flux predictions envelop most of the measurements, the anomalously high values mid-field can likely be explained from those dunes' positions atop a subdued crater rim, though counterexamples are also apparent. It seems height and downwind distance have competing effects on wind strength and hence sediment flux: increases in elevation compress streamlines within the atmospheric boundary layer (ABL, ~2 km thick) and thus increase wind speed and flux (the "Venturi effect"). However, increasing downwind distance allows the IBL to thicken and hence for wind and flux to decrease. For the anomalous midfield fluxes, we propose that topographically-related wind strengthening dominates over IBL-related weakening, though the reverse may be true for other locations within the aeolian field; future modeling efforts may predict the net effect from this interplay.

Table 1: Variables & values used in IBL flux predictions.

Variable	Value	Description
C	3.88	Friction coefficient for sand at Mars' Reynolds number < 10
D	250 µm	Characteristic grain size
D_0	100 µm	Reference grain size (standard)
g	3.7 m/s^2	Mars gravity
I	0.001, 0.005, 0.01 (varied in model)	Intermittency of above-fluid threshold winds
U	20-37 m/s	Free stream air velocity
x	Varies, m	Distance downwind from the upwind margin
z_{0L}	0.0896 m	Lettau roughness height
ν	6.8831 x 10^{-4} m^2/s	Kinematic viscosity
ρ_{air}	0.0154 kg/m^3	Air density
ρ_{solid}	3000 kg/m^3	Density of (basaltic) sand grains

Herschel Center Sand Sheets: The Herschel Center sand sheets are more complex. Without using *a priori* flux knowledge, IBL estimates agree with the range of estimated total fluxes but not necessarily with the flux profiles. Figure 3 shows two sample profiles out of the seven measured sand sheet profiles for Herschel Center.

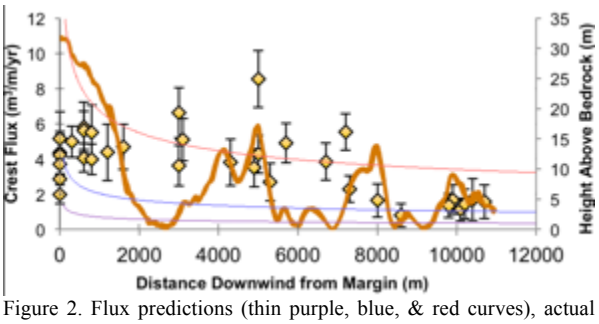

Figure 2. Flux predictions (thin purple, blue, & red curves), actual dune crest measurements (yellow data points), and bedrock topography (thick orange curve). See text for explanation.

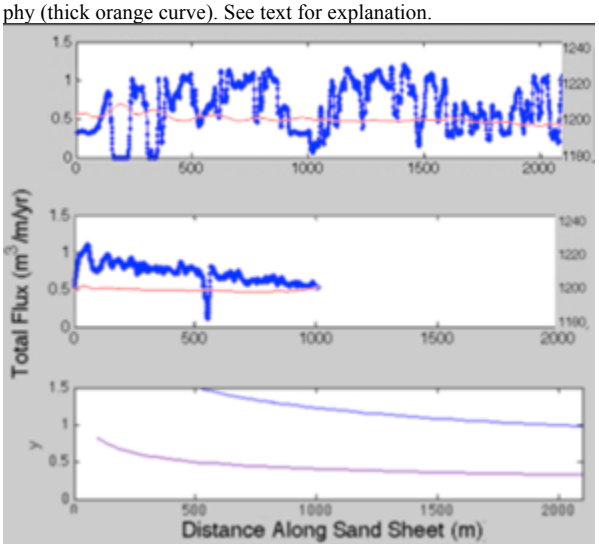

Figure 3. Top two panels show estimated total flux profiles (thick blue squiggles; left-side vertical scale) based on the measured ripple migration rates and a saltation/reptation ratio of 3.5. The thin red squiggles are combined sand sheet/bedrock topography relative to Mars datum (right-side vertical scale). The bottom panel depicts predicted flux profiles from IBL theory, which accurately predicts the overall flux measurements but not necessarily the flux decay profile.

Discussion, Conclusion, & Future Work: Whereas IBL theory seems to dominate the flux decay profile at White Sands, other geophysical factors in Herschel Crater seem to also significantly control aeolian flux profiles, such as the Venturi effect over raised topography. Future work may involve calculating the contribution from the Venturi effect at every point along the transect and comparing with the IBL flux prediction.

References: [1]Jerolmack, D.J. et al., (2012), *Nature Geoscience*, DOI:10.1038/NGEO1381. [2] Anderson, R.S. (1987) *Sedimentology* v. 34, no. *5*, p. *943-956*, doi: 10.1111/j.1365-3091.1987.tb00814.x. [3] Leprince S. et al., (2007) *IEEE Trans. Geosci. and Rem. Sensing, 45, 6.* [4] Bridges N. T. et al. (2012) *Nature 485, 339, doi:10.1038/nature11022*. [5] Tanaka, K.L., et al., (2014), Geologic Map of Mars, *USGS Scientific Investigations Map 3292*. [6] Sullivan R., et al., (2008), *JGR* 13, E06S07, doi:10.1029/2008JE003101.

Acknowledgements: Thanks to Kurt Aikens (Purdue University/Houghton College) for helpful discussions on fluid mechanics; Thanks to Francois Ayoub (Caltech) for his extremely kind patience in serving as "COSI-Corr IT guy."

CONTROLS ON AND IMPLICATIONS OF AEOLIAN GEOMORPHOLOGY ON COMET 67P. K. D. Runyon[1], C. M. Lisse[2], A. F. Cheng[2], N.T. Bridges[1,2], K. Lewis[1], [1]Johns Hopkins University, Dept. of Earth & Planetary Sciences, Baltimore, MD, USA (kirby.runyon@jhuapl.edu), [2]Johns Hopkins University Applied Physics Laboratory (APL), Laurel, MD, USA.

Introduction: Thomas et al. [1] described putative aeolian dunes and/or ripples and wind shadows on the surface of Comet 67P as observed by ESA's spacecraft Rosetta (Figure 1). Purportedly, these formed from cometary jets blowing laterally across the surface and mobilizing surface sediment. This exploratory abstract considers some of the controls and implications of cometary aeolian bedforms.

Prior to this discovery, Cheng et al. [2] invoked aeolian activity to explain much of the geomorphology on comets Wild 2, Hartley 2, and Tempel 1. For Comet Hartley 2, they predicted fluid threshold friction speeds $u_{*\mathrm{ft}}$ of ~5-96 m/s with higher friction speeds required to mobilize smaller particles due to their higher susceptibility to cohesive forces. This threshold velocity is substantially below jet velocities modeled for Comet Hyakutake of ~500-1500 m/s [3]. Additionally, most cometary outgassing occurs from non-jet amorphous outflow that could likely have a lateral velocity component.

Here, using several simple models, we consider the hypothesis that cometary jets can mobilize sediment across the surface, and that particles can be retained on the comet by gravity and cohesion. Thus, the putative aeolian bedforms could indeed be aeolian in nature; whether they are dunes or ripples is not conclusive, though we think ripples are more likely.

Aeolian Theory & Results: Particle speeds at the surface are relatively insensitive to changes in friction shear velocity u_* ([4] and references therein); thus winds much faster than u_{*ft} will generally not produce faster saltating particles. Note that once fluid shear stress initiates saltation, saltating particles are the dominant means of lofting more saltators and not fluid shear stress alone [4]. Additionally, ballistic reptation [6]—which is not a fluid mechanical phenomenon—can launch lower energy grains when a saltating grain impacts the comet's surface. This allows that ripples may be the dominant aeolian bedform on Comet 67P.

Terrestrial Model Applied to Comet 67P: Iverson et al. [7] presented an expression for $u_{*\mathrm{ft}}$, where the variables are described in Table 1:

$$u_{*ft} = A_N \sqrt{\frac{\rho_p - \rho_a}{\rho_a} gD + \frac{\gamma}{\rho_a D}}.$$

The actual wind velocity U at a given height is then expressed by

$$U = \frac{u_*}{0.4} \ln\left(\frac{z}{z_{0L}}\right).$$

where we take $u_* = u_{*ft}$. This assumes a boundary layer profile.

By varying the roughness parameter z_{0L} as indicated in Table 1, we obtain wind speed velocity profiles shown in Figures 2 and 3 assuming the wind is at fluid threshold, calculated at 42.3 m/s. Interestingly, this value is within the range independently calculated for Hartley 2 by [2].

Table 1. Constants and results of terrestrial aeolian theory applied to Comet 67P

A_N	Proportionality Constant (changes for particle friction Re)	0.111
γ	Interparticle strength parameter	2.9×10^{-4} (Kok et al., 2012; value for terrestrial dust & sand)
ρ_p	Water ice density	917 kg/m^3
ρ_a	Air density	2×10^{-5} kg/m^3
g	Gravitation acceleration	10^{-3} m/s^2
D	Particle size	100 μm, 500 μm
z_{0L}	Lettau (1969) aerodynamic roughness height	0.1, 0.01, 0.001 m (varied in calculation)
u_{*ft}	Fluid threshold fiction speed (calculated from above)	42.3 m/s

Jet Velocities: Our simple terrestrial aeolian model as well as [2]'s model agree and are less than the predicted jet velocities of ~450 m/s calculated from

$$V_{\mathrm{outflow}} = \frac{0.65}{\sqrt{r_h}}$$

where r_h is the solar distance in AU and we use $r_h = 2$. Note this is on the low end predicted by [3].

Other Wind Considerations: From the comet's physical size and rotation rate, we find that only a 0.3 m/s wind could be created from rotating within its own coma; we therefore do not consider this a substantial contributor to aeolian dynamics.

While gas velocities are well above escape velocity, mobilized particles would only attain a fraction of this

speed and could remain gravitationally bound to the comet for grain speeds less than the escape velocity of 0.9 m/s [5].

Differential diurnal heating of the comet may also contribute to circum-cometary winds that could contribute a lateral component to other wind sources.

Discussion & Conclusion: *Saltation versus Reptation/Dunes versus Ripples:* As opposed to dunes, which are formed from saltation, the aeolian features on 67P may be giant aeolian ripples caused by reptation. This would allow saltating particles—even those moving above escape velocity—to still occasionally re-impact the comet (possible given the comet's irregular shape) and locally disturb particles on lower energy "hops" where the weak gravity could easily recapture the particles. Additionally, particle speeds necessary to create aeolian bedforms can be used to place upper constraints on grain cohesion.

Conclusion: We have considered that it is possible to mobilize gravitationally-bound sediment on comets and therefore to form aeolian bedforms. Laterally-blowing cometary winds—possibly from jets and/or amorphous outflow—mobilize saltating particles, which can in turn mobilize both saltating and reptating particles, both of which could be re-accreted even in the comet's week gravity. Since reptating particles are slower than saltating particles, it is less likely that they will gravitationally escape; thus the bedforms are more likely to be ripples than dunes. Furthermore, grain energies and values for u_{*fi} place upper bounds on grain cohesion, suggesting that cohesion may be quite low.

Future work is needed to quantitatively constrain grain energies and cohesion on comets. If Rosetta's long-term observations reveal bedform movement, such constraints may be within reach.

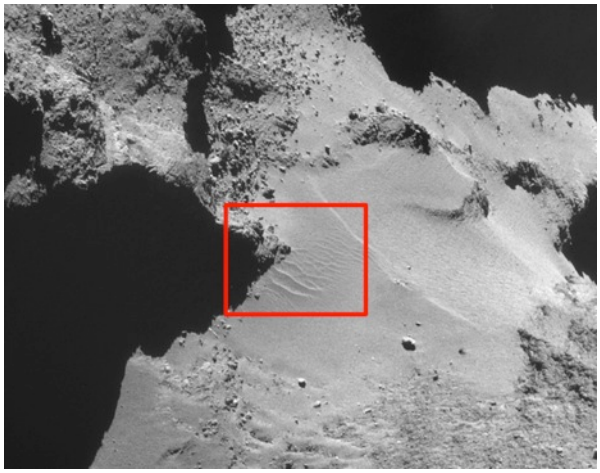

Figure 1. Putative dunes on Comet 67P. Length of the longest "dune" (at the bottom) is ~50 m. Credit: ESA/Rosetta/NavCam/Damia Bouic/Emily Lakdawalla.

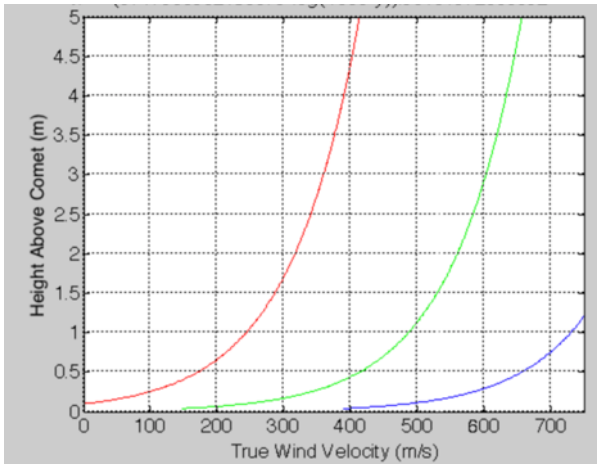

Figure 2. Wind height profiles for 100 µm diameter water ice grains. The only other varied parameter is surface roughness; red (left) = 0.1 m, green (middle) = 0.01 m, and blue (right) = 0.001 m.

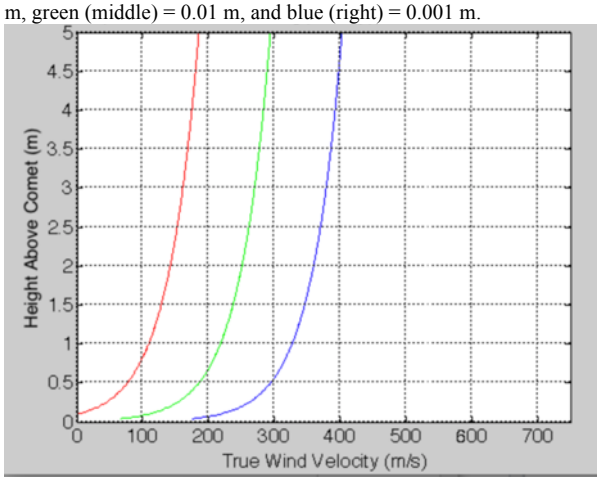

Figure 3. Wind height profiles for 500 µm diameter water ice grains. The only other varied parameter is surface roughness; red (left) = 0.1 m, green (middle) = 0.01 m, and blue (right) = 0.001 m.

References: [1] Thomas, N., et al., (2015) *Science*, 347, DOI: 10.1126/science.aaa0440. [2] Cheng, A. F., et al., (2013) *Icarus*, 222, 808–817, http://dx.doi.org/10.1016/j.icarus.2012.10.004. [3] Combi, M.R., et al., (2005) *in Comets II*, p. 523-552. [4] Kok, J.F., et al., (2012), *Reports in Progress in Physics*, 75, doi:10.1088/0034-4885/75/10/106901. [5] Sierks, H., et al., (2015), *Science*, 347, DOI: 10.1126/science.aaa1044. [6] Anderson, R.S., (1987), *Sedimentology*, 34, 943-956. [7] Iverson, J.D., et al. (1987), *Sedimentology*, 34, 699-706.

AUTOMATED DETECTION OF TRANSVERSE AEOLIAN RIDGES ON MARS USING CONVOLUTIONAL NEURAL NETWORKS AND A FIELD-BASED TERRESTRIAL ORTHOIMAGE TRAINING SET. S. P. Scheidt[1], L. F. Palafox[1], C. W. Hamilton, J. R. Zimbelman[2]. [1]Lunar and Planetary Laboratory, University of Arizona, 1629 E. University Blvd., Tucson, AZ 85721, USA (scheidt@lpl.arizona.edu). [2]CEPS/NASM, Smithsonian Institution, Washington, DC 20013, USA.

Introduction: Dunes on Mars provide evidence of active and ancient aeolian processes and are critical for understanding the planet's stratigraphy and surface modification history. Active sand transport and ripple migration occurring on Mars has been observed using automated image feature correlation and change detection [1, 2, 3], but genetically-related Transverse Aeolian Ridges (TARs) [e.g., 1] appear to have been stationary over recent history. TARs are commonly imaged by the High Resolution Imaging Science Experiment (HiRISE) camera onboard the Mars Reconnaissance Orbiter (MRO), and our goal is to develop an efficient, automated mapping strategy for TARs to understand their spatial distribution, morphological characteristics, and processes of formation.

Methodology: Mapping TARs and including information such as shape, crest spacing, sinuosity and surface albedo is challenging because of their small footprint in HiRISE images. TARs can be found over large areas, but are typically found in isolated patches. To obtain quantitative topographic information about TAR height and morphology, high-resolution (1 m/pixel) digital terrain models (DTMs) can be constructed from HiRISE stereo-image pairs [5] using ISIS and SOCET SET software. These stereophotogrammetry methods are based on feature-matching and the algorithms often have difficulty retrieving three-dimensional (3D) information from smooth surfaces, subtle features, or contiguous ripple textures. TARs typically occupy only a small portion of any HiRISE image, which makes processing an entire DTM for these small features a time-consuming task. Likewise, the area and size of TAR bedforms are generally small and near the limit of detection with respect to the spatial resolution (~1 m/pixel) of the DTMs. Although height information is highly desirable for analysis, the pattern of ripple and TAR ridges seen from HiRISE images alone can reveal information about paleo-wind directions, which is important for understanding Martian climate.

Our initial efforts to map TARs focused on manual digitization of TAR patterns and 3D profile extraction, but it became apparent that automated image processing tools would be better for mapping TARs. Various approaches have been taken to automatically map sand ripples in image data by automatic detection of ripple crest patterns [6] and dunes using supervised machine learning [7]. We initially tested techniques [6] and attempted to map TAR patterns using a Canny edge detection scheme [8]. These essentially could detect edges of TAR crests that correspond to the light and dark image contrast produced from light reflected at the planet's surface. These efforts are still in progress, but they initially resulted in both false positive and negative cases of edge detections.

More recently, improved machine learning techniques, termed Convolutional Neural Networks (CNNs) [9], were used to detect, distinguish, and map volcanic rootless cones (VRCs) and impact craters in Elysium Planitia [10]. Despite the similarity in appearance of VRCs and impact craters in HiRISE images, the technique was successful in distinguishing between the two classes and prompted us to implement CNNs to improve mapping and characterization of TAR ripple patterns. Unlike most computer vision techniques, CNNs are particularly effective for pattern recognition within image data because they do not require preprocessing steps to facilitate accurate classifications [10].

Terrestrial analog training. In this work, we extend the CNN technique [10] by building the supervised training set directly from orthoimage data of terrestrial TAR analogs [11, 12] (Fig. 1).

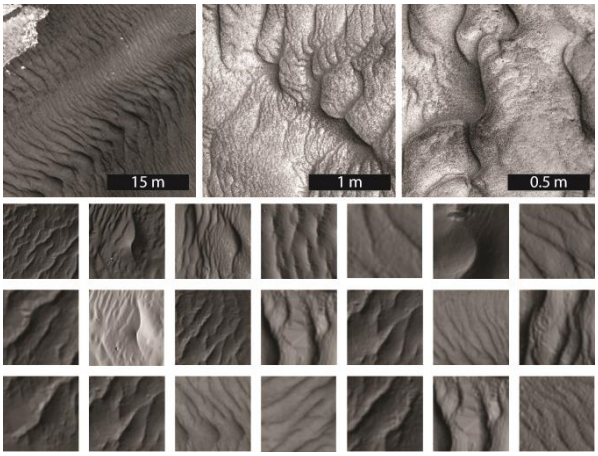

Figure 1. A synthetic orthoimage training set based on 3D models generated from field images of terrestrial TAR analogs in Hawaii, Colorado, and Arizona using multi-view stereo-photogrammetry (MVSP) techniques. The larger top three images show scaled sites, where smaller tiles are dimensional, randomly oriented and are generated both from orthoimages and synthetic DTM models.

Supervised machine learning techniques such as Support Vector Machines (SVMs) [7] and CNNs [9] rely on an image training set that characterizes the features needed for recognition and classification. In planetary remote sensing applications, the training set usually originates from the image source (i.e., the image being classified) and these data lack field-based ground truthing. Fortunately, aeolian bedforms on Earth (e.g., megaripples, granule ripples, and gravel ripples [13–16]), exhibit considerable morphological similarities to those on other planetary surfaces, which implies similarities between their formation mechanisms.

In this study, we employed high-resolution terrestrial orthoimage data (<1 mm/pixel) generated using field-based multi-view stereo-photogrammetry (MVSP) techniques [e.g., 11, 12, 17, 18]. These 3D models have exceptionally high spatial resolution and in the orthoimages (Fig. 1) can be digitally manipulated to have a predefined incidence angle with respect to a synthetic camera. This enables us to use ground-truthed aeolian bedfroms to create a well-characterized terrestrial analog data set with which to train automated landform detection algorithms, such as CNNs.

Results: We show the classification results of training the CNN using a training dataset of 400 points from the original HiRISE image (Figs. 2A and 2B). The results of using the ground-truthed terrestrial training set of 200 synthetic orthoimages under the same conditions (Fig. 2C) is comparable to the CNN application using the martian image training set (Fig. 2B).

Conclusions: CNNs trained using synthetic instrument data, generated from terrestrial analogs, performed comparably to classifications that utilized in-situ HiRISE image training sets. This example demonstrates that well-characterized Earth surface archetypes may be used as training sets for the identifiifation of aeolian bedforms on other planetary surfaces. The immediate benefit of this work is efficient mapping of TARs and the ability to directly link terrestrial bedforms on Earth to planetary image data. However, CNNs may also be trained using terrestrial analog data to search for a range of other Earth-like surface features without introducing a bias by relying exclusively on in-situ training data drawn from planetary remote sensing observations.

References: [1] Silvestro S. et al. (2010) GRL 37(20), doi:10.1029/2010GL044743. [2] Bridges N.T. et al. (2012) Nature, 485(7398, 339-342.[3] Ayoub F. et al. (2012), 3rd Int. Planetary Dunes Workshop, abs. 7026. [4] Bourke M.C. et al. (2010) Geomorphology, 121, 1–14. [5] Kirk R. L. et al. (2008), JGR, 113, E00A24. [6] Vaz D. A. and Silvestro S. (2012), 3rd Int. Planetary Dunes Workshop, abs. 7019. [7] Bandeira L. et al. (2012), 3rd Int. Planetary Dunes Workshop, abs. 7039. [8] Canny J. (1986), IEEE T. Pattern Anal., 8(6), 679-698. [9] LeCun, Y. et al. (1990) *ICPR*, 35–40. [10] Palafox L. F. et al. (2015), LPSC XLVI, abs. 2316. [11] Scheidt S. P. et al. (2014), LPSC XLV, abs. 1446. [12] Scheidt S. P. and Zimbleman J.R. (2015), LPSC XLVI, abs. 1056. [13] Bagnold R.A. (1951) Brit. J. Appl. Phys., 2, 2–29. [14] Sharp R.P. (1963) J. Geology, 617–636. [15] Zimbelman J.R. et al. (2012) Earth Surf. Proc. Land., 37, 120–1125. [16] de Silva, S.L. et al. (2014) LPSC XLV, 45, Abs. #2582. [17] Furukawa Y. and Ponce J. (2010), IEEE Trans. Pattern Anal. Mach. Intell., 32, 8, 1362-1376. [18] Wu C. (2013), Int. Conf. 3DV, doi:10.1109/3DV.2013.25.

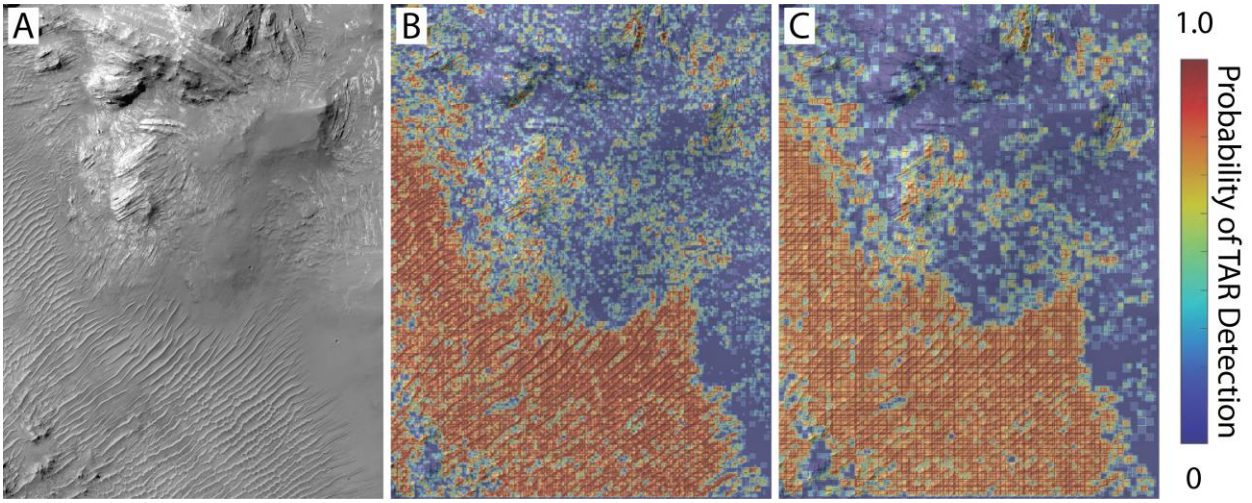

Figure 2. A: Original image (HiRISE ESP_06805_1565) containing TARs emplaced around a layered rock outcrop. B: Results based on the martian HiRISE training set. C: Result using the synthetic terrestrial training set. In B and C the red color of the represent positive TAR detections and blue represent null detections. Map area is 590 × 765 m.

LONGITUDINAL AEOLIAN DEPOSITIONAL FEATURES ON MARS? S. Silvestro[1], D. A. Vaz[2,3], C. Popa[1], F. Esposito[1], [1]INAF Osservatorio Astronomico di Capodimonte, Napoli, Italy (silvestro@na.astro.it), [2]CITEUC - Centre for Earth and Space Research of the University of Coimbra, Portugal, [3]CERENA, Lisboa, Portugal.

Introduction: Mars has abundant aeolian bedforms like dunes, ripples, megaripples and TARs [1]. While dunes can have different morphologies according to the complexity of the wind regime and sediment availability, wind ripples are generally considered to trend perpendicular to the sand transporting winds. Non-transverse aeolian ripples on Earth have only been obtained experimentally under the influence of bi-directional flows [2] and hypothesized to occur on the flank of sand dunes [3]. In this report we propose a couple of possible new interpretations for some ripple patterns/morphologies on Mars that might not be transverse to the resultant wind direction.

Methods: Aeolian bedform are studied on HiRISE data (0.25-0.50 m/pixel). We used HiRISE stereo pairs to build DTMs and to orthorectify the overlapping images. We built the DTMs using SocetSet [4] and the NASA Ames Stereo Pipeline [5]. Ripple migration is measured on overlapping orthorectified HiRISE images [4].

Sand ribbon pattern: In Fig. 1a we show a sand ribbon pattern at Dillon Beach, CA (USA) which consists of longitudinal stripes of coarse/fine grained ripples. Ribbon features or "sand streams" [6-9] represent a mode of self-organization that is still poorly understood, likely due to small scale rotatory flows caused by the change in the roughness at the flow/bed interface [6]. Grain size segregation seems to be the main responsible for the observed wavelength differences. In Figs. 2b and c we show a couple of potential martian analogues. The first one is located in Gale Crater ~7 km SW from the selected Aeolis Mons entry point (Fig. 2b) [10]. In this area ripples are migrating to the SW suggesting winds coming from the NE [13]. Together with the transverse ripples sculpting the slope of the dark dune of Fig. 1b, we also notice several longitudinal stripes of sand running NE-SW [10]. These features are morphologically different from ripples as they do not display clear defect terminations and junctions. In addition, by looking at the same overlapping images analyzed in [11], these rectilinear features do not seem to change over time. One possible explanation is that they are ribbon-like features which form parallel to the main wind direction. In Fig. 2c we show another potential ribbon pattern located in the ESA 2016 landing ellipse in Meridiani Planum [12]. In this area larger wavelength megaripples form an E-W trending pattern extending for tens of kilometers. The pattern shows a clear topographic expression highlighted in the 3D view of Fig. 2c. Remote sensing analysis and in situ investigations [12-14] clearly indicate formative winds blowing from the east, thus the potential ribbons trend parallel to the main flow.

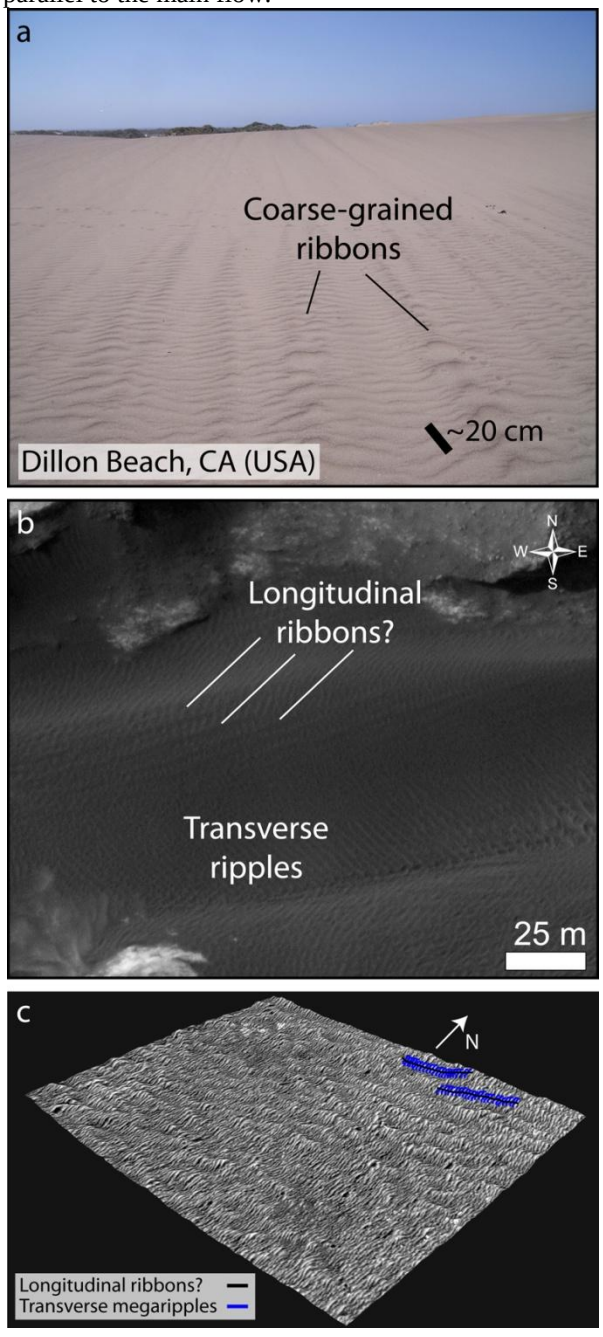

Fig. 1: Sand ribbon patterns **a)** Ribbons over the stoss side of a barchanoid dune, Dillon Beach, CA (USA) **b)** Potential longitudinal ribbon pattern in Gale Crater (Mars) **c)** 3D view of potential ribbons in Meridiani Planum (vertical exaggeration 10x).

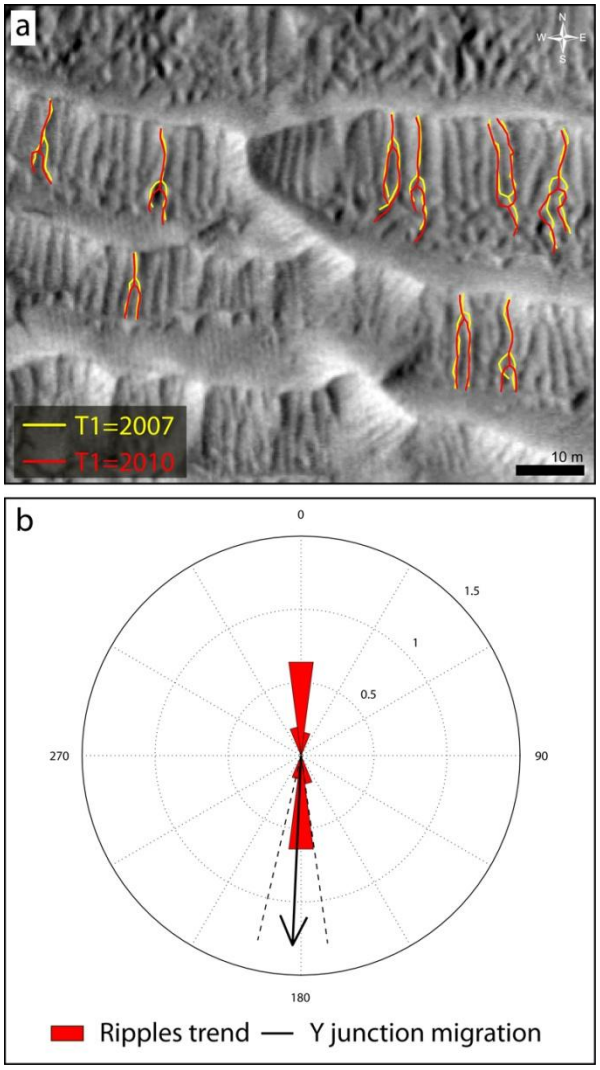

Fig. 2: Longitudinal ripples migration **a)** Mapped crestlines at T1 and T2. Note the longitudinal displacement of the Y junctions at T2 **b)** Rose diagram showing the ripple trend and the direction of the Y junctions migration.

Longitudinal ripples? Recent studies have demonstrated that bedform interactions are similar across scales (ripples, dunes) and environments (air, water) [15,16]. Of particular interest is the migration of the defect terminations (Y junctions) [17-19]. Computer models, laboratory experiments, and field observations have shown that Y junctions tend to migrate downwind when the flow is mostly uni-directional (or when two different flows approach at an acute angle) [17-22]. Conversely, when two flows approach at higher angles, longitudinal bedforms form, with junctures being displaced along the bedform crestlines [18,19] (see movie DR4 and DR6 in [21]). In Fig. 2 we show an example of potential longitudinal ripple migrations by comparing two overlapping HiRISE orthoimages acquired in 2007 and 2010. In this area active ripples trending N-S are located directly downwind of a set of 0.4-0.6 meters tall TARs (main wind deduced from dune migration and morphologies is from north to south). By looking at the overlapping T1 and T2 images we noticed that individual ripples are not migrating toward the East/West as expected. Instead, they seem to elongate downwind with the Y junction terminations being displaced towards the south at T2 (Figs. 2a and b). We hypothesize that flow convergence is probably occurring in this area, causing the ripples to evolve longitudinally. Such a convergence is likely triggered by the particular topographic setting in which ripples are evolving. Results from a preliminary mapping of potential longitudinal ripple migrations will be presented in support to this hypothesis.

Conclusion: In this report we show two examples of potential longitudinal depositional features on Mars. At the pattern scale we show sand ribbons which are formed by longitudinal rows of transverse ripples. If images resolution is not good enough to resolve individual ripples (Fig. 1b), these structures might be mistaken for transverse ripple patterns. At the ripple scale we show that some aeolian ripples might not be completely transverse to the resultant flow direction. The topographic setting in which sand ripples evolve needs to be considered when extracting wind information from images of planetary surfaces. Collectively, our observations suggest that the assumption of the transverse nature of ripples must be used with caution.

References: [1] Bourke M.C. et al. (2010) *Geomorphology* 121, 1–14. [2] Rubin D.M. and R.E. Hunter (1987) *Science* 237. [3] Howard A.D. (1977) *GSA Bulletin*. [4] Mattson S. et al. (2012) *3rd Int. Planet. Dunes Work*. [5] Moratto et al. (2010) *41st LPSC*. [6] Bagnold (1956) Dover Pub. INC. [7] Allen J. R. L. (1968) North-Holland pub. Co. [8] Simons F.S. and G.E. Eriksen (1953) *Bol. Soc. Geol. Perù*, 26, 229-246. [9] Rinker J.N. (1991) *Remote Sensing Field Guide-Desert*. [10] Silvestro et al. (2010) *41st LPSC*, 1820. [11] Silvestro et al. (2013) *Geology* 41 (4), 483-486. [12] Silvestro et al. (2015) *JGR submitted.* [13] Fenton L.K. et al. (2015) *Aeolian Research* pp. 75-99. [14] Golombek M. et al. (2010) *JGR* 111. [15] Ewing R.C. and G. Kocurek (2010) *Sedimentology* 57 (5), 1199-1219. [16] Rubin D.M. (2012) *Earth Science Review* 113, 176-185. [17] Warner B.T. (1995) *Geology* 23 (12), 1107-110. [18] Warner B.T. and G. Kocurek (1997) *Geology* 25 (9), 771-774. [19] Warner B.T. and G. Kocurek (1999) *Geology* 27 (8), 727-730. [20] Reffet E. et al. (2010) *Geology* 38, 6, 491-494. [21] Reffet E. et al. (2010) GSA DataRep. Item2010144, ww.geosociety.org/pubs/ft2010.htm. [22] Lorenz (2011) *Aeolian Research* 3, 229-234.

WIND AT THE NORTH POLE OF MARS: COMPARISONS OF MODELING AND OBSERVATIONS.

Isaac B. Smith[1] (isaac@boulder.swri.edu); Aymeric Spiga[2]; Daniel Tyler[3], Ryan C. Ewing[4]. [1]Southwest Research Institute, Boulder, CO; [2]Laboratoire de Météorologie Dynamique, Paris, France; [3]Oregon State University, Corvallis, OR, USA; [4]Texas A&M University, College Station, Texas.

Introduction: As GCM and mesoscale models develop, it becomes clear that modeling of the Martian atmosphere, with appropriate analysis techniques and comparison with observations, significantly advances in our ability to describe the Martian environment. This is especially true at the poles, where limited ground observations have been made but significant quantities of water reside on the surface, providing nearly the entirety of the Martian water cycle [1,2].

Mars polar regions are some of the most active places on the planet. Winds here strongly influence the surface distribution of water ice and other particulates, especially related to morphologic features such as the spiral troughs and prominent dune fields [3,4]. Understanding the pattern of winds throughout the year is an important step to understanding surface processes.

Prior to this study, no other has completed mesoscale simulations throughout a Mars year for the polar regions with a focus on diurnal, sub-seasonal, and seasonal variability. Here we provide simulations for each 5-10° of solar longitude (L_s) beginning at northern vernal equinox (L_s 0°) and ending at northern autumnal equinox (L_s 180°). Dates outside this range are also simulated, but the seasonal CO_2 ice provides a barrier for modifying the surface, and we exclude them from this discussion.

We find that the retreat of the seasonal CO_2 cap is the primary driver of surface wind speeds for the first half of the season. Once the CO_2 cap has disappeared, other factors, such as large eddies and regional transients play a larger role in determining wind properties. Our simulations of wind speeds and directions closely conform to geologic and atmospheric interpretations of near surface clouds and wind streaks, which afford a valuable check for simulations [3-5].

Methods: We ran simulations at relatively high mesoscale resolutions of 18 km per grid point. They have been completed at latitudes poleward of 75° and are run for three days every 5° or 10° of L_s with increased frequency near the summer solstice.

For one date in our pilot study we ran a three-nested, high resolution simulation for 20 days plus additional spinup. The resolution of each grid was 90 km, 30 km, and 10 km. Inclusion of the many days allows us to perform the detailed analysis first described by [6] and differentiate diurnal from larger timeframe effects.

To improve on previous versions, we have included observations from thermal instruments that detect where CO_2 ice is present on the surface [7] and maps of thermal inertia [8]. This resulted in significant improvements over previously run models, which took input from the LMD GCM to determine the location of CO_2 surface ice and disagreed with observations.

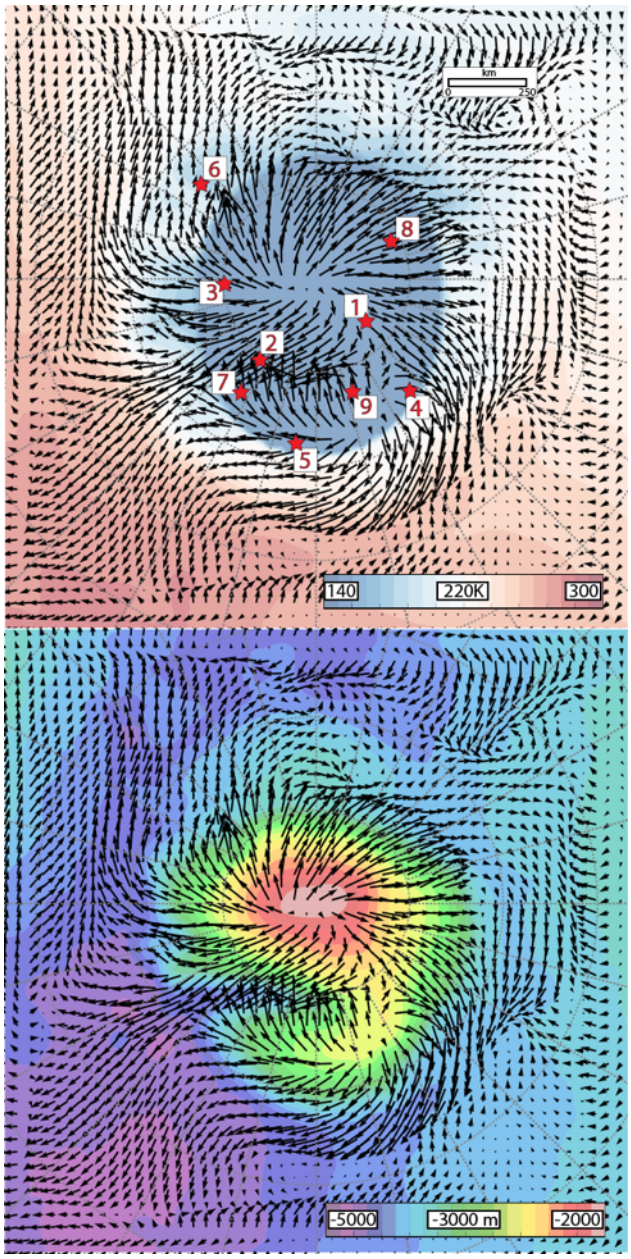

Figure 1: Simulation results for model run at L_s 75. a) Temperature map with overlying wind vectors. Fastest winds are found near boundary between the CO_2 seasonal cap and the newly exposed north polar layered deposits. Numbers are of locations plotted in Figure 2. b) Topographic map with overlying wind vectors at same time and day as (a). Surface slopes a strong influence on wind speeds.

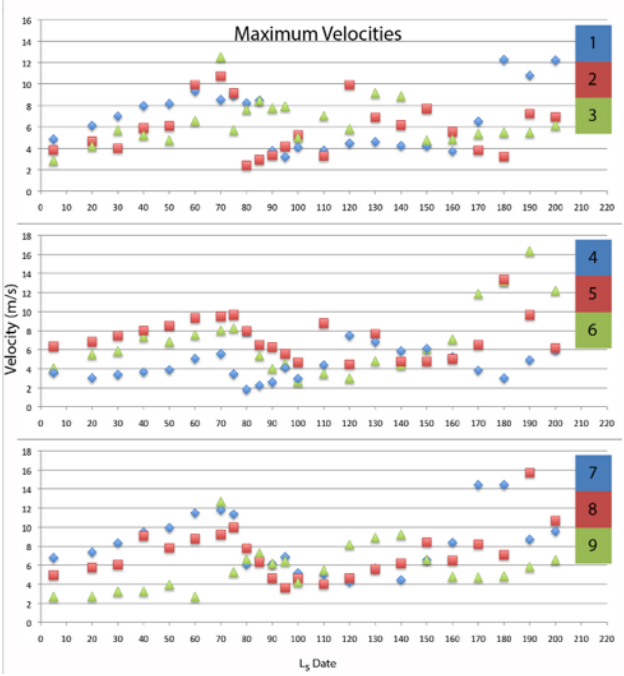

Figure 2: Plotted wind velocities at 9 locations indicated by Figure 1a. Wind speeds increase throughout the spring and peak at different times depending on the location of the CO_2 seasonal cap. After the cap retreats fully, wind speeds drop precipitously until late summer as the CO_2 ice returns.

Results: We find that the seasonal CO_2 frost plays an enormous role in influencing wind direction and speed (Figure 1). This is a direct effect caused by thermal contrast between the interior of the CO_2 cap (inside the crocus line) and outside, where water-ice and lithic material are allowed to warm above the ~150 K sublimation point of CO_2.

After compiling the individual model simulations into a time sequence, each series separate by 5 or 10° L_s, we determined the effect over longer periods. Figure 2 demonstrates the maximum and average simulated wind speeds at 9 polar locations for various dates. Immediately apparent is that the intensity of the wind increases for all locations throughout spring until the seasonal cap retreats to higher latitudes. The timing is different for each location. Wind speeds drop precipitously once the CO_2 retreats past the location. In other words: as the seasonal cap retreats, so do the fastest winds. This matches observations of atmospheric activity, especially in the presence of clouds that result from katabatic jumps. At both poles the clouds retreat at the same rate as the crocus line [9].

Figure 3 demonstrates the usefulness of modeling throughout the year. With this catalog of wind speeds, we can determine the direction and velocity of maximum sustained winds in any given period. Comparisons with inferred wind directions from dune orientations are then straightforward.

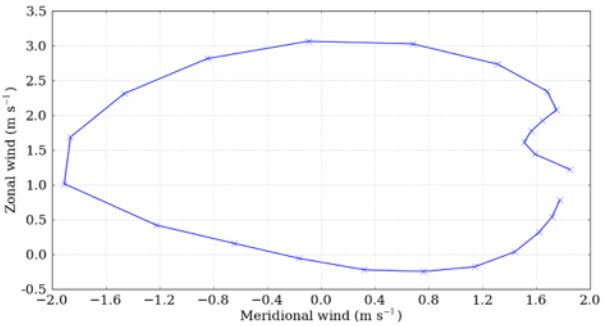

Figure 3: Hodograph of extracted wind speeds (zonal is across longitudes and meridional is across latitudes) at a site for 24 hours of one specific day. The usefulness of this study, with comprehensive modeling across many dates, is that rose diagrams may be made for an entire season for comparison with inferred wind directions from dunes.

Our one, long duration, triple-nested simulation was designed to test the relative effects of CO_2 driven circulation and the larger synoptic structure near the northern ice cap. This was completed at L_s80°, when the CO_2 ice was still present. Results from the analysis show that transients, as pressure and temperature anomalies, do play a role in the strength of katabatic winds; however, near the surface, where winds interact with the spiral troughs and dunes, this is a secondary effect that is mostly observed outside of the crocus line, or seasonal cap boundary. At higher altitudes the larger scale circulation dominates.

Once the seasonal cap has completely disappeared, all wind speeds near the surface at the north pole are reduced, and larger scale transients begin to dominate the synoptic structure [5,10,11].

Conclusions: In this preliminary study of modeling results at high temporal frequency, we were able to observe the direct effect that seasonal CO_2 ice on the surface had on wind speed and direction throughout the sunlit seasons. This is especially important in the late spring, when the seasonal CO_2 ice boundary is within the margin and on the slopes of the North Polar Layered Deposits. At this time (Figure 1), the winds have small diurnal variation inside the crocus line but significant changes in speed and direction outside.

References: [1] Byrne, S. (2009) *Annu. Rev. Earth Planet. Sci.* 37, 535–560. [2] Hvidberg, C. S. *et al.* (2012) *Icarus* 221, 405–419. [3] Smith, I. B. et al. (2013), *J.G.R.*, 118.9 : 1835-1857. [4] Ewing R. C. *et al.* (2010), *J.G.R.* (1991–2012), 115(E8). [5] Howard, A. D. (2000), *Icarus*, 144(2), 267–288. [6] Tyler, D. *et al.* (2008), *JGR*, 113(E3). [7] Titus, T. N. (2005), *36th LPSC*, vol. 36, p. 1993. [8] Putzig, N. E. *et al.* (2014), *Icarus*, 230, 64–76. [9] Smith, I. B. *et al.*, (2014), *Geomorphology.* [10] Tyler, D., and J. R. Barnes (2005), *J.G.R.*, 110(E6), E06007. [11] Tyler, D., and J. R. Barnes (2014), *Icarus*, 237, 388–414.

Wind-blown Sand on Mars: Preliminary Results of Transport Intermittency and Thresholds from Wind-tunnel Simulations. C. Swann[1], R. C. Ewing[1] and D. J. Sherman[2] Department of Geology and Geophysics, Texas A&M University, MS 3115 TAMU, College Station, Texas 77843, [2]Department of Geography, University of Alabama, 204 Farrah Hall, Tuscaloosa, AL 35487.

Introduction: Wind-driven sand transport is inherently intermittent because of the nature of atmosphere-surface energy exchange [1-7]. Boundary layer instability and surface irregularity spawn turbulent flow near the surface. Turbulent flow generates episodic high-energy gusts, followed by low energy lulls, and is identified by significant departures from the mean flow. However, transport models often assume steady-state flow conditions, using time-averaged wind speeds that ignore unsteadiness from turbulent flow [2-4]. Because of this, transport models differ from observed rates in field environments [8-9]. Earth-based field observations using the most commonly cited transport models [10-14] show discrepancies between predicted and observed transport rates on the order of 300% within each model, and up to 700% between Bagnold [10], Lettau and Lettau [14], and Kawamura [11]. The largest deviations from Earth-based models occur at lower transport rates and are attributed to errors in the threshold of motion [15].

Studies of aeolian transport within a simulated Martian environment have relied on the same transport models as have been used for most Earth-based studies. Greeley et al., [16-18], along with others [19-21], initially determined the threshold of movement for sand on Mars. They defined the threshold by "increasing the wind speed through the tunnel until saltation [along the entire wind tunnel] test bed was initiated (following Bagnold [22]). The free stream wind speed was noted and correlated with a standard velocity profile for the wind tunnel" (Greeley et al., [17], p. 418; Greeley et al, [23], p. 12). Four fundamental questions emerged from their definition of threshold. First, these studies did not focus on the intermittent nature of transport before full saltation begins, leaving open the question of how much transport on Mars occurs prior to full saltation. Transport rarely reaches a state of fully developed, continuous saltation. We now recognize an intermittency function, γp, introduced by Stout and Zobeck [3], that describes the portion of time sand transport occurs, and have found saltation rarely occurs more than 50% of the time in any 5-minute period. Lancaster et al. [7] found continuous saltation only to occur 11%-31% of the time during a storm event.

Second, the threshold of motion in those studies, was only evaluated for saltation, and not focused on the movement of bedload before saltation begins. Bedload consists of particles that roll, slide or move in small hops over the surface driven either by the direct force of the wind on the grains or as a result of bombardment from saltating particles [10. 24-26]. Little is known of bedload transport on Mars. Bedload is argued to contribute between 3 and 29% of the total load on Earth [1, 27-28]. This wide range of estimates exists because bedload had never been directly separated from saltation on Earth, until recently [29]. The fluid threshold on Mars is defined by the moment at which full saltation occurs over the wind tunnel, a point where bedload particles are already in motion, evidenced in wind tunnel experiments [16, 30-32]. Threshold predictions for Mars exclude this precursory, intermittent movement before a saltation cloud moves over an entire test bed.

As is widely recognized for threshold-of-motion studies for Earth and Mars, a single wind speed value cannot adequately describe all scenarios when transport begins. An assumption of a single value disregards other controlling factors: modes of movement, different grain size distributions, armoring effects, electrostatics, particle-to-particle contact, compaction, mineral composition of sediments and the exposure of different grains to surface winds. The combination of these factors on a surface makes the threshold of motion occur over a range of values. Intermittent transport, in addition to these factors, produces error in single-value threshold estimates [2-3, 6-7, 33]. Our research generates a range of threshold values related to the intermittency of transport.

The fourth question in Martian threshold predictions is the use of visually-noted free stream velocities, subsequently correlated with typical velocity profiles to resolve the threshold shear velocity. Turbulent shear stress initiates movement with characteristic lag times of the order of 0.5-1s [5, 34-36]. Velocity profiles are altered by the presence of a saltation cloud, producing potential order-of-magnitude errors in estimates of roughness lengths [37-38]. Typical profiles used to calculate shear velocity from free stream velocity must incorporate the variability generated from various levels of saltation transport, including potential changes in the value of the von Karman constant [39].

The presented research uses the MARSWIT to simulate transport conditions on Mars. A new bedload trap is used to individually separate surface creep, reptation and saltation. The initiation of each mode of movement is correlated to instantaneous velocity pro-

files to derive modal threshold shear velocities. Intermittency is calculated to resolve flux distributions prior to 'continuous saltation'.

Our study aims to quantify intermittent aeolian bedload transport under Martian atmospheric pressures using the Planetary Aeolian Facility MARSWIT. Much of the previous work done in MARSWIT focused on quantifying the threshold and sediment fluxes associated with the saltation mode of transport, whereas our research uniquely focuses on the fluxes associated with intermittent transport, primarily bedload that occurs prior to initiation of full saltation. The tasks accomplished in this proposal will improve our understanding of the atmosphere-surface interactions and rates of aeolian resurfacing on Mars by quantifying sediment fluxes associated with high frequency low-intensity wind events under Martian atmospheric conditions.

References: [1] Anderson, R.S. et al. (1991) "A review of recent progress in our understanding of aeolian transport." *Aeolian Grain Transport I: Mechanics*, Wien: Springer-Verlag 1-19. [2] Butterfield, G. R. (1991) "Grain transport rates in steady and unsteady turbulent airflows." *Aeolian Grain Transport I: Mechanics*, Wien: Springer-Verlag 97-122. [3] Stout, J. E. and Zobeck, T. M. (1997) J. Arid. Environ., 44(5): 959-970. [4] Bauer, B. O. et al. (1998) J. Arid. Environ., 39(3), 345-375. [5] Sterk, G. et al. (1998) Earth Surf. Processes Landforms 23(10): 877-887. [6] Schönfeldt, H. J. (2004) Meteorol. Z. 13(5): 437-444. [7] Lancaster, N. et al. (2010) JGR 1115(F3): F03027. [8] Sherman, D. J. et al. (1998) Geomorphology, 22(2): 113-133. [9] Sherman, D. J. et al. (2013) Earth Surf. Processes Landforms, 38: 169-178. [10] Bagnold, R. A. (1937b) Geographical J., 89(5): 409-438. [11] Kawamura, R. (1951) Translated (1965) as U. California Hydraul. Eng. Lab. Rep. HEL 2-8, Berkeley. [12] Zingg, A. W. (1953) Iowa Inst. Hyrdaul. Res. Fifth Hydraul. Conf. Proc., 111–136. [13] Kadib, A. A. (1965) U. California Hydraul. Eng. Lab. Rep. HEL 2-8, Berkeley. [14] Lettau, K. and Lettau, H. (1977) U. of Wisconsin-Madison IES Rep. 101, 110-147. [15] Ellis, J. T. and Sherman, D. J. (2013). *Treatise in Aeolian Geomorphology*, San Diego, 85-108. [16] Greeley, R. et al. (1974) Proc. Royal Soc. London A 341: 331-360. [17] Greeley, R. et al. (1976) Geophys. Res. Lett. 3(8): 417-420. [18] Greeley, R. et al. (1980) Geophys. Res. Lett. 7(2): 121-124. [19] Iversen, J. D. et al. (1976) ICARUS 29: 318-393. [20] Pollack, J. B. et al. (1976) ICARUS 29: 395-417. [21] White, B. R. et al. (1976) JGR 81(32): 5643-5650. [22] Bagnold, R. A. (1941) *The Physics of Wind Blown Sand and Desert Dunes*, Methuen: London, 265. [23] Greeley, R. et al. (1977) NASA Tech. Memorandum 78423. [24] Bagnold, R. A. (1937a) Proc. Royal Soc. London A 163: 250-264. [25] Leatherman, S. P. (1978) Sedimentology 25: 303-306. [26] Anderson, R. S. (1987) Sedimentology 34: 943-956. [27] Tsoar, H. (1994) Prog. Phys. Geog. 18: 91-96. [28] Wang, Z.-T. and Zheng, X.-J. (2004) Powder Technol. 139(2): 123-128. [29] Swann, C. M. and Sherman, D. J. (2013) Aeolian Res. 11: 61-66. [30] Bagnold, R. A. (1936) Proc. Royal Soc. London A 157: 594-620. [31] Nickling, W. G. (1988) Sedimentology 35(3): 499-511. [32] Butterfield, G. R. (1998) J. Arid. Environ., 39(3): 377-394. [33] Stout, J. E. (1998) J. Arid. Environ., 39(3): 395-401. [34] Jackson, D. W. T. and McCloskey, J. (1997) Geophys. Res. Lett. 24(2): 163-166. [35] Baas, A. C. W. and Sherman, D. J. (2005) J. Geophy. Res. 110: F03011, 15pp. [36] Chapman, C. A. et al. (2012) Geomorphology 151-152: 1-12. [37] Bauer, B. O. et al. (1992) Prof. Geographer 44(4): 453-464. [38] Farrell, E. J. and Sherman, D. J. (2006) J. Coastal Res., SI 39: 384-389. [39] Li, B. et al. (2010) Geophys. Res. Lett. 37: L15404.

MORPHOLOGY OF AEOLIAN BEDFORMS ON 67P/CHURYUMOV-GERASIMENKO. D. Tirsch[1], S. Mottola[1], K. Otto[1], E. Kührt[1], R. Jaumann[1,2], G. Arnold[1], H.-G. Grothues[3], M. Hamm[1,4], H. Michaelis[1], I. Pelivan[1], G. Proffe[1], F. Scholten[1], S. Schröder[1], J.-P. Bibring[5]. [1]Institute of Planetary Research, German Aerospace Center (DLR), Rutherfordstrasse 2, 12489 Berlin, Germany, (Daniela.Tirsch@dlr.de); [2] Institute of Geological Sciences, Freie Universität Berlin, Berlin, Germany; [3]Space Management, Space Science, German Aerospace Center (DLR), Bonn, Germany; [4] Humboldt Universtität Berlin, Germany; [5]Institut d'astrophysique spatiale (IAS), Universtité Paris-Sud, Orasy, France.

Introduction: Comets are no typical place to expect dunes at the surface, but surprisingly, aeolian bedforms have been identified on the surface of 67P/Churyumov-Gerasimenko (hereafter named 67P) in OSIRIS (orbiter camera, [1]) and ROLIS (descent imager, [2]) data [3]. Intensive studies aim at finding an answer to the question how to explain aeolian granular transport on a comet with an extremely rarified atmosphere and with almost negligible gravitation, hence, without the fundamental physical mechanisms generally responsible for particle motion [3]. However, conclusive identification of aeolian bedforms indicates that saltation must have happened on 67P. It is not clear, yet, how saltation has been initiated on the comet but conceivable processes are currently under discussion. [3] introduced the term "cometary saltation" for this special type of grain transport, that seem to involve uncommonly coarse particle sizes.

Discussion of Aeolian Bedforms: Dune-like features have first been discovered by [4] in the neck region of the nucleus, called the Hapi region (Fig. 1). The large ripples measure about 60 meters in width and comprise sharp crests and slipfaces, suggesting an "uphill" transport direction in Figure 1. It also is conceivable that the largest crest at the very end of the dune field (downwind/uphill) represents the crest of a mega-barchan, being superposed by the ripples. On planets like Earth or Mars, sharp dune crests often point to relatively fine-grained substrates and active bedforms. It is questionable, though, if the dune-like features of the neck region are composed of finer grained material compared to the bedforms found at other places on 67P since the balance of gravity, gas drag and cohesion is another one on comets.
Further dune-like features on 67P resemble coalesced barchan dunes and are located nearby Philae's landing site in a region called Ma'at.

Other aeolian bedforms, in association with obstacles, have been identified in ROLIS images covering the primary landing site of Philae lander. This is a relatively flat region vastly covered by smooth airfall deposits [3]. OSIRIS images reveal that these bedforms spread over adjacent areas. Particles on 67P can be subject to aeolian motion if gas transport is initiated by sublimation-driven ejection of material [3, 4]. It is noteworthy that the obstacle-associated bedform size on 67P is much larger than those known from Earth and Mars. This might be an effect of low gravitation and coarse grain size. Except for the aeolian ripples in the neck region, all aeolian bedforms identified so far, show rounded crests and a coarser overall shape. Such features generally point to grain-sizes that are coarser than sand and/or to immobile and degraded bedforms [5].

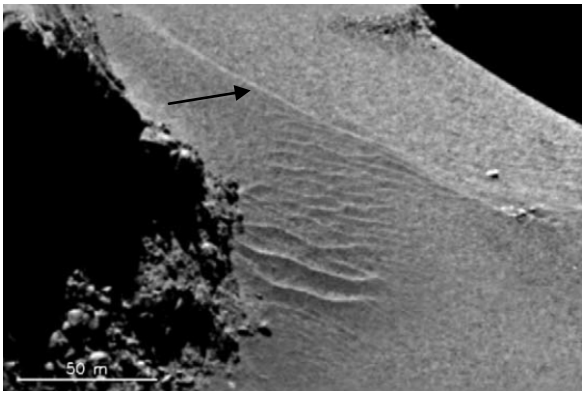

Fig. 1: Large aeolian ripples in the Hapi region, the so-called neck region of the comet. The width of this ripple field is about 60 m. The black arrow marks the crest of a possible mega-barchan. (OSIRIS image NAC_2014-09-18T00.33.01.377Z_ID10_1397549800_F22 [4]) © ESA/Rosetta/MPS for OSIRIS Team MPS/UPD/LAM/IAA/SSO/INTA/UPM/DASP/IDA.

Commentary: Detailed analyses are currently in progress and publications have been submitted. The latest results will be presented at the workshop.

References: [1] Keller H. U. et al. (2007) *Sp. Sci. Rev*. 128, 433–506. [2] Mottola, S. et al. (2007) *Sp. Sci. Rev.* 128, 241-255. [3] Thomas, N. et al (2015) *LPSC*, abstract #1712. [4] Thomas, N. et al. (2015) Science 347, 0.1126/science.aaa0440. [5] Wiggs, G. F. S. (2002) *Aride zone Geomorphology*, Wiley & Sons.

SEDIMENT FLUX MEASUREMENTS AT A MARS ANALOG SITE. T. N. Titus[1], R. K. Hayward[1], R. Bogle[1] and J. Zimbelman[2],[1]U.S. Geological Survey, Astrogeology Science Center, Flagstaff, AZ (ttitus@usgs.gov) [2]Smithsonian Institution, Washington, D.C.

Introduction: Understanding how the surface and atmosphere interact on Mars is important to the safety of future landed missions, as well as being important to the understanding climate evolution and the potential for past life. Before the repeat coverage of High Resolution Imaging Science Experiment (HiRISE) images, the general scientific consensus was that most, if not all, of the dunes on Mars were immobile. However, recent studies have demonstrated that Martian dunes are changing dramatically in the current climate regime [e.g.,1-6]. Bridges et al. [7] documented dune activity in 23 of 57 repeat HiRISE dune targets, concluding that sand is mobile in virtually all parts of the north polar erg and in many non-polar areas. Sand flux rates measured by Bridges et al. [8] show that flux rates at some places on Mars are similar to flux rates on Earth and that dune fields may have formed in as little as 10,000 years. However, both atmospheric modeling and in situ meteorological measurements on Mars suggest that winds are seldom above the saltation threshold [9-13]. Numerical models and wind tunnel experiments indicate that wind speed needed to keep grains saltating on Mars may be 3 to 10 times less than the wind speed required to initiate saltation [14-15]. The goal of the Grand Falls (GF) project was to measure sediment flux at a Mars analog site and to field test whether hysteresis, the continuation of sand transport by lower velocity winds once saltation has been initiated, can be responsible for the flux rate observed by Bridges et al. [8].

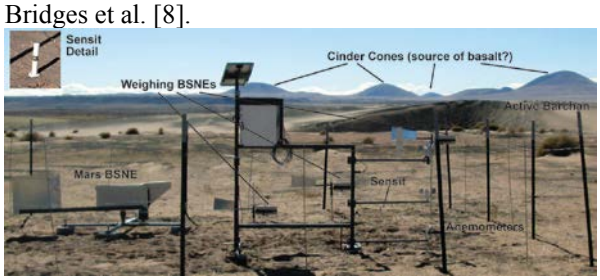

Figure 1: Grand Falls Field Site.

Analog Site: The Grand Falls dune field (~1.6 km x 1 km) is located ~70 km NE of Flagstaff, AZ, and just north of the Little Colorado River (LCR). The dunes at GF are in a relative topographic minimum, migrating toward local topographic maxima that will impede their progress. This setting is analogous to the setting of an estimated 1000 dune fields on Mars that occur within craters and valleys [16-17]. A more detailed description of the analog site can be found in Bogle et al. [18]

Most of the dune sand on Mars is likely of basaltic composition [e.g.,19]. Basalt sand is also present in significant amounts at GF, allowing us to observe its behavior under various atmospheric conditions. Bimodal grain size is another sand characteristic common to both GF and Mars [e.g., 20].

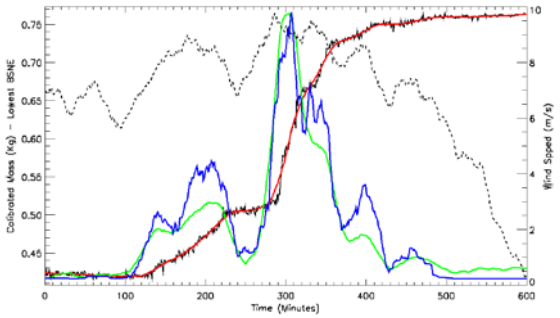

Figure 2: Sediment flux and wind data collected for one 10 hour wind event. The solid black line is the data from the lowest sediment catcher. The red line is the smooth fit to the sediment catcher data. The green line is the gradient of the red line and the blue is the smoothed number of particle impacts from the solid-state saltation sensorS4.

Instrumentation: We installed the following equipment (Figure 1) at GF: one custom-designed sediment sampler, three weighing BSNE (Big Spring Number Eight sediment samplers that passively sample near surface airborne particles and record the weight of the sample at one minute intervals), three anemometers, one directional anemometer, one solid-state saltation sensor (S4), one CR-1000 data logger, two solar panels, and a battery power supply. The equipment has been actively collecting data since November 2013.

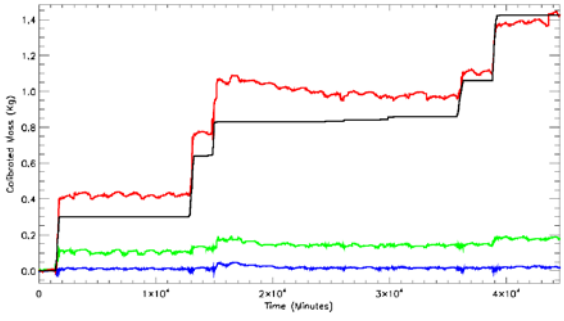

Figure 3: Sediment weight and integrated S4 observations. The red, green, and blue lines are the data from the sediment catchers. The black line is the calibrated data from the S4.

Sediment Flux Calculations: Sediment flux is usually expressed either in units of mass per unit area per unit time (horizontal mass flux (HMF), equation 1)

or as mass per length per unit time (horizontal mass transport (HMT), equation 2) [21]:

$$[1]\ HMF = \dot{q} = \frac{dq}{dt} = {}^{m}/_{At\varepsilon} = \sigma e^{-z/z_0}$$

where m is the sediment mass, A is the areal cross-section of the BSNE opening, t is the integration time, and ε is the BSNE efficiency which is usually 0.4 [22].

If the HMF ($\dot{q}$) is measured at multiple heights (z), then an exponential function can be determined where σ is the HMF at one scale height ($z0$).

$$[2]\ HMT = F = \int_0^\infty \dot{q}\ dz = \sigma z_0$$

Equation 1 is the sediment flux through a unit area at a specified height – which is what an individual BSNE measures. Equation 2 is the sediment flux that passes through a horizontal unit length, vertically integrated from ground level to the top of the atmosphere – thus providing an estimate of the total amount of sediment transported by the atmosphere.

Sediment Flux Results from Bulk Samples: Several large wind events have occurred, providing the opportunity to compare wind events. The scale heights of the sediment flux vary little from wind event to wind event, typically ranging between 17 cm and 22 cm. Sediment flux (HMT) appears to be independent of the sediment flux scale height and can vary from 2.6 to 6.7 kg/m/s.

Table 1: Sediment Flux Rates for Selected Wind Events.

Dates	Event Duration (Hrs)	BSNE-1 Mass (Kg)	BSNE-2 Mass (Kg)	BSNE-3 Mass (Kg)	Flux Scale Ht. (m)	HMT (Kg/m/s)
2/28/14	6.3	0.34	0.029	0.0073	0.22	6.7
3/17/14	5.0	0.17	0.020	0.0047	0.27	4.4
4/25/14	8.2	0.13	0.011	0.00	0.16	2.6
5/11/14	9.4	0.35	0.033	0.00	0.17	6.0

Shear Stress Threshold Calculations: By collecting wind speed data at more than one height AGL, we can calculate the shear stress velocity (U^*), by fitting the observations to equation 3.

[3] $U = U^*/k\ ln(z) - U^*/k\ ln(z_0)$,

where k=0.4, z is height, and z_0 is the aerodynamic roughness scale, to find the roughness factor [23]. Once the shear velocity (U*) and surface roughness (z_0) has been determined, wind speed at any height can be interpolated using this same equation. By comparing U^* to the sediment counts from the S4, we can determine $U^*_{initial}$ and $U^*_{continuous}$.

Hysteresis Calculations: Hysteresis analysis cannot be conducted using the sediment catchers. While the sediment catchers provide a measure of the sediment weight each minute, the uncertainty within those measurements due to vibrations, is larger than any increase in sediment mass over a period of a few minutes. Therefore, the only instrument with sufficient signal-to-noise on sediment flux is the S4. Shear stress above 0.6 m/s clearly initiates saltation; however a lower threshold may be possible.

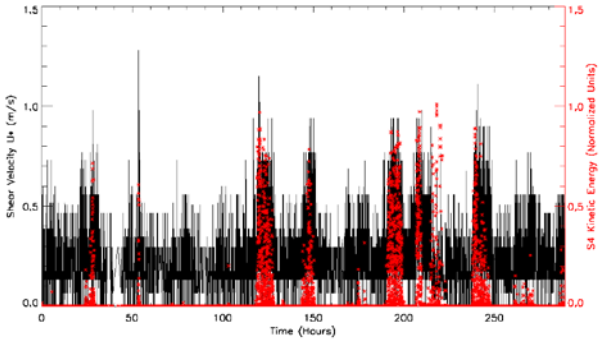

Figure 4: Shear velocity and S4 kinetic energy vs. time. The black lines are the calculated *U over a period of 2 weeks. The red asterisks are the normalized S4 kinetic energy over the same time period. Shear stress above 0.6 m/s clearly initiates saltation; however, a lower threshold may be possible. There are periods when the shear stress should be sufficient to initiate saltation but does not, suggesting that the sediment source may be limited, possibly by environmental factors.**

Acknowledgements: We received MMAMA funding (award number NNH13AV78I) to investigate the role of hysteresis in sediment flux at GF and test a modified sediment sampler for possible use on Mars. We are grateful to the Navajo Nation for allowing us to conduct this experiment on their tribal lands. This project benefits greatly from the efforts of John Vogel and Margaret Hiza.

References: [1] Bourke et al., 2008, *Geomorphology*, **94**, 247-255. [2] Silvestro et al., 2010, *Geophys. Res. Lett.*, **37**, L20203 [3] Chojnacki et al., 2011, *J. Geophys. Res.*, **116**, E00F19 [4] Hansen et al., 2011, *Science*, **331**, 575 [5] Geissler et al., 2010, *J. Geophys. Res.*, **115**, E00F11 [6] Chojnacki et al., 2014, *Icarus*, **232**, 187-219 [7] Bridges et al., 2012a, *Nature*, **485**, 339 [8] Bridges et al., 2012b, *Geology*, **40**, 31. [9] Sullivan et al., 2005, *Nature*, **436**, 58. [10] Greeley et al., 1980, *Geophys. Res. Lett.*, **7**, 121. [11] Hess et al. 1977, *J. Geophys. Res.*, **82**, 4559. [12] Mutch et al., 1976, *Science*, **194**, 87-91. [13] Kok, 2012, *Nature*, **485**, 312-313 [14] Claudin and Andreotti, 2006, *EPSL*, **252**, 30-44. [15] Kok, 2010, *Geophys. Res. Lett.*, **37**, L12202 [16] Hayward et al., 2007, *J. Geophys. Res.*, **112**, E11007 [17] Fenton & Hayward, 2010, *Geomorphology*, **121**, 98. [18] Bogle et al., 2015, *Geomorphology*, **228**, p. 41. [19] Herkenhoff and Vasavada, 1999, *J. Geophys. Res.*, **104**, 16487. [20] Sullivan et al., 2008, *J. Geophys. Res.*, **113**, E06S07 [21] Mendez et al. 2011, *Geomorphology*, **129**, 43-48. [22] Goossens and Offer, 2000, *Atmos. Envir.*, **34**, 1043-1057. [23] von Karman, 1930, *Mechanische Ahnlichkeit und Turbulenz*, Weidmannsche Buchh., Berlin.

THE PUZZLE OF LINEAR DUNES ON PLANETS. H. Tsoar, Department of Geography and Environmental Development, Brn Gurion University of the Negev, Beer Sheva, 84105, Israel. tsoar@bgu.ac.il

The term "linear" or "longitudinal" dunes describes more than one type of dune. In my lecture I will cover what we do and do not know about these dunes. While all linear dunes possess one common characteristic of elongation, they have different shapes and mechanisms of formation and elongation.

McKee [1] differentiated between basic or simple linear dune forms and compound or complex linear forms. The former consists of individual dune forms which are spatially separated from the adjacent dunes. These dunes can also be either convoluted or rectilinear. The mechanism of convoluted seif dunes was studied in the field [2], [3], [4], and by modeling [5]. From its primary formation, the seif dune is affected by two wind directions coming obliquely from both sides of its slopes, at angles of 90^o to 120^o between the two wind directions. Each wind is separated and diverted along the lee slope after reattachment of the separated flow, to blow parallel to the crest-line in a down-dune direction. This process is known as the *flow diversion model*.

The rectilinear dunes are divided between vegetated linear dunes (VLDs) and unvegetated rectilinear dunes. The first is the most widespread dune type that exists in many deserts of the world (mostly in the Australian deserts and the Kalahari). Vegetated-linear dunes are low with rounded profiles. They range in height from a few meters up to dozens of meters. Vegetated-linear dunes may run in parallel for scores of kilometers. Vegetated linear dunes were formed in Late Pleistocene, which had a climate characterized by higher wind power. However, the processes of formation and elongation of VLDs, which are partly or fully vegetated, are not well understood because all contemporary VLDs are stable. It is assumed that vegetation cover is the main reason for VLD formation. It is proposed that VLDs were formed under conditions that prevailed during the Pleistocene but are not present today. Those ancient conditions are characterized by higher wind power and lower rainfall that can reduce, but not completely destroy, vegetation cover, leading to the formation of big nebkhas with lee dunes behind them. The lee dunes connect to the nebkha in front of it, forming one elongated linear vegetated dune. Accordingly, VLDs develop by elongation of lee dunes formed at the downwind side of the nebkhas [6].

The unvegetated rectilinear dunes are found around the north polar region of Mars. On Earth, these dunes are only found at the Qaidam Basin in western China [7]. It is hypothesized that they were also created by the formation of lee dunes when the lee side of a dune (barchan for instance) was cemented. This indurated dune acts as an obstacle that causes a three-dimensional horseshoe vortex and the formation of a lee dune. Once the lee dune is indurated, the process is repeated, and eventually leads to the formation of an elongated rectilinear dune. There are some similarities between the formation of VLDs and unvegetated rectilinear dunes. For example, both are formed by the creation of lee dunes.

Compound and complex linear dunes are wide and high linear megadunes. The first consists of two or more simple linear dunes which have coalesced and are superimposed on the linear megadune. The complex linear dune is composed of two or more non-linear simple dune types which have coalesced and are superimposed on the linear megadune. When we examine aerial low-resolution photographs or satellite images, the small simple superimposed dunes cannot be discerned. That may give the impression that the compound and complex dunes are simple forms. It is plausible that the vast linear dunes on Titan are compound and/or complex forms.

References:

[1] McKee E.D. (1979) *GSPP 1052, 3-19.* [2] Tsoar H. (1982) *JSP, 52, 823-831.* [3] Tsoar H. (1983) *Sedimentology, 30, 567-578.* [4] Tsoar H. et al. (2004) *Geomorphology, 57, 293-302.* [5] Parteli E.J.R. (2009) *PNAS, 106, 22085-22089.* [6] Tsoar H. (2013) *Treatise on Geomorphology, 11, 414-427.* [7] Rubin D.M. and Hesp P.A. (2009) *Nature Geo., 2, 653-658.*

USING LIDAR DATA HAS HELPED IMPROVE THE UNDERSTANDING AND INTERPRETATION OF RESOURCES AT GREAT SAND DUNES NATIONAL PARK AND PRESERVE, COLORADO, U.S.A.

A. D. Valdez, National Park Service, 11500 Hwy 150, Mosca, CO 81146 email: andrew_valdez@nps.gov

Introduction: Great Sand Dunes National Park & Preserve was mapped using lidar (Light Detection and Ranging) in the fall of 2011 as part of a U.S. Geological Survey project [1] that conducted a lidar survey of southern Colorado's San Luis Valley. The project design required a sampling interval of one return per square meter and a vertical accuracy of 15 cm. This is the most accurate topographic mapping of Great Sand Dunes to date and has been used by the National Park Service (NPS) to quantify and visualize the resources it is charged with protecting and interpretation of these resources.

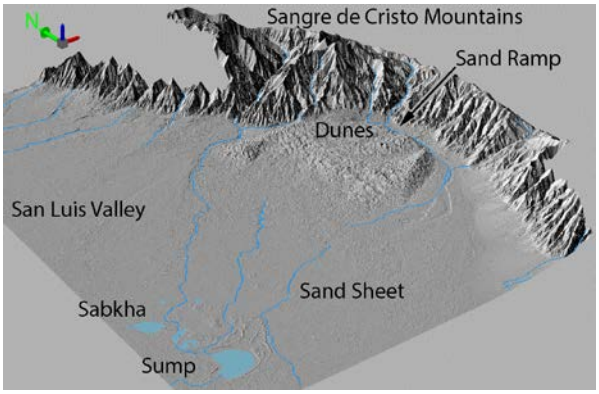

Figure 1: Hillshade of digital elevation model for Great Sand Dunes National Park & Preserve created from the lidar dataset. Vertical exaggeration = 2.

Discussion: Great Sand Dunes is a dynamic landscape where sabkha, sand sheet, dune, and sand ramp deposits have developed along a topographic gradient [2]. Figure 1. The lowest deposit is found in a depression, described as a sump that is the terminus of an internally drained region where playa lakes form [3]. This sump is believed to be the immediate source of sand for the Great Sand Dunes aeolian system [4].

Having a lidar dataset allows the NPS to better understand the relationship between topography, sand deposits, and hydrology. For example, what is the extent of the sump in relation to the distribution of sand? How large would playas become before they overflow the sump and become tributary to the Rio Grande? At what depth to ground water does the sabkha transition to sand sheet?

Accurate topographic data also allows the NPS to make more precise measurements in areas such as determining the sand volume of the dunefield. It also has been used to help develop a systematic method to measure dune height. Great Sand Dunes contains mega-dunes. The summit of the dune is straight forward, but defining the base of such a complex dune form is more complicated. Using elevations at the perimeter of the dunefield, a generalized valley floor can be projected beneath the dunefield. This serves as a base elevation for the dune forms above it. Then the elevation of the dune crest can be subtracted from the elevation of the projected base to give the dune height, making it possible to know the elevation of all dunes in the dunefield. Previously, only a few index dune heights were known as they were surveyed using traditional techniques.

Lidar can give a bare earth perspective, removing vegetation so that landforms stand out. Changing vertical exaggeration and lighting angles can also improve landform identification. In many ways manipulating lidar data can give a better view than seeing an area first hand. In 2010, the Second Planetary Dunes Workshop fieldtrip went to Great Sand Dunes and viewed a crater of unknown origin [5]. Thanks to lidar, the NPS now knows that there is one, possibly more very similar features in that area.

Digital elevation modeled created from lidar data can also be used as a visualization tool. The XYZ data can be projected as 3 dimensional models which are very useful for visualizing landforms, such as dunes, to a non-scientific audience. To enhance this effect it can be presented in stereo 3D. The NPS uses this with positive public response.

References: [1] Giffin C. L. (2011) *USGS Lidar Point Cloud (LPC) CO_San-Luis-Valley_2011*. [2] Valdez A. V. (2007) *Quaternary geology of Great Sand Dunes National Park and Preserve, southern Colorado (Chapter A.)* U.S. Geological Survey, Open-File Report 2007-1193, 3-51. [3] Emery P. A. (1971) *Hydrology of the San Luis Valley, south-central Colorado.* U.S. Geological Survey Hydrologic Investigations Atlas HA-381. [4] Madole R. F. and Romig J. H. (2008) *On the origin and age of Great Sand Dunes, Colorado.* Geomorphology 99, 99–119. [5] Marvin U. B. (1966) *A re-examination of the crater near Crestone, Colorado.* Meteorics, 3(1) 1-10

Additional Information: Lidar and other geographical data sets can be obtained from the USGS at: http://earthexplorer.usgs.gov/

INVESTIGATING THE POLEWARD TREND OF SOUTHERN DUNE FIELD STABILIZATION ON MARS USING THERMOPHYSICAL OBSERVATIONS. S. J. Van Kooten[1,2,†], N. E. Putzig[2], and L. K. Fenton[3]. [1]University of Colorado, Boulder, CO, [2]Southwest Research Institute, Boulder, CO, [3]SETI Institute, Mountain View, CA. [†]Contact: samuel.vankooten@colorado.edu

Synopsis: Dune fields in the southern Martian hemisphere have morphologies indicating a poleward progression toward stabilization starting at 50-60° S. Separately, a near-surface layer of ground ice is suspected to span the hemisphere from ~50° latitude to the pole. We hypothesize that the southward increase in stabilization may be caused by an ice table that is shallower at higher latitudes, a linkage that would allow dune morphology to be used as a tracer of local climate. Thermal inertia measurements and multi-layer thermal modeling can be used to infer near-surface properties, including ice table depth. We have begun an investigation of the thermal properties of the largest 171 southern dune fields with well-defined characteristics. Our analysis of the first two suggests the uppermost portion of the dunes contains a surface of crust overlying dust, rather than sand overlying ice, indicating there is more to the picture than initially suspected.

Background: Recently, evidence has accumulated for a ubiquitous, high-latitude layer of water ice below the Martian surface. Material excavated by fresh, mid-latitude craters has revealed ice within decimeters of the surface [A]. Neutron spectrometry data from Mars Odyssey indicates deposits of 20–100% water-equivalent hydrogen by mass within a meter of the surface poleward of ±50° latitude [B]. Temporal variations in apparent thermal inertia in the northern polar erg have been shown to be consistent with decimeters of dry sand overlying ice-cemented sand [C].

A mapping of 1190 dune fields poleward of 50° S [D] found that sharp-crested dunes are located almost exclusively north of 60° S, and more rounded dunes are primarily south of this line, progressing to flat sand fields near the pole (Fig. 1). This indicates dunes south of 60° S have experienced increased stabilization and are less reflective of current aeolian activity.

Ice, the Leading Suspect: This southward smoothing of dune fields beginning near 60° S is tantalizingly coincident to the southward rise in Odyssey-detected ice beginning near 50° S. Since it is known that interstitial ice retards bedform migration [E], it has been proposed [D] that the transition in dune morphology is caused by sub-surface ice being closer to the surface in more poleward regions. That is, sand is free to respond to local wind when the ice table is low, but a high ice table cements dunes in place, leaving them subject to non-aeolian erosion and causing their rounded, flattened appearance.

High-resolution images do not reveal any craters on these frozen-in-place dune fields, indicating the dune surfaces are young, perhaps even under 100 years old [F]. This suggests that, if the latitudinal progression in dune stability is caused by a progressively shallower ice table, dune morphology is a direct indicator of current climatic conditions.

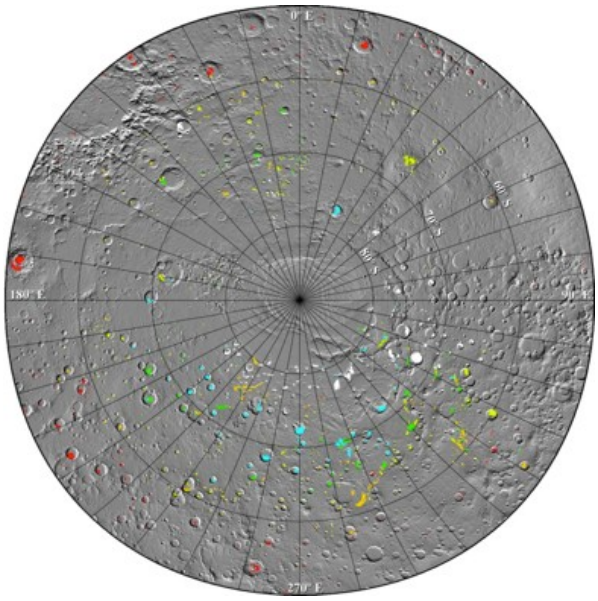

Figure 1. MOLA shaded relief map of the region poleward of 50° S in an oblique equidistant projection. Marked are 1190 dune fields in six morphological classes from [D]. Moving south, sharp-crested dunes (red) give way to rounded dunes (e.g. green) and then to flat sand fields (white).

Investigating with Thermal Inertia: We investigate the ice table depth through comparison of thermal inertia measurements to model results.

Thermal Inertia: Thermal inertia is a bulk material property. For typical materials on the Martian surface, it is dominated by thermal conductivity [G], which is determined by properties such as particle size and porosity, making materials such as dust, sand, and rock easily distinguishable. We determine apparent thermal inertia from individual temperature measurements by the Mars Global Surveyor Thermal Emission Spectrometer (TES) and the Mars Odyssey Thermal Imaging System (THEMIS) using a lookup table which matches temperature to thermal inertia at particular times of day, seasons, latitudes, and atmospheric and surface conditions [H, I].

Thermal Modeling: Once we have determined a dune field's thermal inertia over the course of a year, we compare with predictions from various model surfaces. For a heterogeneous surface, apparent thermal inertia varies with time of day and season [J, K], so observed variations can be matched to a combination of materials (e.g. dust, sand, ice) in a certain configuration (horizontal mixture or vertical layering). Vertical layering is key, as this includes sand layered in some thickness over ice. This technique was used, for instance, to accurately predict sub-surface ice depth at the Phoenix landing site [L] and at the northern polar erg [C].

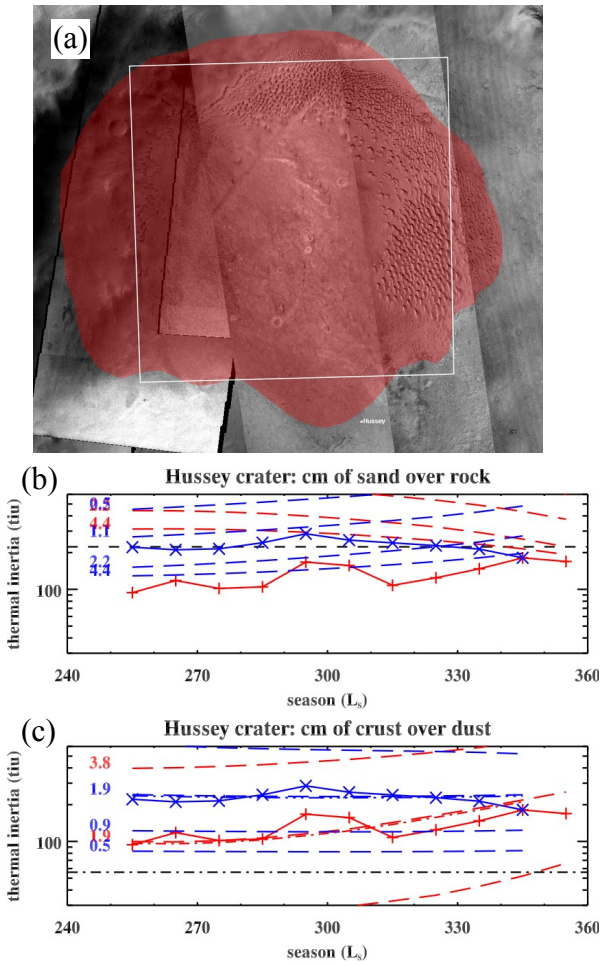

Figure 2. (a) THEMIS visible images showing Hussey crater dune field in red (as defined in [M]), with analysis performed within the white box. (b) and (c) show separate two-layer models (with rock used as thermally equivalent to ice). In each, apparent thermal inertia at 2AM (blue) and 2PM (red) from TES data (symbols connected by solid lines) is compared with that from models (dashed lines) labeled with top-layer thicknesses in cm. Seasons are limited to those when CO2 ice is not present. The data is broadly anti-correlated with the sand (225 tiu)-over-rock (2506 tiu) model, but follows well the crust (889 tiu)-over-dust (56 tiu) lines.

First Looks: We performed an initial analysis on two dune fields, in Hussey crater (233.1° E, 53.1° S) and in the inter-crater plains at 293.7° E, 49.8° S (Fig. 2 & 3). Under the sub-surface ice hypothesis, we might expect thermal inertia measurements at these two sites consistent with a sand-over-rock model (where the model's rock is thermally equivalent to ice). However, both sites are consistent instead with a few centimeters of crust overlying dust. We found similar results in a preliminary analysis of two more poleward, more eroded sites, where shallower ice would be expected. This suggests something more going on, though it does not rule out the presence of deeper ground ice. Of the 1190 dune fields mapped in [D], 171 are larger than 0.25° across (5 pixels in TES data) with a high-confidence morphological classification. We hope analysis of the remaining 167 will help complete this picture.

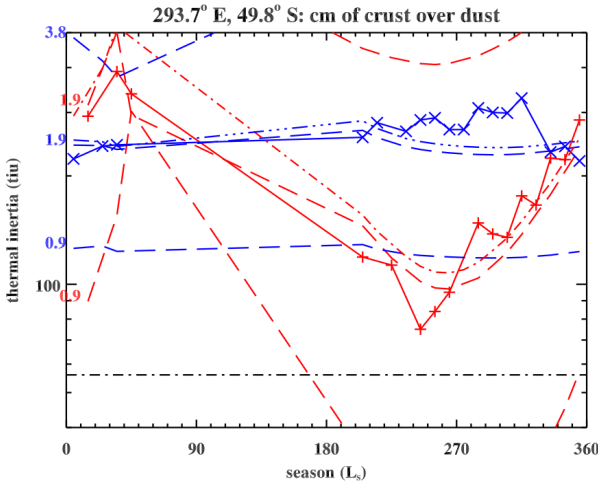

Figure 3. TES thermal inertia and models for the dune field at 293.7° E, 49.8° S, colored and labeled as in Figure 2. As with the Hussey Crater dune field (Fig. 2), a crust-over-dust model provides the best fit whereas a sand-over-ice model (not shown) exhibits an anti-correlated behavior.

References: [A] Byrne, S. et al. (2009) *Science*, 325, 1674-1676. [B] Feldman, W.C. et al. (2004) *JGR*, 109, 13. [C] Putzig, N. E. et al. (2014) *Icarus*, 230, 64-76. [D] Fenton, L. K. and Hayward, R. K. (2010) *Geomorphology*, 121, 98-121. [E] Bourke, M. C. et al. (2009) *Geomorphology*, 109, 148-160. [F] Butcher, A. and Fenton, L. (2011) *LPS XLII*, Abstract #2091. [G] Jakosky, B. M. (1986) *Icarus*, 66, 117-124. [H] Mellon, M. T. et al. (2000) *Icarus*, 148, 437-455. [I] Putzig, N. E. et al. (2004) *LPS XXXV*, Abstract #1863. [J] Mellon, M. T. et al. (2008) in: *The Martian Surface,* Bell, J. F., ed. (2008) Cambridge Univ. Press. [K] Putzig, N. E. and Mellon, M. T. (2007) *Icarus*, 191, 52-67. [L] Putzig, N. E. and Mellon, M. T. (2007) *Icarus*, 191, 68-94. [M] Hayward, R. K. et al. (2014) *Icarus*, 230, 38-46.

OBJECT-BASED DUNE MAPPING AND CHARACTERIZATION ON MARS: DATA COMPARISON AND ACCURACY ASSESSMENT. David A. Vaz[1,2], Pedro T.K. Sarmento[1,3], L. K. Fenton[4], M. T. Barata[1], T.I. Michaels[4], [1]CITEUC - Centre for Earth and Space Research of the University of Coimbra, Observatório Geofísico e Astronómico da UC, Almas de Freire, 3040-004 Coimbra, Portugal (davidvaz@uc.pt), [2]CERENA, Instituto Superior Técnico, Lisboa, Portugal, [3]ESAC - European Space and Astronomy Center, Madrid, Spain, [4]Carl Sagan Center, SETI Institute, 189 N Bernardo Ave, Mountain View, CA 94043, USA.

Introduction: The nearly global coverage of the CTX imagery, at spatial resolutions <10 m/pixel, enables a detailed analysis of dune fields on Mars. Such a large amount of data will be used in the upcoming years to study aeolian processes and to update existing dune catalogs, such as the Mars Global Digital Dune Database [1, 2]. Unless this analysis is totally or partially automated, a considerable human effort must be employed, since it basically relies on manual photointerpretation of orbital imagery.

By adapting the same generic procedure developed for the mapping of aeolian ripples from HiRISE data [3], we have explored the possibility of automated dune pattern characterization [4]. Here we will present the first results, including a preliminary validation of the technique by comparing the results with photointerpretations of the dune fields located in Gale crater and Ganges Chasma.

Data and methodologies: Using ISIS (Integrated Software for Imagers and Spectrometers) we have produced geometrically controlled CTX mosaics with a spatial resolution of 6 and 7 m/pixel, for the Gale Crater and Ganges Chasma areas respectively.

The automated mapping procedure follows the same type of object-based approach described in [3], and it includes: 1) segmentation from the CTX mosaic of the linear bright and dark ridges that can correspond to dune morphologies; 2) vectorization and characterization of the mapped objects (geometric, textural, morphometric and spectral descriptors are computed for each object); 3) supervised classification using neural networks, in order to exclude non-aeolian objects and segment the population of objects that correspond to slipfaces.

In this report we will discuss the accuracy rate of the implemented supervised classification, which constitutes the basis for future analysis. This processing step is fundamental, since it guarantees the segmentation of the objects that represent dune morphologies such as crests or slipfaces.

The obtained results are compared quantitatively and qualitatively with photointerpretations of the same areas. For this purpose we use the same mapping outputs previously discussed in [5] for the Ganges area. The objective is to assess the limitations of the methodology.

Results and discussion: Object descriptors are the input parameters for the classification process. A training dataset with three classes was created, allowing the segmentation of objects that do not correspond to dune morphologies (corresponding in most cases to bedrock features), slipface traces and other dune morphologies (a class that includes dune limbs, ridges, crests, etc.). Figure 1b shows an example of this training dataset, which represents 15% of the total mapped objects. Globally for the two areas, the computed overall accuracy was 94%, with a *k* index of 0.7. These values indicate a significant degree of agreement between the photointerpretations and the mapped objects.

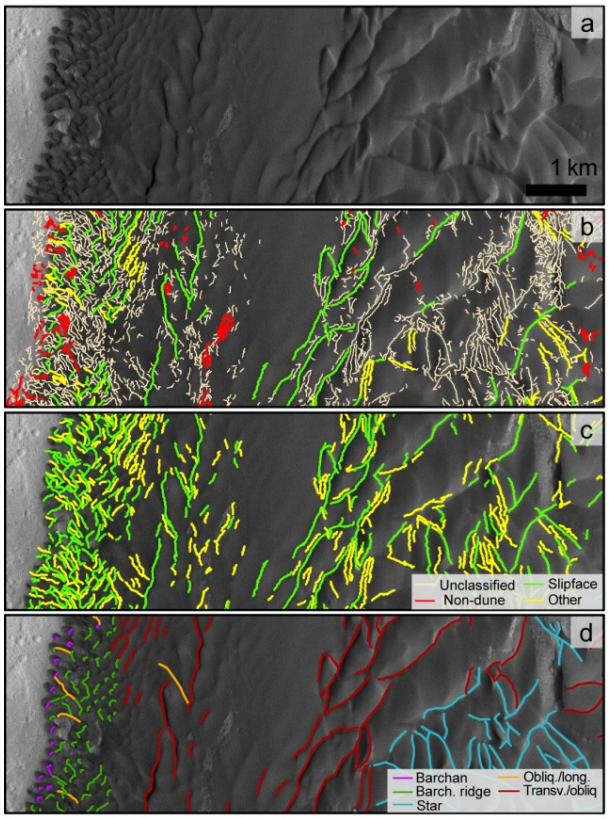

Figure 1 – Classification of the mapped objects, example from the Gale Crater area. a) CTX mosaic; b) mapped objects where the colored lines represent the training dataset; c) results of the supervised classification; d) photointerpreted dataset obtained by visual inspection and manual mapping of the dune morphologies (different classes represent the inferred dune types).

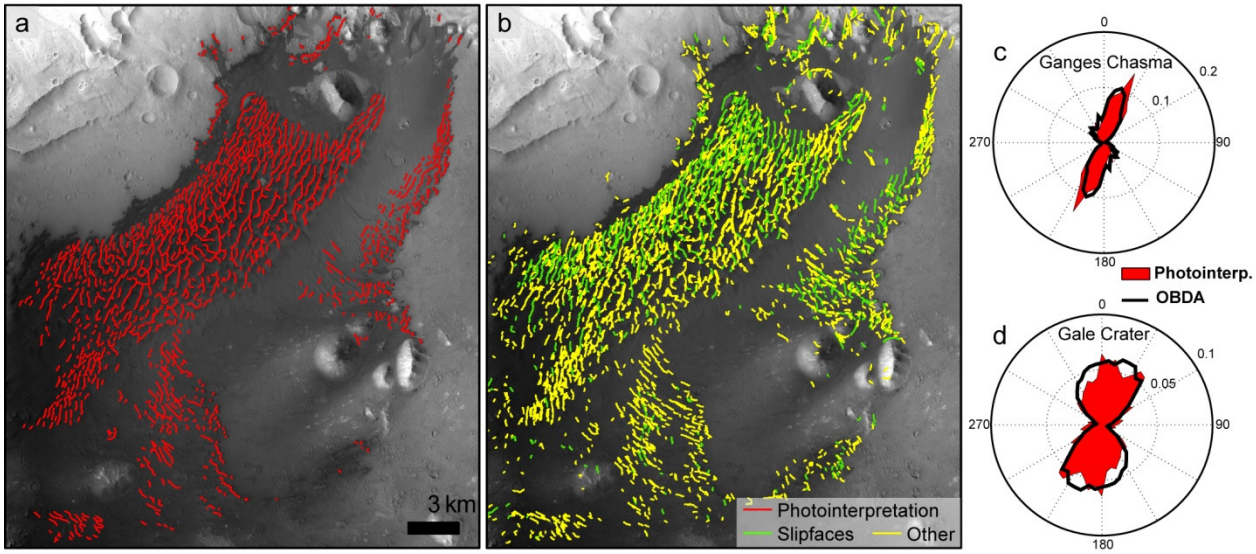

Figure 2 – Mapping results for the Ganges Chasma area and comparison of the circular distributions for the two areas. a) photointerpreted dune morphologies [5]; b) features automatically mapped; c and d) global length-weighted circular distributions for the photointerpreted and automatically derived datasets, note the good agreement between the obtained circular distributions.

Figures 2c and 2d show the global length-weighted circular distributions for the photointerpretations and also for the mapped dune morphologies. The good agreement between the circular distributions for both areas is evident. The angular differences in the trend of the mean axis computed between the two datasets are 5.2º and 4.6º, for Ganges and Gale respectively.

Qualitatively, the similarities in the mapping results are remarkable: compare figures 1c and 1d and 2a and 2b. Since the procedure is tuned to recognize all linear bright/dark regions on the image, it produces better results for larger linear features. Thus, small barchans dunes, which usually present small slipfaces, are not always correctly mapped (Fig, 1). For this dune type, barchans horns and lateral limbs are preferentially mapped. Because they are composed of larger scale linear features, barchanoid ridges, transverse and star dunes are better represented.

Conclusion and future perspectives: The supervised classification which enables the elimination of non-dune morphologies/objects is highly accurate and produces outputs that in qualitative terms are in agreement with the photointerpretations. At a regional level the circular distributions and the average axis of the mapped objects are highly correlated with the results obtained by photointerpretation.

We are currently evaluating the pattern differences at a local level, by implementing a zonal analysis and comparison of the mapped features. This is implemented by creating a sampling grid that is used to integrate the dune pattern characteristics locally. This enables a local quantitative comparison of the mapping results, and a simple integration of these results with mesoscale atmospheric model output.

In summary, we have shown that meaningful dune pattern characterization can be automatically performed for large areas using CTX image mosaics. A more detailed quantitative analysis of the results must still be performed. However, either integrated on a fully automated or semi-automated processing pipeline, the presented approach is potentially useful to implement a new data-driven wide survey of dune fields on Mars. This future survey would probably include automated morphological classification of the dune types and prediction of the sediment transport trends, using the mapped objects as inputs.

References: [1] Hayward R. K., et al. (2007). *Journal of Geophysical Research: Planets,* Vol. 112 (E11),E11007. [2] Hayward R. K., et al. (2014). *Icarus,* Vol. 230,38-46. [3] Vaz D. A. and S. Silvestro (2014). *Icarus,* Vol. 230,151-161. [4] Sarmento P. T. K., et al. (2014) Automated Dune Field Mapping from CTX Imagery, *45th LPSC*, #1777. [5] Fenton L. K., et al. (2014). *Icarus,* Vol. 230,47-63.

Acknowledgements: This work was supported by FCT (Fundação para a Ciência e a Tecnologia) with the grant FRH/BPD/72371/2010 and the contracts PEst-OE/CTE/UI0611/2012-CGUC and PTDC/CTE-SPA/117786/2010.

RIPPLE PATTERN ANALYSIS IN HERSCHEL CRATER. David A. Vaz[1,2], Pedro T.K. Sarmento[1,3], S. Silvestro[4,5], M. Cardinale[6], [1]CITEUC - Centre for Earth and Space Research of the University of Coimbra, Observatório Geofísico e Astronómico da UC, Almas de Freire, 3040-004 Coimbra, Portugal (davidvaz@uc.pt), [2]CERENA, Instituto Superior Técnico, Lisboa, Portugal, [3]ESAC - European Space and Astronomy Center, Madrid, Spain, [4]INAF Osservatorio Astronomico di Capodimonte, Napoli, Italy, [5]Carl Sagan Center, SETI Institute, CA USA, [6]DiSPUTER, Università Degli Studi G.D'Annunzio, Chieti, Italy.

Introduction: Ripples on Martian dark dune fields are actively migrating and being shaped by near-surface winds [1, 2]. Therefore, they are the bedforms that evolve faster, probably recording even daily wind variations. Complex dune topography should also plays an important role, deflecting winds [3, 4] and generating "shadow" zones on the leeside of the dunes.

HiRISE imagery shows a large diversity of ripple patterns. Some ripple sets form regular arrays of straight elongated bedforms, while others can present sinuous traces, resembling linguoid or lunate ripples described in subaqueous environments [5]. Our aim is to understand the meaning of these pattern variations. To achieve this, we have created a dataset that allows the correlation of ripple pattern characteristics, morphometric parameters, migration rates, and a simplified wind effect model [6]. Here we present a preliminary analysis of this integrated dataset.

Data and methodologies: The base data for this work are HiRISE DTMs and orthorectified images. COSI-Corr was used to estimate ripple migrations, and the DTM was used to model the wind effect on the topography [6]. Using the OBRA (Object-Based Ripple Analysis) ripple mapping technique [7] we mapped the ripples on a 15 km^2 area located in Herschel Crater (Fig. 1). The studied dune field consists of asymmetric barchans and barchanoids, with slipfaces elongated obliquely [8].

A regular grid with 10 m spacing was created to integrate the ripple patterns characteristics (length, wavelength, circular mean, modes, circular dispersion, etc.), morphometric parameters (slopes, aspect angles, etc.), migration (magnitude and trend) and a wind effect index. The obtained dataset provides the spatial integration of all these data sources, being ideal to test possible pattern correlations over large areas (Fig. 1).

Results: The compiled dataset combine a large variety of parameters. A complete analysis must then make use of multivariate statistical methods, such as PCA, clustering or multivariate correlations. Here we will simply discuss a first exploratory data analysis, focusing the discussion on one pattern characteristic: the average length of the ripples.

Figures 1b and c show the spatial distribution of the average ripple length. Clusters of ripples presenting higher lengths are visible, suggesting that the spatial distribution of this variable is clearly not random. A North-South variation is also apparent, with a larger concentration of these clusters in the Northern region.

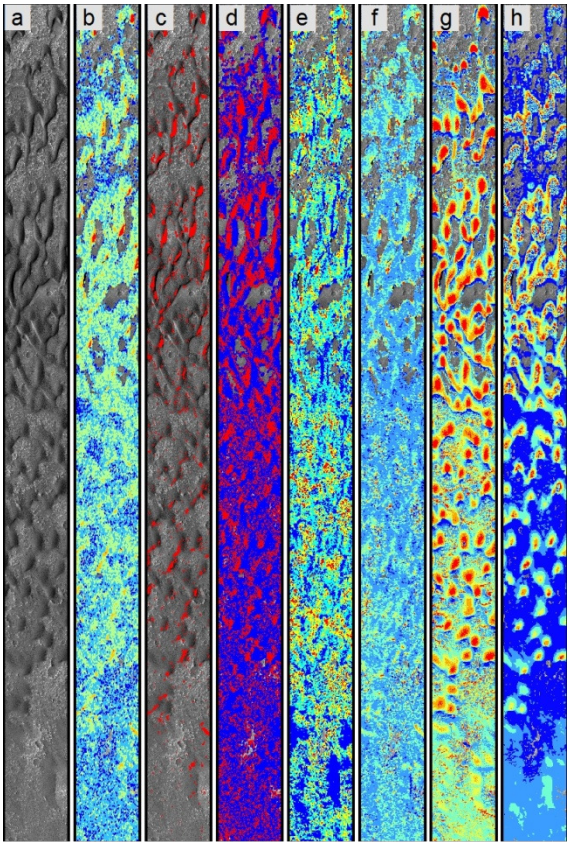

Figure 1 – Study area with some examples of the parameters that were computed. a) HiRISE image; b) average ripple length, note the clusters of longer ripples; c) location of the ripple clusters with average lengths higher than 9 m; d) azimuth of the primary mode, see Fig. 2 for a detailed view of this parameter (N0º-N90º in blue, N90º-N180º in red); e) directional strength ratio; f) ripple average wavelength; g) wind effect on the topography assuming winds blowing from N0º±30º, note the stronger effect of the wind in the windward section of the dunes, and the sheltered areas located in the leeside of the slipfaces; h) magnitude of the COSI-Corr migration vectors, these seem to be positively correlated with the modeled wind effect index.

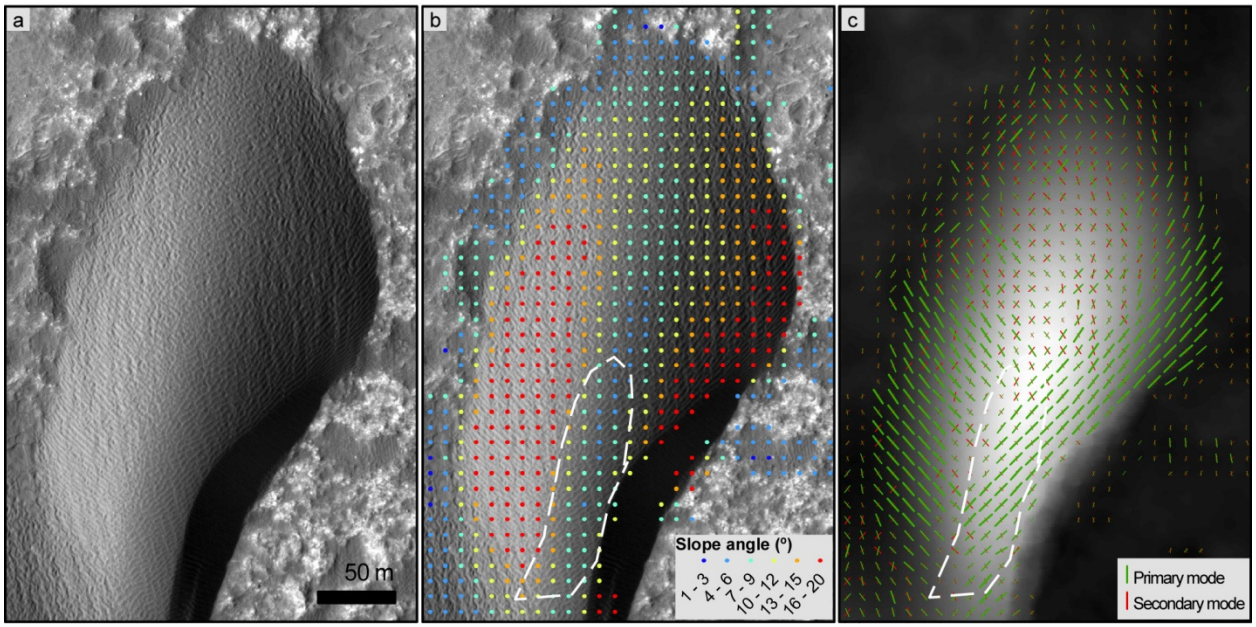

Figure 2 – Detailed view of the ripple pattern over an asymmetric barchan. a) HiRISE image; b) surface slope angle; c) ripple pattern modal trends (primary and secondary modes in green and red respectively), the length of the traces correspond to the kernel modal strength. In this case, nearly orthogonal ripple sets coexist in the stoss slope. Longer ripples seem to be well correlated with higher slopes, but on the dashed area, longer ripples also occur in a relatively flat crest area.

The sub-population of ripples with average lengths higher than 9 m (Fig. 1c) corresponds to sets of long and straight ripples with an average wavelength of 2.6±0.4 m. As shown in Fig. 1c, this sub-population represents a small percentage of the total population (circa 5%). More commonly, the ripples are short and appear in almost orthogonal sets that coexist in the same area.

In most of the cases, the clusters of long ripples appear associated with: 1) dune flanks, in areas presenting higher slopes and with ~N45º and ~N145º trends (Fig. 2); 2) leeside of dome dunes, particularly in the southern region; 3) at the base of slipfaces, where they can sometimes present a North-South trend.

Discussion and conclusion: The example given in this report highlights the use of automated ripple pattern characterization tools for the systematic study of pattern spatial variations. We have limited our analysis only to the average length of the ripples, a pattern characteristic which is considered to be influenced by bed shear stress (straight ripples were associated with lower flow velocities for subaqueous ripples [5]) or across-crest transport flows [9]. The location and morphometric context of the clusters of long and straight ripples that we have identified at Herschel, seems to be consistent with these possible explanations. The association with higher slopes is particularly evident, indicating that gravitational slope transport may be occurring, generating the elongation of the ripples. However, the same physical mechanism cannot be invoked for the other contexts, where upstream topographic obstacles seem to be relevant [10].

References: [1] Silvestro S., et al. (2013). *Geology,* Vol. 41 (4),483-486. [2] Silvestro S., et al. (2011). *Geophys. Res. Lett.,* Vol. 38 (20),L20201. [3] Howard A. D. (1977). *Geol. Soc. Am. Bull.,* Vol. 88,853-856. [4] Zimbelman J. R. and M. B. Johnson (2015). *LPSC 2015*, Abstract 1478. [5] Allen J. R. L., *Current ripples; their relation to patterns of water and sediment motion*. Amsterdam,: North-Holland Pub. Co., 1968. [6] Winstral A., et al. (2002). *J Hydrometeorol,* Vol. 3 (5),524-538. [7] Vaz D. A. and S. Silvestro (2014). *Icarus,* Vol. 230,151-161. [8] Cardinale M., et al. (2012). *Earth Surface Processes and Landforms,* Vol. 37 (13),1437-1443.[9] Rubin D. M. (2012). *Earth-Sci Rev,* Vol. 113 (3-4),176-185. [10] Silvestro S., et al. (2015). This volume.

Acknowledgements: This work was supported by FCT (Fundação para a Ciência e a Tecnologia) with the grant FRH/BPD/72371/2010 and the contracts PEst-OE/CTE/UI0611/2012-CGUC and PTDC/CTE-SPA/117786/2010.

UPDATE ON NASA'S PLANETARY AEOLIAN LABORATORY. D. A. Williams[1], [1]School of Earth and Space Exploration, Arizona State University, Tempe, Arizona 85287-1404 (David.Williams@asu.edu).

Introduction: NASA's Planetary Aeolian Laboratory (PAL) is a facility funded by NASA's Planetary Science Division (PSD) that includes the Mars Wind Tunnel (MARSWIT) and the Titan Wind Tunnel (TWT) located at the Ames Research Center (ARC) at Moffett Field, CA. The purpose of this abstract is to updated the planetary aeolian community on the operational status of the PAL and inform them of the critical need for more proposals to conduct work in the PAL.

Background: The PAL was founded at NASA ARC in 1976 by Dr. Ronald Greeley of Arizona State University (1939-2011) as a facility to conduct controlled experiments in aeolian processes. Funded by NASA's Planetary Geology and Geophysics Program, the PAL initially included the Mars wind tunnel (1976-present) and a Venus wind tunnel (1981-1994), which was remodeled as a Titan Wind Tunnel and became operational in June 2012. The MARSWIT is used to investigate the physics of particle entrainment by the wind under terrestrial and Martian conditions, to conduct flow-field modeling experiments to assess wind erosion and deposition on scales ranging from small rocks to landforms (scaled) such as craters, and to test spacecraft instruments and other components under Martian atmospheric conditions. MARSWIT is a 13-m long open-circuit boundary-layer wind tunnel within a large environmental chamber that operates at atmospheric pressures ranging from 1 bar to 5 millibars, with maximum speeds of 10.5 m/sec at 1 bar and 100 m/sec at 5 millibars. The wind tunnel is an open-circuit design, but sits on the floor of a large pressure chamber with an inside height of 30 m and an interior volume of 13,000 cubic meters. For low-pressure wind tunnel runs, the chamber is sealed and pumped down, and the open-circuit wind tunnel inside is operated within the low-pressure environment. PAL can be evacuated to Mars analog pressure (4 torr) in about 45 minutes. Due to the high cost to operate the vacuum system an agreement was struck in which PAL draws its vacuum almost exclusively only as a ride-along with other NASA-Ames projects/facilities that sponsor the activities of the NASA-Ames steam plant. This arrangement is highly cost-effective, but requires advance scheduling of low-pressure runs (requiring pump-downs) well in advance. Aside from this agreement, reserved vacuum service is available, provided sufficient funding is presented and there are no scheduling conflicts.

The TWT is a closed-circuit, pressurizable (to 20 bars) wind tunnel with an overall dimension of 6-m by 2.3-m. Included in the remodel were upgrades to a newer, higher performance motor, advanced motor controls, and new instrumentation. Overall tunnel pressure is determined by visual observation of a calibrated gauge (manufactured by Wika Instrument Corp., + or – 1psig) attached to the front of the tunnel instrument panel. Differential pressure is measured (for flow velocity calculation) by a custom designed sensor (manufactured by Tavis Corp.). This sensor is connected to a stack valve that determines which pitot tube is being "read" (traversing or fixed). The voltage from the sensor is sent to a data acquisition module (manufactured by Measurement Computing Corp.) and processed for interpretation by TracerDAQ software installed on a laptop computer. A test section is designed to allow the substitution of test plates. A test plate specifically designed for boundary layer profile work already exists and can be installed should the need arise.

Also available to the aeolian community (but not a part of the PAL) is the ambient pressure/temperature wind tunnel (ASUWIT) and the vortex (dust devil) generator (ASUVG) on the Tempe campus of Arizona State University (ASU), which is part of the ASU School of Earth and Space Exploration (SESE) and the Ronald Greeley Center for Planetary Studies. These facilities exist as a "recharge center" as part of ASU, and are available for anyone's use at a cost of $500/day, plus cost of consumables or special equipment.

PAL Status: At the time of this writing (February 2015) the PAL is funded through July 2015. Because there are two currently funded NASA PSD projects requiring use of the PAL facilities in 2015 and 2016, I have recommended to NASA that they grant a 1-year augmentation to the existing grant at the current funding level to continue operating the PAL through July 2016, pending arrangements for a facility review. No decisions have been made on this recommendation.

If the PAL is to continue as a NASA-funded facility, it is imperative that there is an increase in usage by the planetary community, either though an increase in funded proposals to conduct experiments in the PAL, or by requests from funded instrument teams for upcoming missions to test their components in the PAL. Thus, **I encourage members of the aeolian community, who have been thinking about proposeing wind tunnel work, to submit your proposals this year under ROSES-2015!!**

Where to Propose to Use the PAL? The PAL was previously funded by the NASA Planetary Geology and Geophysics (PG&G) program, and as of 2014 is

now incorporated into the "Solar System Workings" Program, where Announcements of Opportunity to Propose (AO) are released annually as part of NASA's Research Opportunities in Space and Earth Science (ROSES), typically available in February of each year. This should be the primary R&A program to submit proposals to conduct laboratory studies with PAL facilities. Funding to use the PAL facilities could also be included in instrument development proposals or proposals to develop instruments for future missions.

Proposers' Information: In ROSES look for information on the PAL in Section C.1. I have made a ***PAL Guidebook to Proposers***, which is available as a PDF through a link in ROSES section C.1. This document contains details on the technical capabilities of the PAL wind tunnels and necessary proposal and budgetary information. Feel free to email me at David.Williams@asu.edu for a copy of this document, or download from this webpage: http://rpif.asu.edu/pal/. For technical feasibility assessments on proposed PAL projects, feel free to contact the PAL Engineer James "Ken" Smith at James.K.Smith@asu.edu

WIND PATTERNS ON THE SOUTHERN END OF THE BRUNEAU DUNES COMPARED TO REMOTE AUTOMATIC WEATHER STATION DATA FROM MOUNTAIN HOME, IDAHO. C. A. Wishard[1,2] and J. R. Zimbelman[2], [1]The University of Alabama MSC 871222, 1831 University Station, Tuscaloosa, AL 35487-0268, cawishard@crimson.ua.edu, [2]CEPS/NASM MRC 315, Smithsonian Institution, Washington, D.C. 20013-7012, zimbelmanj@si.edu.

Introduction: A reversing sand dune is a dune that grows vertically instead of traveling horizontally across the landscape. Seasonal shifts in the dominant wind direction (from the northwest or the southeast) cause the dune to remain stationary throughout the year [1] [2]. The purpose of this study was to determine if the Remote Automatic Weather Station (RAWS) data taken from the Mountain Home Air Force Base (about 20 kilometers from Bruneau Dunes State Park) is an accurate portrayal of the wind patterns on the Bruneau reversing sand dune [3]. This study took data from the RAWS and from the GardenWatchCam (GWC) stationed at the dune and compared the two data types. Should the two data types have a reasonable correlation, RAWS data from the Mountain Home Air Force Base can be used to further study the Bruneau sand dune.

Procedure: In this study, the term "saltation frame" is used to describe a still frame taken by the GWC in which saltation is visible. The term "wind count" is used to describe the number of instances of wind in any specified direction recorded by the RAWS. The RAWS takes data at a one hour interval. Therefore, the wind counts per month would be the number of hour intervals per month in which the RAWS detected wind.

GardenWatchCam: On April 27th, 2011, the GWC was set up on the eastern side of the Bruneau sand dune. The GWC was attached to a pole about five and a half feet off the ground and aimed at the dune. Depending on the data set, the GWC took photos of the dune at one hour, two hours, or one-half hour intervals over the next two and a half years. Data was adjusted to fit a standard one hour interval. From April 27th, 2011, to August 31st, 2013 ten individual photo sets were collected from the GWC.

In this portion of the study, saltation was used as the means to determine if wind was blowing over the dune. It is important to note that saltation to the west or northwest is a sign of wind from the east or southeast and vice versa.

Remote Automatic Weather Station: A wind frequency table with an output of total wind counts was generated each month from May 2011 to February 2013. Based on the Beaufort scale, a wind velocity of 8 m/s was chosen to be the calm threshold for the RAWS data [4].

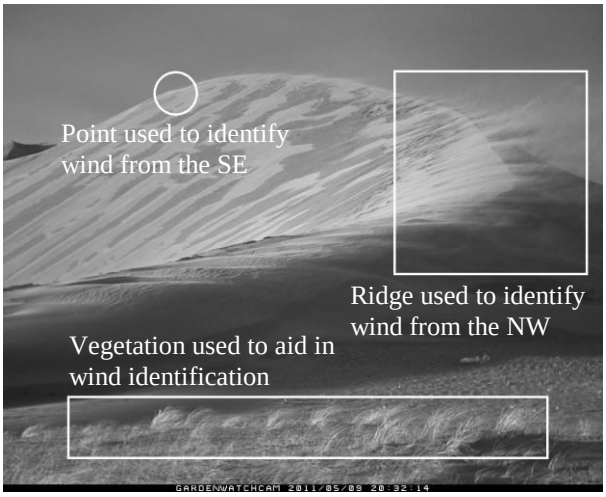

Fig. 1. GardenWatchCam image of the southern end of the Bruneau Dunes. Key areas of the dune have been highlighted. This image shows strong saltation caused by wind from the NW (05/09/11 at 20:32:14).

This table of total counts was divided into 16 cardinal wind directions but because the GWC data could not be reported to that level of accuracy, the RAWS data was simplified in order to compare the two data types. Wind resulting from any of the seven eastern directions was grouped together under southeast as the vast majority of eastern type winds came from the southeast. All northern directions were grouped under northwest in a similar fashion.

Results: The results from the GWC and RAWS were analyzed by wind counts from the SE and NW per month. For the GWC, the number of sightings of saltation per month gives a rough estimate of how often the wind was able to move sand in either the north-western or south-eastern direction per month. For the RAWS, the total amount of wind counts in all directions gives a rough estimate of the amount of strong wind affecting the dune each month.

Discussion: As to be expected from wind causing a reversing sand dune, the wind affecting the Bruneau dune is roughly cyclical. In both 2011 and 2012, the amount of GWC saltation frames and RAWS wind counts drop to below 20 in late summer and early fall. The number of wind counts and saltation frames remains around 10 for a few consecutive months and

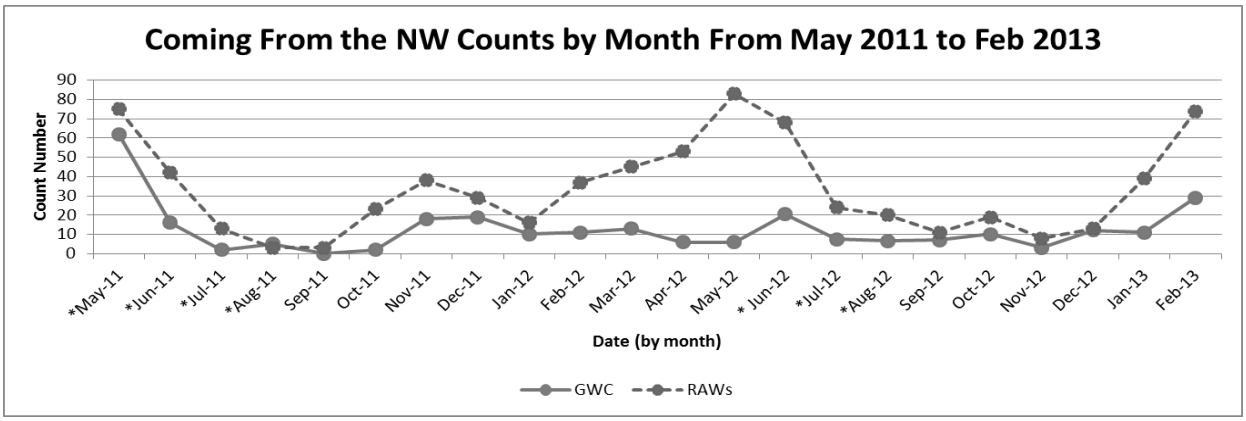

Fig. 2. NW wind counts by month. An "*" denotes a month in which the wind counts were adjusted to fit a one hour interval.

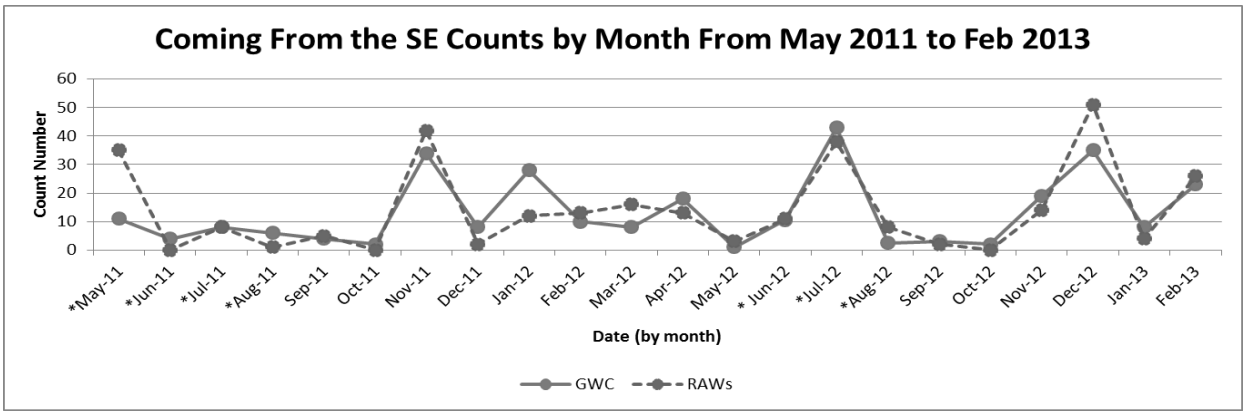

Fig. 3. SE wind counts by month. An "*" denotes a month in which the wind counts were adjusted to fit a one hour interval.

then rises again around November of both years. This is a sign that the winds affecting the dunes are undergoing a change in late summer and early fall.

The NW overlay shows a rough pattern of one large peak during late spring or early summer, followed by a small peak about 6 months later, in late fall early winter (see **Fig. 2**). The SE overlay shows a rough pattern of two large peaks in late fall and mid-summer and a lower continuous period of heightened wind count numbers from mid-winter to late spring (see **Fig. 3**). The SE and NW wind operating on different patterns explains the large dips in wind counts in late summer.

There are two main sources of potential error that could have affected the accuracy of the GWC data. The first is the angle at which the GWC photographed the dune. The GWC was positioned facing north. Because roughly half of the wind affecting the dune came from the SE (causing saltation to the NW), some saltation could have been missed as it blew over the crest of the dune. This would cause the SE GWC saltation frames to be less than the SE RAWS wind counts.

The second potential source of error came in the form of a large gray blur appearing on the lens of the GWC on October 4th, 2012 at 12:27:07. This blur slowly faded away due to rain or wind exposure but it fully did not disappear until December 27th, 2012 at 14:27:07. In this time, GWC data was still taken (as the blur got more translucent with time); however, it is possible that some saltation was missed.

References:

[1] Jackson J.A. (1997). Glossary of Geology, fourth ed. Am. Geol. Inst., Alexandria, 769.

[2] Zimbelman JR., Scheidt SP. (2014). Icarus, 230, 29-37.

[3] Zachariassen, J. et al, (2003). Gen. Tech. Rpt RMRS-GTR-119. U.S. Dept. Agric. and Forest Serv., Ft. Collins, CO.

[4] Met Office (2010). The Beaufort Scale. National Meteorological Library and Archive Fact Sheet, 1-22.

Experimental and numerical study of Sharp's shadow zone hypothesis on sand ripples spacing and implication for Martian sand ripples.

H. Yizhaq[1,2], E. Schmerler[3], I. Katra[3] , H. Tsoar[3] and J. Kok[4]. [1]Swiss Institute for Dryland Environmental and Energy Research, Blaustein Institutes for Desert Research, Ben-Gurion University of the Negev, Sede Boqer Campus, 84990, Israel (yiyeh@bgu.ac.il), [2]The Dead Sea and Arava Science Center. Tamar Regional Council, Israel, [3]The Department of Geography and Environmental Development, Ben-Gurion University of the Negev, Beer Sheva, 84105, Israel, (eschmerler@gmail.com), (katra@bgu.ac.il), (tsoar@bgu.ac.il). [4]Department of Atmospheric and Oceanic Sciences, University of California, Los Angeles, California, USA, (jfkok@ucla.edu).

Introduction: Although many works have been done on sand transport by saltation and reptation, and on the formation of sand ripples, it is still unclear what mechanism determines the linear dependence of ripples dimension on wind speed [1]. We thoroughly studied the formation of normal ripples in a wind tunnel as a function of grains size and wind speed. A linear relationship between the wind shear velocity and the impact angle of saltating grains has been found for different grain sizes. This relationship can explain the increase in ripple wavelength with the shear velocity as was already suggested by Sharp [2] (see Fig.1).

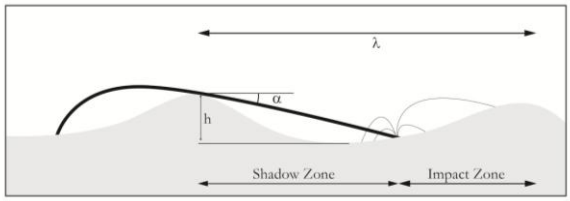

Figure 1. Scematic illustration of the Sharp's impact zone hypothesis. The impact angle of the saltation particle is denoted by α. The sadow zone is the region in the lee side of the ripple that is protected from the bomardemnt of the saltation particles.

In addition to the wind tunnel work we also studied the dependence of the impact angle on wind velocity both on Earth and Mars by numerical simulations with the steady state saltation model COMSALT [3]. COMSALT includes many of the advances of previous models, and in addition it includes: (1) a physically based parameterization of the splashing of surface particles that agrees with experimental and numerical studies [3], (2) a generalization of this splashing process to beds of mixed particle sizes, and (3) a detailed treatment of the influence of turbulence on particle trajectories, which agrees with laboratory measurements. Because of these and other advances, COMSALT is the first physically-based numerical saltation model to reproduce a wide range of experimental data. The model has also been used to show the formation the Basaltic sand ripples in Eagle crater [4].

Materials and Methdes: Quartz sand collected from the northwestern Negev dunefield (Israel) was used for the laboratory wind tunnel experiments on ripple morphology. The sand was taken in the sampling site in the northern Negev– Sekher (in southeren Israel) sands from the upper 10 cm of the sand dunes. Common sizes of the active (loose) sand in Sekher site are at the range of 100-400 µm with modes of 150-200 µm, which are typical of dune saltators. In order to explore the role of particle size in ripple morphology, the sand was segregated into different size fractions due to technical limitation to sieve specific size in natural sands. Three narrow size fractions were obtained using mechanical sieving: 142-200, 200-247, 247-300 µm. These fractions constituted 33.6%, 23.6%, and 12.4% of the bulk sample of Sekher sand, respectively. The aeolian experiments were conducted at the stationary boundary layer wind tunnel of the Aeolian Simulation Laboratory in Ben-Gurion University (BGU) described in [5]. The cross sectional area is 0.7×0.7 m and the working length is 7 m for measurements in the test section. The traps used for measuring the impact angle are shown and described in Fig. 2.

Results: Under high wind velocity conditions the impact angle is smaller, thus the shadow zone grows and the resulting wavelength increases. In addition, the impact angle increases with the grain diameter, thus for unimodal coarse sand, both amplitude and wavelength are small. The shadow zone mechanism is one of the mechanisms contributing to the linear increase of the ripple wavelength with wind speed. The main results of the wind tunnel experiments are shown in Fig.3 and Fig.4; the results of the numerical simulation of the impact angle under Mars conditions (for D=250 µm) is shown in Fig.5.

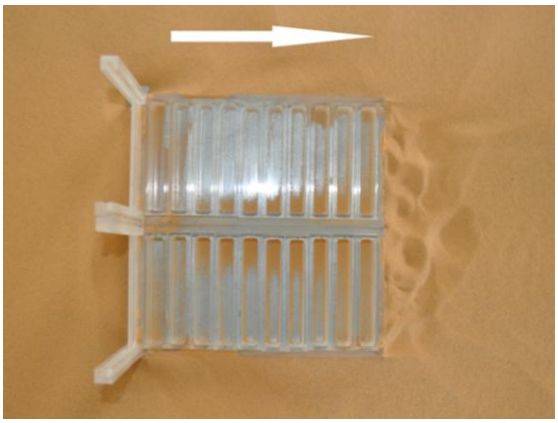

Figure 2: In order to retrieve the impact angle of the saltators, an array of horizontal traps was placed in the test section (the white arrow indicates wind direction). The array is comprised of 10 traps (a cross section of 10 × 1 cm of each). An obstacle at height of 2 cm above the sand bed was installed at the windward side of the array. The obstacle simulated a ripple element while the transported sand accumulated at the windward side to create a ripple slope. Thus the array allows the entering of saltating grains at uniform distances from the obstacle with an interval of 1 cm.

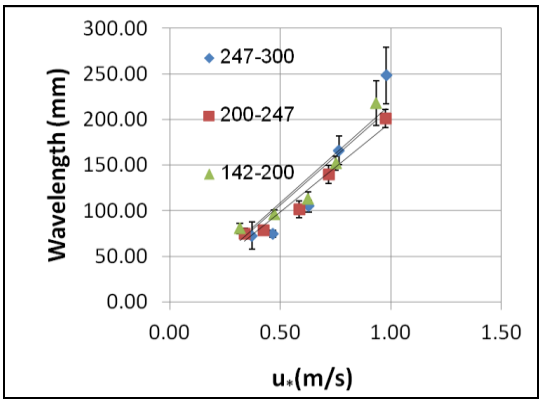

Figure 3. The linear growth of the wavelength with shear velocity is shown, in agreement with previous wind tunnel studies [6]. The largest wavelength was obtained for the fine grain fraction, but the difference between the fractions is quite small and statistically not significant.

Conclusions: Both experimental and numerical results show that the impact angle decreases with the shear velocity as predicted by Sharp [1]. The results also show that the impact angle decreases with the grain diameter in agreement with previous studies [7]. The decrease of the impact angle with the wind speed can explain the linear relation between wavelength and wind speed. For faster winds the impact angle will be shallower and longer wavelength bedforms result. The same behavior was numerically found for Mars (Fig. 5), thus we predict that the linear increase in the wavelength with wind velocity exists also for martian sand ripples. Further study is needed to understand the role of turbulence in ripples formation.

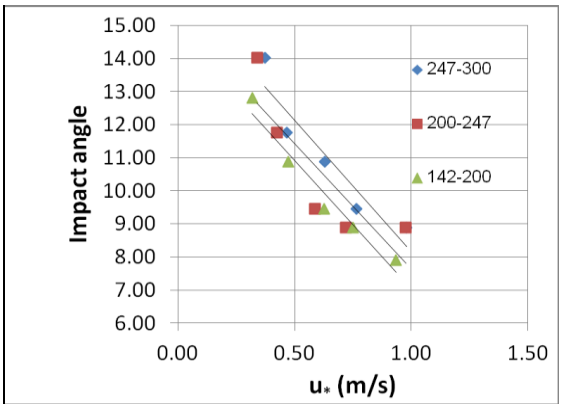

Figure 4: The impact angle of the saltation grains as function of the shear velocity for the three size fractions. The stronger the wind, the smaller is the impact angle, whereas it decreases with the grain diameter as expected by physical consideration of the saltation trajectories.

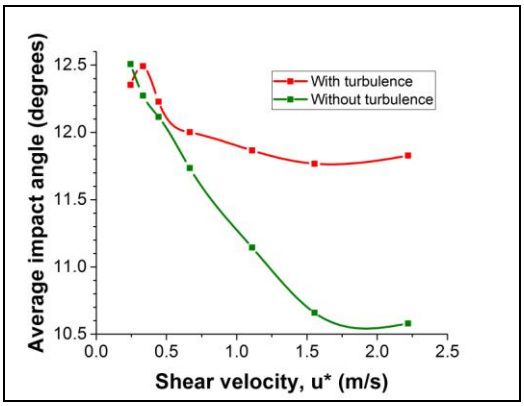

Figure 5: COMSALT simulations of the average impact angle on Mars as a function of the shear velocity with and without turbulence (for D=250 μm).

References:

[1] Durán, O. et al, (2014) *PNAS, 111*, 15665–15668. [2] Sharp R. P. (1963) *J. of Geology, 71*, 617-636. [3] Kok, J. and Renno, N. O. (2009) *JGR*, 114, D17204. [4] Yizhaq et al., (2014) *Icarus, 230*, 143-150. [5] Katra et al., (2014), *GRL, 41*, 858- 865. [6] Andreotti et al., (2006), *PRL*, 96.2: 028001. [7] Willetts et al., (1989), *ESPL, 14*, 719-730.

FIELD TRIP TO THE BRUNEAU DUNES AND THE SNAKE RIVER PLAIN BASALTS. J.R. Zimbelman[1],[1]CEPS/NASM MRC 315, Smithsonian Institution, Washington, D.C., 20013-7012; zimbelmanj@si.edu.

Introduction: A one-day field trip is planned as part of the agenda for the Fourth International Planetary Dunes workshop. On May 20 we will travel in a caravan of personal vehicles from Boise to Bruneau Dunes State Park, located about 10 km east of the small community of Bruneau, a trip of roughly 68 miles each way. Shortly after leaving Boise, we will first make a brief stop at the north bank of a branch of the Boise River where trails provide access to talus accumulated at the base of an exposure of columnar basalt, which is an excellent place to see the materials that comprise the Snake River Plain. Information about the field trip settings, including detailed driving instructions from MapQuest, are available on the workshop web site in a composite pdf file.

Background and Regional Setting: Boise is positioned near the eastern end of a broad NNW-SSE-oriented valley that connects to an even broader valley extending to the ENE, in which the Snake River Plain (SRP) is located (Fig. 1). The western branch of the SRP is a complex graben bounded by a system of normal faults [1], the northern side of which records more than 2.7 km of vertical displacement since Early Pliocene [2]. The structural control for the eastern SRP is less obvious, but a unique style of plains volcanism, based on numerous low-profile small shields, covers the plain [3]. The eastern SRP valley is associated with massive volcanic centers that decrease in age toward the active Yellowstone region at the eastern end of the valley, leading to speculation that the eastern SRP may be the track of the Yellowstone hostpot as plate motion carried North America over the hotspot [4]. The Columbia River Basalt (CRB) province is NNW of the western SRP (Fig. 1), although the earliest CRB eruptions (16.5 Ma) correlate with the location of the Yellowstone hotspot at that time [5]. The Bruneau Dunes are located within an evacuated cut-off meander loop of the Snake River, which flows across a good portion of the SRP [6]; the present sand accumulation at the dunes likely post-dates the Bonneville flood (14.5 Ka [7]), and has grown into the tallest single-structured free-standing sand dunes in North America, with >140 m of relief [6, 8].

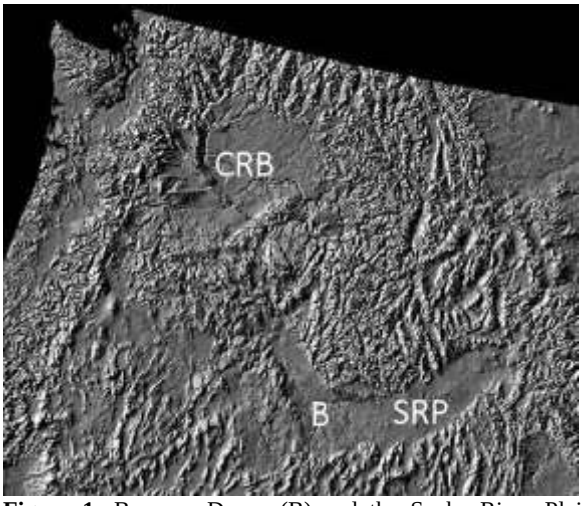

Figure 1: Bruneau Dunes (B) and the Snake River Plain (SRP) shown on a shaded relief image of the northwestern US (geomaps.wr.usgs.gov). The Columbia River Basalts (CRB) are exposed to the NNW of the SRP.

Snake River Plain Basalts: The SRP basalts are both chemically and morphologically distinct from the CRB province, leading Greeley to propose that they represent a form of basaltic "plains" volcanism separate from typical flood volcanism [3]. The western SRP consists of basalt flows of Early Pliocene to Middle Pleistocene age, while the eastern SRP basalts are Late Pleistocene to Holocene age [1]. A stop was chosen to view good exposures of columnar basalt from a parking area on the north side of a branch of the Boise River along Idaho Highway 21 (43° 52' 19.7" N, 116° 5' 33.8" W; Fig. 2). Trails from the parking area go to the base of a talus slope comprised of weathered basalt columns.

Figure 2: Stop for examination of Snake River Plain basalts along Idaho Highway 21, next to a catchment dam on a branch of the Boise River. Oblique Google Earth Pro image. Inset: columnar basalt and talus at the site (JRZ photo).

Bruneau Dunes: The largest sand accumulations at the Bruneau Dunes are interpreted to be reversing dunes (Fig. 3), supported by long-term wind records from nearby Mountain Home [6, 8]. Transverse and barchanoid bedforms do occur arround the main dunes, particularly west of the dunes in an area that Murphy called the 'Little Sahara' [6]. The dunes are preserved

Figure 3: Vertical view of the Bruneau Dunes; Google Earth Pro image. "P" indicates parking lot adjacent to the lake. Red line shows proposed hiking route to the crest of the dunes. White arrow shows orientation of photo in Fig. 4.

as part of the Idaho park system [9], and a daily entrance fee (per vehicle) is required at the entrance. The visit to the dunes will begin at the parking lot adjacent to the main dunes ("P" is Fig. 3; 42° 53' 44.8" N, 115° 41' 50.0" W). The parking area is next to a large lake that is available for non-motorized recreation (Fig. 4).

Figure 4: Oblique view of the Bruneau Dunes, looking south (see arrow in Fig. 3). Note abundant vegetation present both around the lake margin and on the stabilized flanks of the large dunes. JRZ photo, 9/5/12.

From the parking area, we will hike to the crest of the main dunes (red line, Fig. 3). The first half of the hike is basically level, circumventing the lake margin, but the second half of the hike involves moderate exertion to climb up the side of one of the large dunes, portions of which approach the angle of repose. The lowest portions of the large dunes are vegetated and locally stabilized (Fig. 4), but the crests of the tallest dunes are unvegetated and definitely active (Fig. 5). From the crest of the tall dunes, a panoramic view of the surrounding low hills visually confirms that the dunes are situated within a shallow depression, locally named Eagle Cove [6]. Sedimentology supports the interpretation that the dune sands are derived from loose mat-

Figure 5. Frame from a time series obtained by a GardenWatchCam placed to monitor the southern end of the dunes (bottom of Fig. 3). Image shows strong saltation by wind from the northwest, with transverse features over dark (wet) substrate sand. 5/9/11.

erials in the nearby hills, along with equal contributions of basalt fragments and silica sand, the later two likely derived from deposits left by the Bonneville flood [2, 6]. After several hours of exploring the dunes on your own, participants will return to Boise by retracing the path followed in getting to the park. Additional information about the park is available from [9].

References: [1] King J.S. (1977) NASA CR-154621 (R. Greeley and J.S. King, Eds), pp. 45-57. [2] Malde H.E. (1968) U.S. Geol. Surv. Prof. Paper 596, 52 p. [3] Greeley R. (1977) NASA CR-154621 (R. Greeley and J.S. King, eds), pp. 24-44. [4] Christensen R.L. (1990) Volcanoes of North America (C.A. Wood and J. Kienle, Eds.), pp. 263-266, Cambridge Univ. Pr. [5] Hooper P.R. (1997) Large Igneous Provinces (J.J. Mahoney and M.F. Coffin, Eds.), pp. 1-27, AGU Geophy. Mon. 100. [6] Murphey J.D. (1973) The geology of Eagle Cove at Bruneau, Idaho, M.S. thesis, SUNY-Buffalo, 77 p. [7] Currey D.R. (1990) Paleogeo. Paleoclim. Paleoecol. 76, 189-214. [8] Zimbelman J.R., Scheidt S.P. (2012) Icarus 230, 29-37. [9] parksandrecreation.idaho.gov/parks/bruneau-dunes/.

NOTES